

DISS. ETH NO. 26400

Alternative scaffolds for systemic delivery of small interfering RNAs

A thesis submitted to attain the degree of

DOCTOR OF SCIENCES of ETH ZURICH

(Dr. sc. ETH Zurich)

presented by

CHRISTIAN BERK

Pharmacist (State Examination), University of Freiburg

born on 02.08.1989

citizen of Germany

accepted on the recommendation of

Prof. Dr. Jonathan Hall, examiner

Prof. Dr. Karl-Heinz Altmann, co-examiner

2019

Acknowledgements

First of all, I would like to thank Prof. Dr. Jonathan Hall for the supervision of my thesis and his guidance on the various projects. He granted me the freedom to follow my curiosity and reminded me of the necessities when needed. I am deeply grateful for his continued support over the whole PhD.

I would also like to thank

- Prof. Dr. Karl-Heinz Altmann for kindly acting as a co-examiner for my PhD defense
- Prof. Dr. Carlo Catapano and Dr. Gianluca Civenni for the collaboration on the siLin28B project and for hosting my research stay at the IOR
- Sylvia Peleg for the administrative support
- Anne Michelle Lüscher, Marilyn Jayakumar, Chaitra Rao and Diego Lorenzo del Rio Sarasola for their valuable contributions to various research projects. It's been a pleasure to work with such talented and motivated students.
- Dr. Yuluan Wang for the collaboration on the cyCLIP project, long coffee breaks and sport sessions
- Dr. Pascal Röthlisberger, Timo Hagen, Mauro Zimmermann, Matije Lucic, Anna Knörlein and Artur Laski for football talks, sport sessions, bike and ski tours.
- Dr. Mirjam Menzi for the introduction to RNA chemistry and unforgettable ski tours
- Anna Malinowska for long discussions in the chemistry bay
- Verena Schlösser for the introduction to the work with radioactivity
- Francois Halloy, Dr. Ugo Pradère and Dr. Elodie Decuypère for the discussions on chemistry and the entertaining cultural exchange
- Evangelia Lekka for long discussions on Lin28B
- Martina Bigatti for being a great neighbor in the chemistry bay
- Dr. Alok Behera for having everything under control
- Dr. Meiling Li, Dr. Alyssa Hill, Anastasiia Lepikhina, Dr. Alice Ghidini, Dr. Helen Lightfoot and Dr. Pavithra Iyer for joint coffee breaks and various discussions

A special thank you goes to my family for their unconditional and never-ending support

Contents

Acknowledgements	III
List of abbreviations	VIII
Abstract	XIII
Zusammenfassung	XIV
1 Introduction	1
1.1 Chemistry of oligonucleotides	1
1.1.1 Modifications of the phosphodiester backbone	1
1.1.2 Modifications of the nucleobase.....	5
1.1.3 Sugar modifications	7
1.1.4 5'- and 3'-terminal modifications.....	9
1.2 Classes of nucleic acid therapeutics	12
1.2.1 Splice switching oligonucleotides.....	12
1.2.2 RNase H dependent antisense oligonucleotides.....	13
1.2.3 AntimiRs, miRNA mimics and the miRNA interference pathway	14
1.2.4 Small interfering RNAs and functional interplay with the miRNA pathway	17
1.2.4.1 Toxicity aspects of siRNAs	19
1.2.4.2 Metabolic stability of siRNAs.....	20
1.2.4.3 Delivery and pharmacokinetics of siRNAs.....	21
1.2.5 CRISPR/ Cas based systems.....	21
1.2.6 Other classes of RNA therapeutics	23
2 Project 1 – Full PS siRNAs as an alternative scaffold for RNAi therapeutics	25
2.1 Introduction	25
2.1.1 PS modification for siRNAs.....	25
2.1.2 The Lin28/ let-7-axis as a drug target in cancer	26
2.2 Project outline.....	26
2.3 Results and Discussion.....	27
2.3.1 Scale-up of PS ORN synthesis	27
2.3.2 <i>In vitro</i> assessment of PS siLin28B.....	30
2.3.2.1 Cellular activity	30
2.3.2.2 Thermal denaturation and HSA binding of PS and PO siLin28B	31
2.3.2.3 Nuclease stability in mouse serum and rat liver tritosomes	32
2.3.3 Methods to quantify PS siLin28B in tissue biopsies	34
2.3.3.1 TaqMan RT-qPCR for quantification of PS siLin28B.....	35
2.3.3.2 Chemical ligation-qPCR for quantification of PS siLin28B	36

2.3.3.3 Northern blot for quantification of PS siLin28B	38
2.3.3.4 PNA hybridization assay for quantification of PS siLin28B.....	39
2.3.4 Biodistribution of PS siLin28B	40
2.3.5 Investigation of PS siLin28B in a prostate cancer xenograft model	41
2.4 Conclusion and Outlook	43
2.5 Contributions	44
3 Project 2 – Polyamine-siRNA conjugates as novel RNAi reagents	45
3.1 Introduction	45
3.1.1 Biological relevance and nucleic acid binding characteristics of polyamines.....	45
3.1.2 Conjugation of polyamines to oligonucleotides – polyaminooligonucleotides	45
3.1.3 The polyamine transport system (PTS).....	46
3.1.4 The convertible nucleoside approach	47
3.2 Project outline.....	48
3.3 Results and discussion	49
3.3.1 Synthesis of an siRenilla-spermine conjugate library.....	49
3.3.2 UV-melting of siRNA-spermine conjugates.....	54
3.3.3 Activity of siRenilla-conjugates in Dual-Luciferase reporter assays	55
3.3.4 Nuclease stability of siRenilla-spermine conjugates	58
3.3.5 Activity of siLin28B-spermine conjugate	58
3.3.6 Additional modifications introduced via the ‘convertible nucleoside’ approach	59
3.4 Conclusion and outlook	62
3.5 Contributions	62
4 Project 3 – Development of a new chimera-forming CLIP method (cyCLIP)	63
4.1 Introduction	63
4.1.1 Experimental approaches to identify miRNA-RNA interactions – CLIP-based methods	63
4.1.2 Relevance of RNA>p and RtcB as a 2',3'-cyc P/ 3'P RNA ligase.....	65
4.2 Project outline.....	66
4.3 Results and Discussion.....	66
4.3.1 Synthesis of RNA>p.....	66
4.3.2 Ligation of miRNA>p in cell lysate	67
4.3.3 <i>In vitro</i> ligation using RtcB	69
4.3.4 Development of a cyCLIP work-flow.....	71
4.3.5 Use of RNA>p for the synthesis of circular RNAs	75
4.4 Conclusion and Outlook	76
4.5 Contributions	77
5 Side projects.....	78

5.1 Type III CRISPR–Cas systems produce cyclic oligoadenylate second messengers	78
5.2 Covalent linkage of the DNA repair template to the CRISPR-Cas9 nuclease enhances homology-directed repair	79
5.3 One- and two-dimensional high-resolution NMR from flat surfaces	80
5.4 Additional publications	81
6 Conclusion and Outlook	82
7 Experimental part	86
7.1 Oligonucleotide synthesis	86
7.1.1 General conditions for oligonucleotide synthesis	86
7.1.2 Work-up and purification of oligonucleotides	88
7.1.3 LC-MS analysis	89
7.1.4 Synthesis of siRNA conjugates via the convertible nucleoside approach	89
7.1.5 Synthesis of an siRNA-spermine conjugate via click chemistry	90
7.1.6 Synthesis of Cy3 forward primer for CL-qPCR	90
7.1.7 Coating of oligonucleotides on sapphire, borosilicate glass and fused silica	90
7.2 Cell culture	91
7.2.1 General conditions	91
7.2.2 Western blots	91
7.2.3 SYBR Green RT-qPCR	92
7.2.4 TaqMan RT-qPCR	93
7.2.5 Chemical ligation-qPCR	94
7.2.6 Northern blot	95
7.2.7 Dual-Luciferase reporter assays	98
7.3 <i>In vitro</i> experiments	100
7.3.1 Tritosome stability assays	100
7.3.2 Mouse serum stability assays	101
7.3.3 PNA hybridization assay	101
7.3.4 FBS stability assays	102
7.3.5 Thermal denaturation studies	102
7.3.6 Electrophoretic mobility shift assay	102
7.3.7 Fluorescence displacement assay	103
7.3.8 Ligation assay in HeLa lysate	103
7.3.9 RtcB ligation assays	105
7.3.10 2', 3' cycP stability assays	106
7.3.11 RNase T1 digestions	106
7.3.12 cyCLIP	107
7.4 <i>In vivo</i> experiments	107

7.5 Chemistry.....	108
7.5.1 Synthesis of <i>O</i> ⁴ -triazolyluridine-2'- <i>O</i> -TBDMS CED phosphoramidite	108
7.5.2 Synthesis of <i>N</i> ² , <i>N</i> ³ , <i>N</i> ⁴ -tri(tert-butoxycarbonyl)-spermine azide	109
7.5.3 Synthesis of spermine azide.....	109
7.5.4 Synthesis of <i>N</i> ¹ -trityl spermine.....	109
Bibliography	111
Appendix	138
Appendix – Project 1	138
Appendix – Project 2	149
Appendix – Project 3	155
Curriculum vitae	160

List of abbreviations

2'-F	2'-deoxy-2'-fluoro
2'-OMe	2'-O-methyl
4-SU	4-thiouridine
5'-E-VP	5'-E-vinylphosphonate
ACN	Acetonitrile
ACTB	β -actin
AGO2	Argonaute-2
AGO2-IP	AGO2-immunopurification
AMA	aqueous ammonia: methylamine (1:1)
AMD	age-related macular degeneration
AML	acute myeloid leukemia
APCHA	<i>N</i> -(3-aminopropyl)-cyclohexylamine
Apo B-100	apolipoprotein B-100
APS	ammonium peroxodisulfate
AS	antisense
ASO	antisense oligonucleotide
ASPGR	asialoglycoprotein receptor
ATP	adenosine triphosphate
AU	absorbtion units
BHQ-2	black hole quencher 2
BLM-A5	bleomycine A5
BPS	bisphenylsulfonyl
BSA	bovine serum albumin
BTT	5-(Benzylthio)-1H-tetrazole
<i>C. elegans</i>	<i>Caenorhabditis elegans</i>
CARF	CRISPR-associated Rossmann fold
Cas	CRISPR associated
CCC9A	cation-chloride-cotransporter
CCR4	carbon catabolite repressor protein 4
CED	2-cyanoethyl- <i>N,N</i> -diisopropyl
CLASH	crosslinking, ligation and sequencing of hybrids

CLEAR-CLIP	covalent ligation of endogenous Argonaute-bound RNAs-CLIP
CLIP	crosslinking immunoprecipitation
CL-qPCR	chemical ligation quantitative polymerase chain reaction
CNS	central nervous system
CPG	controlled pore glass
CPMG	Carr-Purcell-Meiboom-Gill
CRISPR	clustered regularly interspaced short palindromic repeats
CRISPRa	CRISPR activation
CRISPRi	CRISPR interference
crRNA	crisprRNA
CSD	cold shock domain
CuAAC	copper catalyzed 1,3-dipolar azide-alkyne cycloaddition
cycP	2', 3'-cyclic phosphate
DCA	dichloroacetic acid
dCas9	dead Cas9
DCM	dichloromethane; methylene chloride
DCP 1	mRNA-decapping enzyme subunit 1
DDTT	3-((N,N-dimethylaminomethylidene)amino)-3H-1,2,4-dithiazole-5-thione
DFMO	D, L- α -difluoromethylornithine
DGCR8	DiGeorge Syndrome Critical Region 8
DMEM	Dulbecco's modified Eagle's medium
DMT	dimethoxytrityl
DNB	dinitrobenzhydryl
DNP-SENS	dynamic nuclear polarization surface enhanced NMR spectroscopy
DNSA	dansylamide
dPAGE	denaturing polyacrylamide gel electrophoresis
ds	double stranded
EDTA	ethylenediaminetetraacetic acid
ENA	ethylene nucleic acid
EPR	electron paramagnetic resonance
ESC	Enhanced Stability Chemistry
EtOH	ethanol
FBS	fetal bovine serum

FLU	fluorescence units
FR	folate receptor
GalNAc	<i>N</i> -acetylgalactosamine
GAPDH	glyceraldehyde-3-phosphate dehydrogenase
HDR	homology directed repair
HITS-CLIP	high-throughput sequencing of RNA isolated by crosslinking immunoprecipitation
HPLC	high-performance liquid chromatography
HSA	human serum albumin
iCLIP	individual-resolution crosslinking immunoprecipitation
indels	insertions and deletions
IOR	Institute of oncology research
iPAR-CLIP	<i>in vivo</i> Photoactivatable Ribonucleoside Enhanced Crosslinking and Immunoprecipitation
iPrOH	isopropyl alcohol
i. v.	intravenous
LC-MS	liquid chromatography-mass spectrometry
LLOQ	lower limit of quantification
LMTK3	lemur tyrosine kinase 3
LNA	locked nucleic acid
LNP	lipid nanoparticle
MAS	magic-angle spinning
MeOH	methanol
miRISC	microRNA induced silencing complex
miRNAs	microRNA
MOE	2'- <i>O</i> -methoxyethyl
mRNA	messenger RNA
<i>N</i> -Ac	<i>N</i> -acetyl
<i>N</i> -bz	<i>N</i> -benzoyl
NHEJ	non-homologous end joining
<i>N</i> -iBu	<i>N</i> -isobutyryl
NMP	<i>N</i> -methyl-2-pyrrolidone
NMR	nuclear magnetic resonance

nt	nucleotide
NT2/ D1	NTERA-2 clone D1
NTC	no template control
ODN	oligodeoxynucleotide
ORN	oligoribonucleotide
PABPC1	polyadenylate-binding protein C1
PACT	interferon-induced protein kinase
PADS	phenylacetyl disulfide
PAGE	polyacrylamide gel electrophoresis
PAM	protospacer adjacent motif
PAR-CLIP	Photoactivatable Ribonucleoside Enhanced Crosslinking and Immunoprecipitation
PARN2-3	poly(A)-specific ribonuclease 2-3
PBS	phosphate-buffered saline
PBST	phosphate-buffered saline containing 0.05% Tween
PMO	phosphorodiamidate morpholinos
PMT	photomultiplier
PNA	peptide nucleic acid
PNK	polynucleotide kinase
PO	phosphodiester
PPMO	peptide-conjugated phosphorodiamidate morpholinos
pre-miRNA	precursor microRNA
pri-miRNA	primar microRNA
PS	phosphorothioate
PTS	polyamine transport system
RBP	RNA binding protein
RIG-I	retinoic-acid-inducible-gene-I
RISC	RNA induced silencing complex
RNA>p	RNA-2', 3'-cyclic phosphate
RNAi	RNA interference
RNase	ribonuclease
RP-HPLC	reversed-phase high-performance liquid chromatography
Rpm	rounds per minute

RT	reverse transcription
RT-qPCR	reverse transcription quantitative polymerase chain reaction
s. c.	subcutaneous
SATE	S-acyl-2-thioethyl-phosphotriester
(S)-cEt	(S)-constrained ethyl
sgRNA	single guide RNA
shRNA	short hairpin RNA
siLNA	small interfering locked nucleic acid
siRNA	small interfering RNA
SLC22A16	solute carrier 22A16
SMN	survival motor neuron
SNAP-tag	mutant of O ⁶ -alkylguanine-DNA alkyltransferase
snRNA	small nuclear RNA
SpCas9	<i>Streptococcus pyogenes</i> Cas9
ss	single stranded
SSO	splice switching oligonucleotide
STC	Standard Template Chemistry
TALEN	transcription activator-like effector nucleases
TBDMS	tert-butyldimethylsilyl
TEA	triethylamine
TFA	trifluoroacetic acid
THPTA	tris-hydroxypropyltriazolylmethylamine
TLC	thin-layer chromatography
TLR	toll-like receptors
T _m	melting temperature
TMP	trimethylphenyl
TNRC 6	trinucleotide repeat-containing gene 6
tracr RNA	trans-activating crisperRNA
TRBP	trans-activation response RNA binding protein
TUTase	terminal uridylyl transferase
UTR	untranslated region
VEGF	vascular endothelial growth factor
ZNA	zip nucleic acid

Abstract

Small interfering RNAs (siRNAs) are a promising class of RNA directed therapeutics. While exerting their gene-silencing activity similar to microRNAs (miRNAs) by recruiting the RNA induced silencing complex (RISC) toward messenger RNA (mRNA) targets, siRNAs are capable of inducing Argonaute-2 (AGO2) mediated target RNA cleavage. Despite the recent approval of patisiran, the first siRNA drug, systemic delivery remains a challenge and is currently limited to the liver. Whereas patisiran is dependent on lipid nanoparticle formulation (LNP), potent gene silencing has been achieved through naked administration of *N*-acetylgalactosamine (GalNAc) conjugated siRNAs. However, LNP-independent delivery requires the use of fully chemically modified siRNAs, which have raised concerns with respect to the formation of potentially toxic metabolites. Therefore, the goal of this work was to investigate alternative siRNA scaffolds which do not require a complex mixture of non-natural building blocks for systemic delivery.

In the first approach, we investigated the use of fully phosphorothioate (PS) modified siRNAs. Full PS modification is commonly used in the design of single stranded antisense oligonucleotides (ASOs) and was shown to increase their binding to serum proteins. However, application of PS modifications to siRNA therapeutics has been restricted to the terminal positions due to conflicting reports on the activity and toxicity of full PS siRNAs. Our group recently reported the development of stereochemically biased PS siRNAs and demonstrated a higher activity of *Rp*- than *Sp*-enriched PS siRNAs in mammalian cells. Building on these results, we scaled up our synthesis protocol for PS siRNAs in order to characterize the biodistribution profile and the *in vivo* activity of a PS siRNA directed against the oncogene *Lin28B*. In addition, we investigated the albumin-binding capability and metabolic stability of various siRNA formats in biological fluids.

In a second project, we adopted the previously described convertible nucleoside approach to introduce various chemical modifications into the major groove of siRNAs. We then evaluated polyamine conjugation as a means to increase the cellular uptake and nuclease stability of siRNAs under cell culture conditions.

In a third project, we focused on the development of a new methodology to uncover the targetome of individual miRNAs. For this purpose, we synthesized 2', 3'-cyclic phosphate terminated miRNA mimics (miRNA>p) which can be ligated to their RNA targets through the action of both an endogenous and an exogenously added RNA>p ligase.

In addition, we contributed to several projects in the field of CRISPR-Cas genome editing and the development of a method to characterize surface-bound RNAs in a microarray-like setup.

Zusammenfassung

Small interfering RNAs (siRNAs) sind eine vielversprechende Klasse RNA-basierter Arzneistoffe. SiRNAs sind, ähnlich wie microRNAs (miRNAs), in der Lage den RNA-induzierten-Silencing-Komplex (RISC) zu Ihren RNA Zielstrukturen zu rekrutieren. SiRNAs sind jedoch im Unterschied zu miRNAs vollständig komplementär zur RNA Zielstruktur und können die Spaltung der RNA durch Argonaute-2 (AGO2) induzieren. Trotz der Zulassung von Patisiran, dem ersten siRNA Arzneistoff, ist die systemische Verabreichung von siRNAs eine Herausforderung und die Anwendung ist derzeit auf Zielstrukturen in der Leber beschränkt. Während Patisiran als Lipid-Nanopartikel (LNP) verabreicht werden muss, konnte eine effiziente Gen-Stillegung ohne LNPs durch die Anwendung von *N*-Acetylgalaktosamin (GalNAc)-konjugierten siRNAs erreicht werden. Die LNP-freie Injektion erfordert jedoch den Einsatz vollständig modifizierter siRNAs. Dies hat zu Bedenken im Hinblick auf die Bildung potenziell toxischer Metaboliten geführt. Daher war das Ziel dieser Arbeit die Entwicklung alternativer siRNA Varianten, für die keine Kombination komplexer Bausteine notwendig ist.

Im ersten Projekt haben wir den Einsatz vollständig Phosphorothioat (PS)-modifizierter siRNAs untersucht. Vollständige PS Modifizierung wird bereits in der Entwicklung einzelsträngiger antisense Oligonukleotide (ASOs) genutzt, um eine effiziente Bindung an Serumproteine zu erreichen. Die Anwendung im Bereich der siRNAs ist jedoch aufgrund widersprüchlicher Berichte zur Aktivität und Toxizität auf die terminalen Positionen beschränkt. Unsere Gruppe konnte jedoch kürzlich eine höhere Aktivität von PS siRNAs mit einer erhöhten Zahl an *R_p* Stereozentren gegenüber mehrheitlich *S_p*-konfigurierten Varianten in Zellkultur nachweisen. Darauf aufbauend haben wir unser Protokoll für die Synthese von PS siRNAs angepasst, um die Gewebeverteilung und die *in vivo* Aktivität einer PS siRNA gegen das Onkogen Lin28B zu untersuchen. Zudem haben wir die Albumin-Bindung und die metabolische Stabilität verschiedener siRNA Varianten in unterschiedlichen biologischen Flüssigkeiten untersucht.

In einem zweiten Projekt haben wir ein konvertierbares Nukleosid eingesetzt, um verschiedene Modifikationen in die grosse Furche von siRNAs einzubringen. Dann haben wir die Konjugation an Polyamine zur besseren zellulären Aufnahme sowie erhöhten Nukleasestabilität untersucht.

Im dritten Projekt haben wir uns auf die Entwicklung einer neuen Methode zur Identifizierung der Zielstrukturen individueller miRNAs konzentriert. Zu diesem Zweck haben wir miRNA-Analoga mit einem terminalen 2', 3' zyklischen Phosphat (RNA>p) synthetisiert. Diese haben wir dann zur Ligation an die RNA Zielstrukturen mittels endogener und exogener RNA>p-Ligasen verwendet. Darüber hinaus waren wir an verschiedenen Projekten auf dem Gebiet der CRISPR-Cas basierten Genomeditierung sowie an der Entwicklung einer Methode zur Charakterisierung oberflächengebundener RNA beteiligt.

1 Introduction

The field of nucleic acid therapeutics emerged in 1978 with the observation that an oligonucleotide that was antisense to *Rous sarcoma virus* 35S RNA could be used to inhibit viral replication[1, 2]. To date, we can differentiate several classes of RNA-targeted therapeutics which operate via a diverse set of mechanisms in different compartments of the cell. In the following, the currently most advanced RNA-targeting platforms will be introduced together with the chemistry that is used to construct them.

1.1 Chemistry of oligonucleotides

The properties and functions of oligonucleotides depend on the combination of the nucleotide sequence, the structural format and their chemical architecture[3-5]. Potential sites for chemical modification are the nucleic acid backbone, the nucleobase, the sugar moiety and the 5'- and 3'-termini (Figure 1.1). We have recently described several aspects of oligonucleotide chemistry with respect to their roles as therapeutics or tools for chemical biology[6].

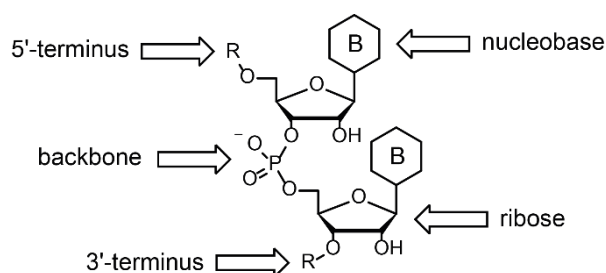


Figure 1.1. Potential sites for chemical modifications

1.1.1 Modifications of the phosphodiester backbone

One of the first and still most prominent chemical modifications that was introduced into the oligonucleotide field was the substitution of one of the non-bridging oxygens of the phosphodiester (PO) linkage by sulphur[7, 8]. The resulting phosphorothioate (PS) linkage provides a remarkable increase in nuclease resistance[3, 7, 9, 10] and, although often under debate for its potential contribution to mechanism-independent side-effects[11-14], remains widely used or even considered “the most useful modification to date”[4]. A reason for its widespread use, particularly in single stranded therapeutics, is the ability of PS oligonucleotides to bind to a wide range of proteins, including serum and cellular surface proteins, which enables a broad biodistribution and facilitates cell uptake [15-18]. Another strength of the PS backbone modification is that it supports RNase H as well as RNA interference (RNAi) dependent mechanisms[4, 8]. The general utility of this modification is reflected by its use in the FDA-approved drugs mipomersen[19], nusinersen[20], inotersen[21]

as well as most small interfering RNAs (siRNAs) and antisense oligonucleotides (ASOs) that are currently in clinical trials[8]. A drawback of the PS modification is a general loss in binding affinity to complementary oligonucleotides, which is usually compensated by the use of additional modifications, especially at the 2'-hydroxyl position[7, 9, 22]. In nature, PS linkages are found in bacterial DNA as part of an epigenetic mechanism to protect host DNA during degradation of invader genomic material[23].

The substitution of only one of the non-bridging oxygens converts a prochiral PO linkage into a new stereocenter[24]. Unless chiral auxiliary groups are used to conduct the oligosynthesis in a stereospecific fashion[25-32], *Rp* and *Sp* linkages occur in an approximately 1:1 ratio[9, 33] (Figure 1.2). Mechanistic studies revealed that, when following the commonly used phosphoramidite approach for solid-phase synthesis, the major determinant of PS stereochemistry is the coupling reaction between the support-bound oligonucleotide chain and the incoming phosphoramidite[9, 34, 35]. At least in the case of oligodeoxynucleotides (ODNs), subsequent oxidation of the resulting phosphite triester linkage (P(III) linkage) with a sulphur transfer reagent occurs rapidly and proceeds with stereoretention[36, 37].

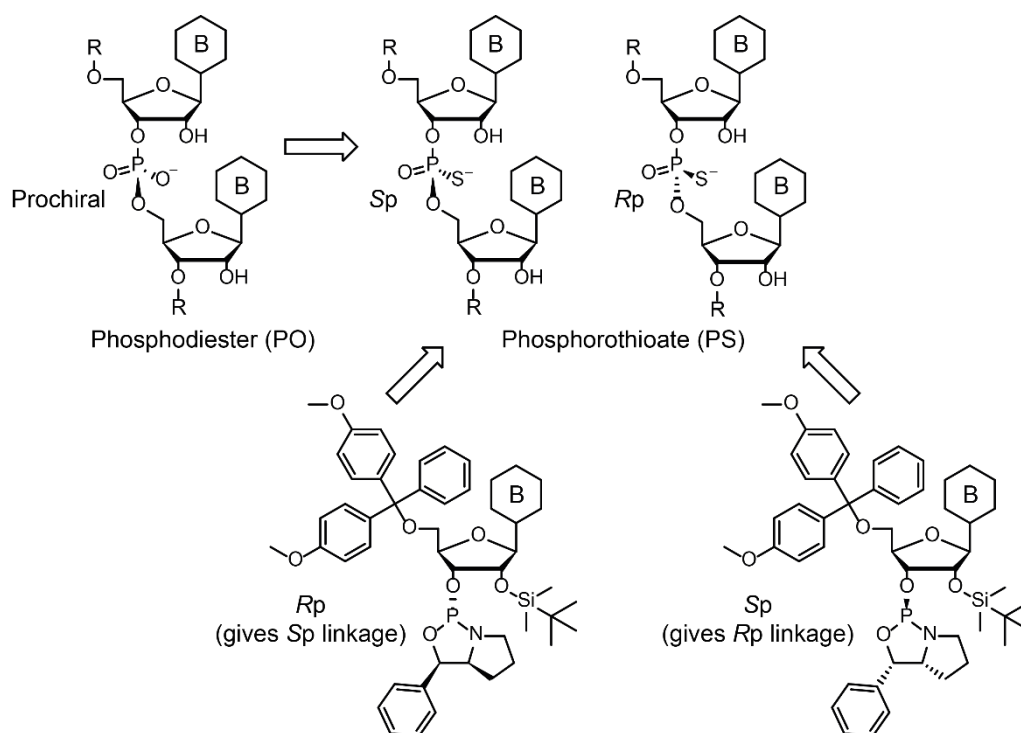


Figure 1.2. Modification of a PO linkage with sulphur yields 2 diastereoisomers (top) unless stereopure phosphoramidites with chiral auxiliary groups are used (bottom)

Our group has previously shown that the choice of activator during chemical synthesis of oligoribonucleotides (ORNs) influences the stereochemistry at the PS linkage, introducing a distribution bias of roughly 2:1 for either *Rp* or *Sp* stereochemistry[9]. Although geometrically similar to PO oligonucleotides[22, 38, 39], substitution of oxygen with the larger sulphur[40] atom changes the electronic properties of the linkage[41, 42]. Whereas the electron density is

equally distributed between the two non-bridging oxygens of a PO linkage, it is shifted towards either oxygen or sulphur in a PS backbone. The electron density distribution in a PS linkage depends on the chemical environment, particularly on the presence of different hard or soft cations[42, 43]. Counterintuitively, the negative charge appears to be predominantly centred on the sulphur atom instead of the more electronegative oxygen[41-44]. The observation that PS linkages exhibit a generally increased resistance towards nuclease mediated cleavage can be superficially explained by the notion that a PS oligonucleotide is not the natural target for vertebrate nucleases. On the molecular level, major contributors to the increased resistance are PS-induced structural perturbations of the nuclease active site[45] and a reduced affinity of Mg^{2+} towards sulphur[46]. Replacement of Mg^{2+} by the more thiophilic Mn^{2+} has been shown to restore cleavage of PS linkages through the endonuclease domain of Ago2[47, 48]. Moreover, susceptibility to nuclease mediated cleavage is dependent on the PS stereochemistry, with Sp linkages showing a superior stability towards most nucleases compared to Rp, at least in ODNs[49, 50] and 2'-O-methoxyethyl (MOE) oligonucleotides[30]. However, in the case of full PS siRNAs, a bias towards Rp stereochemistry seems to be beneficial not only for cellular activity but also for nuclease resistance[9]. This is possibly due to an increased thermal stability which is thought to limit the so-called breathing of the duplex and thereby protecting against nuclease attack[51]. With respect to gapmer ASOs, an optimized stereochemical composition has recently been suggested, comprising a 3'-SpSpRp-5' motif for optimal RNase H activation[30]. Overall it can be assumed that the stereochemistry at each position needs to be optimized individually for different classes of therapeutics or potentially even for each individual candidate molecule to modulate activity, tissue specific metabolic stability, lipophilicity[30] and protein binding[7]. This might also be a means to specifically tailor the biodistribution profile.

The biodistribution profile of 2'-MOE and DNA ASOs has been shown to primarily depend on the PS backbone which mediates binding to serum proteins that hold the oligonucleotides in circulation and prevent rapid renal clearance[15, 16, 18]. Efficient protein binding of 2'-MOE PS ASOs has been shown to be length-dependent, with an increase of the unbound ASO fraction >10% when the ASO metabolite was shorter than 10 nucleotides (nt) [52-54]. Furthermore, PS backbone chemistry has been linked to free uptake in certain cell lines[55-59]. Free uptake has been further classified in productive and unproductive pathways which lead to either cytosolic delivery or lysosomal accumulation[58, 60]. A number of cell lines have been identified which show productive uptake of PS ASOs[61]. Although a variety of PS ASO binding proteins have been catalogued[16, 62, 63] and a role of lysobisphosphatidic acid in endosomal trafficking[64] as well as the involvement of certain cell surface receptors in ASO uptake has been demonstrated[65], the exact mechanisms underlying productive uptake remain elusive. However, apart from the positive aspects such as prolonged circulation and

increased tissue accumulation, unspecific protein binding has been identified as a potential source of toxicity[12, 66-70] and mechanism-independent therapeutic effects[71]. Therefore, the development of PS oligonucleotides as drugs requires special care to identify sequences which can be safely applied in humans. However, as more and more RNA-targeted therapeutics enter the clinic, it becomes clear that this is not only true for PS oligonucleotides but also for all other classes of nucleic acid therapeutics and corresponding screening efforts have been vastly increased[72, 73].

In addition, a single PS linkage can be further derivatized through reaction of the nucleophilic thiol with haloacetyls such as 4-azidophenacyl bromide to generate photoactivatable RNA probes for mapping RNA-protein interactions[74-77]. A difficulty when tethering functional groups to the RNA backbone is an elimination of the label through an attack of the neighbouring 2'-hydroxyl group[74, 78]. This side-reaction can be avoided through the replacement of the 2'-hydroxyl group by a single 2'-methoxy (2'-OMe) or a deoxyribose moiety[74].

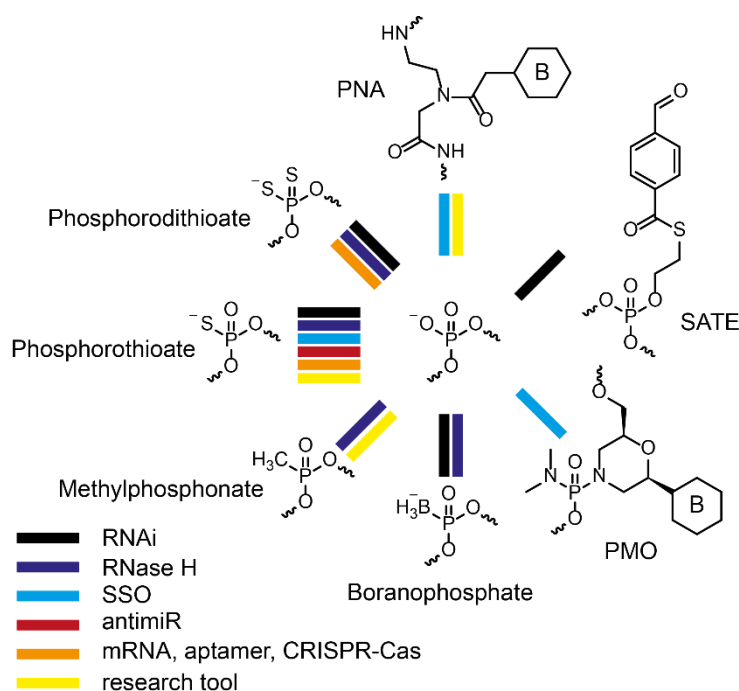


Figure 1.3. Selected backbone modifications and their primary applications

Other backbone modifications that have been designed to improve the pharmacokinetic properties of oligonucleotides include phosphorodithioates[79-81], methylphosphonates[82], boranophosphates[83-85] and S-acyl-2-thioethyl-phosphotriesters (SATE)[86] (Figure 1.3). Phosphorodithioates are particularly interesting for future therapeutics as they have not only shown good activity when used in siRNAs[86] but also convert the chiral phosphorothioate back to a prochiral center. This might be of particular relevance for future approval by the various drug admission authorities. The use of SATE backbone chemistry has triggered initial excitement as it offers a new possibility to reversibly mask the phosphodiester charge and

creates a handle for the attachment of additional functional moieties[86-88], but is not widely used. A disadvantage is the added complexity to already complex macromolecules, which is a concern both in terms of production-scale chemistry and potential metabolites. Furthermore, the negatively charged sugar-phosphate backbone can be replaced entirely by amide bonds in peptide nucleic acids (PNA)[89, 90] or phosphorodiamidate morpholinos[91] (PMO or PPMO when conjugated to a peptide). The non-charged PMOs have demonstrated a good safety profile[92, 93] but do not bind sufficiently to proteins and therefore showed unfavourable pharmacokinetics[4]. PMO chemistry has been used in the design of the exon-skipping oligonucleotide eteplirsen which has recently received conditional FDA approval as the results of a phase III study were not conclusive and have come under scrutiny[94-96]. Similar results for Sarepta's new exon-skipping DMD drug golodirsen recently prompted the FDA to reject accelerated approval, raising concerns on renal toxicity and infusion related infections[97]. Neutrally charged PNAs bind their targets with high affinity but clinical development has been complicated by sequence-dependent solubility issues and rapid excretion in the urine[98-103]. These challenges have been addressed through conjugation to short peptide stretches[104-106].

Although initially intended to benefit therapeutic strategies, some backbone modifications have been developed into RNA chemical biology tools to identify specific protein-RNA interactions (methylphosphonate)[82] or functional RNA domains (PNA interference mapping)[107]. Currently PNAs also find growing applications as probes in PNA hybridization assays to detect oligonucleotides in tissue biopsies[108-113].

1.1.2 Modifications of the nucleobase

The nucleobase offers several potential sites for chemical modification which are dependent on the specific base (Figure 1.4). Key considerations when introducing modifications on the nucleobase are the spatial orientation of the newly added moiety and whether the modification affects the ability for base pairing. Nucleobase modifications can either point towards the major or minor groove, a feature which has generally been shown to largely impact the properties of the modified oligonucleotide[114-116].

The only nucleobase modification that is currently used in the clinic is 5-methylcytidine[4]. 5-methylcytidine has been used instead of the canonical, unmethylated form in the design of the FDA approved drugs mipomersen, nusinersen and inotersen[8]. 5-methylation of cytidine has been shown to result in an increased hybridization affinity[117] along with reduced immunostimulatory effects[118, 119]. 5-methylcytosine has also been found as a component of natural DNA, where it is thought to be involved in the epigenetic regulation of gene expression[120].

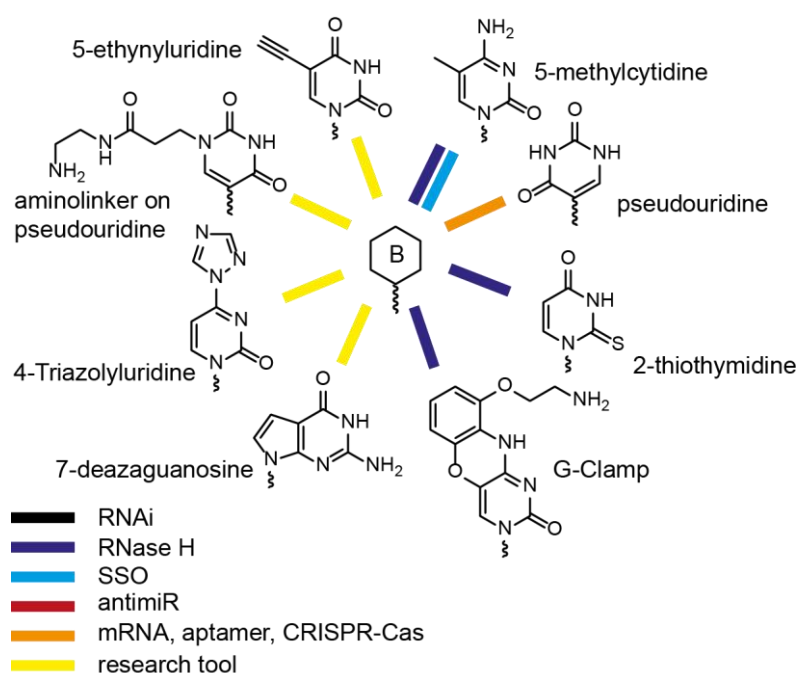


Figure 1.4. Selected nucleobase modifications and their primary applications

Another cytosine-analogue that supports RNase H activity is the so-called G-clamp in which the nucleobase is replaced by an aminopropyl-substituted phenoxazine or guanidium derivatives thereof. This resulted in an unprecedented increase of 13-18°C in the melting temperature of DNA-DNA and DNA-RNA duplexes[121-125].

In the field of mRNA therapeutics, substitution of uridine by the naturally occurring pseudouridine has been used to increase translation efficiency and nuclease stability. This has been related to changes in the secondary structure of modified mRNAs[3, 126-128]. In addition, 2-thiothymidine has been applied to the design of ASOs but is not widely used[129].

In research, nucleobase-modification is often achieved through a copper catalyzed 1,3-dipolar azide-alkyne cycloaddition (CuAAC)[115, 130, 131] or strain-promoted copper-free click chemistry[132, 133]. One example from our group was the introduction of spermine in the 5-position of uridine through a click reaction between 5-ethynyl-2'-O-methyluridine and spermine-azide[115]. Conjugation via CuAAC leads to the formation of a rigid 1, 2, 3-triazole linker. More flexible linkers have been used for the introduction of trivalent GalNAc moieties via amide bond formation[134]. An elegant methodology for the introduction of nucleobase modifications is the convertible nucleoside approach, in which a leaving group containing building block is incorporated during solid-phase oligosynthesis that is afterwards replaced through a nucleophilic attack of the chemical modality of interest[135-142]. So far this method has been limited to the use of thiol and amino nucleophiles as well as to the exocyclic amino positions of uridine, adenosine and guanosine.

7-deazaguanosine is an example of a nucleobase modification that disturbs Hoogsteen base-pairing and can therefore be used as a control for studies related to G-quadruplex formation[143, 144].

1.1.3 Sugar modifications

The most common site for chemical modification of RNA-targeted therapeutics is the ribose 2'-hydroxyl position (Figure 1.5). This position plays a key role for nuclease stability, as ribonucleases (RNase) typically catalyse cleavage of the phosphodiester linkage through a nucleophilic attack of the neighbouring 2'-hydroxyl group[145, 146]. A common strategy to enhance metabolic stability of therapeutic RNAs is hence the replacement of the 2'-hydroxyl group by 2'-Fluoro (2'-F), 2'-OMe or 2'-MOE moieties[3, 4, 147-149]. In addition to simply masking the 2'-hydroxyl group, 2'-modifications influence the sugar pucker and thereby the overall geometry of the oligonucleotide[150-152]. 2'-F, 2'-OMe as well as 2'-MOE all favour the C3'-endo conformation typically found in A-form duplexes[152-155]. In contrast, 2'-deoxyribose preferably adopts a C2'-endo conformation leading to a B-form duplex. Whereas A-form duplexes have a narrow and deep major and a wide and shallow minor groove, B-form duplexes have a wide and deep major and a narrow and deep minor groove[156, 157]. Although 2'-F as well as 2'-OMe substituents both favour the formation of A-form duplexes, 2'-F slightly overwinds (more stacking) and 2'-OMe slightly underwinds (less stacking) the double-helix[3]. Since major and minor grooves are typical sites for protein and ligand interactions[158, 159], it is conceivable that changes in the duplex geometry also affect biodistribution and immunostimulation through a distinct subset of binding partners. Oligonucleotides which adopt a C3'-endo conformation also show a higher binding affinity for RNA and DNA targets[147, 152].

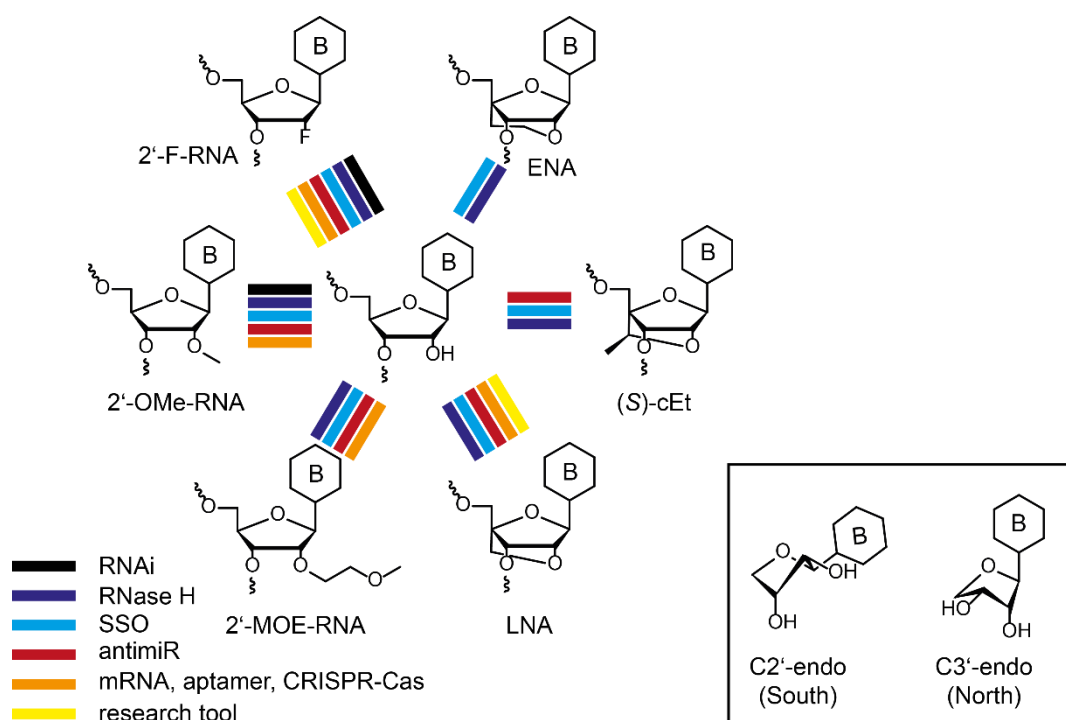


Figure 1.5. Selected ribose modifications and their primary applications

This principle was ultimately exploited through the introduction of synthetically demanding constrained nucleosides such as locked nucleic acids[160-162] (LNA, also known as 2',4'-bridged nucleic acid[163, 164]), (S)-constrained ethyl ((S)-cEt)[165, 166], and ethylene nucleic acids (ENA)[167-169] which are chemically locked in a C3'-endo conformation. LNA and cEt, in which the 2'-oxygen is linked to the 4'-carbon, are currently used in the development of anti-miRNAs[170, 171] and RNase H activating ASOs[166, 172]. LNA and cEt, its methylated analogue, show increased hybridisation affinities of 4°C to 8°C per nucleoside when binding RNA[161-163] and exhibit improved nuclease stability[173, 174]. This translated into ASOs which were 5-10 fold more potent than 2'-MOE oligonucleotides *in vivo*[4]. At least in the case of LNAs this was accompanied by hepatic and renal toxicities as well as injection site inflammation[170-172, 175].

The currently most widely used sugar modification for single stranded therapeutics is the 2'-MOE moiety[4, 149]. 2'-MOE groups greatly improve nuclease stability, reduce immune stimulation and enhance the target binding affinity[4, 152]. The 2'-MOE moiety winds along the minor groove and leads to the formation of a distinct hydration pattern around the 3'-phosphate, thereby increasing the steric bulk and shielding the linkage against nuclease attack[176]. The increased hybridisation affinity of 2'-MOE oligonucleotides has been explained by a conformational preorganization for binding[176]. Because full 2'-MOE oligonucleotides are not capable of eliciting RNase H mediated effects, a gapmer ASO design was developed in which a central DNA region is flanked by 2'-MOE wings[165]. Full 2'-MOE modification has been

used in the design of the recently approved splice switching oligonucleotide (SSO) nusinersen[20].

2'-OMe and 2'-F substitutions were among the earliest oligonucleotide modifications and exhibited improved nuclease resistance and target binding affinity compared to RNA[177-180]. Nevertheless, they were shown to be less useful for antisense therapeutics than 2'-MOE because effects on nuclease stability were less pronounced[148, 181]. However, as 2'-MOE oligonucleotides are not compatible with the RNA interference (RNAi) mechanism, 2'-OMe and 2'-F modifications have found a renaissance for applications in siRNAs, but careful positioning of these modifications is required[182-184]. Most siRNAs that have advanced in clinical trials contain 2'-OMe modifications[4, 8, 185]. All siRNAs of the Alnylam development pipeline are additionally modified with 2'-F, although the 2'-F content has been steadily reduced in favour of 2'-OMe over the development cycles[183]. Improvements in nuclease stability for 2'-OMe are decreased compared to 2'-MOE but larger than for 2'-F[148, 181, 183]. In addition, 2'-OMe has not raised toxicity concerns such as the use of 2'-F nucleosides[4, 69, 186-188]. Therefore, newly developed siRNAs are typically screened for positions in which 2'-OMe substituents are tolerated and only at sites that do not allow 2'-OMe moieties, it is replaced by the sterically less demanding 2'-F[183]. However, additional modification patterns such as LNA-modified pre-sliced siRNA (siLNAs)[189, 190] as well as siRNAs which are composed of glycol-phosphorothioate units[191] have been investigated.

1.1.4 5'- and 3'-terminal modifications

Functionalisation of 5'- and 3'-terminal positions has been used for both, therapeutic and analytical purposes (Figure 1.6). Synthetic oligonucleotides, unlike *in vitro* transcribed RNAs, have free 5'- and 3'-OH termini, unless specifically modified. However, a 5'-phosphate (5'-P) group is required for RISC loading of siRNA guide strands and miRNA mimics[192-196]. Whereas unmodified siRNAs are readily phosphorylated by ubiquitous CLP 1 kinase[194, 196] and thus phosphorylation is not a rate-limiting step *in vivo*[197], heavily modified siRNAs suffer from a poor phosphorylation efficiency[112, 198, 199]. Although chemical introduction of natural 5'-P could theoretically alleviate this problem, rapid phosphatase-mediated dephosphorylation would lead to inactivation of modified siRNAs. Therefore, a number of phosphatase resistant phosphate-analogues has been developed[112, 198, 199]. So far, 5'-E-vinylphosphonate (5'-E-VP) emerged as the phosphate cap of choice and has been used in the context of double stranded (ds) [112, 198, 199] as well as single stranded (ss) siRNAs[200, 201]. 5'-E-VP has been shown to improve activity of heavily modified siRNAs *in vivo* and to enhance tissue deposition of GalNAc[199, 202] and lipid siRNA conjugates[112]. Enhanced biodistribution has been correlated with an additional increase in stability against nuclease mediated degradation[112]. 5'-Z-VP, its other diastereoisomer, showed a decreased activity

because of unfavourable positioning of the 5'-phosphonate within the RISC binding pocket[201, 203]. In addition, 5'-PS and 5'-methylphosphonate were shown to increase nuclease stability of ss siRNA while maintaining activity, although effects were less pronounced than for 5'-E-VP[201]. 5'-blocking groups such as 5'-OMe can be used to prevent undesired RISC loading and activity of the passenger strand[194, 204].

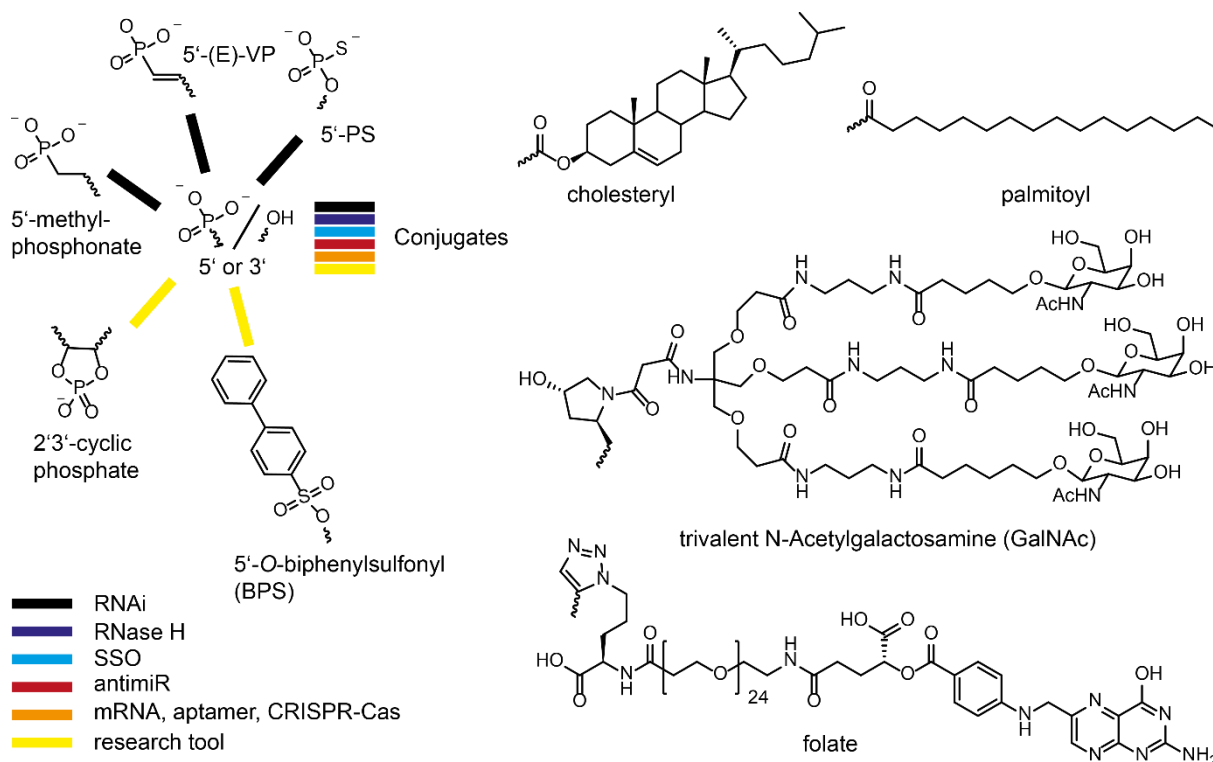


Figure 1.6. Selected 5'- and 3'-terminal modifications and conjugates

On the other hand, natural 5'-phosphate groups can be used in ligation approaches for the synthesis of long, modified RNAs. One way to chemically introduce a 5'-phosphate during solid-phase oligosynthesis is the use of a dinitrobenzhydryl (DNB)-phosphoramidite that has been developed in our group[205]. An advantage of the DNB-phosphoramidite is its compatibility with conventional reversed-phase high-performance liquid chromatography (RP-HPLC) purification. After isolation of the DNB-capped oligonucleotide, the 5'-phosphate group can be unmasked under mild UV irradiation (Figure 1.7).

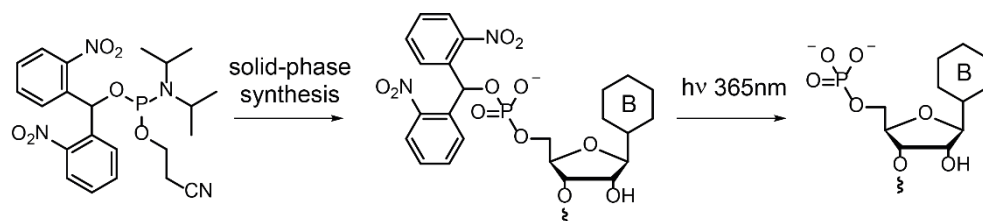


Figure 1.7. Use of the photocleavable DNB-phosphoramidite for the synthesis of 5'-phosphorylated RNA

Furthermore, 5'-bisphenylsulfonyl (BPS) capped DNA has been used in conjunction with 3'-PS terminated DNA for template dependent chemical ligation reactions in order to alleviate the need for enzymatic reverse transcription (RT) of an RNA into a DNA template prior to oligonucleotide quantification via quantitative polymerase chain reaction (qPCR) [206, 207]. Whereas 2'-OMe and 2'-F modified siRNAs have been successfully converted into DNA enzymatically[183, 208], 2'-MOE oligonucleotides are not amenable to reverse transcription and therefore benefit from a chemical ligation approach[206].

Moreover, 2', 3'-cyclic phosphate (cycP) terminated RNAs (RNA>p) are of particular biological importance and their widespread roles in small nuclear RNA (snRNA) 3'-uridylation[209], tRNA splicing[210-213] and as intermediates in RNase mediated degradation[145] become increasingly recognized[6]. In collaboration with the group of Martin Jinek, we have used A6>p as a tool to establish cyclic oligoadenylates as a novel type of second messengers in type III CRISPR Cas systems[214, 215]. RNA>p have also been used to capture 5'-hydroxyl terminated RNAs in cells by using their potential to undergo RtcB mediated ligation[216], a property that was also exploited in our investigation on the use of miRNA>p mimics for the identification of miRNA target sites in CLIP-type (CrossLinking and ImmunoPrecipitation) protocols. RNA>p are enzymatically accessible through the use of *E. coli* MazF toxin[217, 218]. Synthetically, RNA>p are accessible via solid phase synthesis on a dedicated solid support[219]. 2', 3'-cycP diribonucleosides and 2', 3'-cyclic phosphorothioate oligonucleotides have been prepared in solution[220, 221].

In addition to the various phosphate analogues, the terminal positions are a classical site for the conjugation to targeting groups such as trivalent GalNAc for delivery to hepatocytes via targeting the asialoglycoprotein receptor (ASGPR)[222]. Other currently explored delivery strategies are conjugation to folate[223, 224], peptides[225, 226] as well as various hydrophobic ligands such as cholesterol and fatty acid moieties[113, 227-229] (Figure 1.6). General strategies for conjugate-mediated delivery of RNA-targeted therapeutics have been reviewed by R. Juliano[230] and lipid conjugates in particular have been reviewed by M. Osborn and A. Khvorova[231]. Interestingly, fatty acid conjugation to gapmer ASOs has been recently shown to result in increased activity in the skeletal muscle after subcutaneous (s.c.) injection. Activity was dependent on fatty acid chain length and albumin binding, but appeared to be independent of the degree of saturation. The most promising strategy was palmitoyl conjugation[232]. In addition, docosahexanoic acid conjugation has been used to achieve a longer retention of siRNAs after direct injection into the brain[113].

1.2 Classes of nucleic acid therapeutics

A general classification can be made based on whether oligonucleotide functions via a so-called “occupancy-only” mechanism or through “occupancy-mediated degradation” as well as on structural aspects[4]. In the following, the currently most advanced nucleic acid based platforms will be introduced.

1.2.1 Splice switching oligonucleotides

SSOs are a class of oligonucleotide therapeutics that function via an “occupancy-only” mechanism, meaning that in principle they do not mediate enzymatic RNA degradation such as RNase H dependent ASOs or siRNAs[4] (Figure 1.8). Nevertheless, they interfere with the RNA splicing machinery by binding to certain splice sites or to regions which are otherwise involved in the regulation of splicing. The principle behind the design of SSOs is that binding to a particular splice site and thereby sterically blocking its accessibility to the splicing machinery, can modulate splicing in cases where normal splicing is disrupted. Hence, only little restrictions in terms of the chemical architecture apply. Therefore, a large variety of affinity and metabolic stability enhancing modifications can be used in the design of SSOs, albeit for clinical development the chemical space has been mostly limited to 2'-MOE, PMO, LNA and (S)-cEt building blocks, usually combined with PS backbone chemistry[3, 4, 8]. Long DNA stretches should be avoided to prevent RNase H mediated RNA degradation. The single stranded nature of these modalities in combination with PS backbone chemistry results in amphiphilic molecules, in which the hydrophobic nucleobases are exposed[3, 4]. Hence, single stranded PS oligonucleotides show a sequence-dependent protein binding[52] which is not observed for duplex RNAs in which the nucleobases face the inside of the double helix[3, 4]. Two SSOs, nusinersen[20] and eteplirsen[95], have been recently approved by the FDA, although FDA-approval of eteplirsen (Exondys 51, Sarepta therapeutics) was only conditional and EMA approval was not granted due to unclear results in a phase III clinical trial[92, 94-96]. Both drugs have in common that they have been developed for rare diseases. Eteplirsen is a non-charged PMO targeting exon 51 of dystrophin pre-mRNA to induce exon skipping and thereby restore functional dystrophin generation in a subset of Duchenne muscular dystrophy (DMD) patients with a particular frameshift mutation (approximately 13% of DMD patients)[95, 233, 234]. Protein binding of eteplirsen is relatively low[235] (6.1-16.5%)[236], which is consistent with a generally low protein binding of PMOs. Eteplirsen is given weekly by intravenous (i. v.) infusion at 30 mg/ kg[236].

On the other hand, nusinersen (Spinraza, Ionis and Biogen) has received FDA and EMA approval for the treatment of patients suffering from spinal muscular atrophy with a mutation in the *SMN1* gene, encoding for survival motor neuron (SMN) protein[20]. Loss of *SMN1* can

be partially compensated by low amounts of SMN protein produced from the homologous *SMN2* gene but only a fraction of *SMN2*-transcripts (approximately 10%) leads to expression of functional SMN protein due to dominant exon 7 skipping, leading to a truncated protein which is rapidly degraded[4, 237]. Nusinersen is a full 2'-MOE PS oligonucleotide targeting an inhibitory cis-element in the *SMN2* gene to promote exon 7 inclusion in order to increase total levels of functional SMN protein[20]. It is administered at a dose of 12 mg every 4 months by intrathecal injection to the central nervous system (CNS)[4].

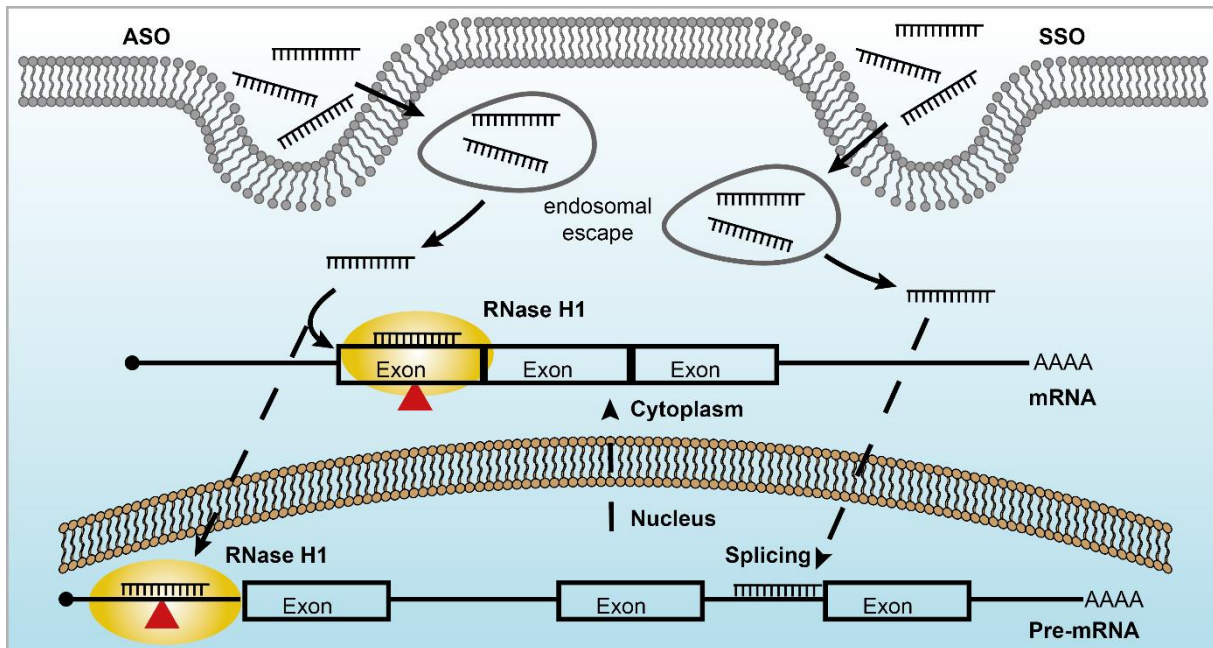


Figure 1.8. Mechanisms of ASOs and SSOs

1.2.2 RNase H dependent antisense oligonucleotides

RNase H dependent ASOs are a means to downregulate disease-causing proteins mainly through enzymatic degradation of the pre-mRNA inside the nucleus. RNase H, particularly RNase H1, is a non-sequence-specific endoribonuclease which cleaves the RNA strand of a DNA/ RNA duplex and is predominantly located inside the nucleus, although it is also present in the cytosol[238] (Figure 1.8). The first generation of this type of ASOs were simple DNA-PS oligonucleotides and biodistribution was solely dependent on the PS backbone chemistry. In order to increase therapeutic efficacy through a combination of enhanced metabolic stability and RNA binding affinity, a so-called gapmer design was developed in which a central DNA gap, which is required to elicit RNase H1 mediated RNA cleavage, is flanked by 2'-MOE wings[3, 4, 152]. As described in 1.1.3, 2'-MOE modification leads to increased hybridization affinity[152, 176] and prolonged tissue half-lives of 2-4 weeks[18, 54, 239]. Mipomersen (Kynamro), the first FDA-approved ASO (01/ 2013) was developed by ISIS pharmaceuticals (now IONIS) in collaboration with Genzyme and was designed in a gapmer 2'-MOE-DNA-PS format in order to target apolipoprotein B-100 (Apo B-100) pre-mRNA in the liver for the

treatment of patients with the genetic disease homozygous familial hypercholesterolemia[19, 240]. In addition, all cytosine bases in the DNA gap as well as in the 2'-MOE wings have been replaced by 5-methylcytosine. Although mipomersen was not commercially successful, it was an important milestone in the development of RNA-targeted therapeutics[8]. 2'-MOE-PS gapmer ASOs are highly bound to plasma proteins (>85%) and accumulate mostly in the liver[15, 18, 52, 239]. The rather high dose of 200 mg mipomersen per week was accompanied by hepatotoxicity and inflammatory reactions at the injection site[4, 8]. A third generation of liver-directed ASOs are currently developed as (S)-cEt gapmer-GalNAc conjugates. Second generation 2'-MOE gapmer GalNAc conjugates were 6-10-fold more potent and third generation (S)-cEt-GalNAc gapmers were ~60-fold more potent than the unconjugated 2'-MOE parent molecules[241]. The increase in potency has been attributed to a productive receptor-mediated uptake from the extracellular matrix into hepatocytes[242].

1.2.3 AntimiRs, miRNA mimics and the miRNA interference pathway

The first miRNA was discovered in 1993, when it was noticed that a short RNA produced from the *lin-4* gene in *Caenorhabditis elegans* (*C. elegans*) was able to post-transcriptionally downregulate levels of *lin-14* mRNA[243-245]. Although initially thought to be limited to nematodes, it quickly became clear that post-transcriptional gene regulation by short non-coding RNAs was a widespread phenomenon across diverse animal phyla[246, 247] and plants[248-251]. Mature microRNAs (miRNAs) are short ds non-coding RNA molecules, which are approximately 22 nt in length[252, 253]. MiRNAs are usually transcribed as primary miRNAs (pri-miRNAs) by RNA polymerase II and fold into a stem-loop structure which is flanked by single stranded regions[254-256]. After transcription, pri-miRNAs associate with the nuclear microprocessor complex, consisting of the RNA binding proteins DiGeorge Syndrome Critical Region 8 (DGCR8, dimeric) and Drosha (Figure 1.9). Upon binding, DGCR8 orients the RNase III domain of Drosha in such a way, that an approximately 70 nt long hairpin, called precursor-miRNA (pre-miRNA) is released[257, 258]. 5'-P and the two-nucleotide 3'-overhang (3'-OH) that can be found in pre-miRNAs are characteristic of RNase III processing and are recognized by the nuclear shuttle protein Exportin-5. After association of Exportin 5 with Ran-GTP, pre-miRNAs are exported into the cytoplasm[259-261] and further processed by the RNase III protein Dicer[262-265]. Dicer, in conjunction with the dsRNA binding proteins trans-activation response RNA binding protein (TRBP)[266-268] and interferon-induced protein kinase (PACT)[269-271], interacts with the 5'- and 3'-termini as well as the loop region of the pre-miRNA and cuts off the loop, yielding an imperfect miRNA duplex consisting of a 5p and 3p arm[272-274]. Again, each strand has the typical 5'-P and a two-nucleotide 3'-overhang[257, 265]. Correct processing and ATP-dependent[275] loading of the mature miRNA duplex into the miRNA-induced silencing complex (miRISC) is achieved via the RISC-

loading complex, consisting of Dicer, TRBP and one of the Argonaute family members (AGO I-IV)[276, 277]. Upon association of the miRNA duplex with AGO I-IV[278], the minimal RNA-silencing complex, the miRNA duplex is unwound and only one of the strands, referred to as the guide strand, is retained whereas the other, the passenger strand, is ejected from the complex and subsequently degraded[279-282]. In principle, both strands of a mature miRNA can function as a guide strand and the mechanism of strand selection is not yet fully understood. Computational analysis revealed that in the majority of cases, the strand with the thermodynamically less stably paired 5'-end (in other words the one that has less GC basepairs at its 5'-end) is selected as the guide strand[282, 283]. In addition, a 5'-uridine or adenine has been identified as a positive selection factor for loading miRNA (or siRNA) guide strands into AGO2[284, 285]. Nevertheless, the process of strand selection is probably much more complex. For example, the cell-type specific abundance of individual miRNA strands and the regulation of a tissue specific targetome have been reported[286-289]. It is tempting to speculate that the cell-type or -state specific presence of certain RNA binding proteins, or particular isoforms thereof, are involved in tissue specific miRNA biogenesis and strand selection[268, 290-294].

Upon association with AGO I-IV and generation of an active miRISC, miRNAs typically recognize a target sequence in the 3'-untranslated region (3'-UTR) of mRNAs by base pairing with nt 2-8, counting from the miRNA 5'-end. This region is called the miRNA seed and is the main determinant of canonical miRNA target recognition[295]. Crystal structure analysis revealed that upon seed-mediated target recognition, the AGO complex undergoes a structural change to enable additional base pairing between the rest of the miRNA and the target[296]. Although sequence complementarity in the seed region is the main determinant of canonical target recognition[297-299], additional complementarity in the 3'-half of the miRNA can compensate for mismatches in the seed region (supplementary region)[300-303]. Preferred mRNA target sites have an adenine facing nt 1 (t1A) of the miRNA[304]. Although t1A does not base pair with the miRNA, it is recognized through a specific binding pocket inside AGO2[305, 306]. Association of the target mRNA with miRISC results in translation arrest and mRNA deadenylation followed by decapping and decay[307-309]. mRNA deadenylation is a consequence of association of AGO with a variety of RNA binding proteins, including trinucleotide repeat-containing gene 6 (TNRC 6) proteins[310-313], polyadenylate-binding protein (PABPC)[314], deadenylase complexes poly(A)-specific ribonuclease 2 (PARN2)-PARN3[315, 316] and carbon catabolite repressor protein 4 (CCR4)-NOT[317-319]. In turn, deadenylation triggers decapping through the mRNA-decapping enzyme subunit 1 (DCP1)-DCP2[316], thereby facilitating 5'-3' exonuclease mediated degradation[320]. In addition, a variety of non-canonical pathways for miRNA processing, miRNA homeostasis and target

regulation have been described and have been extensively reviewed[252, 253, 293, 308, 309, 321].

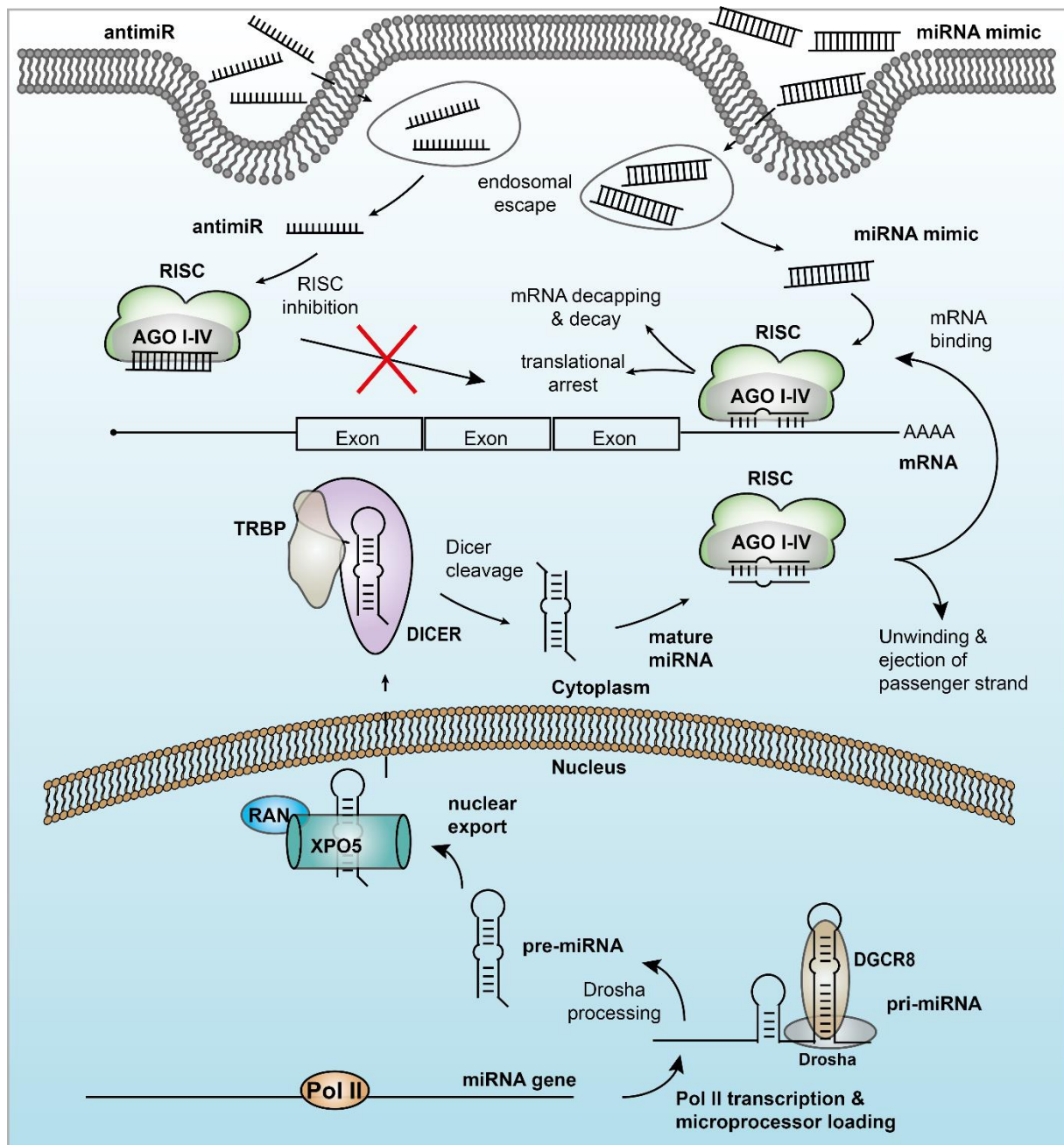


Figure 1.9. MiRNA biogenesis, the miRNA interference pathway and therapeutic applications thereof. MiRNA biogenesis was adapted from[322].

Given that 60% of the human protein-coding genome have been predicted to contain miRNA target sites[323], it is appealing to exploit this regulatory network therapeutically. Moreover, a variety of diseases have been linked to miRNA deregulation[324, 325] and global downregulation of miRNAs is considered to be a hallmark of cancer[308, 326]. Nevertheless, some miRNAs are also known to promote tumor development and are referred to as oncomiRs[327]. Therapeutic modulation of miRNA function is mainly achieved by following two

strategies: Either by using miRNA mimics which can substitute miRNAs that have been downregulated in a disease state such as the tumor-suppressor miR-34a in several forms of cancer[328] and let-7 in different cancers[329, 330] and diabetes[331, 332] or by inhibiting miRNA function with so-called antimiRs[333] (or antagomiRs, when conjugated to cholesterol[334]) which bind to miRNAs inside RISC[335]. MRX34, a liposomal miR-34a mimic, has been investigated by Mirna therapeutics for treatment of multiple cancers, but clinical development was discontinued after a series of immune-related adverse events[336-338]. A prominent example for the latter strategy was the development of miravirsen by Santaris Pharma, a DNA-LNA mixmer designed to inhibit miR-122 function for the treatment of hepatitis C virus infections[171, 339, 340]. In addition to blocking miRNA function after association with AGO, miravirsen has been shown to invade the pre-miR-122 stem-loop structure and prevent miRNA processing[341]. However, clinical development was suspended due to the approval of the curative treatment sofosbuvir. Similarly, development of RG-101, a GalNAc conjugated antimiR against miR-122 developed by Regulus Therapeutics[342], has been halted due to the occurrence of severe jaundice[343]. Moreover, particularly short LNA phosphorothioates that only bind to the miRNA seed region (tinymer) have been developed as a new anti-miR format[344].

1.2.4 Small interfering RNAs and functional interplay with the miRNA pathway

The journey of siRNAs began in 1998 with the observation that dsRNA was more effective at gene silencing than was either strand individually[345]. The discovery of the RNAi pathway in *C. elegans* was followed up by the first siRNA silencing experiment in mammalian cells in 2001[346] and was honoured with the noble prize for A. Fire and C. Mello in 2006. SiRNAs are short dsRNAs with a length of approximately 19-24 nt and exploit the previously described RNA interference pathway for gene silencing[3, 4]. In contrast to miRNAs, which typically show imperfect base pairing and can function equally via all 4 AGO family members[308], siRNAs are perfectly complementary to their target sequences and mainly operate via AGO2 (Figure 1.10). A unique property of AGO2 is the ability to cleave a target RNA which is fully complementary to the siRNA guide strand at a single phosphodiester linkage opposite to nts 10 and 11 of the guide strand when counting from the 5'-end[347, 348]. These positions are referred to as 'g10' and 'g11', respectively. AGO2 is therefore also called the "slicer protein". Nevertheless, siRNAs can also be loaded into other AGO family members and mediate seed-dependent miRNA-like effects which can be both, on- or off-target[349, 350]. The standard siRNA format is considered to be a 21 nt duplex with a 19 nt complementary region and the RNase III characteristic two-nucleotide 3'-overhang[346]. Historically, the 3'-overhang consists of two thymidine residues due to a cheaper and more efficient chemical synthesis from solid supports that have been pre-loaded with dT. Nowadays, a large variety of siRNA designs are

in use, including single stranded siRNAs, blunt ended duplexes, asymmetric duplexes as well as chemically diverse overhang modifications[351]. In addition, the use of long dsRNAs and short hairpin RNAs (shRNAs) has been propagated as more efficient RNAi reagents due to a Dicer dependent processing which is thought to facilitate RISC loading[352]. Therapeutic development however focussed on short duplex formats, as long dsRNAs have an increased immunostimulatory potential and heavy chemical modification can interfere with Dicer processing[353, 354].

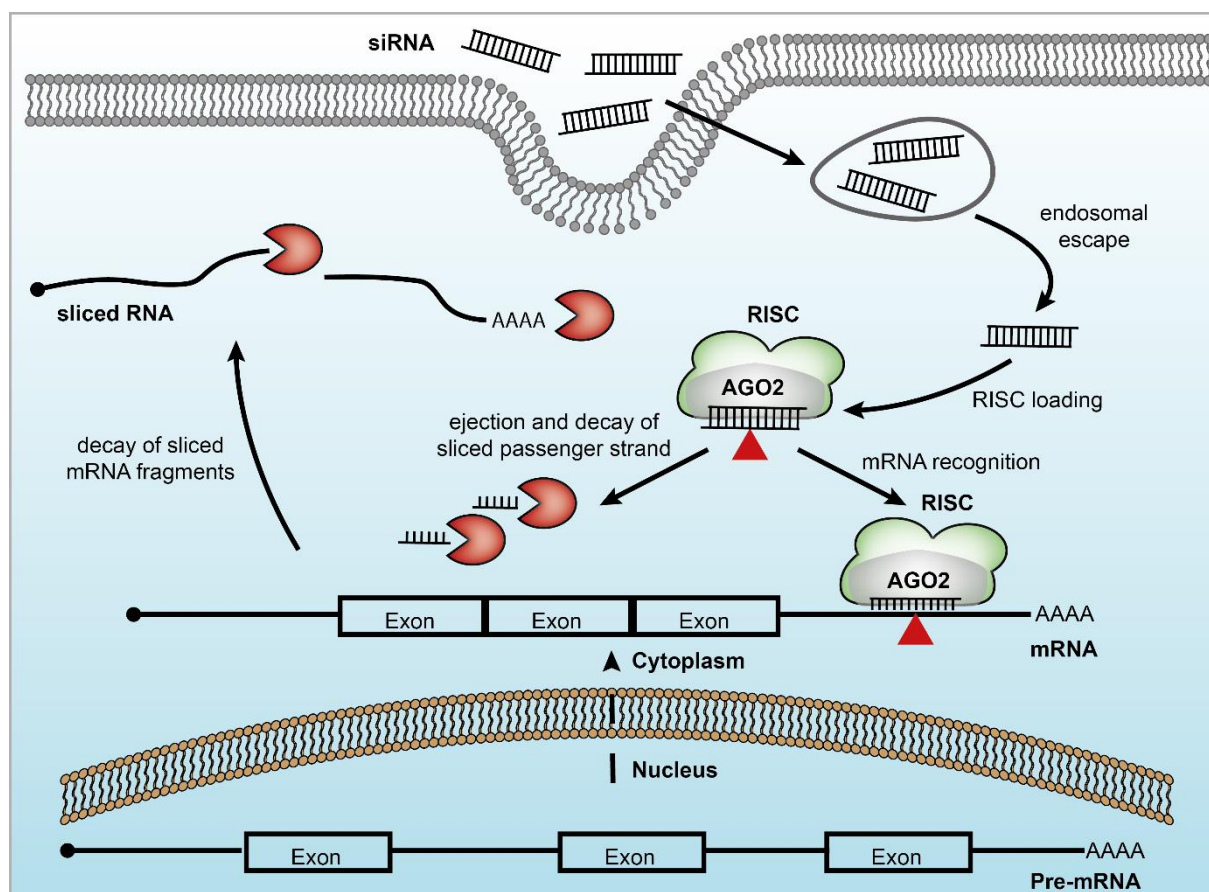


Figure 1.10. Mechanism of siRNAs

To date, patisiran is the only siRNA that received market authorization by the FDA and EMA (both 08/ 2018)[355]. Patisiran is a mildly modified, unconjugated siRNA, which is given as a lipid nanoparticle formulation. It consists of two 21 nt RNA strands and contains a total of 11 2'-OMe modifications and a 2 nt 3'-dT overhang on both strands[4, 8]. Due to the immunogenicity of the LNP formulation, an anti-inflammatory pre-treatment of patients with a combination of corticosteroids, acetaminophen and antihistamines is required[4, 356, 357]. Therefore, most siRNAs that are currently under clinical development rely on naked delivery, mostly achieved through GalNAc-mediated targeting to hepatocytes[8]. Hence, despite the approval of patisiran, key challenges for broad *in vivo* applications remain.

1.2.4.1 Toxicity aspects of siRNAs

One concern regarding the safe use of siRNAs is the potential for seed-driven off-target effects[349, 350]. In principle, each siRNA also has the ability to function as a miRNA and to recognize a range of targets due to seed complementarity. Such miRNA-like behaviour is thought to be the main cause for liver toxicity. To minimize this risk, computational as well as experimental screening efforts have been vastly increased[72]. Potential side-effects from passenger strand loading have been addressed through chemical modification of the passenger seed region[358, 359] and capping of the passenger strand in order to prevent the 5'-phosphorylation required for RISC loading[194, 204]. For heavily modified siRNAs, passenger strand loading is a lesser concern as endogenous 5'-phosphorylation is less efficient and therefore chemical phosphorylation of the guide strand is required[112, 198, 199].

The stimulation of the innate immune system by exogenously delivered RNAs is a well-known risk. SiRNA-induced immune responses are mainly mediated by toll-like receptors (TLR) and retinoic-acid-inducible-gene-I (RIG-I)[354, 360-364]. Chemical modifications such as 2'-OMe offers a convenient means to reduce the immunogenicity of siRNAs but do not eliminate the need for extensive screening procedures[365, 366].

In addition, the risk of a global competition between siRNAs and endogenous miRNAs for RISC loading has been an early concern[367-369] but so far no clinical evidence has been found to support this hypothesis[4]. As RNA-targeted therapeutics are increasingly modified with a wide range of chemically modified building blocks, a key question for future development will be the in-depth characterisation of the resulting metabolites, including but not limited to the associated risk for genotoxicity. A modification that has attracted a lot of attention in this respect is the use of 2'-F nucleotides as it has been associated with a risk of genotoxicity[4] and a loss of paraspeckle proteins[186, 188]. In response, Alnylam Pharmaceuticals has undertaken efforts to reduce the 2'-F content of siRNAs in their development pipeline and several companies attempt to increase the metabolic stability of their drugs to limit patient exposure[183]. For example, whereas the transthyretin targeting GalNAc-siRNA revusiran was dosed at 500 mg/week[4], Alnylam's newly developed isosequential drug vutrisiran (ALN-TTRSC02)[370] can be administered at 25 mg every 3 months[371]. Revusiran, for which a phase 3 trial was terminated due to a mortality imbalance in the treatment and placebo arms[372], was constructed using the so-called "Standard Template Chemistry" (STC). For the next-generation "Enhanced Stability Chemistry" (ESC) drug vutrisiran (Table 1.1), 2'-F content has been reduced from a total of 22 to 9 building blocks with a concomitant increase of 2'-OMe nucleosides from 22 to 35 and an increase in PS linkages from 2 to 6[370].

Table 1.1. STC vs ESC siRNA design

Compound	Strand	Sequence (5' - 3')	Target
Revusiran (STC)	AS	u <u>C</u> u <u>U</u> g <u>G</u> U <u>U</u> a <u>C</u> a <u>u</u> g <u>A</u> a <u>A</u> u <u>C</u> c <u>C</u> a* <u>U</u> *c	Transthyretin
	S	<u>U</u> g <u>G</u> g <u>A</u> u <u>U</u> u <u>C</u> A <u>U</u> g <u>U</u> a <u>a</u> c <u>C</u> a <u>A</u> g <u>A</u> L	
Vutrisiran (ESC)	AS	u* <u>C</u> *uug <u>G</u> uu <u>A</u> caug <u>A</u> a <u>A</u> uccca*u*c	Transthyretin
	S	u*g*ggau <u>U</u> u <u>C</u> A <u>U</u> guaaccaagaL	
QPI-1002	AS	uGaAgGgUgAaAuAuUcUc	p53
	S	GaGaAuAuUuCaCcCuUcA	

Upper case= RNA, upper case + underlined= 2'-F, lower case = 2'-OMe, * = PS linkage, L = trivalent GalNAc. Sequences taken from [370] and [185]

Long-term safety data and regulator's response will tell, whether the future of RNAi therapeutics will rather be a mix of several chemical modifications or whether more uniform patterns such as simple alternating 2'-OMe modifications as in QPI-1002[185] will win through.

1.2.4.2 Metabolic stability of siRNAs

As mentioned above, recent research focussed on the metabolic stability of siRNAs in order to

- Improve therapeutic efficacy
- Limit drug exposure of patients
- Increase patient compliance through convenient dosing regimens
- Reduce overall costs of therapy due to less frequent dosing

The main determinant for metabolic stability of siRNAs has been found to be the resistance towards 5'-exonuclease mediated degradation in the endo-lysosomal compartment after uptake into hepatocytes[182]. Whereas nuclease stability of single stranded therapeutics is usually increased through the use of 2'-MOE, LNA or (S)-cEt sugar modifications, these moieties are less useful for RNAi therapeutics[3, 373]. Hence, for siRNA chemistry, a combination of 2'-OMe and 2'-F building blocks along with terminal PS modifications is routinely used and an overall modification pattern has been suggested based on an analysis of the functionality of 1,890 Alnylam siRNAs[183]. Still, specific patterns have to be optimized for individual sequences and combinations of guide and passenger strands[183]. On one hand, high metabolic stability is desired for long-term treatments with infrequent injections, on the other hand it raised the concern that such long-lived drugs pose a danger in case of unexpected side-effects. This might be of particular concern for first-in-man clinical trials and therefore short high-affinity LNA antidotes have been developed which bind the siRNA guide strand inside AGO to stop drug action[374]. This strategy resembles the tinymer approach introduced for antimirs[344] but does not offer an emergency solution in case of inflammation.

1.2.4.3 Delivery and pharmacokinetics of siRNAs

Systemic delivery of siRNAs has been regarded as the main challenge that hampered the transition of RNAi therapies from a biochemical tool to the clinic[375]. Whereas single stranded PS oligonucleotides are amphiphilic and capable of binding to serum proteins, the hydrophobic nucleobases of RNA duplexes are buried inside the helical structure and protein binding is much weaker for ds therapeutics[3, 4]. Delivery of siRNAs therefore used to rely on LNP formulation to enable delivery to the liver after association with lipoproteins. Although LNP formulation triggers an immune response, this delivery approach paved the way for the approval of the first RNAi drug patisiran in 2018[355]. The next key development in the field of RNAi therapeutics was GalNAc conjugation to heavily modified siRNAs, which enabled naked delivery to hepatocytes[222]. This strategy is currently used for all drug candidates in the Alnylam pipeline and is also employed for newly developed single stranded therapeutics[4, 8]. Future delivery strategies are likely to focus on the development of novel conjugation approaches that will enable target inhibition beyond the liver. The currently most promising strategy is conjugation to lipid moieties[113, 227, 228, 231, 232]. Other delivery options include conjugation to peptides[376], aptamers[377] and small molecules such as folic acid[223] (Figure 1.6). However, development of a “new GalNAc” is considered to be a major challenge. It has been estimated that 2,000 -10,000 cytosolic siRNA molecules are required to achieve robust gene silencing. Given that only 0.1 – 2% of endocytosed siRNAs actually reach the cytosol, a requirement for the simultaneous occupation of 1 million cell surface receptors has been estimated[375]. ASPGR, the target for GalNAc ligands, are expressed in 500,000 – 1,800,000 copies per hepatocyte and are rapidly internalized and recycled[378-380]. In mouse models of reduced ASPGR expression, mimicking diseases such as alcoholic cirrhosis and hepatocellular carcinoma, GalNAc-siRNAs that require dosing >5 mg/kg were not able to achieve maximum knockdown efficiency due to limited ASPGR capacity[379]. One option is the targeting of folate receptor (FR) overexpressing tumors. FR abundance in certain forms of cancer has been reported to be 1 – 10 million copies per cell, exceeding expression levels in healthy tissues by a factor of 100-300[223, 381]. In addition, local delivery to the CNS has been successfully demonstrated for SSOs[20] and conjugate-independent uptake of naked siRNAs into proximal tubular epithelial cells has been reported[185, 382]

1.2.5 CRISPR/ Cas based systems

The discovery of CRISPR (clustered regularly interspaced short palindromic repeats) – Cas (CRISPR associated) antiviral defence systems in bacteria and archaea has added a new facet to nucleic acid based therapeutics. In prokaryotes, CRISPR sequences are derived from the DNA of viruses that have previously infected the host cell[383-385]. These acquired DNA stretches are incorporated as spacers into CRISPR loci with the help of Cas1 and Cas2

proteins. CRISPR-Cas systems can be roughly divided into two classes which are further characterized as class 1 type I, III and IV and class 2, type II, V and VI[386]. Whereas class I systems use large multiprotein effector complexes, class II systems require only a single Cas protein. Therefore, class 2, and more specifically type II, CRISPR systems served as the basis for the development of an ensemble of methods, now generally referred to as CRISPR-Cas based genome editing[387]. In type II systems, crisprRNAs (crRNA) that are transcribed from the CRISPR locus associate with a trans-activating crRNA (tracrRNA) to recruit the DNA targeted endonucleases Cas9 towards a complementary target sequence. However, as a genetic tool, genomic CRISPR sequences are not required but only a Cas protein, typically Cas9, is used in conjunction with a dual crRNA/ tracrRNA system or with a single guide RNA (sgRNA)[388].

Type II CRISPR-Cas systems now serve as the key molecular engine to drive targeted genome editing[387]. Before the advent of the CRISPR-Cas approach, genome editing has been achieved through zinc finger nucleases[389] and transcription activator-like effector nucleases (TALEN)[390], which had to be specifically engineered for the recognition of individual target sequences. The strength of CRISPR-Cas systems is that the target sequence can be identified through the introduction of target specific sgRNAs, alleviating the need for laborious protein engineering[387]. A common feature of all genome editing approaches is the dependence on the cellular DNA repair machinery[391]. Two major pathways for the repair of dsDNA breaks, introduced through Cas proteins or other endonucleases, are known: The more frequent one is non-homologous end joining (NHEJ), which leads to an error prone direct ligation of the double-strand break and is exploited for gene knockout through the formation of insertions and deletions (indels) [392]. The other one is homology-directed repair (HDR), which requires the presence of a template DNA that can be used for guided repair of the double-strand lesion[393]. Co-delivery of specific repair templates is used for precise genome editing, as the desired insert can be encoded in the repair template[394]. A prerequisite for binding is the presence of short Cas recognition motifs in the flanking region of the target sequence, termed protospacer adjacent motif (PAM)[395, 396]. The PAM sequence for the currently most widely used *Streptococcus pyogenes* Cas9 (SpCas9) is 5'-NGG-3'[397]. Other currently investigated Cas proteins are Cas12a (type V) for the cleavage of ss and dsDNA substrates[398] and Cas13a (type VI) for targeting ssRNA[399, 400]. Furthermore, RNA targeted Cas13d has been used to degrade misspliced tau mRNA in a neuronal model of frontotemporal dementia[401].

Type III systems are markedly different from the others in the respect, that they do not only lead to targeted cleavage of particular RNAs or DNAs, but instead invader RNA sensing by an RNA-targeted multisubunit complex is linked to global degradation of cellular RNAs via the standalone RNase Csm6[402]. Interestingly, Csm6 activation is triggered through the

formation of cyclic oligoadenylate second messengers via the Cas10 subunit of the interference complex[214, 215].

Despite its classical use in genome editing, CRISPR-Cas systems have found versatile applications. Point mutations in the Cas9 RuvC and HNH endonuclease domains result in a catalytically inactive, dead Cas9 (dCas9) which has opened up new possibilities for CRISPR-Cas technologies including CRISPR interference (CRISPRi) and CRISPR activation (CRISPRa)[403]. CRISPRi can be used to inhibit transcription through steric interference of dCas9 with the initiation of transcription and elongation[404]. Fusion of dCas9 to transcriptional activators is the basis for CRISPRa to enhance gene expression[405]. A recent development was the generation of so-called base editors through fusion of dCas9 proteins with either adenosine or cytosine deaminases. In this setup, a dCas9-sgRNA complex is used to recruit the covalently bound deaminase to specific sites in the genome in order to convert A-T to G-C and C-G to T-A base pairs[406-408] without induction of DNA double-strand breaks. However, frequent off-target editing has been revealed as a major challenge[409-411].

To date, a number of clinical trials has been launched which will shed light on the clinical applicability of current CRISPR-Cas technologies[412]. Key questions will be the safety profile of this novel technology platform and the identification of suitable delivery vehicles. Currently, delivery through lentiviral or lipid nanoparticles is most widely used[413] but recent reports suggest that a direct delivery of Cas proteins might be advantageous with respect to off-target editing[414, 415].

1.2.6 Other classes of RNA therapeutics

In addition to the therapeutic modalities highlighted above, a multitude of nucleic acid focussed research areas exists, comprising structurally and chemically diverse oligo- and polynucleotide species. An emerging field is the use of mRNA therapeutics as cancer vaccines and for protein replacement therapy[416, 417]. Because long polynucleotides are currently not accessible via chemical synthesis, mRNA therapeutics are produced through *in vitro* transcription, which has limited the exploration of site specific chemical modifications. Nevertheless, the use of chemical modifications is under investigation and in particular substitution of uridine by pseudouridine showed promising effects on translation efficiency and nuclease stability[126-128]. In addition, chemical synthesis of particular mRNA regions and subsequent ligation offers a means to selectively explore the chemical space[205]. A drawback is the current requirement for the use of LNP formulation[418].

Another promising approach involves targeting of cell-surface components as well as subcellular structures through the use of aptamers. In contrast to other nucleic acid based approaches, aptamers evolve through dedicated selection procedures to recognize their target

structure by shape complementarity rather than base pairing[419]. In this respect, aptamers are often viewed as the nucleic acid counterpart of antibodies. A variety of chemical modifications has been used in the development of novel aptameric structures[419] and aptamers are currently investigated as targeting moieties for other therapeutic platforms[420, 421] as well as in sensor technologies[422]. Of note, the anti-vascular endothelial growth factor (VEGF) aptamer pegaptanib has received market authorization by the FDA in 2004 for the treatment of neovascular age-related macular degeneration (AMD)[423].

Additional approaches include the use of immunostimulatory oligonucleotides to activate the immune system for cancer therapy[424] and infectious diseases[425] as well as ribozymes for targeted destruction of RNA targets[426].

2 Project 1 – Full PS siRNAs as an alternative scaffold for RNAi therapeutics

2.1 Introduction

2.1.1 PS modification for siRNAs

siRNAs are a promising class of drugs in the emerging field of RNA therapeutics. A key difference between siRNAs and other classes of RNA-targeted therapeutics is its double-stranded nature. In an siRNA duplex, one strand, commonly referred to as the passenger or sense (S) strand, can be viewed as a carrier molecule that delivers its cargo, the guide or antisense (AS) strand, into the cell and facilitates RISC loading[3, 4]. On one hand, the double stranded format provides stabilization against nucleases but on the other, it imparts a broad biodistribution due to a reduced binding to serum proteins which are generally exploited as carrier molecules to keep ASOs in circulation[4]. Consequently, patisiran, the only approved siRNA drug to date, depends on lipid nanoparticle formulation for efficient *in vivo* delivery[355]. Due to the immunostimulatory effects of these lipid nanoparticles, an antiinflammatory pretreatment of patients with glucocorticoids, acetaminophen and antihistamines is required[4]. Of note, the mode of delivery appears to be of general importance for activation of the immune system, indicating that naked injection of synthetic siRNAs is less prone to trigger an immune response than lipid-nanoparticle encapsulated siRNAs[427-429]. Therefore, current research focusses on the development of siRNA-conjugates that do not require lipid-formulation[3, 8]. Such siRNA-conjugates are usually fully chemically modified to increase their metabolic stability. However, despite recent success in clinical trials using fully modified GalNAc conjugates, the clinically most advanced GalNAc-siRNA, revusiran, failed in a phase III study due to a mortality imbalance between the treatment and placebo groups[372]. Although the mortality imbalance has been related to an underlying distribution bias of patients into the treatment and placebo arms, a contribution of the drug could not be excluded[3]. In light of emerging reports on potential toxicity aspects of the use of 2'-deoxy-2'-F nucleotides[4, 69, 186-188], an investigation of alternative siRNA scaffolds that convey metabolic stability but alleviate 2'-F-related toxicity concerns is required.

One option is to use phosphorothioate substitutions across large parts of the siRNA[113, 430-432]. Whereas unconjugated PO siRNAs are known to be rapidly cleared from the bloodstream by renal filtration[190], at least single stranded PS oligonucleotides are shielded against urinary excretion through binding to serum proteins[15]. Despite conflicting reports on activity and toxicity of PS siRNAs[67, 68, 433-435], our lab developed full PS siRNAs with good *in vitro* activity and limited toxicity[9]. A key aspect of this development was the use of an activator that introduces a mild bias towards *Rp*-stereochemistry during the synthesis of PS-ORNs.

Moreover, an increased serum stability of partially PS substituted siRNAs was observed *in vivo*[190, 432], further encouraging the investigation of PS siRNAs.

2.1.2 The Lin28/ let-7-axis as a drug target in cancer

Lin28 has been initially identified as a critical regulator of developmental timing in *C. elegans*[436] and has been afterwards described in animals and humans[437, 438]. In the healthy body, Lin28 is highly expressed during early development and afterwards downregulated in most tissues[436-439]. Two Lin28 paralogues have been described in humans, Lin28A and B. Both paralogues contain an N-terminal cold shock domain (CSD) and two C-terminal CCHC zinc finger domains through which they can bind a GGAG motif in the terminal loop regions of let-7 precursors[440-442]. Whereas Lin28B contains a nuclear localization signal and is hence commonly found in the nucleus, Lin28A is mostly present in the cytosol[443]. However, localization of both paralogues may vary between different cell types and Lin28A has been suggested to be able to shuttle between the nucleus and the cytosol[444, 445]. Despite its various roles in transcription and splicing, the most prominent role of Lin28 in cancer is the downregulation of the potent tumor-suppressor miRNA let-7[445]. The binding of Lin28 to miRNA precursors leads to inhibition of pri-let-7 microprocessor cleavage in the nucleus and Dicer processing in the cytosol[445]. In addition, Lin28 has been shown to recruit terminal uridylyl transferases (TUTase), thereby marking the pre-miRNA for degradation[446, 447]. As let-7 targets a large variety of potent oncogenes such as c-MYC, Ras and HMGA2, Lin28 overexpression has been recognized as an important driver of several cancers[445]. Moreover, overexpression of Lin28B has been reported to be sufficient to drive tumor development in mouse models of hepatic carcinoma[448] and to be critical for the maintenance of cancer stem cells in prostate cancer xenografts[329].

2.2 Project outline

The goal of this project was to conduct a detailed investigation of a model PS siRNA in order to investigate this promising scaffold as a novel strategy for systemic delivery of siRNAs. This included several steps:

- a clean scale-up of our PS ORN synthesis protocol from a few micrograms to several milligrams
- *in vitro* tests to evaluate the metabolic stability and human serum albumin (HSA) binding capability
- the development of a suitable method for the detection of PS siRNAs in tissue biopsies and the evaluation of the biodistribution profile in mice
- a xenograft study to evaluate the *in vivo* activity of a PS siRNA directed against Lin28B

Lin28B was selected as a model target due to its prominent role in different types of cancer[445], including prostate cancer[329], as well as a history of Lin28B focused projects in our group[449, 450].

2.3 Results and Discussion

2.3.1 Scale-up of PS ORN synthesis

As a prerequisite for a detailed investigation of PS siRNAs, our current protocol for oligonucleotide synthesis[9] needed to be scaled up. Difficulties regarding a clean synthesis of PS ORNs have been acknowledged in the literature. Furthermore, reports on cell toxicity and lack of activity have been linked to synthesis related impurities. For example, Corey and coworkers noted that “oligomers with phosphorothioate modification can be relatively difficult to purify and that impurities that remain after synthesis can increase toxicity upon transfection into cultured cells”[431]. These difficulties originate mainly from two challenges. One challenge is to achieve an efficient sulfurization of the P (III) linkage in the presence of the bulky 2'-O-tert-butyldimethylsilyl (TBDMS) protecting group, which are commonly used in RNA synthesis. Particularly large purine stretches are a challenge in terms of efficient sulfur transfer[451]. Inefficient sulfurization leads to the persistence of a P (III) phosphite triester linkage which is subsequently cleaved during the DCA treatment in the deblock step (Figure 2.1). This leads to a range of truncated sequences with internal deletions[451]. As the growing oligonucleotide chain is not capped at the internal deletion site, the synthesis proceeds to completion, yielding 5'-dimethoxytrityl (DMT) protected shortmers. Such shortened sequences are particularly difficult to remove because PS ORNs usually elute as broad peaks during HPLC purification (Figure 2.2). This is because PS ORNs are synthesized as a mixture of 2^n diastereoisomers (n = number of PS linkages) unless chiral auxiliary groups are employed[25-28, 30, 31]. In contrast to the prochiral phosphodiester linkage of natural PO RNA, each sulfurization gives rise to a new stereocenter. Therefore, separation of failure sequences from full length products depends on the presence or absence of the hydrophobic 5'-DMT group. In other words, only PS ORNs that are truncated from the 5'-end and therefore lack DMT protection can be efficiently separated from full-length DMT-on sequences.

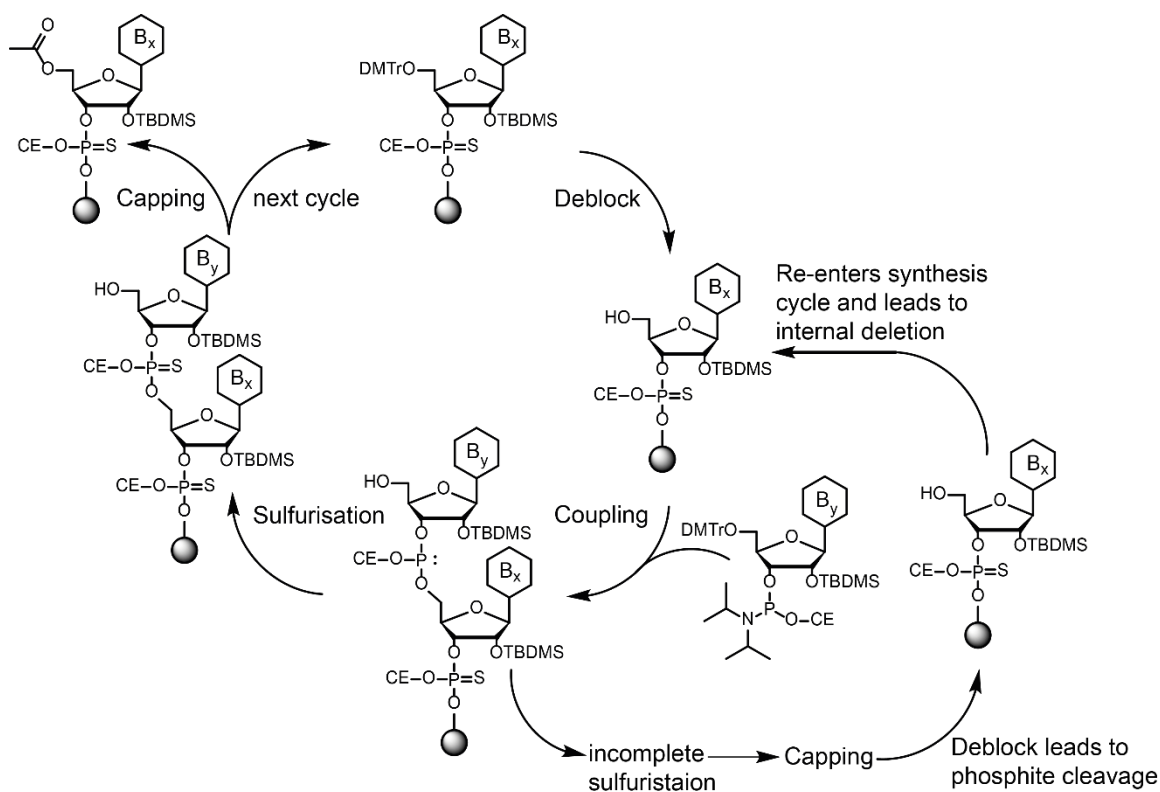


Figure 2. 1. Synthetic cycle for PS ORNs and formation of internal deletions. Support-bound growing ORN chains undergo iterative synthetic cycles. Insufficient sulfuration can lead to phosphite cleavage and re-entry of truncated sequences into the synthesis cycle.

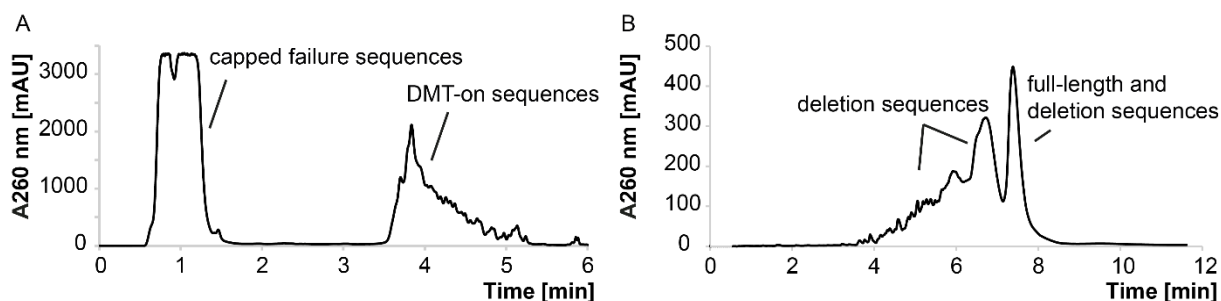


Figure 2. 2. HPLC chromatograms after large-scale PS ORN synthesis before optimization A) HPLC chromatogram of crude (DMT-on) purification of PS ORN. High levels of 5'-truncated failure sequences elute at 1 min, full length and internally truncated DMT-on sequences elute at 4 min. B) DMT-on sequences from crude purification were collected, detritylated and HPLC purified. Multiple shortened sequences are resolved during DMT-off purification of the peak isolated from A. mAU= milli absorption units.

An efficient sulfuration was achieved through increasing the concentration of the sulfur transfer reagent 3-((*N,N*-dimethylaminomethylidene)amino)-3H-1,2,4-dithiazole-5-thione (DDTT) from 0.05 M to 0.1 M and extending the contact time from 2 to 10 min. A comparable sulfuration efficiency was achieved using aged solutions of 0.2 M phenylacetyl disulfide (PADS) [452-454]. Because of a similar sulfuration efficiency at comparable costs, the more defined fresh solution of DDTT was used instead of an aged PADS solution which contains a mixture of polysulfides[453, 454]. In addition, each reagent volume and contact time had to be carefully optimized. Furthermore, regular calibration of reagent pressure, valve opening times

and adjustment of vacuum strength are necessary, particularly when new solvent ratios are tested.

In the next step, the work-up procedure had to be optimized. The routinely applied on-column deprotection using gaseous methylamine led to a $m+14$ side-product (Figure 2.3), presumably corresponding to an *N*-methylated impurity arising through nucleophilic displacement of cytidine N^4 -acetyl or adenosine N^6 -benzoyl protecting groups by methylamine[138, 455]. This was not observed for on-column deprotection using 50 nmol columns.

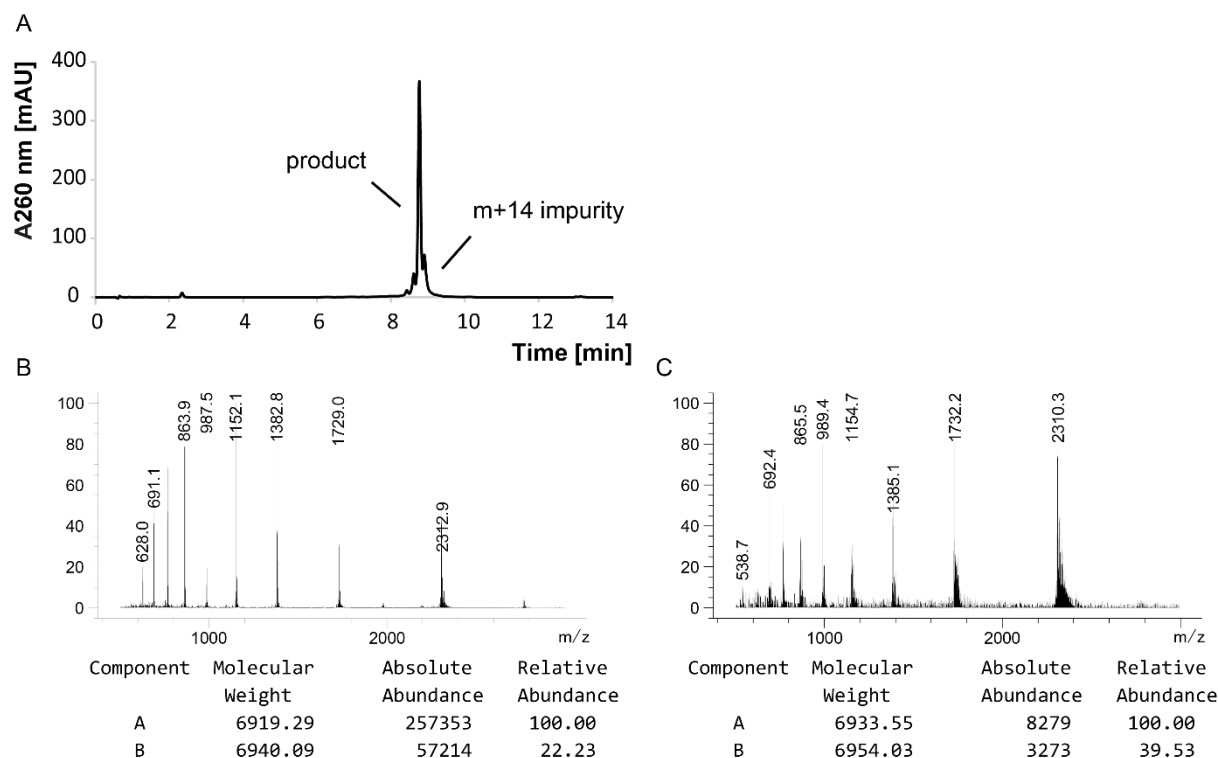


Figure 2. 3. LC/ MS analysis reveals work-up related impurity. A) UV trace of purified PS siLin28B guide strand after gaseous methylamine deprotection. B) MS of main peak at 8.8 min from A. C) MS of side-peak at 8.9 min from A. M calc= 6920.38

The use of a suspension procedure using a 1:1 mixture of 40% aqueous methylamine and 25% ammonia (AMA) at either 65°C for 1 h or 30°C for 6 h resolved the problem. A standard 2 h desilylation procedure using a fresh mixture of *N*-methyl-2-pyrrolidone/ triethylamine/ triethylamine trihydrofluoride (NMP/ TEA/ TEA.3HF) at 70°C was efficient for the removal of 2'-TBDMS groups. After optimization of the gradients for DMT-on and DMT-off RP-HPLC purification, a routine synthesis of ~18 mg (~1.3 μ mol) PS ORNs/ synthesis column was achieved at a purity >95%. Considering the use of 300 mg controlled pore glass (CPG) solid support per column with an average loading of 40 μ mol/ g, this corresponds to a theoretical yield of 11%. For comparison, the commercial supplier Integrated DNA Technologies states an average coupling yield for unmodified RNA of 98%[456] leading to a theoretical yield of 65% for a 21mer of which only 40-70% can be recovered after a single HPLC purification[457].

Interestingly, DMT-on PS ORN diastereoisomers elute as two peaks on our RP-HPLC system (Figure 2.4 A) and migrate as a single peak after detritylation (Figure 2.4 B).

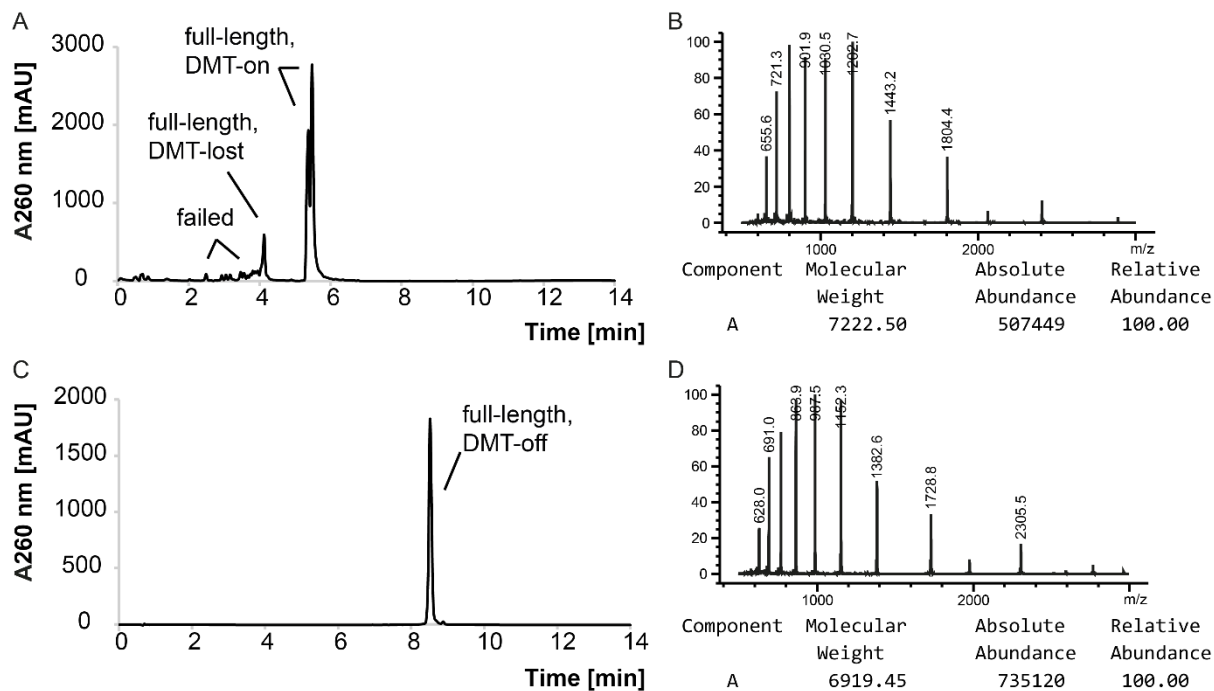


Figure 2. 4. Large-scale synthesis of PS ORNs after optimization. A) UV trace of LC-MS analysis of crude PS siLin28B guide strand B) MS of peak at 5.3-5.5 min from A. M calc (DMT-on) = 7222.75 C) UV trace of LC-MS analysis of PS siLin28B guide strand after purification and detritylation. D) MS from peak at 8.5 min from C. M calc (DMT-off) = 6920.38

2.3.2 *In vitro* assessment of PS siLin28B

After a clean synthesis protocol for milligram (μmol) quantities of PS ORNs was established, the *in vitro* properties of PS siRNAs were evaluated, building on our previously published results[9, 329]. Lin28B was selected as a target for the in-depth characterization of a PS siRNA.

2.3.2.1 Cellular activity

As a first step, the activity of our PS siLin28B was confirmed by SYBR Green RT-qPCR and Western Blot analysis in HEK293T cells (Figure 2.5, data was previously shown in [322]). As measured on the RNA and protein level, the activity of the PS siRNA was only slightly reduced compared to the PO parent duplex in the presence of Lipofectamine 2000 as a transfection reagent. Activity after free uptake at 1 μM concentrations was neither observed for the PO nor the PS duplex. Limited toxicity was observed in HEK 293T cells and toxicity was vastly increased after transfection into HeLa cells, suggesting a cell line dependent sensitivity towards full PS siRNAs. Cellular toxicity after transfection reagent mediated delivery however does not necessarily reflect the *in vivo* situation as the transfection reagent itself appears to be an important aspect of the toxicity mechanism[427-429].

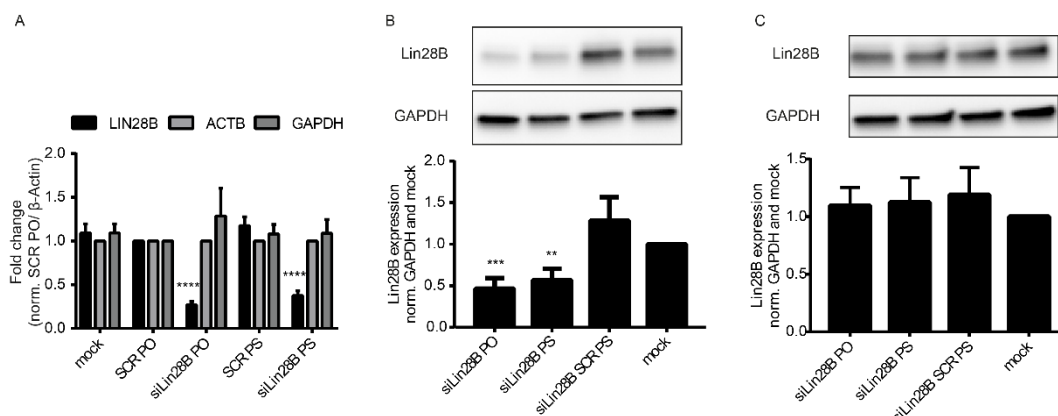


Figure 2. 5. In vitro activity of PS siLin28B. A) RT-qPCR of Lin28B, β -actin and GAPDH after transfection of 40 nM siRNAs (Lipofectamine 2000) in HEK 293T cells. Results normalized to GAPDH and scrambled PO siLin28B. SCR PO and SCR PS are scrambled PO and PS siLin28B, respectively. B) Western Blot analysis of Lin28B and GAPDH after transfection of 40 nM siRNAs (Lipofectamine 2000) in HEK 293T cells. Results normalized to GAPDH and mock. C) Western Blot analysis of Lin28B and GAPDH after gymnosylation of 1 μ M siRNAs in HEK 293T cells. Results normalized to GAPDH and mock. Mean \pm SD of all experiments are the results of 3 independent replicates. Mock treatment was Lipofectamine 2000 alone. Asterisks indicate statistical significance to 0 nM treatment calculated by one-way ANOVA and Dunnett's post-hoc test. (**) $P < 0.01$; (***) $P < 0.001$; (****) $P < 0.0001$.

2.3.2.2 Thermal denaturation and HSA binding of PS and PO siLin28B

As a next step, the thermal duplex stability and the albumin binding characteristics of PS and PO siLin28B were analyzed (Figure 2.6). The melting temperature (T_m) of an ORN duplex is a surrogate for the hybridization affinity and was measured through the increase of UV absorption at 260 nm during thermal denaturation of the duplex (Figure 2.6 C). As expected, the T_m of PS siLin28B ($59.3 \pm 0.5^\circ\text{C}$) was reduced in comparison to the PO duplex ($66.7 \pm 0.1^\circ\text{C}$). A reduced T_m of PS oligonucleotides is well documented in the literature[7, 9].

Then, we assessed the HSA-binding affinity of the PS siRNA as HSA could potentially serve as a vehicle for biodistribution. Although dsRNAs are known to bind serum proteins to a much lesser extent than single strands[3, 4], we hypothesized that the increased PS content might increase albumin binding as has been reported for PS substitution in single stranded oligonucleotides[15]. We used two techniques to assess albumin-binding: a gel-shift assay on a native polyacrylamide gel (Figure 2.6 B) and a competition assay based on displacement of fluorescent dyes specific to albumin binding sites I and II (Figure 2.6 A). In the gel shift assay we observed comparable albumin bound fractions between the PO and PS duplex but in the PS samples, an additional smear that was dependent on the albumin concentration was visible. This was rationalized as a weak transient binding of the PS duplex that was resolved during migration. The fluorescent displacement assay confirmed the weak albumin binding.

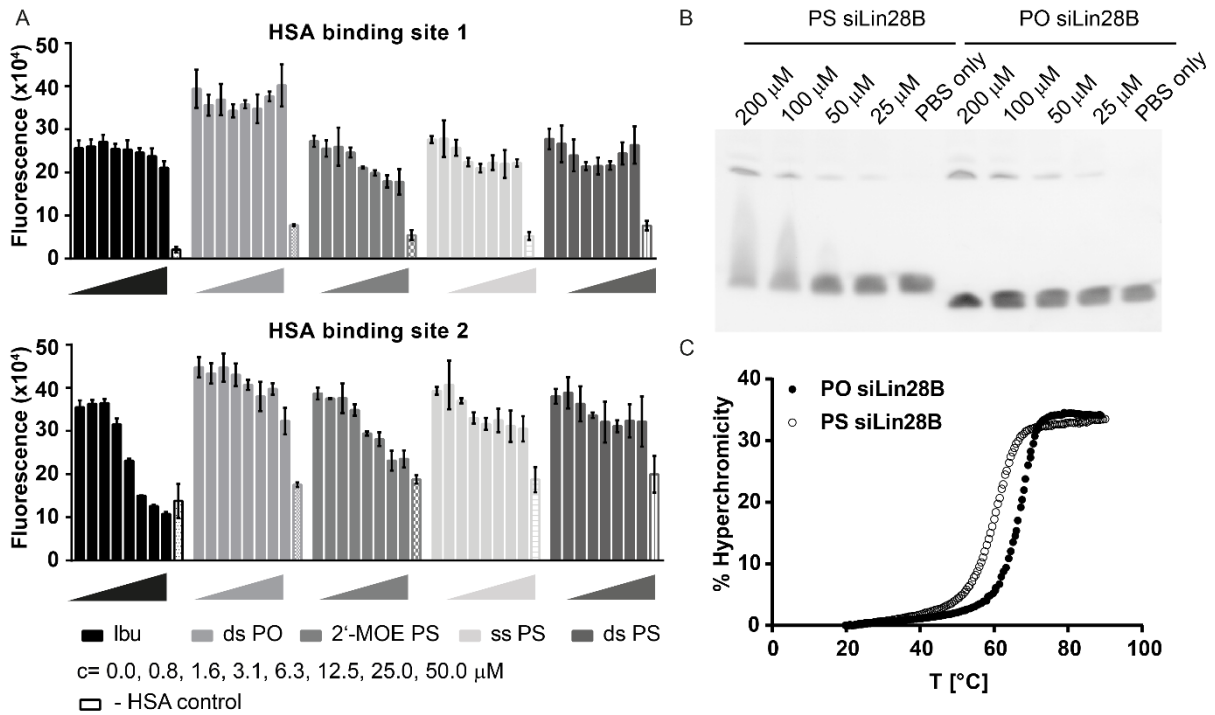


Figure 2. 6. Hybridization affinity and HSA binding assays of PS and PO siLin28B. A) Fluorescent displacement assay for HSA binding sites I and II. Fluorescent dyes were dansylamide (binding site I) and BD140 (binding site II). Ds PO and ds PS= PO and PS siLin28B respectively, ss PS= siLin28B guide strand, 2'-MOE PS= unrelated 19mer 2'-MOE-PS. HSA concentration was kept constant at 100 μ M. Last bar of each series represents the corresponding 50 μ M ORN/ dye mix without HSA. N= 3 B) Gel-shift assay on a 4-20% polyacrylamide gradient gel after incubation of 0.5 μ M siRNAs with different concentrations of human albumin. Representative gel shown. N= 3. C) UV melting of 3 μ M PS and PO siLin28B. T_m PS siLin28B= 59.3 +/- 0.5°C; T_m PO siLin28B= 66.7 +/- 0.1°C.

2.3.2.3 Nuclease stability in mouse serum and rat liver tritosomes

Upon injection, the siRNA will be in contact with serum nucleases during circulation. After tissue distribution and extravasation, the siRNA needs to enter the cytosol. Although many mechanistic aspects regarding the cell entry of oligonucleotides remain elusive, all investigated siRNAs so far are transported in endosomal vesicles that are subsequently fused with lysosomes[60, 230, 375]. Whereas several nanoparticle or polymer based formulations have been developed to facilitate endosomal escape[413], metabolic stability during endosomal trafficking is required for the naked administration of oligonucleotides and has been identified as the main determinant of *in vivo* efficacy of GalNAc siRNAs[182]. An *in vitro* surrogate for the endosomal compartment are rat liver tritosomes, which represent the lysosomal fraction of livers isolated from rats that have been treated with Triton WR 1339 (also called Tyloxapol) to facilitate purification[458, 459]. Therefore, nuclease stability of several siRNA formats was assessed in rat liver tritosomes and a subset of these was additionally tested in 50% mouse serum.

Based on literature reports, we established an assay that involved incubation of the query molecule in the respective medium followed by ion-exchange HPLC analysis[182]. Selected

time points were adjusted to the specific medium. The higher sampling rate at early stages of the tritosome assay thereby reflects the aggressiveness of the lysosomal milieu compared to serum. Besides the full PO and PS siRNAs mentioned above, a range of additional scaffolds were investigated (Table 2.1). Figure 2.7 shows a summary of tritosome (Figure 2.7 A) and serum stability assays (Figure 2.7 B). Corresponding chromatograms can be found in the appendix (Figures 7.1 and 7.2). Nuclease stability of PS and PO siLin28B was compared to an isosequential siLin28B that was either modified with 2'-OMe/ 2'-F-nucleotides + terminal PS linkages (siLin28B II, designed according to Foster et al. [183]), or with a combination of 2'-OMe/ RNA PS nucleotides + terminal PS linkages (siLin28B III). Furthermore, nuclease stability of the PS siLin28B guide strand alone (ss PS guide), the siRNA component of patisiran (hereafter referred to as patisiran) as well as the siRNA core of fitusiran (without GalNAc conjugation; hereafter referred to as fitusiran), were investigated.

Table 2.1. Sequences of oligonucleotides used in this study

Compound	Strand	Sequence (5'-3')	M calc	M found
PS siLin28B	AS	A*A*A*U*C*C*U*U*C*C*A*U*G*A*A*U*A*G*U*T*T	6920.38	6919.45
	S	A*C*U*A*U*U*C*A*U*G*G*A*A*G*G*A*U*U*U*T*T	6977.40	6976.11
scrambled PS siLin28B	AS	A*U*A*A*G*U*A*C*G*U*U*C*A*C*U*A*C*U*A*T*T	6920.38	6918.60
	S	U*A*G*U*A*G*U*G*A*A*C*G*U*A*C*U*U*A*U*T*T	6977.40	6976.12
PO siLin28B	AS	AAAUCCUCCAUGAAUAGUTT	6599.07	6598.83
	S	ACUAUUCAUGGAAGGAUUUTT	6656.09	6655.29
siLin28B II	AS	a* <u>A</u> *auc <u>C</u> uuccaug <u>A</u> a <u>U</u> agu*u*u	6913.65	6912.87
	S	a*c*uauu <u>C</u> a <u>U</u> G <u>G</u> aaggauuu*u*u	6970.65	6969.91
siLin28B III	AS	a*A*aucC*uuccaugA*aU*agu*u*u	6953.86	6953.01
	S	a*c*uauuC*aU*G*G*aaggauuu*u*u	7026.93	7025.93
ss PS guide	AS	A*A*A*U*C*C*U*U*C*C*A*U*G*A*A*U*A*G*U*T*T	6920.38	6919.45
Patisiran	AS	AUGGAAuACUCUUGGUuACTT	6660.07	6659.25
	S	GuAAccAAGAGuAuuccAuTT	6764.32	6763.61
Fitusiran	AS	u* <u>U</u> *g <u>A</u> <u>G</u> <u>A</u> <u>A</u> ugg <u>U</u> <u>g</u> <u>U</u> <u>U</u> <u>AC</u> c*a*g	7675.03	7674.09
	S	<u>G</u> *g* <u>U</u> <u>u</u> <u>A</u> <u>a</u> <u>C</u> <u>a</u> <u>C</u> <u>C</u> <u>A</u> <u>u</u> <u>U</u> <u>u</u> <u>Ac</u> <u>U</u> <u>u</u> <u>C</u> <u>a</u> <u>A</u>	6784.26	6783.30

Upper case = RNA, upper case + underlined = 2'-F, lower case = 2'-OMe, * = PS linkage. Patisiran sequence retrieved from [460] and fitusiran sequence retrieved from [461].

PO siLin28B was degraded more rapidly in serum than the PS analogue, but was still detectable after 10 h although not after 24 h. In the tritosome extract the PO siRNA was degraded immediately whereas the PS version showed intermediate degradation. Degradation of PS siLin28B was much more pronounced in tritosomal extracts than in mouse serum, with a half-life of approximately 2 h in tritosomes and 24 h in serum. Similar to the PO duplex, the PS single strand was degraded instantly in the tritosome extract, reflecting the increased nuclease stability of duplex RNA compared to single strands. On the other hand, siLin28B II

showed little degradation in serum and no degradation in the tritosome extract. Substitution of 2'-F nucleotides with RNA PS linkages led to increased degradation in tritosomes (~80% siLin28B III remaining after 24 h compared to ~100% for siLin28B II). To our surprise, patisiran was degraded immediately in the tritosome assay, despite displaying a serum stability profile that was comparable to PS siLin28B. As patisiran is approved as a LNP formulation, problems related to nuclease stability during trafficking were circumvented for the approved drug composition[4, 8]. Nevertheless, the striking differences between the stability profiles of patisiran in serum and tritosomes compared to the PS siRNA raised questions regarding the different mechanisms of degradation operating in serum and the lysosomal compartment and which chemical modifications are most suitable for the respective environments. Literature reports suggest, that 3'-exonuclease digestion is the main degradation path in serum[50], whereas 5'-exonuclease stability is required for endosomal trafficking and is the main determinant for efficacy of GalNAc siRNAs[182].

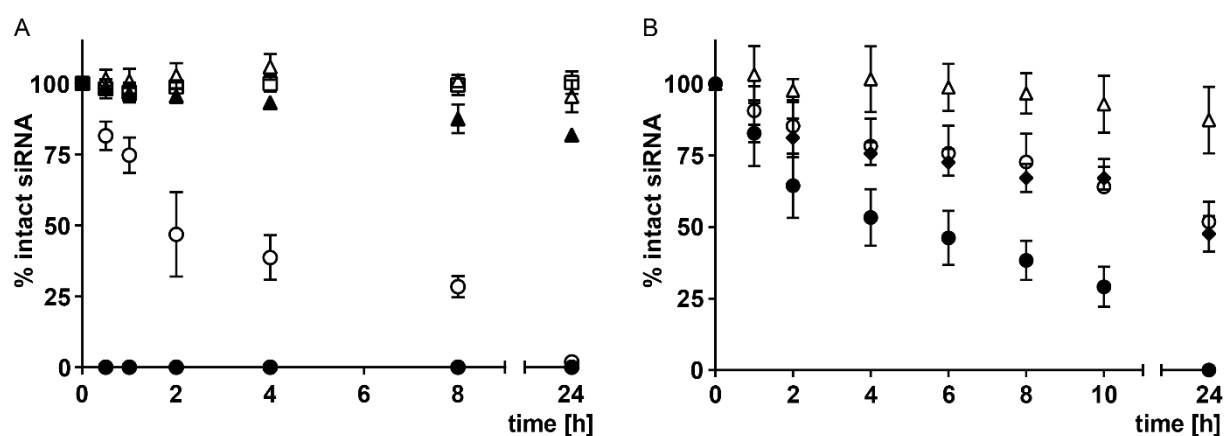


Figure 2. 7. Nuclease stability of different siRNA formats in mouse serum and rat liver tritosomes. A) Stability after incubation in rat liver tritosomes, pH= 5 at 37°C. ○ PS siLin28B, ● PO siLin28B, △ siLin28B II, ▲ siLin28B III, □ fitusiran. Complete degradation of patisiran and ss PS guide occurred instantaneously as for PO siLin28B and was omitted from the plot for the sake of clarity. Mean +/- SD shown from 3 independent replicates. B) Stability after incubation in 50% murine serum at 37°C. ○ PS siLin28B, ● PO siLin28B, △ siLin28B II, ◆ patisiran. Mean +/- SD shown from 3 independent replicates.

2.3.3 Methods to quantify PS siLin28B in tissue biopsies

Having established an efficient large-scale synthesis protocol along with the *in vitro* characteristics of a full PS siRNA directed against Lin28B, we turned towards the assessment of the biodistribution profile of the selected model PS siRNA. As a first step, a suitable method for the detection of PS siRNAs in tissue biopsies had to be developed. Due to the well documented influence of commonly used tags such as fluorescent dyes or radiolabels on the tissue distribution of oligonucleotides and frequent misinterpretations through detection of the free label, we decided to focus on label-free techniques[190, 462, 463]. Four different techniques have been investigated for tissue detection of PS siLin28B: Chemical ligation-qPCR (CL-qPCR), TaqMan RT-qPCR, northern blot and a PNA hybridization assay.

2.3.3.1 TaqMan RT-qPCR for quantification of PS siLin28B

TaqMan RT-qPCR (similarly stem-loop RT-qPCR [182]) is a widely used technique to quantify small RNAs such as miRNAs that are normally too short for efficient PCR amplification. Therefore, special stem-loop primers are used to increase the length of the amplicon. The fluorescent signal which is used to quantify the target RNA is generated through the Taq DNA polymerase mediated degradation of a so-called TaqMan probe during chain elongation. TaqMan probes are short oligonucleotides that are dually labelled with a fluorescent dye on the 5'-terminus and a quencher at the 3'-end. While the probe is intact, fluorescence is quenched through the proximity of the dye and the quencher moiety. With each round of amplification, an exponentially increasing amount of the fluorescent tag is released through degradation of TaqMan probes due to the 5'-nuclease activity of the Taq DNA polymerase. Quantification is based on the number of amplification cycles that are needed to cross a certain fluorescence threshold (Cp value). A scheme illustrating the TaqMan RT-qPCR work-flow is shown in Figure 2.8 A.

In order to quantify PS siLin28B, a set of specific primers and the TaqMan probe were designed by ThermoFisher. Primer and probe sequences were not revealed by the company. Initial attempts to quantify PS siLin28B according to the manufacturer's protocol failed due to an unexpectedly low Cp value for the no-template control (NTC) at 22 cycles (TaqMan set 1; Figure 2.8 C). A step-by-step troubleshooting suggested an unspecific self-amplification of the stem-loop RT primer in the presence of reverse transcriptase (Figure 2.8 B). Of note, DNA-dependent DNA polymerase activity is an often forgotten feature of reverse transcriptases[464]. The observed unspecific amplification could be reproduced after a new batch of TaqMan primers of the same design was provided by the company. Thereafter, a new assay kit with a new reverse primer design was provided and a small but insufficient reduction of the non-specific amplification was achieved (TaqMan set 2; Figure 2.8 C). Replacement of the routinely used MultiScribe Reverse Transcriptase by heat-resistant SuperScript III allowed us to perform the RT reaction at elevated temperature. We hypothesized, that an increased RT temperature might help to break potential secondary structures of the stem-loop primer that might cause the observed self-amplification. However, although non-specific amplification could be further reduced, a suitable linear range could not be reproducibly obtained. Additional reasons for the insufficient linear range could be the competition between the stem-loop primer and the passenger strand for annealing to the guide strand, a reduced activity of the reverse transcriptase on PS ORNs as well as an error-prone siRNA denaturing-transfer procedure prior to reverse transcription (see methods section and [208]). Adding Mn²⁺ to the reverse transcription buffer[465] could not reproducibly improve performance. Another important aspect regarding the overall sensitivity of TaqMan RT-qPCR is the requirement to dilute the

input sample for the RT reaction to 10-100 ng/ μ l total RNA as higher total RNA concentrations inhibit the reverse transcriptase. For example, 100 mg of liver biopsy typically yielded around 350 μ g of total RNA and therefore needed to be dissolved in at least 3.5 ml H₂O of which 1.25 μ l were used for RT.

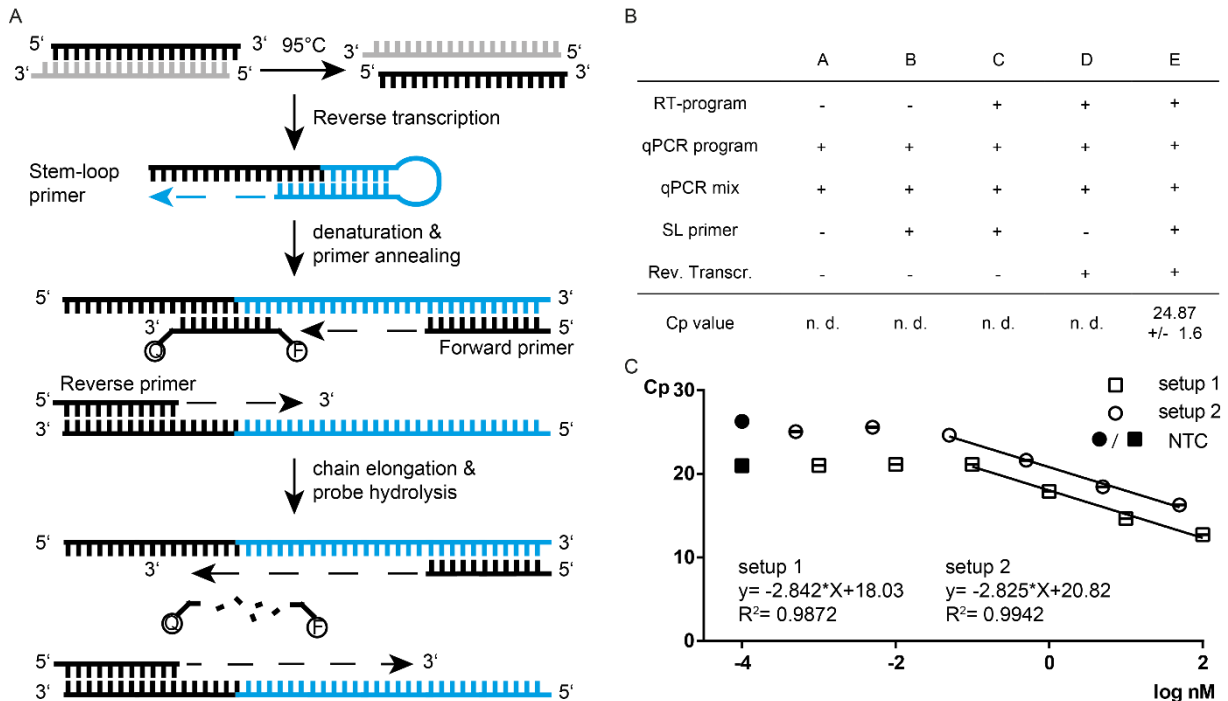


Figure 2. 8. TaqMan RT-qPCR for quantification of PS siLin28B. A) Scheme of TaqMan RT-qPCR quantification. B) Troubleshooting to identify unspecific amplification. A-E= reactions including the listed steps and reagents. C) Calibration curve of PS siLin28B. Setup 1= PS siLin28B in H₂O. Quantification using TaqMan set 1 and multiscribe reverse transcriptase at 37°C (□). Setup 2= PS siLin28B in mouse liver lysate (100 ng/ μ l total RNA). Quantification using TaqMan set 2 and SuperScript III reverse transcriptase at 55°C (○). Mean + / - SD from 3 technical replicates. NTC= No template control containing only matrix (H₂O or liver lysate) without PS siLin28B.

2.3.3.2 Chemical ligation-qPCR for quantification of PS siLin28B

Chemical ligation-qPCR (CL-qPCR) is a technique that was developed for the quantification of highly modified nucleic acids[206] and has been successfully used in our group to quantify anti-miRNAs inside RISC[207]. In the CL-qPCR protocol, the enzymatic reverse transcription step to convert RNA into DNA strands that are accessible to qPCR quantification is replaced by a template-dependent chemical ligation between sequence-specific 5' and 3' ligators (Figures 2.9, 2.10). The 3'-ligator binds to the 3'-half of the target sequence and has a 3'-PS terminus. The 5'-ligator is specific to the 5'-region of the query molecule and bears a 5'-BPS leaving group which can be replaced through a proximity driven nucleophilic attack of the 3'-PS group of the 3'-ligator. Because each ligator is otherwise composed of standard DNA, the nucleophilic substitution leads to the formation of a regular DNA strand in which a single bridging-oxygen at the ligation site is replaced by Sulphur. For the subsequent qPCR step, a fluorescently-labelled forward primer is used. Fluorescence of excess forward primer is

quenched through a complementary black-hole-quencher (BHQ) labelled anti-primer, which dissociates from the forward primer during chain extension. This results in an exponentially increasing fluorescence signal at the elongation step

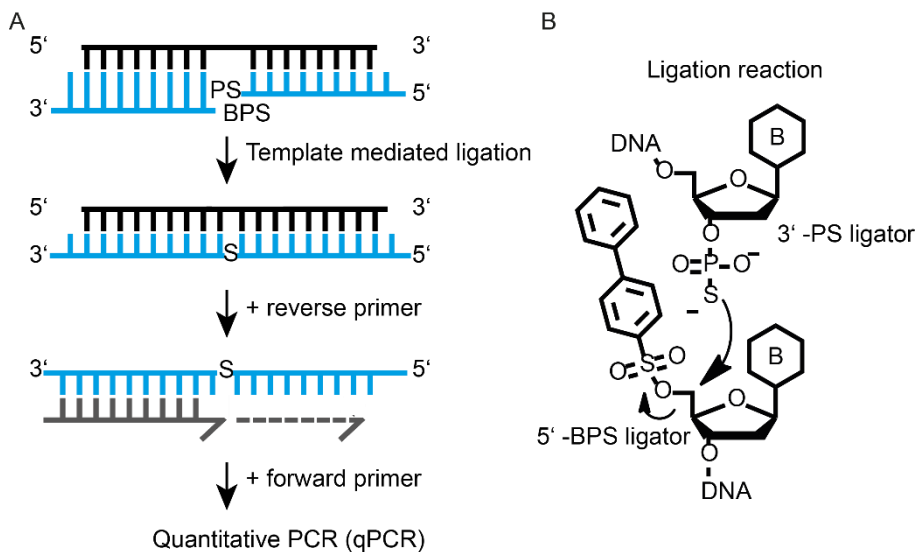


Figure 2. 9. Principle of CL-qPCR quantification. A) Scheme of CL-qPCR. B) Chemical ligation reaction.

Initial ligators and primers targeting the PS siLin28B antisense strand were designed according to Brunschweiler et al[207], but following the previously described protocol for 2'-OMe anti-miR quantification did not result in detectable signals for PS siLin28B standards. As a first step, the qPCR protocol was adjusted using a synthetic DNA ligation product, two different primer designs and different annealing temperatures (Figures 2.10 and 2.11 A, B).

AAAUCCUCCAUGAAUAGUTT	siLin28B guide
3'-TGACCAATTTAGGAAGGT-BPS-5'	5'-BPS ligator
3'-PS-ACTTATCAAAAACCAAATT-5'	3'-BPS ligator
3'-TGACCAATTTAGGAAGGTACTTATCAAAAACCAAATT-5'	ligation product
5'-ACTGGTTAAATCCTTCC	reverse primer
5'-ACTGGTTAAATCCTTCCATGAATAGTTTTGGTTAA-3'	1st amplification
3'-TTATCAAAAACCAAATTTAGCTCCCTCCCTC-Cy3-5'	forward primer 1
3'-GGTACTTATCAAAAACCAAATTTAGCTCCCTCCCTC-Cy3-5'	forward primer 2
5'-AAATCGAGGGAGGGAG-BHQ-3'	anti-primer

Figure 2. 10. Sequence scheme and comparison of forward primer designs 1 and 2. Ligator overhangs (adapters) are indicated in cyan, reverse primer sequence marked in magenta.

Due to the superior performance of primer design II, this setup was used to optimize chemical ligation conditions for the PS siRNA (Figure 2.11 C) and finally a calibration curve was prepared in liver lysate of untreated mice (liver tissue provided by Dr. Paulina Cwiek; Figure 2.11 D). Overall, the method was not suitable for the quantification of PS siLin28B in tissues under the tested conditions. In particular, elevated Cp values at higher concentrations prevented a reliable quantification. One reason for the inferior performance of CL-qPCR for PS

siRNA quantification compared to previously reported applications could be the reduced hybridization affinity of PS compared to PO ORNs, which is a key factor for efficient chemical ligation. Another reason could be the competition of the passenger strand with the ligators. In line with these explanations, CL-qPCR has been previously used for quantification of ssRNA with affinity-enhancing modifications such as 2'-MOE.

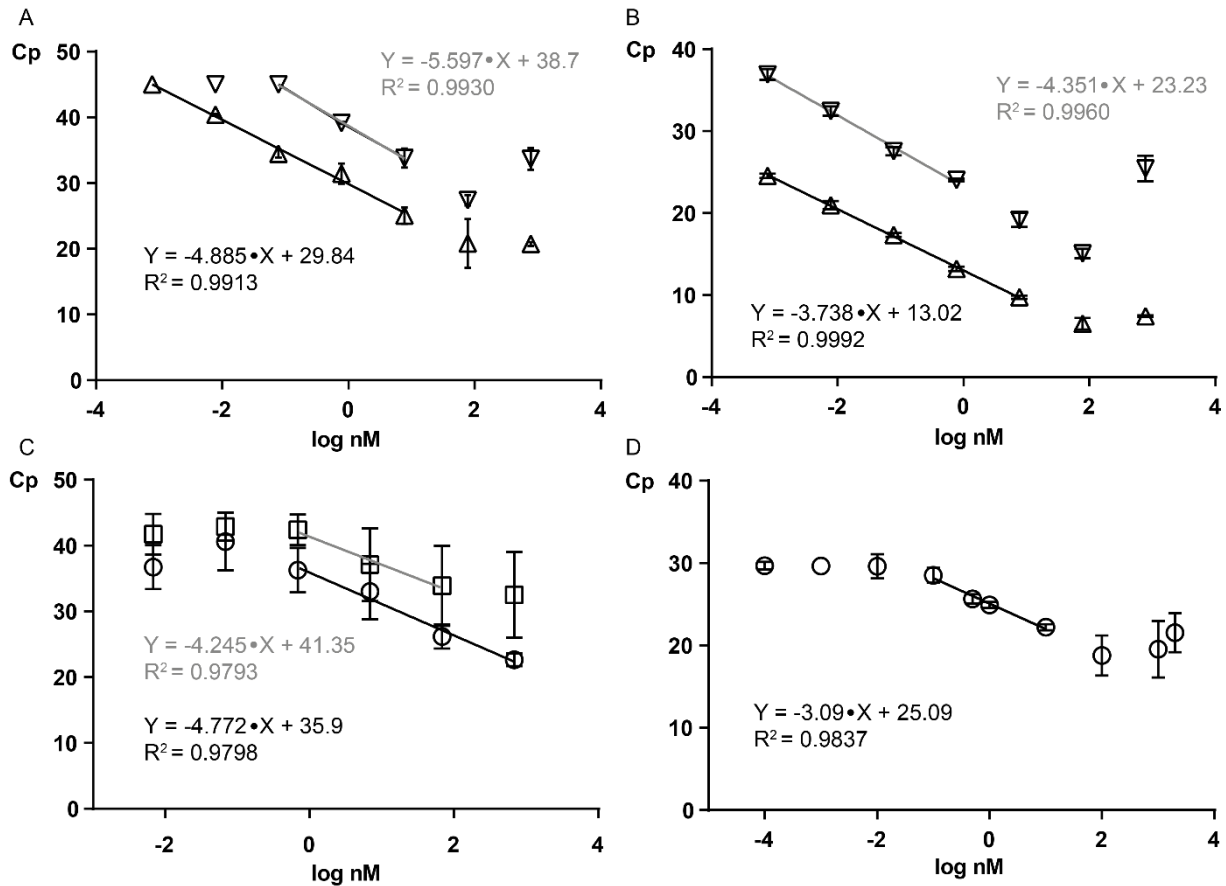


Figure 2. 11. CL-qPCR for quantification of PS siLin28B. A) qPCR with synthetic DNA ligation product with forward primer design 1 (∇) and 2 (Δ) in H_2O . Annealing temperature (T_a) at qPCR step was $45^\circ C$. B) qPCR with synthetic DNA ligation product with primer design 1 (∇) and 2 (Δ) in H_2O . $T_a = 48^\circ C$. C) CL-qPCR of PS siLin28B in H_2O using primer design 2, $T_a = 48^\circ C$. CL at $31^\circ C$ (\square) or $33^\circ C$ (\circ). D) Optimized CL-qPCR of PS siLin28B in mouse liver lysate using primer design 2, $T_a = 48^\circ C$ and CL at $33^\circ C$. Mean \pm SD from 3 technical replicates.

2.3.3.3 Northern blot for quantification of PS siLin28B

As a third method, northern blot was evaluated for tissue detection of PS siLin28B. This technique has previously been used in our group to detect PS siLin28B in Ago2-immunoprecipitates after transfection into HeLa cells[9]. An attractive feature of northern blotting is that no dilution of the input sample is required, partially compensating the generally lower sensitivity of the method compared to PCR based techniques. Nevertheless, the observed detection limit of 500 fmol (10 μ l, 50 nM) of PS siRNA in liver lysate was too high to be used for tissue detection after naked delivery (Figure 2.12). The low sensitivity is probably due to the relatively low affinity of the RNA probe towards the PS RNA. An attempt to increase

the sensitivity by the use of an LNA-enhanced northern probe was not successful. On the contrary, sensitivity was even reduced compared to the detection with an RNA probe (data not shown). Probably this is due to a lower phosphorylation efficiency of the LNA substrate by T4 polynucleotide kinase (PNK). In that case, the additional “cold”, non-phosphorylated LNA probe would compete with the radioactively labelled species and thereby reduce the overall sensitivity.

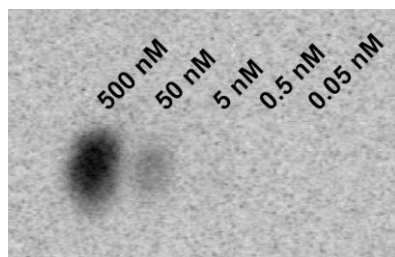


Figure 2. 12. Northern blot for quantification of PS siLin28B. Northern blot of decreasing concentrations of PS siLin28B in mouse liver lysate. 10 μ l of tissue lysate with indicated concentrations was loaded. Detection with a 32 P-labelled 21 nt RNA probe complementary to the PS siLin28B guide strand.

2.3.3.4 PNA hybridization assay for quantification of PS siLin28B

A recent development in the field of RNA therapeutics is the use of a PNA-hybridization assay to study the biodistribution of oligonucleotides[108-113]. The assay is based on the hybridization of the siRNA guide strand with a fluorescently labelled PNA probe in tissue lysate. Due to the high binding affinity of the PNA to the siRNA guide strand, the labelled probe can displace the competing passenger strand during a denaturation-annealing protocol. The resulting fluorescently labelled RNA-PNA hybrid duplex is then analyzed by anion-exchange HPLC (Figure 2.13). Because the PNA probe is not charged, the excess probe elutes in the void volume of the column together with other fluorescent matrix components whereas the PNA-RNA duplex is retained and elutes at higher salt concentrations. Integration of the fluorescence peak area can be used for quantification of the siRNA. An advantage of the hybridization assay in comparison with qPCR based methods is that it also delivers information on the integrity of the monitored RNA. Starting from literature examples[108-113], the HPLC gradient was optimized for detection of the PS siRNA. The lower limit of quantification (LLOQ) was 4.2 ng PS siLin28B (0.3 pmol) in 1 ml of tissue lysate. This is comparable to an LLOQ of 1 ng/ ml previously reported by Arrowhead pharmaceuticals[108] and 8 ng/ ml reported by Alnylam[182]. The higher sensitivity reached by the Arrowhead group can be explained by the use of a more sensitive fluorescence detector (Shimadzu RF-20Axs, H₂O Raman S/ N = 2000 compared to S/ N= 900 for our Hitachi Elite LaChrom L-2485). The lower sensitivity observed at Alnylam is probably due to the use of an atto425-labelled RNA probe instead of a high affinity PNA (termed atto probe assay instead of PNA hybridization assay). Based on the evaluation of the PNA hybridization assay, a protocol could be established that allowed the quantification

of PS siLin28B in tissue lysate in the anticipated concentration range of the biodistribution study (Figure 2.13 B, C)

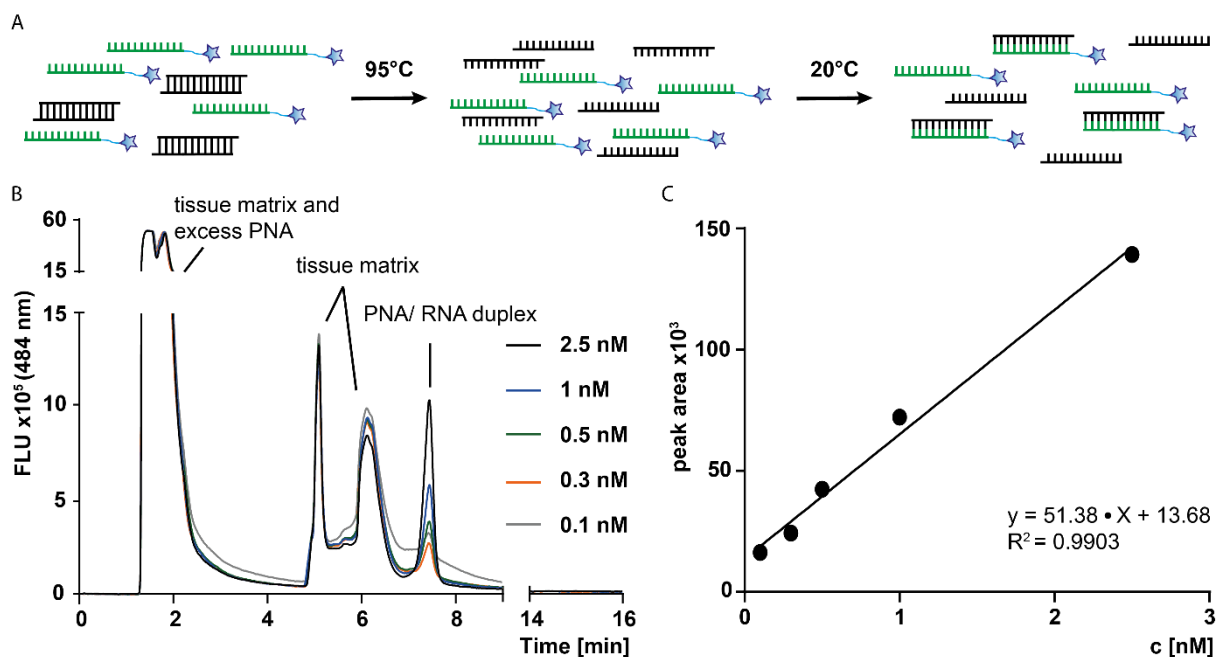


Figure 2. 13. PNA hybridization assay for detection of PS siLin28B in tissue lysate. A) Principle of siRNA detection with fluorescently labelled PNA probes. B) Superimposed fluorescence traces of anion-exchange HPLC after spiking decreasing concentrations of PS siLin28B into mouse liver lysate. Please note that the y-axis scale is changed above the break. C) Calibration of PNA hybridization assay in mouse liver lysate. Fluorescence peak area is plotted against concentration of PS siLin28B.

2.3.4 Biodistribution of PS siLin28B

A biodistribution study was performed in nude mice. Mice were s.c. injected with a single dose of 50 mg/ kg PS siLin28B in phosphate-buffered saline (PBS) or PBS alone and sacrificed 4 h after the injection. Selected tissues were snap-frozen after collection. All *in vivo* experiments were performed by Dr. Gianluca Civenni at the Institute of Oncology Research Bellinzona (IOR). Samples were then shipped to ETH for analysis using the PNA hybridization assay described above. The total distribution of PS siLin28B including metabolites is shown in Figure 2.14. Representative chromatograms are shown in the appendix (Figure 8.3). In general, PS siLin28B was detected in all analyzed tissues including prostate. Main sites of accumulation were liver and kidney, in line with previous reports of naked administration of chemically modified siRNAs[432, 466, 467]. Lowest levels were found in blood, consistent with a fast excretion and tissue distribution of circulating siRNAs. Total amounts of siRNA in tissues were comparable to previous studies that used dedicated formulations[108] and approximately 10-100x lower compared to a GalNAc conjugated fully modified siRNA[182]. However, amounts of siRNAs in the cytosol are generally much lower than the total tissue deposition[182]. One possibility to measure cellular uptake is the quantification of the 5'-phosphorylated fraction of an originally unphosphorylated siRNA[109]. In the case of PS

siLin28B a separation of the 5'-phosphorylated and unphosphorylated species was not possible due to the broad peaks corresponding to the PS RNA-PNA duplex (Figure 2.13 B and Figure 8.4). Quantification of siRNA-GalNAc conjugates in Ago2 tissue immunoprecipitates has been reported by RT-qPCR but not hybridization based HPLC analysis[182].

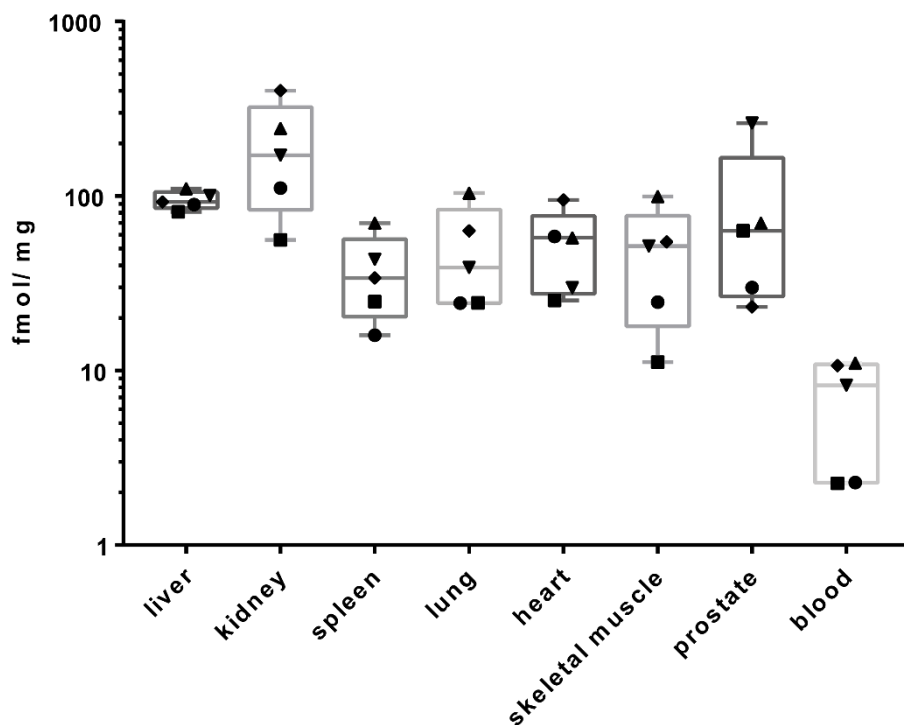


Figure 2. 14. Biodistribution profile of PS siLin28B in mice. Symbols indicate individual mice. Median is indicated by a horizontal mark. The edges of each box mark the 25th and 75th percentile. Whiskers extend to lowest and highest values. 1 fmol/ mg tissue corresponds to 0.014 ng/ mg.

2.3.5 Investigation of PS siLin28B in a prostate cancer xenograft model

The broad biodistribution of PS siLin28B (Figure 2.14) in conjunction with the good silencing activity in mammalian cells (Figure 2.5) prompted us to investigate the performance of this reagent in a mouse model of human prostate cancer. In collaboration with the group of C. Catapano (IOR Bellinzona), we have previously described the importance of Lin28B for the maintenance of CSCs in prostate cancer xenografts[329]. In close collaboration with the Catapano group, we designed a PC3 xenograft study that involved three s.c. injections per week of 50 mg/ kg PS siLin28B or scrambled control for two weeks (table 2.2). The dose of 50 mg/ kg was based on our biodistribution study and previous reports on the therapeutic administration of naked siRNAs[227, 228]. As a positive control, mice received s.c. injections of 5 mg/ kg PO siLin28B in complex with *in vivo* jetPEI.

Table 2.2. Treatment schedule for PC3 xenograft study

Compound	Dose (mg/kg)	Formulation	Schedule	number of mice
PS siLin28B	50	PBS	3 inj. /week	7
Scr PS siLin28B	50	PBS	3 inj. /week	7
PO siLin28B	5	In vivo jetPEI	3 inj. /week	7

In accordance with the treatment schedule, we applied our previously established synthesis protocol for the manufacture of 96 mg of PS siLin28B and the scrambled control, as well as 9.6 mg PO siLin28B (calculated for 64 injections and an average weight of 30 g per mouse). Individual doses (1.5 mg or 0.15 mg per injection) were lyophilized in screw-cap tubes and shipped to Bellinzona. As before, all *in vivo* experiments were performed by Dr. G. Civenni at the IOR.

Unfortunately, treatment with 50 mg/ kg PS siLin28B did not lead to a reduced tumor growth compared to administration of the scrambled control duplex (Figure 2.15). In general, tumor growth in both groups was slower than expected. Similar observations have been made by other researchers at the IOR who conducted similar, but unrelated, xenograft experiments at the time. Nevertheless, as the treatment with *in vivo* jetPEI formulated PO siLin28B showed a trend towards reduced tumor growth, we decided not to repeat the study.

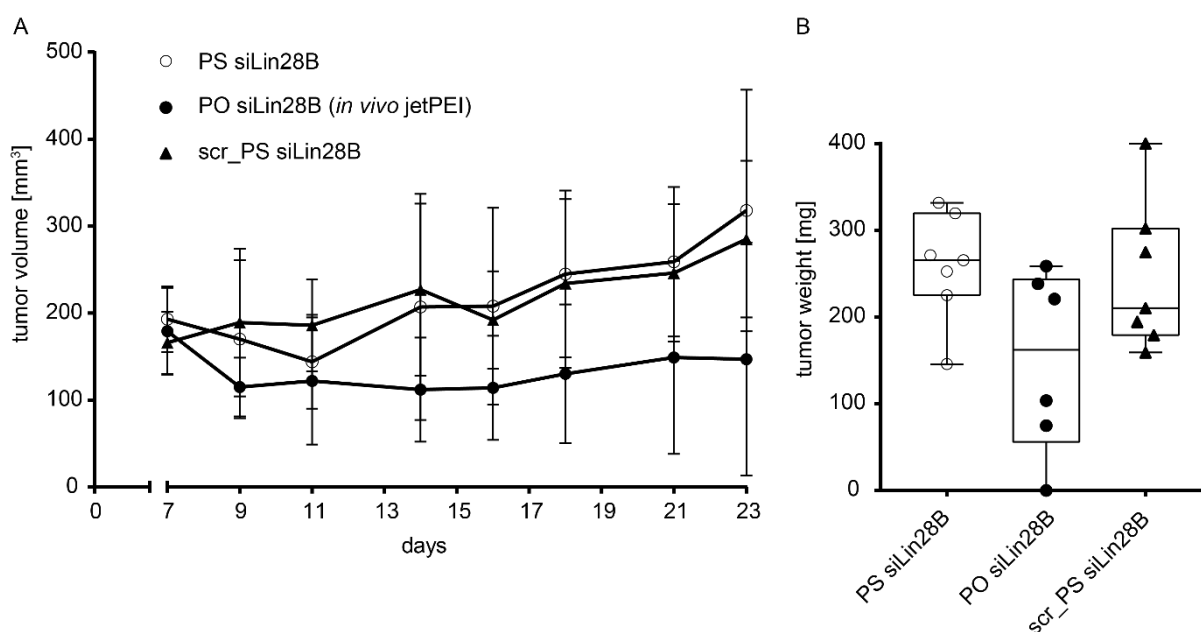


Figure 2. 15. Activity of PS siLin28B in a PC3 xenograft model. A) Tumor volume after repeated injections of PS siLin28B (50 mg/ kg in PBS), scrambled PS siLin28B (50 mg/ kg in PBS) or PO siLin28B (5 mg/ kg, in vivo jetPEI). Days are indicated as days after injection of PC3 cells. B) Tumor weight at the end of the study. Median is indicated by a horizontal mark. The edges of each box mark the 25th and 75th percentile. Whiskers extend to lowest and highest values. Symbols indicate individual mice. N= 7.

As reported previously, productive uptake of ORNs from the extracellular matrix is generally low[58, 182] and can be viewed as a two-step process: Productive internalization and endosomal escape. Productive uptake could be stimulated through specific targeting of cell surface receptors, as has been successfully demonstrated for GalNAc siRNA[134] and gapmer conjugates[241]. Nevertheless, despite receptor-mediated internalization, a high metabolic stability during endosomal trafficking is required[182, 183]. Although a number of cationic peptides[468] and small molecules[230, 469] have been investigated to facilitate endosomal escape, their use has been limited by cellular toxicity. Moreover, the endo-lysosomal compartment can serve as a cellular reservoir for sustained release of metabolically stable siRNAs[470]. Hence, combination of the full PS backbone with currently used ribose modifications may offer a route towards improved RNAi therapeutics.

2.4 Conclusion and Outlook

Building on our previous results[9], we have scaled-up the synthesis of full PS siRNAs from several micrograms to ~18 mg per synthesis run (Figure 2.4). This enabled a detailed investigation of this promising siRNA scaffold. We could demonstrate a good gene silencing activity of a model PS siRNA in mammalian cells (Figure 2.5) along with vastly improved nuclease resistance compared to the PO duplex (Figure 2.7). In line with previous reports on a lower protein binding capability of duplex RNAs compared to single stranded 2'-MOE PS ORNs[4], we observed a weak albumin-binding of our model PS siLin28B. However, protein-binding of PS siLin28B was increased compared to the PO analogue, at least under the conditions of the gel-shift assay (Figure 2.6 B). Furthermore, we identified a PNA hybridization assay as a suitable method to quantify PS siRNA accumulation in tissue biopsies (Figure 2.13). We then used this assay to characterize the biodistribution profile of PS siLin28B (Figure 2.14) and investigated its activity in a xenograft model (Figure 2.15). Despite the broad biodistribution of PS siLin28B in nude mice, no reduction in tumor growth was observed after repeated injections in a PC3 xenograft model of human prostate cancer. Although the lack of activity could be partially explained by the generally weak tumor growth, reduction of the tumor volume upon treatment with *in vivo* jetPEI formulated PO siLin28B points towards a weak uptake of the PS siRNA into the tumor cells. Another reason could be a poor penetration of the naked siRNA into the tumor tissue.

For the future, a combination of the full PS scaffold with additional ribose modifications might offer an attractive route to develop RNAi therapeutics with improved PK properties. Another option is the use of PS RNA building blocks for the replacement of 2'-F nucleotides, in case further evidence for 2'-F-related toxicity builds up[4, 186, 188]. Furthermore, substitution of the PO backbone with stereodefined PS linkages might be a possibility to specifically tailor the PK properties of siRNAs while maintaining their potency. The broad biodistribution of the model

PS siRNA indicates that application of the PS backbone chemistry might be particularly useful to reach tissues beyond the liver. For this purpose, conjugation of PS siRNAs to different targeting moieties might be investigated in order to promote productive uptake after tissue deposition.

2.5 Contributions

Scale-up optimization was performed by Mauro Zimmermann and Christian Berk. Synthesis of oligonucleotides, gel-shift assays, melting studies, CL-qPCR, northern blots and nuclease stability assays were performed by Christian Berk. Western Blot and SYBR Green RT-qPCR was performed by Dr. Yuluan Wang. TaqMan RT-qPCR was done by Anne Lüscher, Dr. Yuluan Wang and Christian Berk. PNA-hybridization assays were performed by Dr. Christian Steuer and Christian Berk. *In vivo* experiments were performed by Dr. Gianluca Civenni.

3 Project 2 – Polyamine-siRNA conjugates as novel RNAi reagents

3.1 Introduction

3.1.1 Biological relevance and nucleic acid binding characteristics of polyamines

The natural polyamines putrescine, spermidine and spermine are ubiquitously biosynthesized in mammalian cells and are involved in various physiological processes such as immunity, aging, hair growth and wound healing[471]. Polyamines are well-known to interact with DNA as well as RNA, although with a higher affinity for RNA, and to influence the 3D structure of nucleic acids[472, 473]. These interactions are not limited to ionic interactions of the positively charged amino groups with the negatively charged nucleic acid backbone but also involve hydrogen-bonding to the nucleobases[474] and 2'-hydroxyl groups [475]. X-ray, NMR and molecular docking studies indicate that free spermine preferentially binds to the major groove of RNA[474, 476-478] and that spermine has a higher affinity for dsRNA than ssRNA[479, 480]. Therefore, various polyamines have been used for conjugation to DNA and RNA oligonucleotides in order to increase their hybridization affinity (reviewed in [114]). In addition, spermine and various synthetic analogues have been developed as novel delivery vehicles for the transfection of nucleic acids[481, 482].

3.1.2 Conjugation of polyamines to oligonucleotides – polyaminooligonucleotides

Since polyamines offer a simple way to modulate the hybridization properties of synthetic oligonucleotides, they have been widely used for nucleic acid chemistry. The various synthetic approaches of grafting spermine onto DNA and RNA oligomers have been reviewed by Menzi et al[114]. In brief, among the various polyamines, spermine has been most frequently used for conjugation at various positions of oligonucleotides. The most notable example of these so called polyaminooligonucleotides (Figure 3.1) is the conjugation of oligophosphospermine-units to the 5' end of DNA. Such ODNs have been commercialized as zip nucleic acids (ZNA) for the fine-tuning of primer melting temperatures[483, 484]. The same approach using RNA oligonucleotides resulted in the generation of cationic siRNAs which have shown increased serum stability *in vitro* and sub-micromolar activity under free uptake conditions in mammalian cells[485, 486]. However, a large number of terminally conjugated phosphospermine units was necessary to achieve cellular uptake ($N/P > 1.5$), leading to a tedious and inefficient purification process.

Additionally, spermine has been attached to the 2'-O-position of RNA and various locations on the nucleobase with a general trend of increased duplex melting temperatures[114]. Of particular interest for this project is the conjugation to major groove binding positions on the nucleobase. Prakash et al. introduced spermine at the 4 position of 5-methyl-2'-deoxycytidine

and incorporated this modified building block into short DNA sequences, which resulted in a slightly decreased melting temperature of the ODN-DNA duplex[487]. In a later account, the Markiewicz group used a similar strategy to incorporate *N*⁴-spermine-tethered 2'-deoxycytidine into DNA oligomers at different positions and found an increase in duplex stability by 4°C per modification[488]. These apparent inconsistencies can be rationalized in view of a recent NMR study which showed that a propargyl-residue attached to the *N*⁴-position of dC is preferentially oriented toward the Watson-Crick face of the ODN, thus slightly reducing the duplex melting temperature by 1°C. However, when an additional 5-methyl group was present, thus impeding the rotation of the propargyl moiety, a drastic drop in melting temperature of 10°C has been observed[489]. Furthermore, an NMR study with an octamer ODN carrying a spermine-tether at the *N*⁴-position of dC indicated that the covalently bound spermine resides in the major groove of an ODN-DNA duplex, pointing towards the 3' terminus of the modified strand and only loosely aligned to the phosphodiester backbone[488]. More recently, Menzi et al. showed that a single polyamine residue conjugated to the 5-position of uridine (major groove) of 2'-OMe ORNs (12 nt in length) led to an increase in *T*_m of up to 12°C[115]. Additional studies have been conducted using aminated 2'-amino-LNA (minor groove)[490], *N*⁶-spermine-tethered dA (major groove)[491, 492] and *N*²-spermine-tethered dG (minor groove)[493-495], again demonstrating an increased thermodynamic stability of ODN-DNA duplexes while maintaining mismatch discrimination.

3.1.3 The polyamine transport system (PTS)

Albeit polyamine transport into cells has been the subject of several recent studies, little is known about the molecular architecture of the mammalian transporters involved. The first human polyamine transporter, a member of the cation-chloride-cotransporter family (CCC9a, SLC12A8A) has been identified in 2009[496]. CCC9a has been shown to promote polyamine uptake in stably transfected HEK293T cells, with a preference for spermidine over spermine and putrescine.

Recent interest in the mechanism and structural requirements for selective uptake via the polyamine transporters has grown since many tumor cells have been reported to express an overactive PTS[497-499]. So far different small molecules, such as anthracene[500], naphthalimide[501], benzazepine[502] and stigmasterol[503] have been successfully conjugated to polyamines to achieve cell-type specific cytotoxicity. The most interesting examples of this conjugation approach are two high-molecular-weight cytotoxic agents. One is the anticancer drug F14512 (Figure 3.1), which is currently investigated in clinical trials and consists of an epipodophyllotoxin core coupled to a spermine side chain[504]. The cytotoxicity of this compound in 13 leukemia cell lines showed strong correlation with the level of PTS activity as measured using a spermine-conjugated fluorescent probe[505, 506]. An adaption

of this protocol for blood, bone marrow, ovarian cancer and acute myeloid leukemia (AML) samples was used to select patients for clinical trials[507-510].

The other is bleomycin-A5 (BLM-A5), a naturally occurring glycopeptide with a molecular weight of 1440 Da (Figure 3.1). BLM-A5 is a spermidine-conjugate of the anticancer drug bleomycine. *In vitro* data suggests that specific uptake of BLM-A5 is mediated by the human carnitine transporter SLC22A16 (also referred to as hCT2, OCT6, OKB1, CT2 or Flip2), which was thereby shown to play an important role in polyamine uptake[511]. SLC22A16 has been previously characterized as a testicular carnitine transporter with 12 transmembrane domains and has been associated with the bidirectional transport of L-carnitine[512] and doxorubicin uptake into cancer cells[513]. Of note, the highly SLC22A16 expressing testicular cancer cell line NTERA-2/ cl. D1 (NT2/ D1) was 4-fold more sensitive to BLM-A5 than to the commonly used BLM-A2, which does not contain a polyamine moiety, or blenoxane, which contains a mixture of various bleomycine derivatives. Furthermore, addition of L-carnitine to the growth medium protected NT2/D1 cells from BLM-A5 cytotoxicity and overexpression of SLC22A16 in otherwise BLM-A5 resistant HCT116 cells led to a 3-fold increase in fluorescein-labeled-BLM-A5 uptake and increased cytotoxicity, whereas response to control treatment with cisplatin was not altered[511]. SLC22A16 shows a tissue-specific expression pattern with a high abundance in testis and moderate levels in the bone marrow. In addition, an RT-qPCR screen identified several SLC22A16 expressing tumor cell lines of which the well-established hepatocarcinoma cell line Huh7 showed the highest expression levels[513].

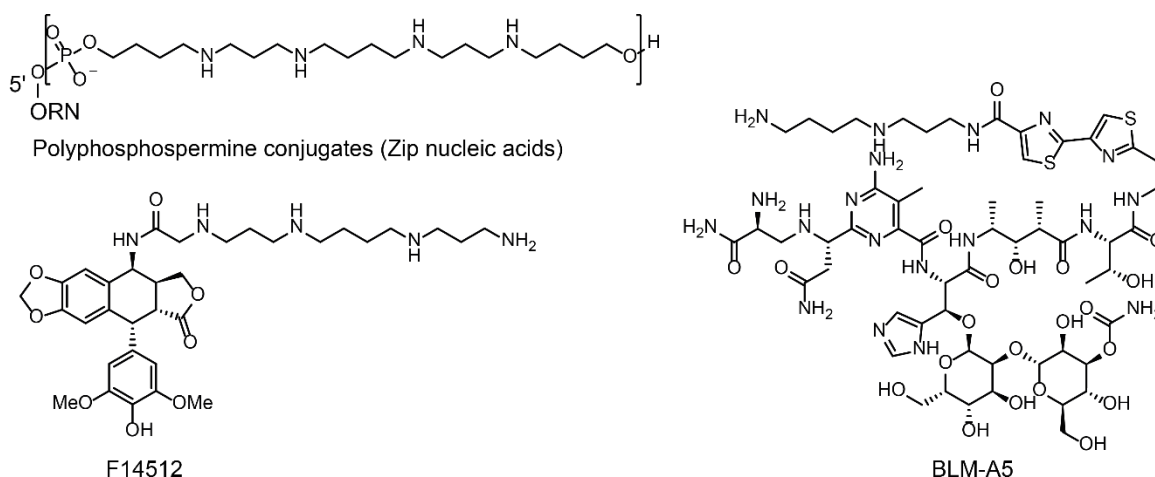


Figure 3. 1. Structures of ZNA and small molecule-polyamine conjugates

3.1.4 The convertible nucleoside approach

The basis of the ‘convertible nucleoside’ approach is the use of nucleoside analogues which contain a leaving group that can be displaced in a nucleophilic substitution reaction by different thiol or amino-containing molecules[514]. Such ‘convertible nucleosides’ are typically inserted into the oligonucleotide chain during solid-phase synthesis and subsequent substitution leads

to site-specific functionalization of the ORN. Nevertheless, substitution can also be performed on the phosphoramidite level, prior to oligonucleotide synthesis. The approach was first described in the early 90's as a means to site-specifically label various positions on the nucleobase and a number of leaving groups were investigated. The first example was the use of an *O*⁴-trimethylphenyl-dU (TMP dU) phosphoramidite for the generation of N⁴-alkyl dC residues[515]. Shortly thereafter, the scope of the method has been extended to N⁶-adenosine using *O*⁶-phenyl[137] and p-chlorophenyl leaving-groups[136, 516] and to the guanosine N²-position via *O*-6-(p-nitrophenyl)-2-fluorodeoxyinosine units[495, 516, 517]. Our studies have focused on the use of the convertible nucleoside *O*⁴-triazolyluridine, which has been initially reported by Shah et al.[139, 140, 142] and has been previously used in our group to generate N⁴-methylated ORNs[518].

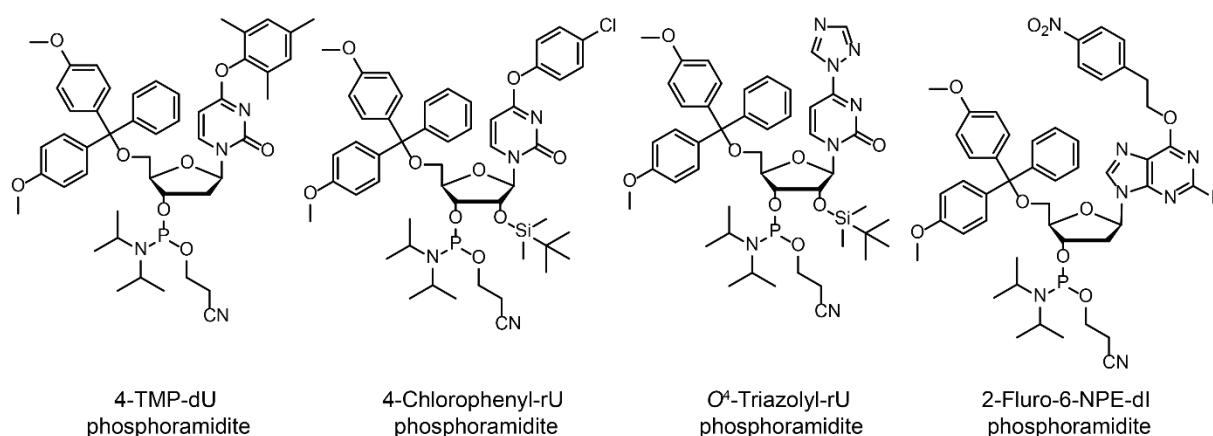


Figure 3. 2. Structures of various convertible nucleosides

3.2 Project outline

The goal of this project was the investigation of major-groove spermine-siRNA conjugates as a novel type of RNAi reagents. The basis of the project were findings of Menzi et al. who described an increase of up to 12°C in *T*_m upon major groove modification of 2'-OMe ORNs with spermine[115]. The tremendous increase in *T*_m was specific to the major groove directed C5 position of cytidine compared to the 2'-O position, which points towards the minor groove. We hypothesized that an increase in *T*_m would enhance the stability of siRNAs against nuclease degradation by limiting the “breathing” of the duplex. Reducing the spontaneous dissociation of the terminal base pairs is important for the metabolic stability of siRNAs because nuclease digestion preferentially occurs on single stranded regions of the duplex[51]. This is in line with earlier reports that siRNAs with an increased *T*_m generally exhibited a greater nuclease stability than those with a lower *T*_m[9]. Increased thermal duplex stability has also been correlated with increased on-target and reduced off-target activity due to a preferential loading into Ago2 compared to the other Argonaute family members[519]. Spermine conjugation was also demonstrated to influence the kinetics of target binding by

increasing the k_{on} , which is thought to be beneficial in catalytic mechanisms such as RISC induced RNA cleavage[115]. Furthermore, spermine conjugation was reported to facilitate gymnotic delivery of siRNAs in cell culture, albeit only at N/ P ratios > 1.5[485, 486]. Another aspect of the project was an evaluation of the practicability of the convertible nucleoside approach for the introduction of various moieties into a major groove binding position of RNA.

3.3 Results and discussion

3.3.1 Synthesis of an siRenilla-spermine conjugate library

In order to characterize the influence of major groove spermine conjugation on the activity and nuclease stability of siRNAs, the “convertible nucleoside” 5'-DMT-2'-O-TBDMS-O⁴-triazolyluridine-CED-phosphoramidite was synthesized from commercially available 5'-DMT-2'-O-TBDMS-uridine-CED-phosphoramidite in a one-step procedure as described by Shah et al. [142] (Figure 3.3 A). The convertible nucleoside O⁴-triazolyluridine served as the basis for the solid-phase synthesis of a site-specifically modified siRenilla library (Figure 3.3 B, Table 3.1).

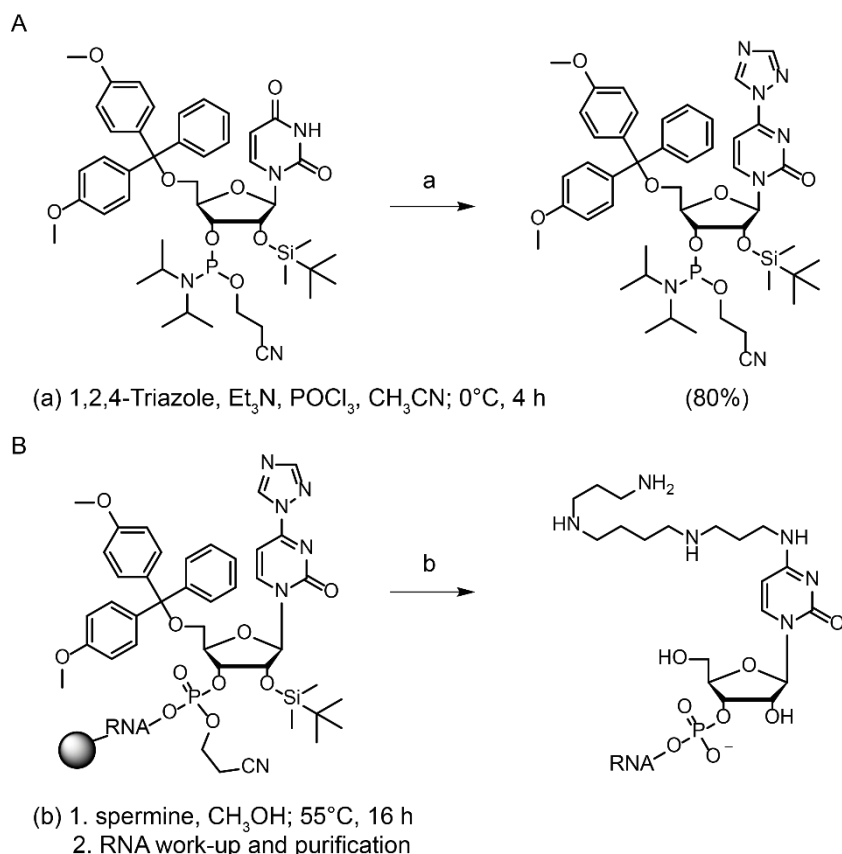


Figure 3. 3. Synthesis of ORN-polyamine conjugates. A) Synthesis of the convertible nucleoside O⁴-triazolyluridine. B) Incorporation of the convertible nucleoside into RNA and displacement by spermine.

In a first step, the convertible nucleoside was used for the synthesis of a single-modified siRenilla-spermine antisense strand (si-spm4 AS, table 3.1) in order to identify suitable

conditions for spermine conversion. For this purpose, a large batch of the siRenilla-conjugate was synthesized. The CPG was divided into 20 mg portions and different conditions for spermine conversion were tested. Best results were obtained after overnight incubation of ORNs with a solution of 1 M spermine in MeOH at 55°C followed by desalting via Glen-Gel Pak columns and additional AMA deprotection for 1 h at 65°C (Figure 3.4).

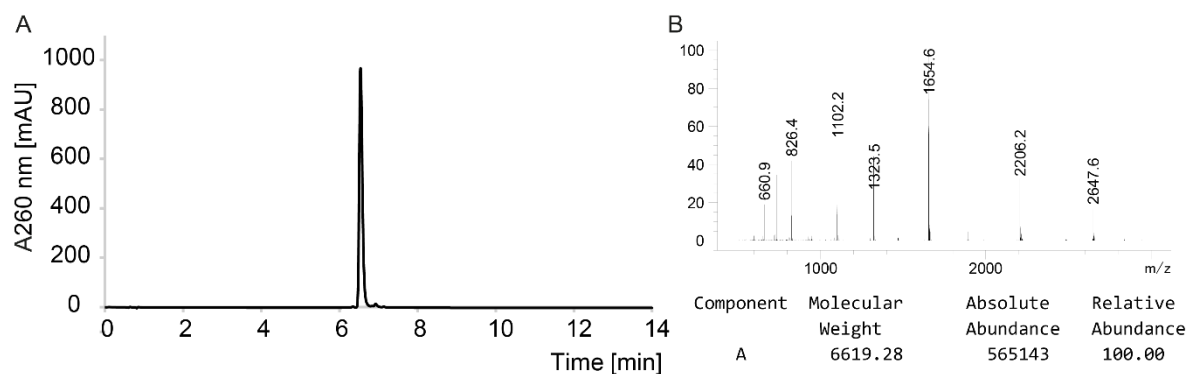


Figure 3. 4. LC-MS analysis of si-spm4 AS after HPLC-purification. A) UV-trace. B) MS at 6.5-6.6 min, M calc= 6621.02.

In order to gain insights into the regioselectivity of the spermine conversion, nucleophilic substitution was performed in the presence of diethylamine and spermine (1:1 and 2:1 ratio). Even in the presence of excess diethylamine, only 9% of the ORN had reacted with diethylamine, indicating a preferred nucleophilic attack via the primary amino groups of spermine (Figure 3.5). This in line with earlier reports which showed a higher nucleophilicity of the primary amino groups of polyamines[491, 520, 521].

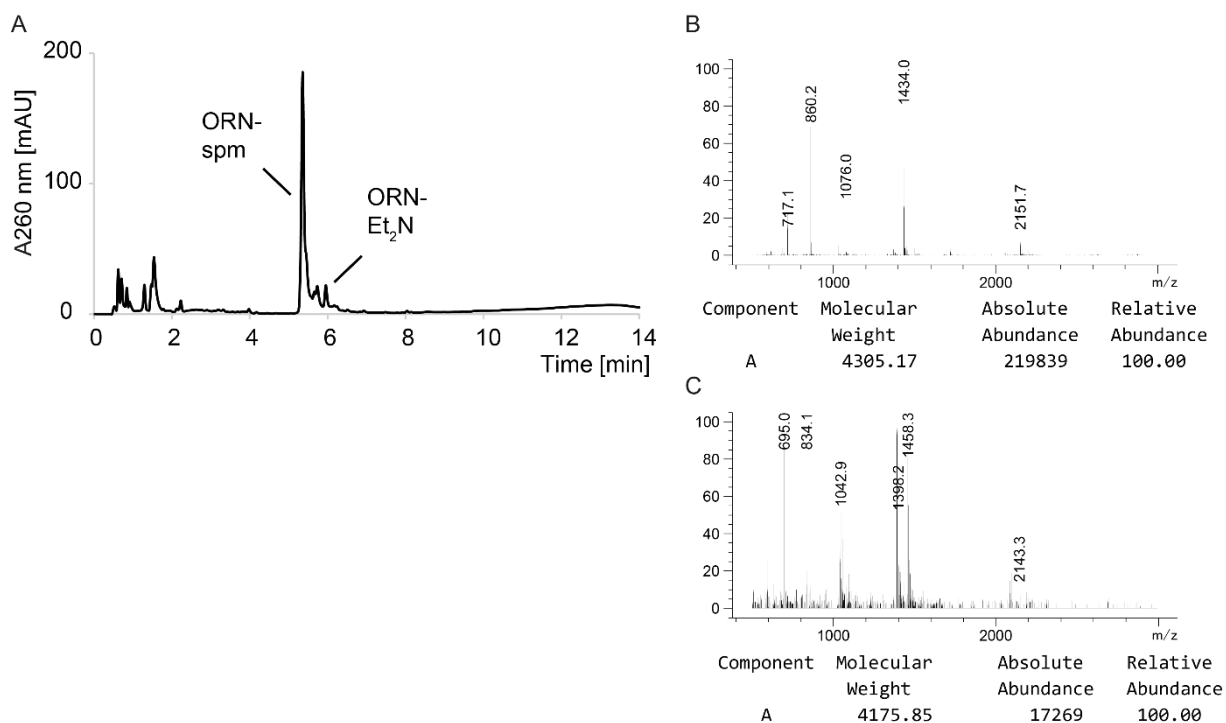


Figure 3. 5. LC-MS analysis of crude ORN (DMT-on) after competition between spermine and diethylamine (1:2) for nucleophilic substitution. A) UV trace. B) MS at 5.4 min. M calc (DMT-on, ORN-spm) = 4305.97. C) MS at 6.0 min. M calc (DMT-on, ORN-Et₂N) = 4176.86

A drawback of all procedures using free spermine was the appearance of side products in the crude ORN mixture (m+42 and in some cases also m+84, Figure 3.6 A-D). This is consistent with an intramolecular transamidation in which an acetyl protecting group from *N*⁴-acetylcytidine is transferred to a free amino group of spermine. The impurities could be removed during RP-HPLC purification (Figure 3.6 E-F).

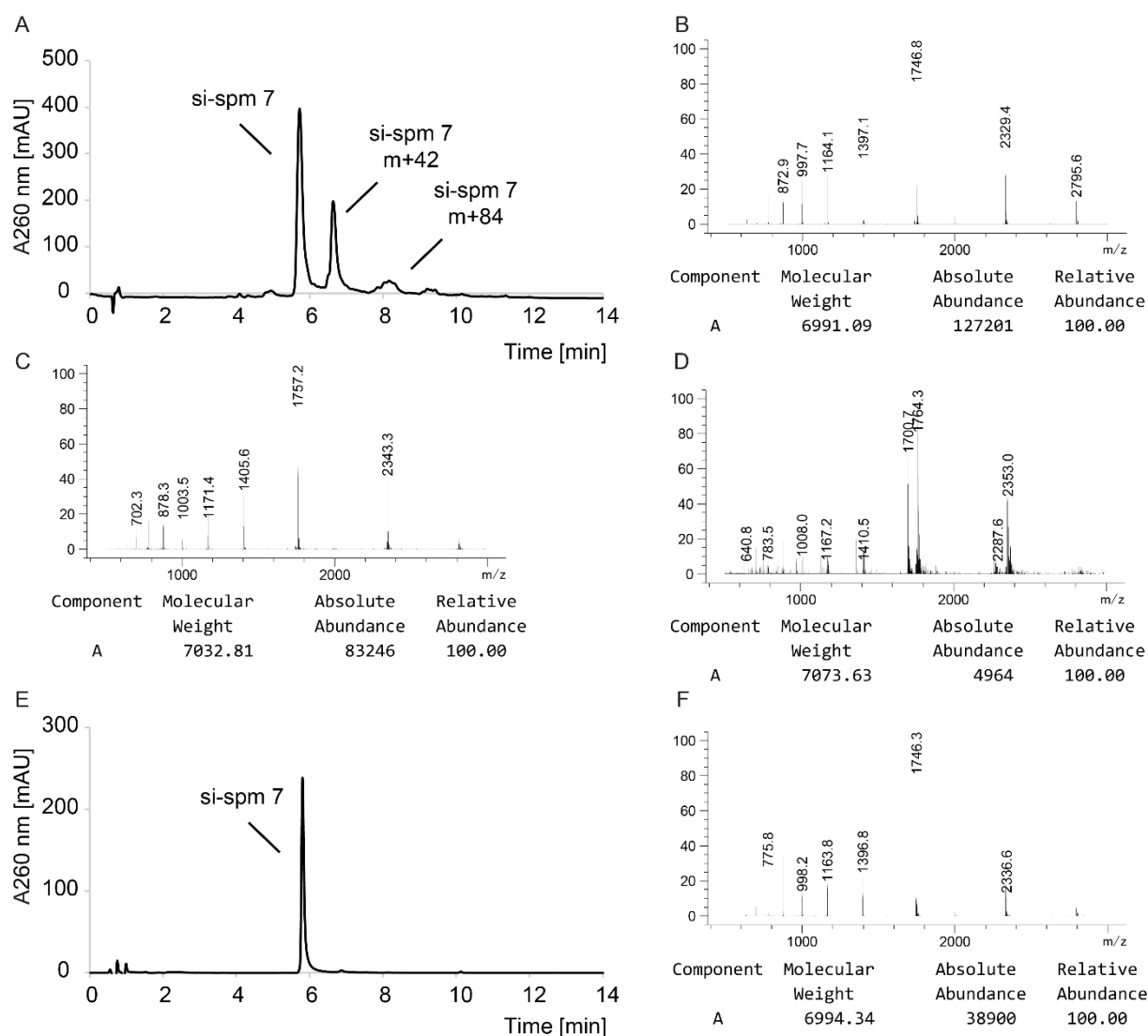


Figure 3. 6. LC-MS analysis of si-spm7 AS after detritylation (A-D) and HPLC purification (E-F). A) UV trace before purification. B) MS from A at 5.7-5.8 min. C) MS at 6.6-6.7 min. D) MS from A at 8.1-8.3 min. E) UV trace after purification. F) MS from E at 5.8-5.9 min. M calc= 6991.44.

In order to prevent acetylation, the monoprotected spermine derivatives *N*¹-trityl spermine and spermine azide were synthesized[522, 523] (Figure 3.7) and tested for applicability in the convertible nucleoside approach. Unfortunately, no conjugation product could be isolated after reaction of ORNs with protected spermine derivatives. In the case of *N*¹-trityl spermine, no crude oligonucleotide could be detected after work-up. Although a crude ORN was detected after conversion with spermine azide, the yield was too low to recover the siRNA-conjugate after RP-HPLC purification. Spermine azide was further used for the synthesis of si-spm8 via click reaction with a 3'-terminal 2'-O-propargyl cytosine modified siRenilla sense strand (appendix, Figure 8.15).

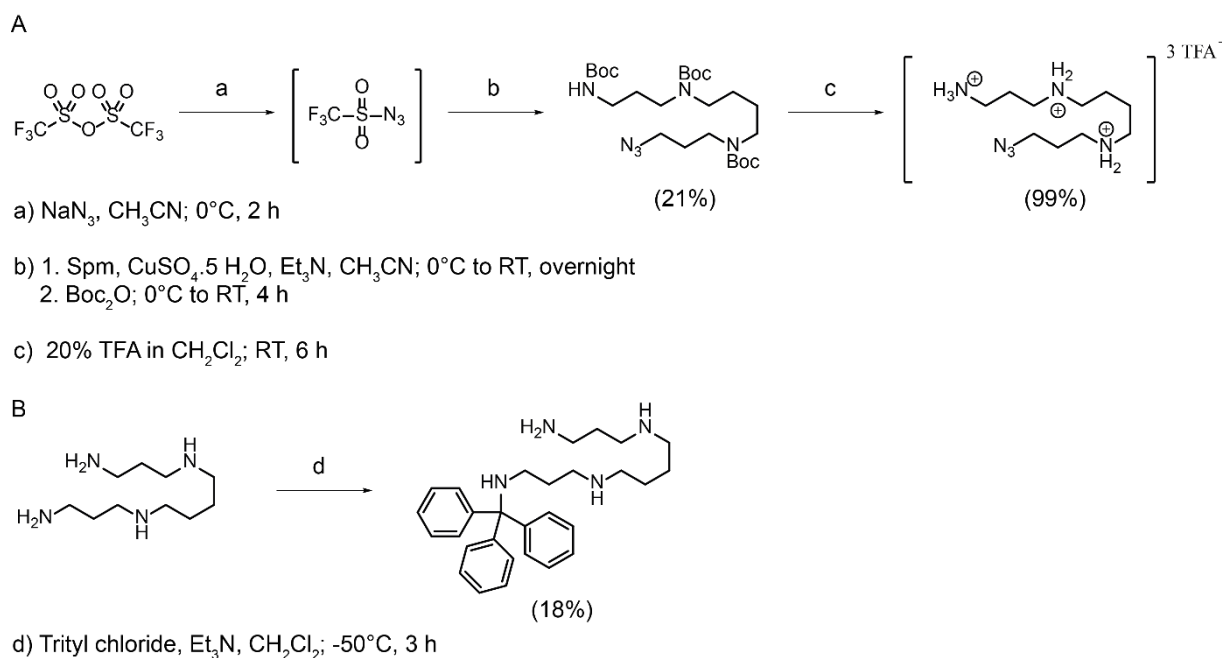


Figure 3. 7. Synthesis of protected spermine derivatives. A) Synthesis of spermin- $\text{N}_3 \cdot 3\text{TFA}$ according to Yamada et al.[523] B) Synthesis of N^1 -trityl spermine modified from Krakowiak et al. [522]

Due to the markedly reduced conjugation efficiency with monoprotected spermine derivatives, we decided to pursue the simpler conjugation strategy with unprotected spermine and synthesized an siRenilla-spermine-conjugate library consisting of single and multi-modified ORNs. Spermine modifications were introduced at various positions across the antisense strand in order to evaluate position-dependent effects on the activity of siRenilla-spermine-conjugates (Table 3.1).

Table 3. 1. siRenilla-spm library

Compound	Strand	Sequence (5'-3')	M calc	M found
siRenilla	AS	UUUCUCGCCCUCUUCGCUCUU	6436.80	6436.16
	S	GAGCGAAGAGGGCGAGAAAUU	6901.29	6901.23
Scr_si-spm	AS	CUUCUCCUUCGCGUUCUCCUX	6621.02	6620.04
	S	GAGGAGAACGCGAAGGAGAAG	6963.37	6962.34
si-spm1	AS	UUUXUCGCCCUCUUCGCUCUU	6622.01	6621.60
si-spm2	AS	UUUCUCGCCCUCUUCGCUCXU	6621.02	6620.47
si-spm3	AS	UUUCUCGCXCUCUUCGCUCUU	6622.01	6620.93
si-spm4	AS	UUUCUCGCCCUCUUCGCUCUX	6621.02	6620.26
si-spm5	AS	UUUCUCGCCCUCUUCGCUCXX	6805.25	6803.98
si-spm6	AS	UUUCUCGCCCUCUUCGCUXXX	6990.46	6989.87
si-spm7	AS	UUUXUCGCCCUCUUXGCUCXU	6991.44	6989.37
ORN-spm/ Et ₂ N	-	DMT-CGXGAGAAAUUC	spm 4305.97	4305.17
			Et ₂ N 4176.86	4175.85

All linkages are RNA-PO. X indicates spm-C after replacement of O⁴-triazolyluridine.

3.3.2 UV-melting of siRNA-spermine conjugates

The T_m of siRenilla-spermine conjugates could not be accurately measured because the melting curve did not reach a plateau due to the high T_m of the unmodified duplex (Figure 3.8). However, an increased T_m could be qualitatively inferred from a shift of the asymptotic phase in the melting curve of the spermine-conjugate towards higher temperatures and is in accordance with previous observations on the thermodynamic stability of major-groove polyamine conjugates[114, 115]. However, the increase in T_m appears to be milder than previously observed[115].

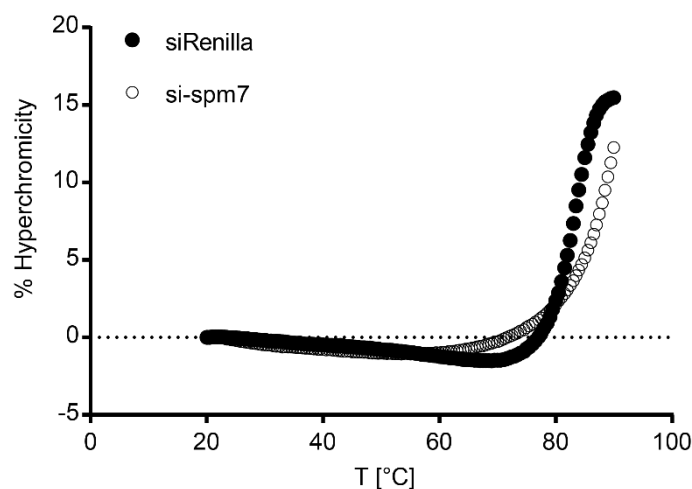


Figure 3. 8. UV melting of 3 μ M siRenilla and si-spm7. T_m siRenilla \approx 82.6°C. T_m of si-spm7 could not be measured.

3.3.3 Activity of siRenilla-conjugates in Dual-Luciferase reporter assays

To evaluate position-dependent effects of spermine-conjugation, the siRenilla library was evaluated in a Dual-Luciferase reporter assay after Lipofectamine 2000 mediated delivery into HeLa and Huh7 cells (Figure 3.9). A single spermine modification in the 5'-region of the antisense strand mildly reduced the activity (si-spm1). Conjugation was well tolerated at the 3' terminus (si-spm1), including a consecutive triple substitution (si-spm6). Interestingly, spermine modification on position 9 nearly abolished activity of the siRNA. Of note, position 9 is in close proximity of the RISC cleavage site[347, 348] and therefore the covalently bound spermine moiety might induce structural perturbations at the AGO2 active site or affect the local RNA duplex geometry. Alternatively, spermine could prevent the efficient release of the passenger strand or the target and thereby reduce the cleavage rate of the RISC complex.

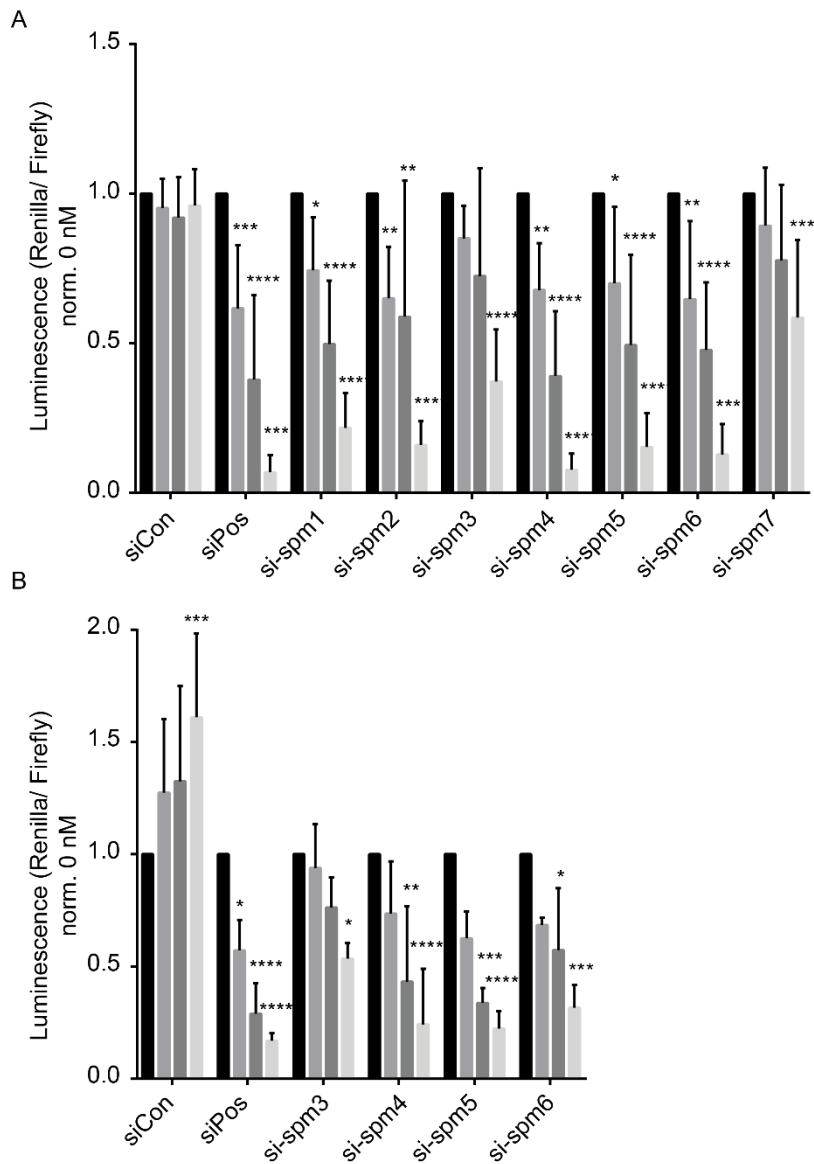


Figure 3. 9. Activity of the siRenilla-spm library in (A) HeLa and (B) Huh7 cells. Increasing siRNA concentrations from left to right. HeLa: 0, 1.25, 5, 20 nM. Huh7: 0, 2.5, 10, 40 nM. siCon was scr_si-spm and siPos was siRenilla. Asterisks indicate statistical significance to 0 nM treatment calculated by two-way ANOVA and Dunnett's post-hoc test. (*) $P < 0.05$; (**) $P < 0.01$; (***) $P < 0.001$; (****) $P < 0.0001$. $N = 3-6$ for HeLa and $n = 3$ for Huh7 cells.

In order to test the ability of siRenilla-spermine conjugates to permeate the cell membrane through receptor mediated free uptake via the PTS, Dual-Luciferase assays were also attempted in NT2/ D1 cancer stem cells. NT2/ D1 cells have been reported to express high levels of the polyamine transporter SLC22A16[511]. Moreover, NT2/ D1 cells have been used to demonstrate PTS-dependent uptake of the novel anticancer drug BLM-A5[511]. However, results of the Dual-Luciferase assays in NT2/ D1 cells were not reproducible. Confocal microscopy using NT2/ D1, HeLa and Huh7 cells revealed the morphological heterogeneity of NT2/ D1 cells, which could explain the difficulties with the reporter assay in this cell line (Figure 3.10). NT2/ D1 are pluripotent cancer stem cells that can differentiate into neurons upon exposure to retinoic acid[524], but morphological and proteome heterogeneity has also

been described before induction of differentiation[525]. In addition to investigating the reasons for the difficulties with the Dual-Luciferase assay in NT2/ D1 cells, we attempted to visualize expression of the polyamine transporter SLC22A16. Unfortunately, SLC22A16 expression was not detectable in any of the cell lines. As a positive control for the preparation of microscopy samples, Rbfox-2 was detected in the nuclei of all three cell lines. Furthermore, expression of the second control protein Lin28B was visible in the nucleus and cytosol of NT2/ D1 cells but neither in HeLa nor Huh7 cells. The detection of Lin28B protein in NT2/ D1 but not in Huh7 cells was probably because the Lin28B antibody had not been specifically validated for use in confocal microscopy and was thus only able to detect the high amounts of Lin28B protein present in NT2/ D1 cells. HeLa cells served as a negative control for Lin28B expression[526]. The inability to detect SLC22A16 can be explained by the localization of the transporter in the cell membrane, making it difficult to visualize the protein by immunofluorescence.

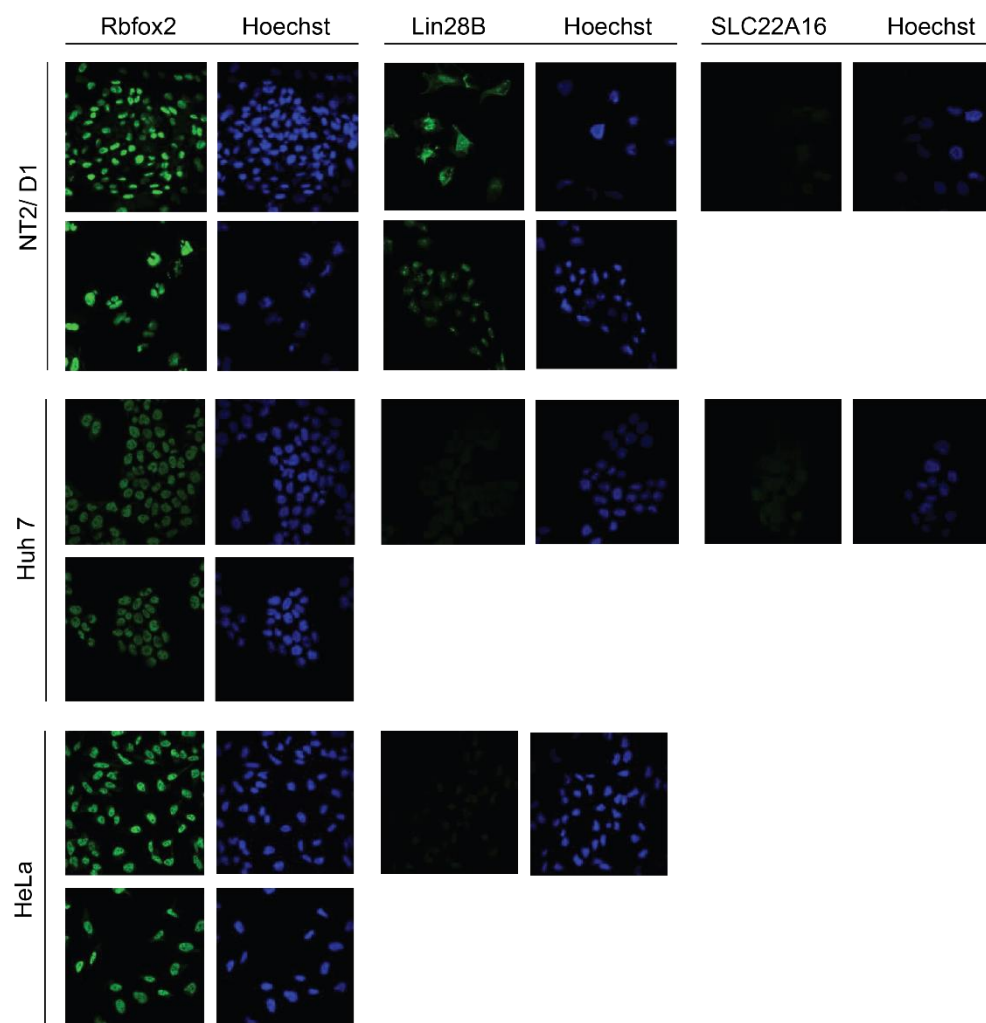


Figure 3. 10. Immunofluorescence staining of Rbfox2, Lin28B and SLC22A16 in NT2/ D1, Huh7 and HeLa cells. Hoechst dye was used for nuclear staining. Each staining was performed in a separate experiment. Different representative sections of each cell population are shown. No data for SLC22A16 in HeLa cells was obtained.

Because of the heterogeneity of the NT2/ D1 cells, we turned towards Huh7 cells to evaluate free uptake of the conjugate library. Huh7 cells have also been reported to express high levels of SLC22A16[513]. However, no activity of siRenilla conjugates was observed under free uptake conditions at concentrations of up to 1 μ M (data not shown). We hypothesized that uptake of spermine-conjugates might be increased upon polyamine depletion, but pretreatment of Huh7 cells with a combination of 100 μ M *N*-(3-aminopropyl)-cyclohexylamine (APCHA) and 500 μ M D, L- α -difluoromethylornithine (DFMO) led to extensive cell death. Conditions for efficient polyamine depletion in HeLa cells have been described by Lightfoot et al. [527] but effects may vary depending on the cell line.

3.3.4 Nuclease stability of siRenilla-spermine conjugates

To evaluate effects of spermine conjugation on nuclease stability, the most promising 3'-terminal siRenilla-conjugates were tested for their nuclease stability under cell culture conditions. For this purpose, siRNAs were incubated in 10% fetal bovine serum (FBS) and the degradation was analyzed by native polyacrylamide gel electrophoresis (PAGE; Figure 3.11). In general, spermine conjugation appeared to mildly increase the nuclease stability of the siRNAs. Nuclease stability of the triple-modified si-spm6 was comparable to the stability the mono-modified si-spm4.

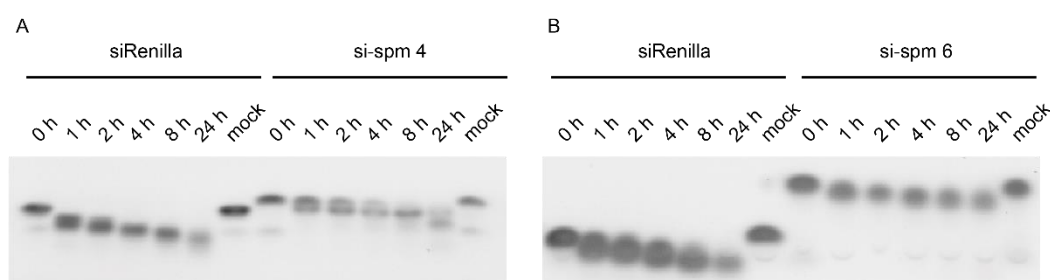


Figure 3. 11. Nuclease stability of (A) siRenilla, si-spm4 and (B) si-spm6. 12 μ M siRNAs were incubated at 37°C in 10% FBS for the indicated time and analyzed on a native 4-20% polyacrylamide gel. Representative gels shown, n= 3.

3.3.5 Activity of siLin28B-spermine conjugate

In order to assess the effect of spermine conjugation on the siRNA silencing activity for an endogenous target, we synthesized a spermine conjugate of the previously used siLin28B. Because spermine conjugation to siRenilla antisense strands did not increase their gene silencing activity (Figure 3.9), we adopted the more commonly applied delivery strategy of introducing the conjugate moiety at the 3'-terminus of the sense strand. For this purpose, we performed a western blot analysis after Lipofectamine 2000 mediated transfection of the siLin28B-spm conjugate into Huh7 cells (Figure 3.12). As for the siRenilla antisense strand conjugates, activity was slightly reduced compared to the unmodified duplex.

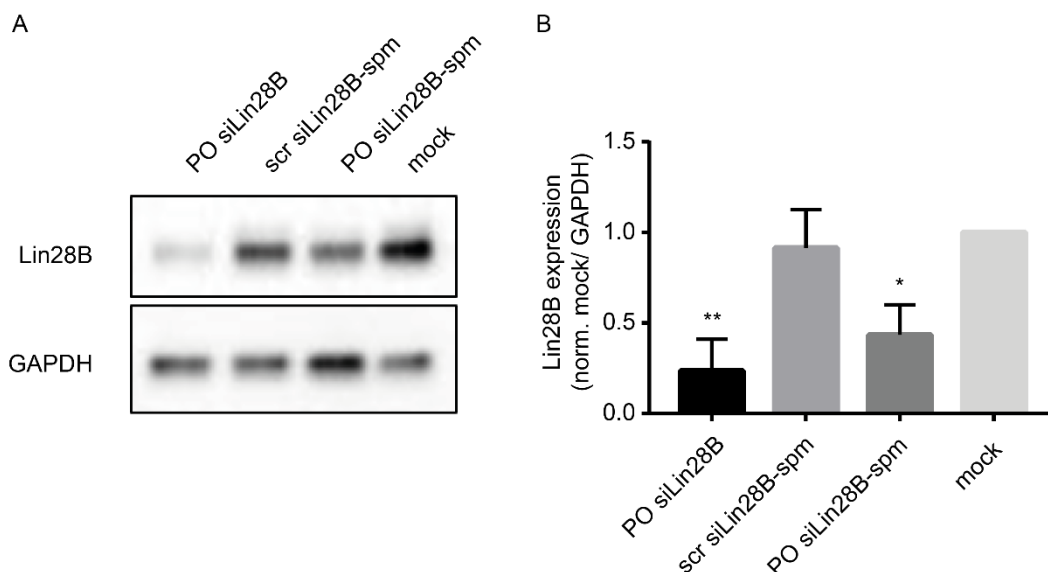


Figure 3. 12. Activity of siLin28B-spm. A) Representative western blot after transfection of 40 nM siLin28B-spm or controls in Huh7 cells. B) Analysis of three independent replicates. Mock treatment was Lipofectamine 2000 alone. Asterisks indicate statistical significance to mock treatment calculated by one-way ANOVA and Dunnett's post-hoc test. (*) $P < 0.05$; (**) $P < 0.01$, $n = 3$.

3.3.6 Additional modifications introduced via the 'convertible nucleoside' approach

After exploring spermine conjugation to siRNAs in order to improve their therapeutic properties, the introduction of additional modifications was attempted using the 'convertible nucleoside' approach. For this purpose, conjugation with phenethylamine, glucosamine, ethanolamine, methylamine and dimethylamine was investigated. Whereas substitution with phenethylamine occurred in a clean fashion even at multiple positions (Figure 3.13 A-B), no conjugation-product could be obtained after reaction with glucosamine or ethanolamine (data not shown). Substitution with methylamine or dimethylamine occurred efficiently across a range of sequences (Figure 3.13 C-J) as reported earlier[518].

The activity of siRenilla-phenethylamine conjugates was evaluated in a Dual-Luciferase reporter assay in HeLa cells as described for siRenilla-spermine conjugates (Figure 3.14). Phenethylamine-conjugation was well tolerated at 3'-terminal positions but appeared to mildly impair activity at position 9 of the AS strand, at least at 1.25 and 5 nM concentrations. This is in line with the results obtained with siRenilla-spermine conjugates (Figure 3.9), although the inhibitory effect of conjugation to position 9 was less pronounced and not observed at the 20 nM treatment. Mono- and dimethylated versions of pre-miR-20b were further used by Verena Schlösser for protein binding studies and Pol1/ Pol2-dmC were provided to the Polacek group (Uni Bern) for use in a ribosome stalling study[141]. A list of additional conjugates is shown in table 3.2.

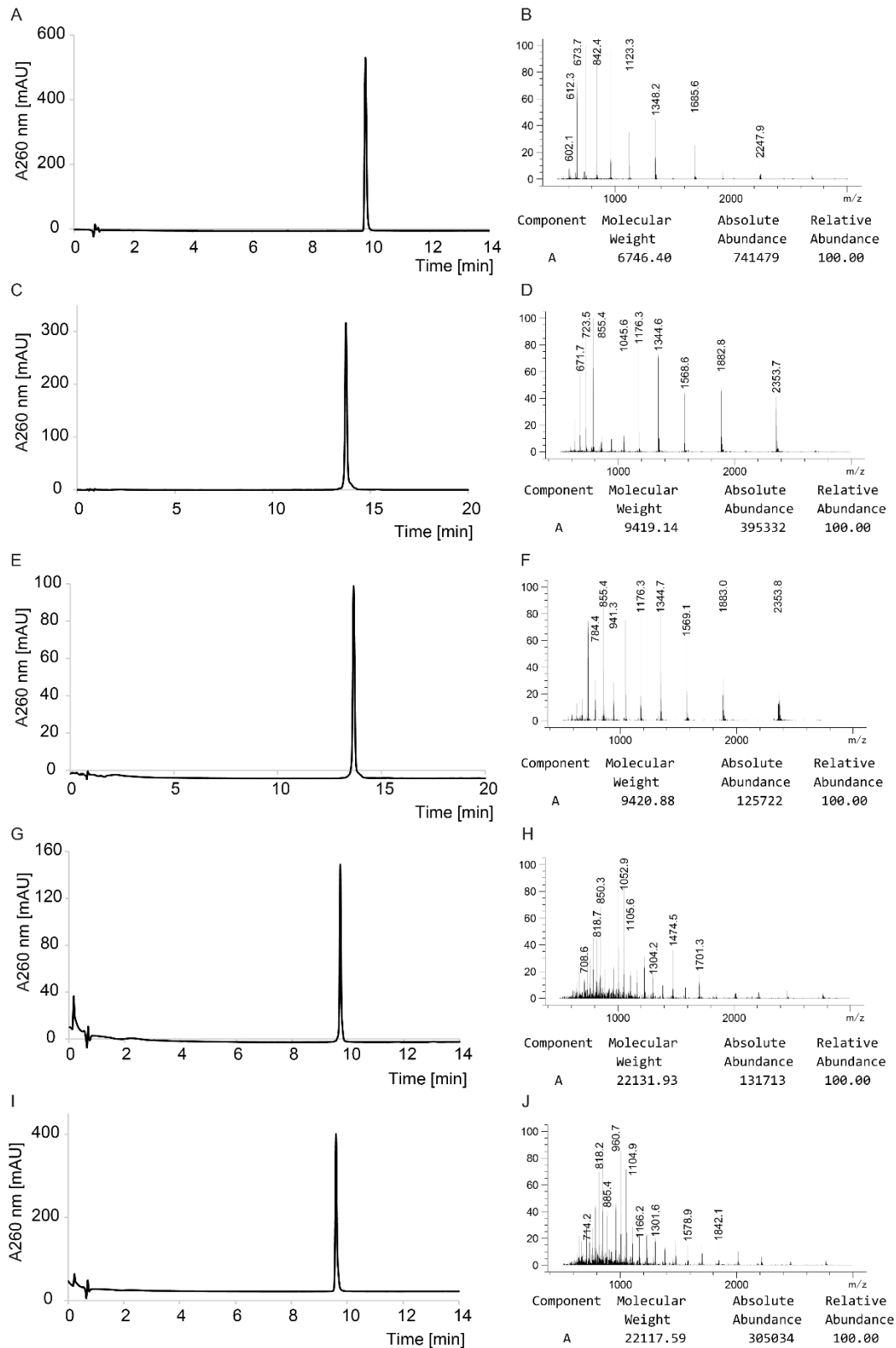


Figure 3. 13. LC-MS analysis of various ORNs synthesized via the convertible nucleoside approach. A) UV-trace of si-phen6. B) MS of (A) at 9.8-9.9 min. C) UV-trace of Pol1-dmC. D) MS of (C) at 13.7-13.8 min. E) UV-trace of Pol2-dmC. F) MS of (E) at 13.6-13.7 min. G) UV-trace of pre-miR-20b-dmC. H) MS of (G) at 9.7-9.8 min. I) UV-trace of pre-miR-20b-mmC. J) MS of (I) at 9.6-9.7 min. LC-MS analysis of Pol1/ Pol2-dmC deviated from the standard DMT-off gradient and was performed with 5-30% eluent B over 20 min. M calc for all samples are listed in table 3.2.

Table 3. 2. Additional ORNs synthesized via the convertible nucleoside approach

Compound	Strand	Sequence (5'-3')	M calc	M found
Scr_si-phen	AS	CUUCUCCUUCGCGUUCUCCU W	6539.96	6539.03
	S	GAGGAGAACGCGAAGGAGAAG	6963.37	6962.34
si-phen3	AS	UUUCUCGC W CUCUUCGCUCUU	6540.95	6540.25
si-phen4	AS	UUUCUCGCCCUUCUUCGCUCU W	6539.96	6539.11
si-phen6	AS	UUUCUCGCCCUUCUUCGCU WWW	6747.28	6746.40
pre-miR20b	-	AGUACCAAAGUGCUCAUAGUGCAGGU		
-dmC	-	AGUUUUGGY/ Z AUGACUCUACUGUAGU	22133.31	22131.39
-mmC	-	AUGGGCACUCCAGUACU	22119.29	22117.59
Pol1-dmC	-	GCGGCACGCGAGCUGGGU Y CAGAAC	9419.78	9419.14
		GUCG		
Pol2-dmC	-	GCGGCACGCGAGCUGGGU Y YAGAAC	9420.77	9420.88
		GUCG		

All linkages are RNA-PO. Bold letters indicate modification after replacement of O^4 -triazolyluridine. W= phenethyl-rC, Y= dimethyl-rC, Z= monomethyl-rC. Sense strand of si-phen3-6 was the same as for siRenilla.

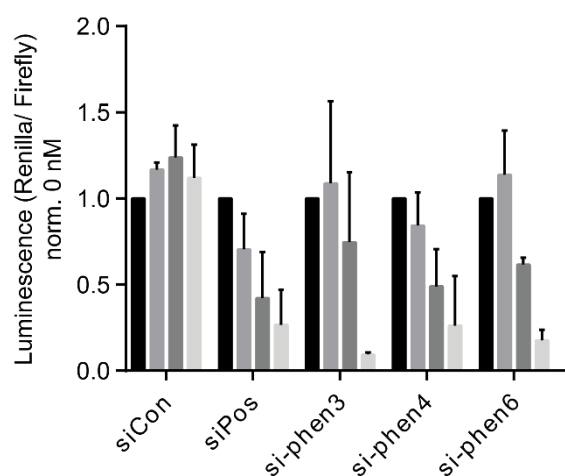


Figure 3. 14. Activity of siRenilla-phenethylamine conjugates in a Dual-Luciferase reporter assay in HeLa cells. Increasing siRNA concentrations from left to right: 0, 1.25, 5 and 20 nM. Renilla/ Firefly luminescence was normalized to 0 nM treatment. SiCon was scr_si-phen and siPos was siRenilla. N= 2.

3.4 Conclusion and outlook

Most siRNAs that are currently under investigation rely on heavy chemical modification and conjugation to targeting ligands in order to avoid complex LNP formulation[3, 4, 8]. We have investigated spermine conjugation to siRNAs in an effort to identify natural modifications that enable the construction of potent RNAi reagents without the need for the excessive use of non-natural building blocks. Conjugation of oligonucleotides with spermine has previously been reported to facilitate free uptake at N/ P ratios > 1.5[485, 486]. Although the exact mechanism of polyspermine-dependent free uptake is not clear, the stringent requirement for an overall positive charge and free amino groups to act as a 'proton sponge' resembles the cellular uptake mediated by polycationic transfections reagents such as polyethylenimine (e.g. jetPEI)[528]. Nevertheless, spermine conjugation to siRNAs is of interest for systemic delivery. A study on small molecule-polyamine conjugates suggested that free primary amino groups are important for efficient uptake by PAT[500]. This structural requirement has not been met by previous polyphosphospermine-conjugates (Figure 3.1). Although conjugation to spermine did not increase the cellular activity of siRNAs, polyamine conjugation might be of value for targeted delivery *in vivo*. For this purpose, conjugation to spermine derivatives such as recently introduced dendrimer-like star-shaped polyamines[481] could be investigated as a means to trigger productive cellular uptake. Furthermore, polyamine conjugation could be used in combination with other chemical modifications to eliminate the need for 2'-F building blocks in the design of siRNAs. Another approach that could benefit from polyamine conjugation is the use of full PS siRNAs since one factor that is potentially limiting the metabolic stability and therapeutic efficacy of these reagents is the considerable loss in thermodynamic duplex stability (Figure 2.6). Major groove polyamine conjugates therefore offer an attractive means to fine-tune the biophysical properties of PS siRNAs[114, 115].

3.5 Contributions

Synthesis of spermine-siRNA conjugates was performed by Anne Michelle Lüscher and Christian Berk. Synthesis of alkyl- and aryl-RNA-conjugates was performed by Chaitra Rao and Christian Berk. Dual-Luciferase reporter assays were performed by Anne Michelle Lüscher, Diego Lorenzo Del Rio Sarasola and Christian Berk. Synthesis of *O*⁴-triazolyluridine and *N*¹-trityl spermine was performed by Anne Michelle Lüscher and Christian Berk. Synthesis of spermine azide was performed by Anne Michelle Lüscher, Dr. Elodie Decuypère and Christian Berk. Immunofluorescence and western blot experiments were performed by Anne Michelle Lüscher. Nuclease stability assays were performed by Christian Berk.

4 Project 3 – Development of a new chimera-forming CLIP method (cyCLIP)

This project was a collaborative effort with Dr. Yuluan Wang and has been previously described in Dr. Wang's thesis "Tailoring CLIP-based methods for exploring the miRNA targetome"[322].

4.1 Introduction

4.1.1 Experimental approaches to identify miRNA-RNA interactions – CLIP-based methods

Recognition of the widespread regulation of cellular functions by miRNAs has triggered the development of a variety of methods to uncover the miRNA targetome. Despite the development and continuous improvement of a number of computational miRNA-target prediction algorithms, such tools are traditionally limited by our current understanding of miRNA targeting and are therefore prone to miss yet undescribed interactions[529]. For example, the most frequently used prediction tool TargetScan was originally developed to identify miRNA-target sites based on seed-complementarity and conservation of the target sites in 3'-UTRs[530, 531], reflecting the lack of knowledge about non-canonical miRNA targeting at the time. Experimental approaches for delineating miRNA-target interactions are hence of central importance and have been reviewed in detail by Steinkraus et al[532] and Lee et Ule[533]. In brief, the history of experimental high-throughput determination of miRNA-targets via crosslinking approaches began with the development of "high-throughput sequencing of RNA isolated by crosslinking immunoprecipitation" (HITS-CLIP)[534], which uses UV irradiation to covalently crosslink RNAs to their protein interaction partners, followed by RNase digestion and immunoprecipitation of AGO-RNA complexes. After purification and reverse transcription of isolated RNAs, samples are subjected to sequencing, yielding separate datasets for miRNAs and their respective targets. Importantly, this methodology did not enable the identification of exact miRNA target sites as miRNA/ target RNA complexes were not covalently connected. Following the protocol of the "Photoactivatable Ribonucleoside Enhanced Crosslinking and Immunoprecipitation" (PAR-CLIP) method[535-538], UV-induced crosslinking efficiency between RNAs and RNA binding proteins (RBPs) could be improved through the addition of a photoactivatable nucleoside such as 4-thiouridine (4-SU) to the growth medium, which is subsequently incorporated into endogenously synthesized RNAs. In addition to improving the RNA-protein crosslinking efficiency, incorporation of 4-SU produces a thymidine to cytidine transition in the resulting cDNA library, which can be used to map the exact protein binding site. In parallel, our group developed a method termed miR-CLIP that focusses on the elucidation of individual miRNA targetomes rather than global miRNA-RNA interactions, thereby increasing specificity and providing a more detailed analysis of single

miRNA targets[539]. This is achieved through dual chemical modification of the miR-CLIP probes with a psoralen crosslinking moiety and a biotin affinity tag, which permits the use of a stringent washing procedure.

With the advent of a method termed “crosslinking, ligation and sequencing of hybrids” (CLASH)[540], a ligation step was introduced into CLIP-type protocols, which for the first time allowed the unambiguous identification of miRNA target sites through formation of miRNA-target chimeras. Thereafter, the original PAR-CLIP protocol was extended by incorporation of a ligation step, resulting in the generation of the modified *in vivo* PAR-CLIP (iPAR-CLIP) method, which has been used to identify sites of miRNA-target interactions in *C. elegans*[541]. To the authors’ surprise, miRNA/ target-RNA chimeras were also detected in the absence of exogenously added ligase. These chimeras were mostly composed of truncated miRNAs bound to their respective targets, indicating that a 2',3'-cyclic phosphate terminus, presumably resulting from RNase T1 digestion, was used for this conjugation. This observation is in line with earlier reports that described the presence of an endogenous RNA ligase capable of ligating 5'-hydroxyl to 2',3'-cyclic phosphate (cycP) terminated RNAs (RNA>p) in mammalian cells[210, 211, 542]. In addition, the presence of an endogenous RNA-3'-P-cyclase, capable of converting a 3'-P into a 2',3'-cycP end, has been described[211] and experiments with siRNAs carrying a 3'-P antisense strand revealed an unexpected ligation to the corresponding sense strand in HeLa lysate[194].

Moreover, through re-analysis of published CLIP data from PAR-CLIP and HITS-CLIP experiments, more than 11,000 human and ~2,000 mouse miRNA-target chimeras were identified, although in none of these experiments an exogenous ligase had been added[541]. Importantly, in these cases >80% of the chimeric reads contained 3' truncated miRNAs. In the following, the inventors of the HITS-CLIP method adapted their original strategy by including a ligation step and termed their new method “covalent ligation of endogenous Argonaute-bound RNAs-CLIP” (CLEAR-CLIP)[543]. Applying CLEAR-CLIP to mouse brain and Huh7.5 cells further validated that miRNA-target chimeras can also be found in the absence of an exogenously added ligase. These chimeras also showed significant seed-enrichment which provided further evidence that these interactions are real. Therefore, the authors investigated mammalian transfer RNA ligase HSPC117 as a potential source of chimera-ligation. However, neither overexpression of HSPC117 nor its depletion in Huh7.5 cells significantly affected the frequency of miRNA-target chimeras[543]. Moreover, Broughton et al. found that application of their newly developed *in vivo* individual-resolution crosslinking immunoprecipitation (iCLIP) protocol in *C. elegans* resulted in the generation of full-length miRNA-target chimeric reads, although the protocol does not include a dedicated chimera-ligation step[303]. Therefore, the authors concluded that most iCLIP chimeras formed in fact during adapter-ligation in the

preparation of the sequencing library. Nevertheless, the authors acknowledged that approximately 20% of chimeric reads were comprised of truncated miRNAs, for which an endogenous ligase might be responsible.

However, despite the development of a number of chimera-generating CLIP procedures, the efficiency of chimera generation remains low (0.2-5%)[529]. As a consequence, many target sites have been identified by only a single chimeric read[529]. Furthermore, in the modified iPAR-CLIP data, less than 20% of chimeric reads occurred more than once[529, 541]. Consequently, computational TargetScan prediction of functional miRNA-target sites was more accurate than inferring target sites from experimental CLASH chimeric reads[304]. Hence, the development of more efficient chimera-generating methods is needed.

4.1.2 Relevance of RNA^{>p} and RtcB as a 2',3'-cyc P/ 3'P RNA ligase

RNA^{>p} have been recognized for their central role in tRNA splicing[544, 545] and their detailed investigation shed light on an unusual ligation mechanism that is used to covalently link RNA^{>p} to 5'-hydroxyl RNAs[210, 211, 544, 546-553]. Whereas in classical ligation mechanisms, 5'-P RNA is activated as an AMP-adduct and subsequently attacked by a 3'-hydroxyl RNA[554-556], direct ligation of RNA^{>p} to 5'-OH RNAs has been observed in HeLa lysate[210, 211]. The human tRNA ligase HSPC117 has been suggested as the responsible enzyme[544]. Mechanistic studies on the bacterial orthologue RtcB have provided evidence for a Mn²⁺ and GTP dependent, three-step mechanism in which (i) RtcB reacts with GTP to form a covalent RtcB-(histidinyl-N)-GMP intermediate from which (ii) a guanylate is transferred to an RNA-3'-P, which (iii) is subsequently attacked by a 5'-hydroxyl RNA[546-553]. This mechanism requires initial hydrolysis of the 2',3'-cycP end to 3'-P and the authors consequently described RtcB as a 3'-P rather than a 2',3'-cycP RNA ligase. However, ligation in HeLa lysate has been reported to occur preferentially on 2',3'-cycP RNAs and ligation of 3'-P RNAs was preceded by cyclisation via an endogenous 3'-P cyclase[210, 211, 544] (Figure 4.1).

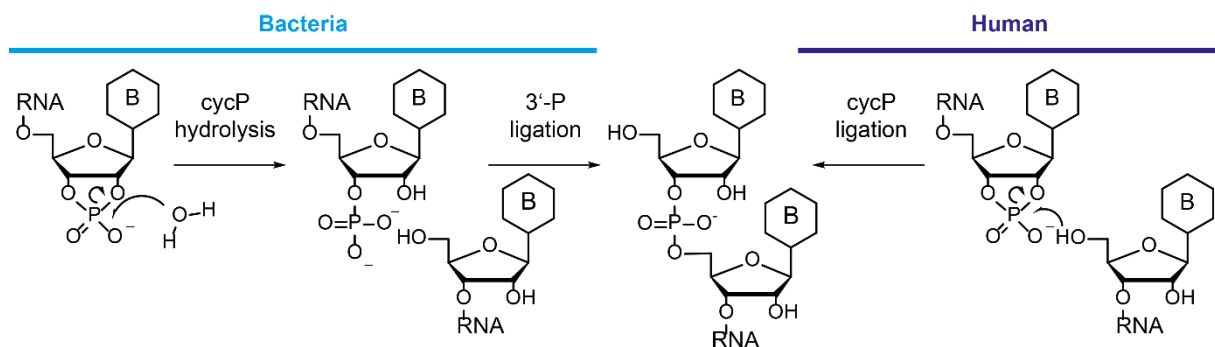


Figure 4. 1. Different mechanisms suggested for bacterial and human RNA^{>p} ligation

4.2 Project outline

We set out to investigate a novel chimera-generating approach by using chemically synthesized miRNA>p probes and recently commercially available *E. coli* RtcB. The new method was termed cyCLIP, reflecting the 2',3'-cycP probe design. We hypothesized that miRNA>p probes could undergo ligation at different stages. The first possibility would be in HeLa lysate through the action of the previously reported endogenous 2',3'-cycP ligase[210, 211, 544] upon binding of the probe to its RNA target inside RISC and subsequent RNase trimming. RISC bound RNA regions would thus be shielded from RNase digestion[557] (Figure 4.2). A second ligation could occur after AGO2-immunopurification through addition of exogenous RtcB 2',3'-cycP/ 3'-P ligase. In addition, we planned to evaluate the possibility of non-enzymatic ligation of RNA>p probes[558-563] and to assess potential alternative applications of 2',3'-cycP RNAs.

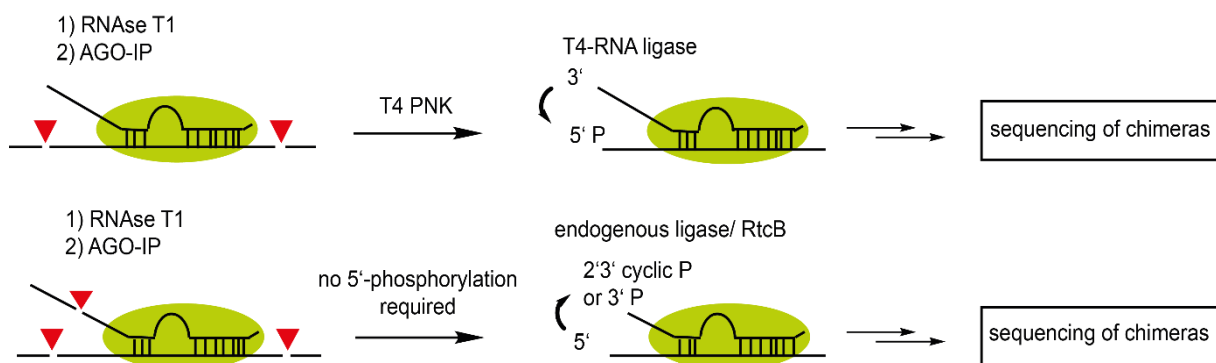


Figure 4. 2. Principle of classical chimera-forming methods (top) vs cyCLIP approach (bottom).

4.3 Results and Discussion

4.3.1 Synthesis of RNA>p

RNA>p were synthesized on a dedicated, commercially available solid support[6, 214, 219] (Figure 4.3). All RNA>p species were synthesized in DMT-off mode because of the lability of the 2', 3'-cycP group under acidic conditions.

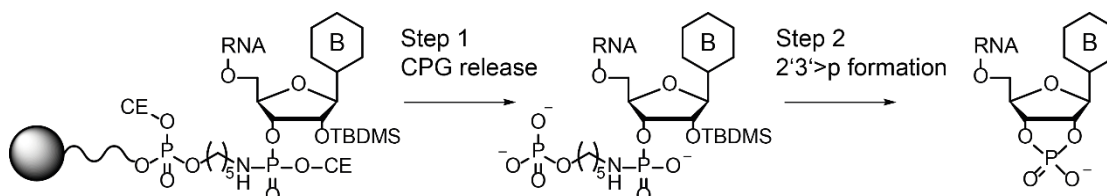


Figure 4. 3. Synthesis of RNA>p from a commercially available solid-support

A list of all ORNs used in this study and the LC-MS analysis of RNA>p can be found in the appendix (Figure 8.16 and Table 8.1).

4.3.2 Ligation of miRNA>p in cell lysate

As a proof of principle experiment, we evaluated the ligation of miR-34a-5p>p duplexed to a ~40 nt counterstrand in HeLa lysate. Counterstrand designs were based on the literature-reported miR34a-target site on Lemur Tyrosine Kinase 3 (LMTK3) mRNA[564, 565]. Specifically, we investigated ligation to 4 different counterstrands (Figure 4.4). Two counterstrands contained the natural, 8 nt complementary target site but varied in their 5'-overhang, thereby changing the spacer length between the miRNA>p and the target during ligation. These counterstrands are hereafter referred to as 8CS(+n), where 8 indicates the 8 nt complementarity to the miRNA seed region and n indicates the length of the counterstrand 5'-overhang. The other constructs contained an artificial 14 nt complementary target site but were otherwise identical to the natural counterstrands. Correspondingly, these counterstrands are referred to as 14CS(+n).

In order to follow the ligation reaction by denaturing PAGE (dPAGE), miR-34a-5p>p was marked with a radioactive 5'-³²P label. The enzymatic 5'-labelling has to be performed using a phosphatase deficient PNK mutant, as regular T4 PNK would remove the 2',3'-cycP end[566]. To gain further insight into favorable geometric arrangements of the miRNA>p and the target for the ligation, we added a bridging ORN, which was fully complementary to the miRNA>p/8CS(+8) ligation site. We hypothesized that inclusion of the bridging ORN would favor a linear arrangement of the miRNA>p/ target complex. Furthermore, we evaluated the potential of non-enzymatic miRNA>p ligation in a buffer system, as reported earlier[558, 561, 562].

outcome was desired, as chimera-ligation after RISC binding would need to occur in a duplex format. Moreover, ligation efficiency increased with increasing duplex complementarity and decreasing 5'-overhang length. Non-enzymatic ligation in a buffer system was dependent on the presence of the bridging oligo, but was generally weak and not reproducible.

4.3.3 *In vitro* ligation using RtcB

After the promising ligation outcomes in HeLa lysate, we turned towards the use of bacterial RtcB to boost ligation efficiency. For this purpose, miR-34a-5p>p and WT strands were incubated with LMTK3 counterstrands in the presence of RtcB in RtcB ligase buffer (Figure 4.5).

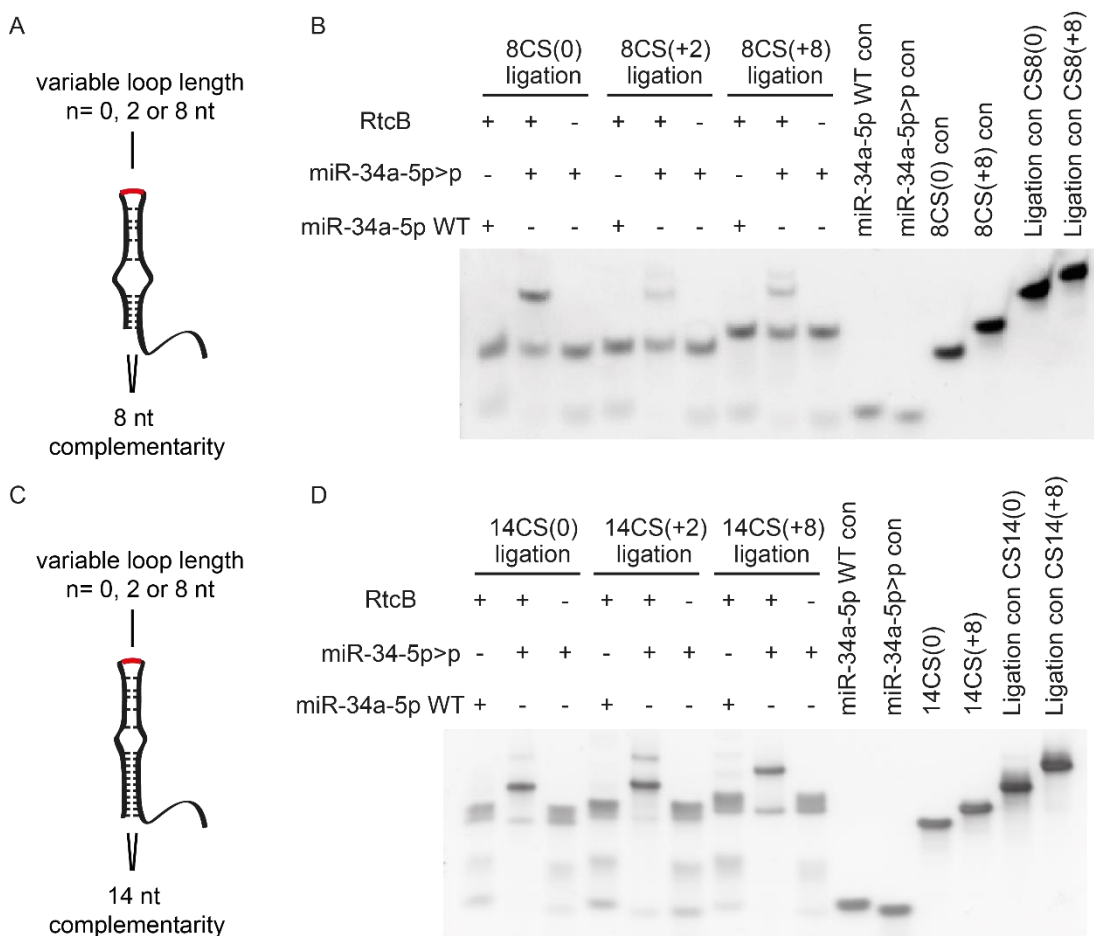


Figure 4. 5. *In vitro* RtcB ligation of miR-34a-5p>p to LMTK3 CS constructs. A) Cartoon showing assumed ligation product of miR-34a-5p>p/ 8CS complexes with indication of 5'-overhang influence. B) RtcB ligation of miR-34a-5p>p and WT to 8CS LMTK3 constructs in buffer. C) Cartoon showing assumed ligation product of miR-34a-5p>p/ 14CS complexes with indication of 5'-overhang influence. D) RtcB ligation of miR-34a-5p>p and WT to 14CS LMTK3 constructs in buffer. Representative gels shown. N= 3. Staining with SYBR Gold. Adapted from[322].

Again, appearance of bands that were consistent with the formation of intermolecular ligation products was dependent on the presence of a 2',3'-cycP terminus and RtcB. This was expected, as the experiment was performed in the absence of lysate. As in the previous

experiment, ligation efficiency increased with shorter 5'-overhangs, particularly in the case of the 8CS constructs (Figure 4.5 B). For 14CS constructs, ligation proceeded efficiently also with increased 5'-overhang length, indicating a generally higher ligation efficiency (Figure 4.5 D). In some samples we observed an additional, slower migrating band. We reasoned, that these bands may correspond to a ligation product between the chimeric sequence and additional miR-34a-5p>p.

As a next step, we tested the tolerance of the RISC machinery toward miRNA>p duplexes as miRNA mimics. For this purpose, we evaluated the dose dependent knockdown efficiency of three miRNA>p duplexes in a Dual-Luciferase reporter assay: miR-34a, miR-106a and let-7g (Figure 4.6). As indicated by the comparable knockdown efficiencies between all tested miRNA>p and their WT analogues, the 2', 3'-cycP terminus did not impart efficient RISC loading and silencing activity.

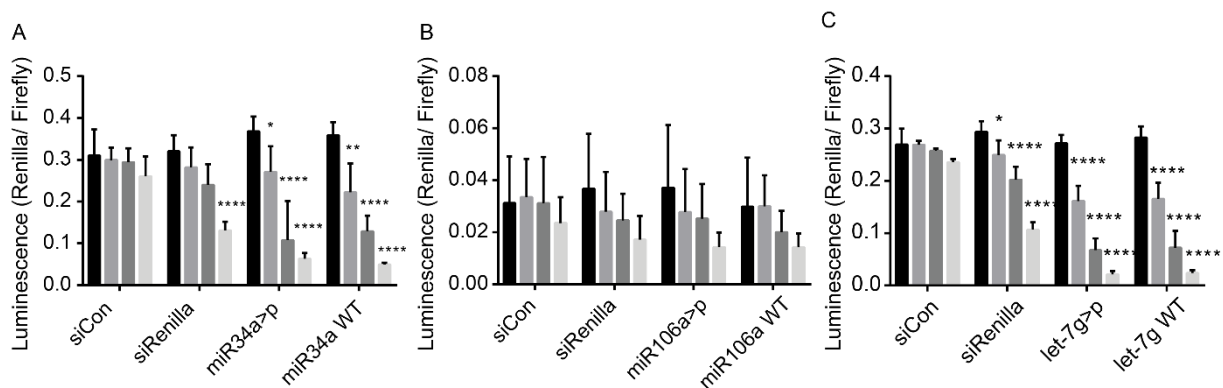


Figure 4. 6. RISC tolerance toward miRNA>p. Activity of miR-34a>p (A), miR-106a>p (B) and let-7g>p (C) in Dual-Luciferase reporter assays in HEK293T cells (2',3'-cycP on 5p strands). Increasing concentrations from left to right: 0, 2.5, 10 and 40 nM. Assays were performed with psi-CHECK 2 plasmids containing 3x fully complementary target sites for miR-34a-5p (A) or 1x fully complementary target site for miR-106a-5p (B) or let-7g-5p (C). Mean +/- SD shown from three independent experiments. Asterisks indicate statistical significance to 0 nM treatment calculated by two-way ANOVA and Dunnett's post-hoc test. (*) P<0.05, (**) P<0.01, (****) P<0.0001. Adapted from[322].

Due to the reported siRNA interstrand ligation between a 3'-P guide and a 5'-OH passenger strand[194], we evaluated two capping strategies to prevent unintended intra-miRNA ligation: 5'-C₆-acetamide (Figure 4.7 A, left) and UniCap (Figure 4.7 A, right) modifications of miRNA passenger strands. We evaluated both capping strategies for their ability to block ligation for miR-34a and miR-106a probes (Figure 4.7 D and E) in dPAGE ligation assays. Whereas the 5'-C₆-acetamide cap surprisingly still permitted a low efficiency ligation, ligation was abolished through UniCap modification. Luciferase silencing activity of 'guide>p – UniCap-passenger miRNA probes' was investigated for miR-34a (Figure 4.7 B) and miR-106a (Figure 4.7 C) and was comparable to the corresponding unmodified duplexes.

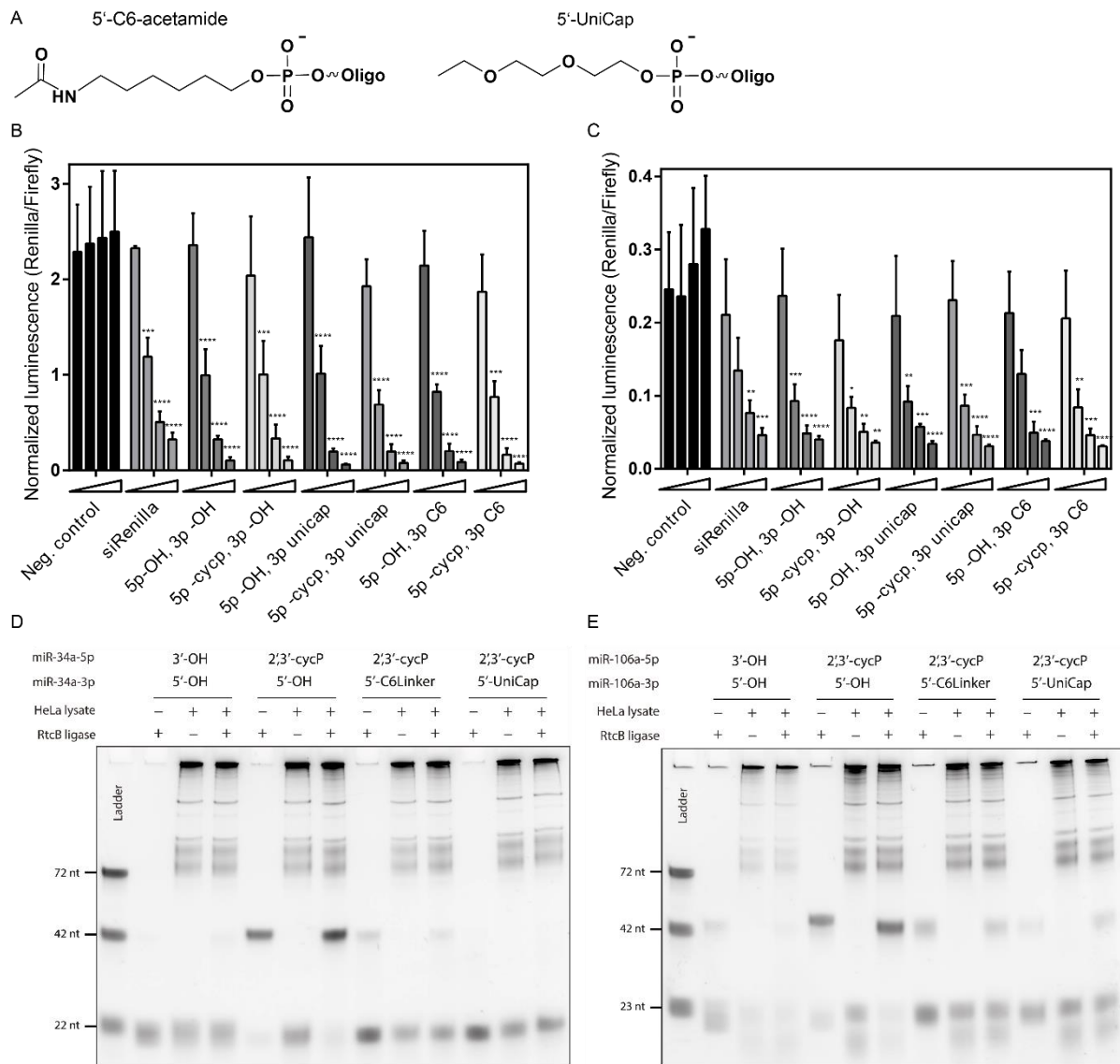


Figure 4. 7. Evaluation of 5'-capping groups to prevent intra-miRNA ligation. A) Structures of 5'-C6-acetamide and 5'-UniCap groups. B) Dual-Luciferase reporter assay for different miR-34a formats. Psi-CHECK 2 plasmid contained 3x fully complementary target sites for miR-34a-5p. Labelling indicates 3'-terminus of 5p strand and 5'-terminus of 3p strand. Increasing concentrations from left to right: 0, 2.5, 10, 40 nM. N=3. Asterisks indicate statistical significance to 0 nM treatment calculated by two-way ANOVA and Dunnett's post-hoc test. (*) P<0.05, (**) P<0.01, (***) P<0.001, (****) P<0.0001. C) Dual-Luciferase reporter assay for different miR-106a formats. Psi-CHECK 2 plasmid contained 1x fully complementary target site for miR-106a-5p. Labelling, doses and statistical analysis as in B. D) RtcB ligation in buffer of miR-34a and (E) miR-106a formats. N= 1. Staining with SYBR Gold. Adapted from[322].

4.3.4 Development of a cyCLIP work-flow

Having established the principle of the approach, we designed a work-flow for the new method based on previous experience with the miR-CLIP protocol[539]. The new method was termed cyCLIP (Figure 4.8).

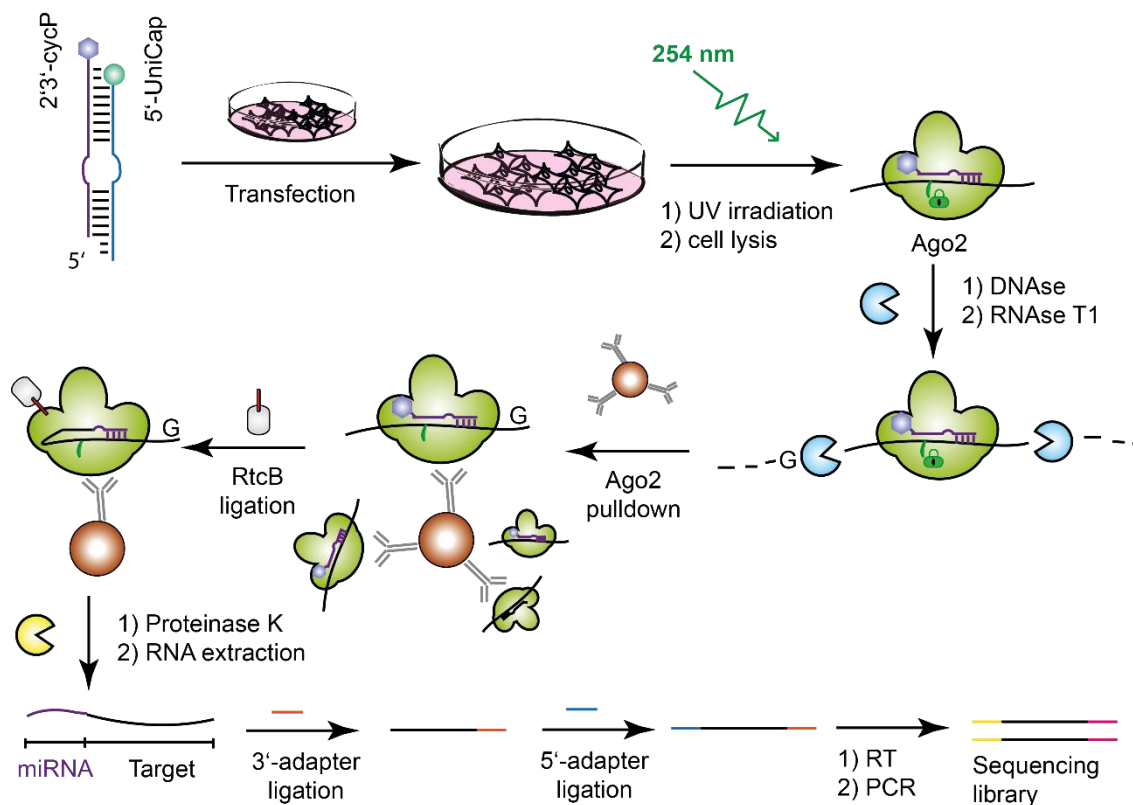


Figure 4. 8. Proposed cyCLIP work-flow. Adapted from[322].

Based on the proposed work-flow, we focused on the optimization of the RNase digestion step, as this has been previously identified as a critical step in CLIP protocols[533]. RNase T1 was selected based on its reported use in chimera generating CLIP methods[536, 541, 543]. Of note, RNase T1 digestion was thought to be responsible for the generation of the 2',3'-cycP termini required for previously observed unintended ligations[541]. Based on the *in vitro* results, which indicated a preference for short 5'-overhangs, we aimed for an RNase trimming to an approximate size of 23-70 nt, thereby removing most of the non-RISC protected RNA. In order to identify suitable conditions for RNase digestion, we followed the cyCLIP protocol until the Ago2-immunopurification step. RNase digested Ago2-bound RNAs were liberated from the Ago2-complex through a proteinase K treatment and RNase trimming was evaluated by dPAGE (Figure 4.9). Best results were obtained with 1.865 U/ μ l RNase T1 in HeLa lysate. On-beads digestion after AGO2-immunopurification (AGO2-IP) was attempted, but no RNA could be recovered. Therefore, the on-beads digestion strategy was not further pursued.

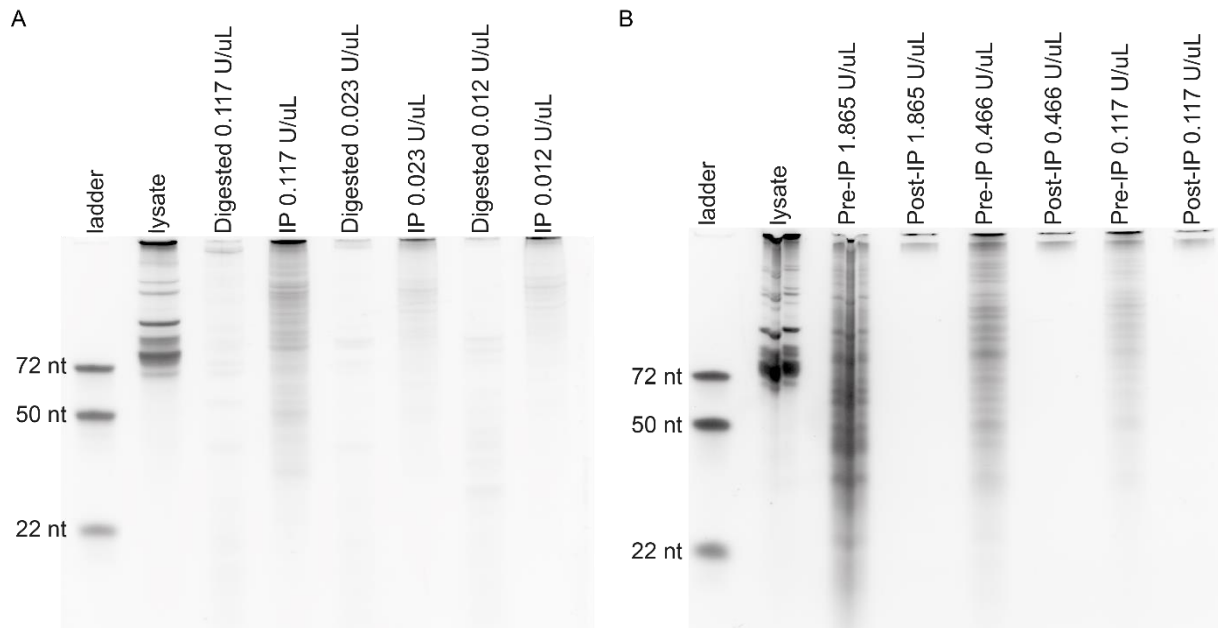


Figure 4. 9. Optimization of conditions for RNase T1 trimming. Samples were collected after UV-crosslinking, Ago2-IP and RNase T1 digestion in HeLa lysate. Staining with SYBR Gold. Adapted from[322].

Before proceeding to the final sequencing experiments, we performed a control-experiment based on Northern-Blot detection of chimeric ligation products. We therefore co-transfected miR-106a-cyCLIP probes with a Luciferase plasmid containing a validated SIRPa1 target site[567]. After following the cyCLIP protocol, total RNA extracts and in-process controls (input samples for AGO2-IP, samples after RNase digest and the cyCLIP supernatant) were separated by dPAGE and transferred to a Hybond NX membrane (Figure 4.10). We hypothesized that consecutive probing with 5'-³²P-labelled probes targeting either miR-106a-5p or the SIRPa1 target site would indicate the presence of a chimeric product. As expected, SIRPa1-ligation controls were detected with both probes and the miR-106a control was only detected by the miR-106a-probe. Furthermore, miR-106a and SIRPa1 were detected in the AGO2-IP input samples and were absent in AGO2-IP supernatants (not bead-bound fraction). Surprisingly, no signals were detected in the RNase-digestion in-process controls. Nevertheless, appearance of a smear, spanning the range of the expected ligation products in the final cyCLIP extracts, encouraged us to proceed with the sequencing experiments.

Unfortunately, sequencing of the first cyCLIP library after transfection of a miR-106a probe into HeLa cells did not reveal useful chimeric reads. We reasoned that either the cyCLIP probe was not sufficiently stable after transfection or that the endogenous ligase and RtcB were not able to efficiently ligate miRNA/ target complexes inside RISC.

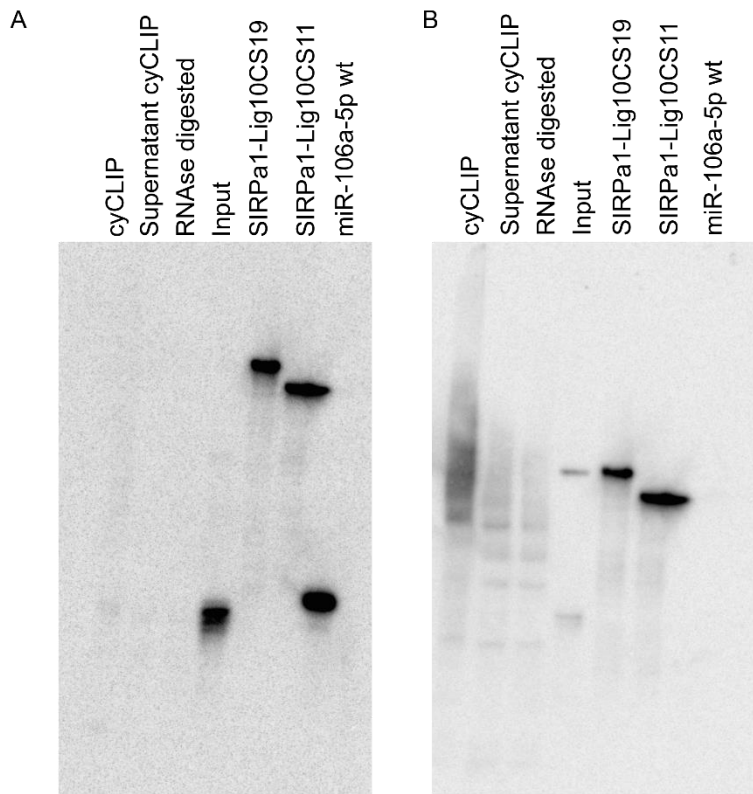


Figure 4. 10. Chimera northern blot. Cotransfection of miR-106a cyCLIP probe and psi-CHECK 2 plasmid containing the miR-106a target site on SIRPa1 mRNA into HeLa cells. Samples were collected after completing the cyCLIP protocol. Membrane was probed for miR-106a (A) and the SIRPa1 target site (B). N= 1. Adapted from[322].

In order to monitor the stability and the ligation capability of the probe, miR-106a-5p>p and WT duplexes were incubated in HeLa lysate. Lysate digestion was quenched at the indicated time points (Figure 4.11) through addition of proteinase K. Then, proteinase K was inactivated and RtcB was added. The positive control (no lysate incubation) showed the expected ligation band at ~45 nt. Surprisingly, a slightly faster migrating band was also observed in the WT sample at t= 0 min. The unexpected band at t= 0 min could be explained through a rapid 3'-end removal of 1-2 nt, yielding a 2', 3'-cycP terminus which could be efficiently ligated by RtcB. This is consistent with the appearance of yet faster migrating "ligation-bands" at later time points and lower intensity in the WT sample. The miR-106a-5p>p duplex showed a strong band at t= 0 min, which was migrating at the same level as in the positive control. However, the band intensity decreased considerably after prolonged lysate incubation. This indicated a decreased ligation capability of miR-106a-5p>p after incubation, possibly explaining the failure of the sequencing experiment. Correspondingly, degradation of miR-106a-5p>p and WT duplexes (bands at ~23 nt) was observed. Nevertheless, degradation of the miR-106a-5p>p duplex appeared to be slower than for the WT sequence. We hypothesized that the slight shift of the upper ~23 nt band in miR-106a-5p>p samples indicated hydrolysis of 2', 3'-cycP and subsequent removal of 3'-P. Slower gel migration of RNA-3'-OH compared to the corresponding RNA>p species has been observed before (Figure 4.5 and [568]).

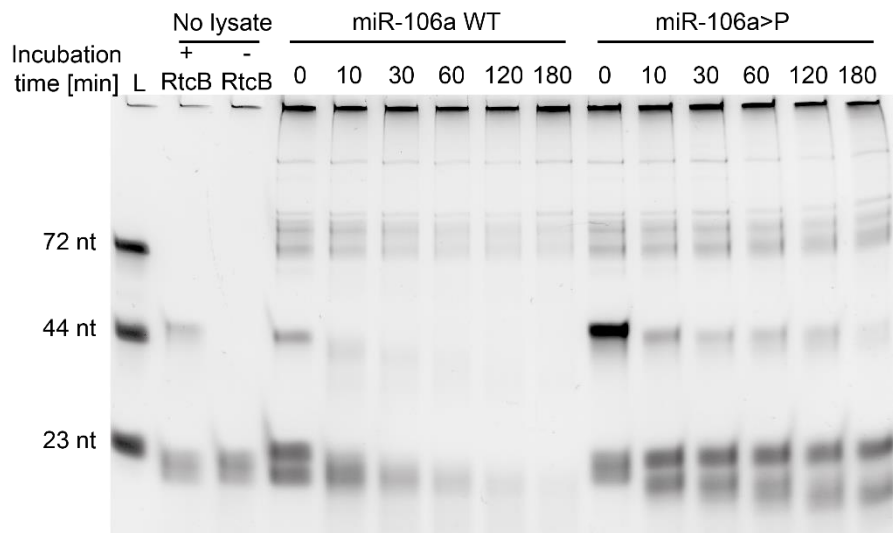


Figure 4. 11. Ligation ability of miR-106a WT or miR-106a>p (2', 3'-cycP on 5p strand) after incubation in HeLa lysate. Incubation in HeLa lysate was quenched at the indicated time points and RtcB was added. Size of the expected inter-strand ligation product is 45 nt. Staining with SYBR Gold. L= ladder. N= 1. Adapted from[322].

4.3.5 Use of RNA>p for the synthesis of circular RNAs

In addition to the originally intended use of RNA>p probes in the cyCLIP methodology, we investigated RtcB mediated intrastrand ligation to obtain circular RNAs[211, 547, 548]. For this purpose, we analyzed the intramolecular ligation of two RNA>p species: One was a truncated RNA>p hairpin based on the pre-miR-20b stem-loop. The other one was a dumbbell-shaped siLin28B hairpin, which was designed according to previously established guidelines[569-571]. Successful cyclization was indicated by the appearance of a faster migrating band in both cases (Figure 4.12 A, B). Faster dPAGE migration of cyclic RNAs compared to their linear analogues has been reported previously[547, 548, 569]. Having demonstrated the successful cyclization of the siLin28B hairpin, we investigated the biological activity of the resulting siLin28B dumbbell by RT-qPCR in HEK293T cells (Figure 4.12 C). In line with previous reports, similar knockdown efficiencies of the dumbbell RNA and a standard siLin28B duplex indicated efficient Dicer processing and RISC loading of the cyclic siRNA[569-571].

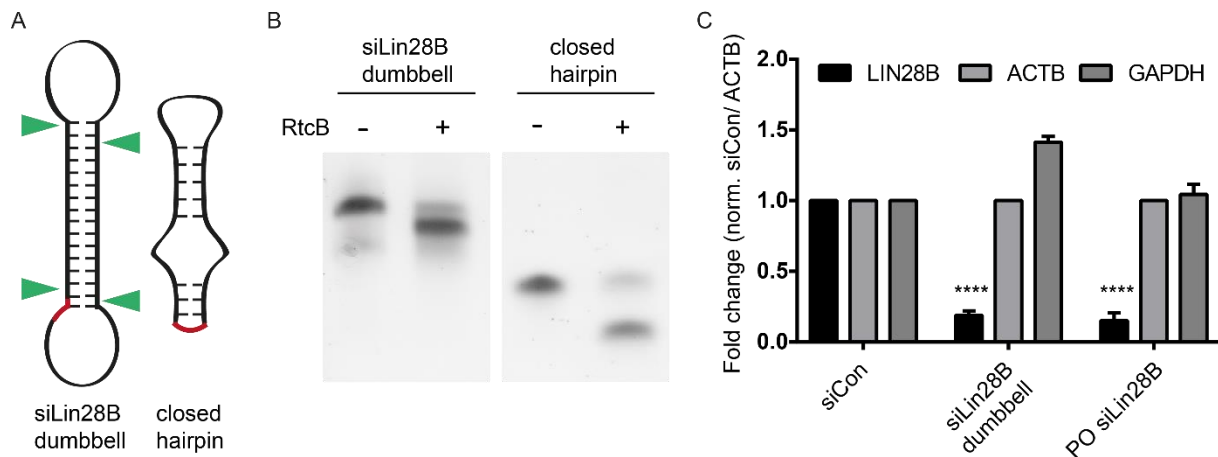


Figure 4.12. RNA \gt p circularization by RtcB. A) Structures of siLin28B dumbbell and closed hairpin after ligation. Newly formed junctions are indicated in red, Dicer processing sites are marked with green wedges. B) Intramolecular ligation of siLin28B dumbbell and closed hairpin. Representative gels shown. N= 3. C) RT-qPCR results for Lin28B after transfection of 40 nM siLin28B dumbbell or PO siLin28B into HEK293T cells. Asterisks indicate statistical significance to 0 nM treatment calculated by one-way ANOVA and Dunnett's post-hoc test. (****) $P < 0.0001$. N= 3.

4.4 Conclusion and Outlook

Despite the development of several CLIP protocols by various groups, the ligation efficiency remains generally low and limits the rate of chimera formation. As a consequence, many miRNA-target sites have been identified by single chimeric reads, making the sequencing results less reliable and increasing the chance of missing potentially interesting interactions[529]. We therefore aimed to develop a new CLIP-protocol to unambiguously identify miRNA target sites in mammalian cells with increased rates of chimera generation. For this purpose, we explored an unusual ligation mechanism involving 2', 3'-cycP terminated miRNA probes.

We were able to demonstrate the ligation of miRNA \gt p to chemically synthesized RNA targets in HeLa lysate through an endogenous RNA ligase. We furthermore found an improved ligation of miRNA \gt p species through the addition of bacterial RtcB. We evaluated different strategies to prevent unintended intra-miRNA ligation and identified a 5'-UniCap modification as a suitable 5'-cap to prevent guide-to-passenger ligation while maintaining biological activity. Based on our previous experience with miR-CLIP experiments[539], we designed a convenient CLIP work-flow and investigated suitable conditions for RNase digestion. Unfortunately, the final sequencing experiment did not yield the expected chimeric reads, presumably due to an insufficient stability of the miRNA \gt p probes in cells. We thus investigated alternative applications of 2', 3'-cycP RNAs and used such species for the synthesis of circular RNAs. Finally, we were able to show the cyclization of an siLin28B hairpin to a dumbbell siRNA. The maintenance of gene silencing activity comparable to a standard siLin28B duplex indicated efficient Dicer processing and RISC loading of the circular RNA.

4.5 Contributions

Oligonucleotide synthesis and *in vitro* miRNA>p ligation assays were performed by Stylianos Tsagkris and Christian Berk. Ligation of truncated pre-miR-20b>p and siLin28B>p dumbbell were performed by Christian Berk. Dual-Luciferase reporter assays for RISC tolerance of miRNA>p were performed by Eloise Baumann. Ligation assays for evaluation of 5'-capping groups and miRNA>p ligation assays after lysate incubation were performed by Stylianos Tsagkris. Dual-Luciferase reporter assays for RISC tolerance of 5'-capping groups, optimization of RNase T1 digestion, TaqMan RT-qPCR after transfection of siLin28B dumbbell and cyCLIP with subsequent library preparation was performed by Dr. Yuluan Wang. CyCLIP with northern blot detection was performed by Dr. Yuluan Wang and Christian Berk. Sequencing analysis was performed by Dr. Alexander Kanitz.

5 Side projects

5.1 Type III CRISPR–Cas systems produce cyclic oligoadenylate second messengers

In this work, we contributed to the identification of cyclic oligoadenylates as a novel class of second messengers in type III CRISPR-Cas systems[214]. In many prokaryotes, type III CRISPR-Cas systems contribute to the host's antiviral defense system through the coordinated degradation of both the invader DNA and its transcripts through a multisubunit effector complex[402]. In addition, target RNA binding leads to activation of the CRISPR-associated protein Csm6, which contributes to the immunity reaction through global degradation of cellular RNAs[572]. However, how invader DNA/ RNA sensing was linked to Csm6 activation remained unclear.

We could show that target RNA binding of the effector complex leads to the conversion of ATP to cyclic oligoadenylates via the Cas10 subunit. In turn, cyclic oligoadenylates function as second messengers to allosterically activate the standalone RNase Csm6 by binding to its CRISPR-associated Rossmann fold (CARF) domain. An important step in the identification of cyclic oligoadenylates as second messengers was the direct comparison of the endogenously synthesized second messenger to the corresponding isomeric RNA₄>p variants.

Individual contribution: The project was designed and led by Dr. Ole Niewoehner, Dr. Carmela Garcia-Doval and Prof. Dr. Martin Jinek. Christian Berk synthesized RNA₄>p variants and performed LC-MS analysis of endogenous second messengers and synthetic RNA₄>p standards. Jakob T. Rostøl performed phage infection assays. Dr. Frank Schwede synthesized rA₄>p. Laurent Bigler performed LC-MS analysis of additional Csm6-activators.

This work led to the following publication[214]:

Ole Niewoehner, Carmela Garcia-Doval, Jakob T. Rostøl, Christian Berk, Frank Schwede, Laurent Bigler, Jonathan Hall, Luciano A. Marraffini and Martin Jinek. *Type III CRISPR–Cas systems produce cyclic oligoadenylate second messengers*. Nature, 2017. 548(7669): p. 543.

5.2 Covalent linkage of the DNA repair template to the CRISPR-Cas9 nuclease enhances homology-directed repair

Type II CRISPR-Cas9 systems are commonly used as a tool for targeted genome editing in mammalian cells and hold great promise for therapeutic applications[387]. However, the existence of two competing dsDNA repair pathways poses a challenge for precise genome editing[573]. DNA repair via NHEJ leads to an error-prone direct ligation at the lesion site and is used as a tool for gene-knockout through indel formation. On the other hand, HDR can be exploited to precisely edit a specific DNA locus through a template guided repair of the double-strand break[387].

In this work, we demonstrated that covalent linkage of the DNA repair template to the Cas9 nuclease increases the rate of HDR and thus facilitates precise genome editing[394, 574]. Conjugation was achieved through reaction of a 5'-O⁶-benzylguanine labeled repair template with a fusion protein of Cas9 and an O⁶-alkylguanine-DNA alkyltransferase mutant (SNAP-tag).

Individual contributions: Dr. Natasa Savić, Femke C.A.S. Ringnalda and Gerald Schwank designed and led the project. Dr. Helen Lindsay analyzed the sequencing data. Christian Berk performed HPLC purification and LC-MS analysis. Katja Bargsten expressed recombinant proteins. Yizhou Li performed additional HPLC purification and LC-MS analysis.

This work led to the following publications[394, 574]:

Natasa Savić, Femke C.A.S. Ringnalda, Helen Lindsay, Christian Berk, Katja Bargsten, Yizhou Li, Dario Neri, Mark D. Robinson, Constance Ciaudo, Jonathan Hall, Martin Jinek and Gerald Schwank. *Covalent linkage of the DNA repair template to the CRISPR-Cas9 nuclease enhances homology-directed repair*. eLife, 2018. 7: p. e33761.

Natasa Savić, Femke C.A.S. Ringnalda, Christian Berk, Katja Bargsten, Jonathan Hall, Martin Jinek and Gerald Schwank. *In vitro Generation of CRISPR-Cas9 Complexes with Covalently Bound Repair Templates for Genome Editing in Mammalian Cells*. Bio-protocol, 2019. 9(1): p. e3136

5.3 One- and two-dimensional high-resolution NMR from flat surfaces

The atomic-level characterization of small amounts of analytes which are deposited on flat surfaces poses a challenge for analytical chemistry. Nevertheless, it is of high relevance for multiple applications including batteries, electronic circuits and advanced biosensors, such as microarrays[575-577].

In collaboration with the group of Prof. Dr. Lyndon Emsley (EPFL Lausanne) we could show that a combination of dynamic nuclear polarization surface enhanced NMR spectroscopy (DNP-SENS) and Carr-Purcell-Meiboom-Gill (CPMG) multiple-echo acquisition can be used to record one- and two-dimensional ^{31}P solid-state NMR spectra from 80 pmol of oligonucleotides, which have been adsorbed on sapphire wafers. For this, we synthesized a series of structurally diverse ORNs and ODNs with either PS, PO or mixed backbones and obtained magic-angle spinning (MAS) NMR spectra after deposition on fused silica, sapphire or borosilicate glass. We could detect a shift of the ^{31}P signal of two PS linkages which were embedded in a PO ODN upon hybridization with hsa-miR-34a-5p on sapphire. We hypothesized that this shift was the consequence of a conformational change due to bulge formation at the PS site after binding to the miRNA. In addition, we were able to monitor the unmasking of a DNB-capped 5'-phosphorothioate ORN after exposure to UV radiation.

Individual contributions: Dr. Brennan J. Walder and Prof. Dr. Lyndon Emsley designed and led the project. Christian Berk performed oligonucleotide synthesis, LC-MS analysis and optimized the procedure for adsorption of oligonucleotides on different surfaces. Dr. Wei-Chih Liao, Dr. Aaron Rossini and Dr. Martin Schwarzwälder prepared additional samples and consulted for the DNP-SENS CPMG MAS-NMR studies. Dr. Ugo Pradère synthesized and immobilized an ORN containing a 3'-terminal 2'-O-propargyl moiety on azide-functionalized glass plates via CuAAC.

This work resulted in the following publication[576]:

Brennan J. Walder, Christian Berk, Wei-Chih Liao, Aaron J. Rossini, Martin Schwarzwälder, Ugo Pradère, Jonathan Hall, Anne Lesage, Christophe Copéret and Lyndon Emsley. *One- and Two-Dimensional High-Resolution NMR from Flat Surfaces*. ACS Central Science, 2019. 5(3): p. 515-523.

5.4 Additional publications

The following additional publications were associated with this thesis[6, 31, 207]:

Pascal Röthlisberger, Christian Berk and Jonathan Hall. *RNA Chemistry for RNA Biology*. CHIMIA International Journal for Chemistry, 2019. 73(6): p. 368-373

Meiling Li, Helen L. Lightfoot, Francois Halloy, Anna L. Malinowska, Christian Berk, Alok K. Behera, Daniel Schümperli and Jonathan Hall. *Synthesis and cellular activity of stereochemically-pure 2'-O-(2-methoxyethyl)-phosphorothioate oligonucleotides*. Chemical Communications, 2017. 53(3): p. 541-544.

Andreas Brunschweiler, Luca F.R. Gebert, Matije Lucic, Ugo Pradère, Hartmut Jahns, Christian Berk, Jürg Hunziker and Jonathan Hall. *Site-specific conjugation of drug-like fragments to an antimiR scaffold as a strategy to target miRNAs inside RISC*. Chemical Communications, 2016. 52(1): p. 156-159.

6 Conclusion and Outlook

The work described in this thesis covers several aspects of RNA chemical biology with respect to the development of nucleic acid therapeutics. In the first project, we have evaluated the use of an *Rp*-enriched phosphorothioate backbone as an alternative scaffold for the systemic delivery of siRNAs. The stereochemical bias towards *Rp*-linkages was achieved during RNA synthesis through the use of BTT as an activator for the phosphoramidite coupling step as previously described[9]. We successfully scaled up the solid-phase synthesis of PS ORNs to produce sufficient quantities for the *in vitro* and *in vivo* investigation of a model PS siRNA directed against the oncoprotein Lin28B, which was recently shown to play an important role in the maintenance of CSCs in prostate cancer[329]. We could show that the PS scaffold increased the nuclease resistance of siLin28B in comparison to the parent PO duplex as well as to LNP-free patisiran, while maintaining gene silencing activity. Furthermore, binding studies with human serum albumin indicated an increased, although transient, protein binding of PS siLin28B compared to the PO variant. Therefore, we hypothesized that serum albumin could serve as a potential carrier protein to facilitate the tissue distribution of the PS siRNA *in vivo*. In order to investigate this, we evaluated four different methods for the detection of chemically modified RNAs and identified a PNA hybridization assay[108-113] as a suitable method to quantify PS siRNAs in tissue biopsies. In collaboration with the group of Prof. Catapano at the IOR Bellinzona, we showed that the PS siRNA could be recovered from several tissues after naked administration of a single dose of 50 mg/ kg PS siLin28B in nude mice. The main sites of accumulation were liver and kidney and lowest levels were found in blood, indicating a rapid tissue distribution and clearance. These results are in line with previous reports on the naked delivery of siRNAs *in vivo*[432, 466, 467]. In addition, the PS siRNA could be recovered from prostate tissue, further supporting the investigation of *Rp*-enriched PS siLin28B in a mouse xenograft model of prostate cancer. However, a 16 days' treatment involving eight s.c. injections of 50 mg/ kg PS siLin28B did not lead to a reduction in tumor growth in comparison to the treatment with a scrambled PS siRNA. We concluded that the metabolic stability of the PS siRNA, although increased compared to the PO variant, was not yet sufficient to achieve an anti-tumor effect *in vivo*.

A possible continuation of the project could involve the use of PS linkages with defined stereochemistry at the terminal positions in order to further reduce exonuclease-mediated degradation. Furthermore, the influence of a stereochemical bias at the terminal PS linkages in state-of-the-art ESC-GalNAc siRNAs could be investigated. In addition, combination of the PS scaffold with chemical modifications at different positions of the ribose or the nucleobase moiety offers a possibility to further modulate the properties of PS siRNAs.

In a second approach we investigated major-groove polyamine modification in order to improve the cellular uptake and nuclease stability of siRNAs. For this purpose, we synthesized a library of otherwise unmodified siRenilla conjugates via the convertible nucleoside approach[514] and compared their activity in a Dual-Luciferase reporter assay. We found a strong position dependence of the tolerance of spermine moieties across the siRenilla AS strand. Whereas the polyamine moieties were well tolerated at the 3'-terminus, even at multiple consecutive positions, modifications near the 5'-seed region modestly decreased the silencing activity. The strongest effect was observed with spermine modification at position 9. We hypothesized that the decrease in activity was due to the close proximity of this position to the RISC-cleavage site, potentially inducing structural perturbations at the RNase III domain inside AGO2. We then evaluated the potential of siRenilla-spm conjugates for gymnotic gene silencing in Huh7 and NT2/ D1 cells, both of which have been reported to express the polyamine transporter SLC22A16[511, 513]. However, we did not detect any silencing activity in these cell lines in the absence of transfection reagents. In addition, we found that results obtained in NT2/ D1 cells were generally difficult to reproduce due to the heterogeneity of this cell line as indicated by confocal microscopy studies. Furthermore, polyamine modification of the AS strand only modestly increased the stability of the duplex after incubation in 10% FBS. Nevertheless, results obtained after LNP-mediated transfection of siLin28B-spm conjugates indicated that spermine modification was also tolerated at the 3'-terminus of the passenger strand. Moreover, we demonstrated the applicability of the convertible nucleoside approach for the introduction of structurally diverse amine moieties and evaluated the RISC tolerance towards major groove phenethylamine modifications. Although similar trends were observed between aryl- and spermine siRenilla-conjugates, position-dependent effects of phenethylamine moieties were less pronounced. In addition, the convertible nucleoside approach was used to synthesize mono- and dimethylated pre-miRNA hairpins and rRNA fragments which served as probes for protein binding and macrolide-dependent ribosome stalling studies. Although our experiments indicate that modification with a limited number of natural spermine moieties is not sufficient to improve the cellular uptake and nuclease stability of siRNAs, conjugation to chemically modified spermine derivatives such as star-shaped dendrimer-like polyamines[481] might offer a possibility to achieve receptor-mediated uptake via the PTS. Furthermore, the convertible nucleoside approach can serve as an elegant methodology for the introduction of structurally diverse amine or thiol moieties and therefore offers a convenient route for the generation of siRNA-conjugate libraries.

In a third project, we changed the focus from improving the properties of RNA therapeutics to the development of a new methodology for the identification of miRNA targetomes in order to better understand the complex regulatory roles of non-coding RNAs in the cell. A thorough understanding of these regulatory networks is essential to select new targets for RNA

therapeutics. Despite the development of a number of experimental techniques for the identification of miRNA target sites, the efficiency of the ligation step that is required for the generation of miRNA-target chimeras remains low[529, 532]. As a consequence of this, many miRNA target sites have been identified by a single chimeric read, thereby limiting the reliability of the inferred targetomes[304, 529]. We therefore adopted a new strategy for chimera generation which relies on the ligation of chemically synthesized 2', 3'-cycP terminated miRNA probes to free 5'-hydroxyl ends of the target RNA. Such ligase activity has been previously observed in mammalian cell lysates[194, 210, 211] and recently, the bacterial RNA^{>p}/ 3'-p ligase RtcB has been made commercially available[550, 552].

We have synthesized a series of miRNA^{>p} probes and demonstrated the ligation of 5'-³²P-labelled miR-34a^{>p} to different target RNA constructs by an endogenous ligase present in HeLa lysate. We were able to improve the ligation efficiency through the use of recombinant *E. coli* RtcB in a suitable buffer system and evaluated the use of two 5'-capping groups to avoid unintended ligation between the two miRNA strands. We showed that 5'-unicap modification efficiently prevented miRNA guide-to-passenger ligation and did not impair RISC activity. Then, we designed a work-flow for this novel CLIP-type approach (termed cyCLIP) and prepared a sequencing library after applying the cyCLIP protocol in HeLa cells. Unfortunately, sequencing of the library did not yield the expected chimeric reads. We hypothesized that the lack of chimeric reads was due to an instability of the 2', 3'-cycP moiety in the cytoplasm. We therefore incubated the miRNA^{>p} probes in cell lysate for different time points and evaluated the ligation efficiency. A rapid decrease in ligation efficiency after 10 min of incubation suggested that the stability of the miRNA^{>p} probe was not sufficient. Alternatively, the bead-bound miRNA^{>p}/ target RNA duplex might not be accessible to the exogenously added RtcB. We thus investigated additional applications for the use of RtcB for the intramolecular ligation of RNA^{>p} variants. Finally, we were able to use RtcB for the circularization of a siLin28B^{>p} hairpin to a dumbbell structure with equal gene silencing ability as the unmodified siLin28B duplex.

In summary, we have addressed three key questions for the development of RNA therapeutics, namely

- nanoparticle-free delivery of siRNAs *in vivo*
- metabolic stabilization of siRNAs while avoiding potentially genotoxic chemical modifications
- reliable identification of miRNA target sites as a prerequisite for the development of novel therapeutic oligonucleotides.

In addition, we contributed to the elucidation of a novel mechanism linking invader RNA sensing to Csm6 activation via cyclic oligoadenylate second messengers in type III CRISPR-Cas systems [214] and the development of an improved method for Cas9-mediated genome editing through covalent linkage of the DNA repair template to the Cas9 nuclease [394, 574]. We therefore believe that the work described in this thesis contributes to our current understanding of RNA biology as well as the development of novel RNA therapeutics.

7 Experimental part

7.1 Oligonucleotide synthesis

7.1.1 General conditions for oligonucleotide synthesis

Chemicals for oligonucleotide synthesis were purchased from Sigma Aldrich (Steinheim, Germany), Fluorochem (Hadfield, United Kingdom) and TCI (Eschborn, Germany). Phosphoramidites were obtained from Thermo Fisher Scientific (Waltham, MA, USA). Oligonucleotides were synthesized on a MM12 synthesizer from Bio Automation (BioAutomation Corp., Irving, TX, USA) and standard 2'-TBDMS phosphoramidites (ThermoFisher, Waltham, MA, USA) were used. Phosphoramidites (PA) were prepared as 0.08 M solutions in dry acetonitrile (ACN), the activator 5-(Benzylthio)-1H-tetrazole (BTT; Biosolve BV, Valkenswaard, Netherlands) was prepared as a 0.24 M solution in dry ACN. Oxidizer was prepared as a 0.02 M I₂ solution in THF/ pyridine/ H₂O (70:20:10, w/v/v/v); Sulfurization was carried out using a 0.1 M solution of DDTT (Glen Research, Sterling, VA, USA) in dry pyridine/ ACN (9:1). Capping reagent A was THF/ lutidine/ acetic anhydride (8:1:1) and capping reagent B was 16% *N*-methylimidazole/ THF. Detritylations were performed using 3% dichloroacetic acid (DCA) in dichloromethane. 500 or 1000 Å UnyLinker CPG (ChemGenes, Wilmington, MA, USA) had an average loading of 40 μmol/ g. 2', 3' cyclic phosphate RNAs were synthesized on 5'-DMT-2', 3'-cyclic phosphate adenosine (*N*-Bz), uridine, cytidine (*N*-Ac) or guanosine (*N*-iBu) 1000 Å CPG (catalog no N-8501-XX, ChemGenes, Wilmington, MA, USA). 5'-BPS ligators for CL-qPCR were synthesized on a 500 Å dT-Q-CPG (Glen Research), using Pac-dA and iPr-Pac-dG CED phosphoramidites (Glen research) and a 5'-BPS-thymidine CED phosphoramidite previously synthesized by Martina Bigatti according to Boos et al.[206]. Deprotection of the 5'-BPS ligator was performed with 25% ammonia for 4 h at 25°C. 3'-PS ligators for CL-qPCR were synthesized on a 3'-phosphate-ON Icaa 1000 Å CPG (ChemGenes) with an initial sulfurization step. A 5'-phosphorothioate group was introduced via a DNB phosphoramidite as previously described[205] in combination with a sulfurization step. The 5'-DNB protecting group was removed after deposition of the ORN on sapphire through irradiation at 365 nm for 30 min/ side.

Conditions for small scale and large scale ORN synthesis are given in table 6.1 and 6.2, respectively.

Table 7. 1. Conditions for small scale ORN synthesis

Step	Reagent	Amount	Contact time
Loading	500 or 1000 Å UnyLinker CPG	5 mg	-
Deblock	3% DCA	2x 120 µl	2x 30 s
Coupling	0.08 M PA 0.024 M BTT	2x 50 µl 2x 100 µl	2x 90 s
Oxidation	0.02 M iodine	120 µl	60 s
Sulfurization	0.1 M DDTT	120 µl	360 s
Capping	Capping reagent A Capping reagent B	80 µl 80 µl	45 s

Table 7. 2. Conditions for large scale ORN synthesis

Step	Reagent	Amount	Contact time
Loading	500 or 1000 Å UnyLinker CPG	300 mg	-
Deblock	3% DCA	2x 2.5 ml	2x 90 s
Coupling	0.08 M phosphoramidite 0.024 M BTT	600 µl 1.2 ml	300 s
Oxidation	0.02 M iodine	2.0 ml	90 s
Sulfurization	0.1 M DDTT	2.0 ml	600 s
Capping	Capping reagent A Capping reagent B	1.6 ml 1.6 ml	90 s

7.1.2 Work-up and purification of oligonucleotides

Oligonucleotides were cleaved from the solid support and the protecting groups on the exocyclic amino groups and the backbone were removed using a 1:1 mixture of 40% aqueous methylamine and 25% aqueous ammonia (AMA) for 1 h at 65°C. For large scale synthesis, 300 mg CPG were divided into 50 mg portions and 600 µl AMA mix including 10 µl 1 M tris(hydroxymethyl)aminomethane (Tris). 2'-O-TBDMS groups were removed using a fresh mixture of NMP (120 µl), TEA (60 µl) and TEA.3HF, 80 µl) at 70°C for 2 h. Desilylation was quenched with trimethylethoxysilane (400 µl), then diisopropyl ether (200 µl) was added to precipitate the oligonucleotide. The precipitate was dissolved in H₂O and purified DMT-on (table 6.3) on an Agilent 1200 series HPLC fitted with a Waters XBridge Oligonucleotide BEH C18 column, 10 × 50 mm, 2.5 µm at 65 °C. Fractions were pooled, dried in a SpeedVac and treated for 15 min with 40% acetic acid at room temperature. After drying in a SpeedVac, oligonucleotides were dissolved in H₂O and subjected to a second purification on RP-HPLC (table 6.4). Eluent A was 0.1 M triethylammonium acetate, pH 8.0. Eluent B was acetonitrile.

Table 7. 3. Gradient for DMT-on RP-HPLC purification

Time (min)	Eluent A (%)	Eluent B (%)	flow rate (ml/ min)
0	90	10	5.0
5.0	50	50	5.0
6.0	5	95	5.0
6.5	5	95	5.0

Table 7. 4. Gradient for DMT-off RP-HPLC purification

Time (min)	Eluent A (%)	Eluent B (%)	flow rate (ml/ min)
0	98	2	5.0
8.0	80	20	5.0
9.0	5	95	5.0
9.5	5	95	5.0

For *in vivo* experiments, oligonucleotides were precipitated as their respective Na⁺ salts by adding 3 M sodium acetate (pH 5.5) to a final concentration of 0.3 M and 3 volumes of ethanol. Supernatant was discarded, pellet was washed 4x with 75% ethanol and dissolved in RNase free H₂O. Then RNA was sterile-filtered through 0.2 μm PVDF Unifo filters (GE Healthcare).

6.1.3 LC-MS analysis

The integrities of purified oligonucleotides were confirmed by LC-MS analysis (table 6.5) on an Agilent 1200/ 6130 system fitted with a Waters acquity UPLC OST C-18 column (2.1×50 mm, 1.7 μm) at 65 °C. Eluent A was aqueous hexafluoroisopropanol (0.4 M) containing triethylamine (15 mM). Eluent B was methanol.

Table 7. 5. Gradient for LC-MS analysis

Time (min)	Eluent A (%)	Eluent B (%)	flow rate (ml/ min)
0	95	5	0.3
14.0	65	35	0.3
15.0	5	95	0.3
16.0	5	95	0.3

6.1.4 Synthesis of siRNA conjugates via the convertible nucleoside approach

O⁴-triazolyluridine phosphoramidite was incorporated into the growing ORN chain during solid-phase synthesis without deviations from the standard protocol. 20 mg support bound ORN was suspended in 200 μl of 1 M spermine in MeOH and incubated at 55°C on an Eppendorf ThermoMixer (Eppendorf, Hamburg, Germany) for 14 h. The suspension was filtered to remove the CPG and the filtrate was desalted on a Glen Gel-Pak desalting column (Glen Research) according to the manufacturer's protocol. Deprotection was completed through a standard AMA treatment and work-up continued as for unmodified ORNs. For competition experiments with spermine/ diethylamine mixtures, diethylamine was added to the reaction mixture at a final concentration of 1 M (1:1 ratio) or 2 M (1:2 ratio). Methylamine or dimethylamine conjugation was achieved through incubation of the CPG in 40% aqueous methylamine or dimethylamine at 45°C for 2.5 h. Then, an equal volume of 25% aqueous ammonia was added and temperature increased to 65°C for 30 min. For phenethylamine conjugation, the spermine solution (1 M in MeOH) was replaced by 200 μl neat phenethylamine. Unlike spermine, phenethylamine does not cleave the ORN from the CPG

and therefore excess reagent was removed by filtration. The CPG was washed with EtOH and subsequently worked-up in the same manner as unmodified ORNs.

7.1.5 Synthesis of an siRNA-spermine conjugate via click chemistry

The protocol was adapted from Pradère and Hall[578]. 2'-O-propargyluridine CED phosphoramidite was incorporated into the growing ORN chain during solid-phase synthesis without deviations from the standard protocol and work-up was identical to unmodified ORNs. Spermine-N₃.3TFA was dissolved in MeOH and incubated with polymer-bound tris(2-aminoethyl)amine overnight (200-400 mesh, Sigma Aldrich). The resin was removed by filtration and the filtrate was evaporated under vacuum. To 10 µl of a 150 µM solution (1.5 nmol) of purified siRenilla sense strand containing a 3'-terminal 2'-O-propargyl uridine building block were added 15 µl water, 28.5 µl PBS buffer (pH 7.4), 2.5 µl of aqueous 50 mM tris-hydroxypropyltriazolylmethylamine (THPTA), 1.25 µl of 40 mM spermine-N₃ in DMF, 1.25 µl 20 mM aqueous CuSO₄·5 H₂O and 2.5 µl 100 mM aqueous Na-ascorbate. The reaction mixture was shaken at 45 °C for 2 hours. After cooling to room temperature, the reaction mixture was diluted with 150 µl H₂O and extracted 3x with 200 µl EtOAc. 25 µl 3 M sodium acetate and 800 µl EtOH/ iPrOH (2:1) were added to the aqueous phase and RNA was precipitated at -20°C overnight. After centrifugation for 10 min at 12'000 rpm at 4°C the supernatant was removed and the pellet was dissolved in 200 µl H₂O for HPLC purification using the standard DMT-off gradient (table 6.4).

7.1.6 Synthesis of Cy3 forward primer for CL-qPCR

Cy3-N₃ and 2'-O-propargyl cytidine CED phosphoramidite were previously synthesized by Martina Bigatti according to [579]. 2'-O-propargyl cytidine CED phosphoramidite was incorporated during the solid-phase synthesis under standard coupling conditions. To crude CL-qPCR forward primers 1 and 2 containing a 3'-terminal 2'-O-propargyl cytidine, was added 150 µl PBS, 150 µl MeOH, 20 µl 25 mM TBTA in DMF, 20 µl 50 mM Cy3-N₃ in DMF, 10 µl 50 mM aqueous Na-ascorbate and 10 µl 5 mM aqueous CuSO₄·5H₂O. The reaction mixture was shaken overnight at 45 °C. The CPG was isolated by filtration and washed with 3x 200 µl DMF, then 3x 200 µl aqueous 0.1 M ethylenediaminetetraacetic acid (EDTA, pH 8.2), 3x 200 µl DMF, 3x 200 µl ACN and 3x 200 µl chloroform. Cleavage from solid support and work-up/purification was performed as for unmodified oligonucleotides with the exception that the DMT-off gradient was 5-40% eluent B in 10 min.

7.1.7 Coating of oligonucleotides on sapphire, borosilicate glass and fused silica

Sapphire cover slips (WST-102; diameter= 10 mm, thickness= 0.20 mm; U.Q.G. Optics Limited, Cambridge, England) were coated on each side with the amount of oligonucleotide

corresponding to 0.9 nmol of each phosphate species (PS or PO) out of 80 µl aqueous solutions. For example, to coat a sapphire disk with 200 pmol of ORN, 80 µL of a 1.25 µM solution was deposited on each side of the disk and air-dried overnight. Coating of ORNs on borosilicate glass disks (diameter= 12 mm, thickness= 0.13 to 0.16 mm, Thermo Scientific Menzel, Loughborough, England) was performed in the same manner. Coating on fused silica was achieved by freeze drying the oligonucleotide solution in a fused silica electron paramagnetic resonance (EPR) tube fitted with a self-made teflon coated insert to ensure thin-layer coating on the inner wall. The teflon-coated insert and a cooling block for lyophilisation of ORNs in EPR tubes was prepared with the help of Markus Küpfer in the mechanical workshop (HCI D192.3).

7.2 Cell culture

7.2.1 General conditions

HeLa, HEK293T and Huh7 cells were maintained in Dulbecco's modified Eagle's medium (DMEM; Invitrogen) supplemented with 10% fetal bovine serum (Sigma). All cell culture handlings were performed under a laminar flow cabinet (Biowizard Golden Line, Kojair).

7.2.2 Western blots

40'000 HEK 293T or Huh7 cells were seeded in each well of a 24-well plate. Transfection of siRNAs at a final concentration of 40 nM using Lipofectamine 2000 (Thermo Fisher) was performed according to the manufacturer's instructions 12 h after seeding. For naked delivery, siRNAs were added to a final concentration of 1 µM without transfection reagent. Cells were harvested 48 h post-transfection using RIPA lysis buffer (Sigma). Protein concentrations were determined using a BCA assay (Thermo Fisher) according to the manufacturer's recommendations. 2 µg total protein were prepared in 1x Lämmli buffer (BioRAD) and boiled at 95 °C for 5 min, followed by PAGE-separation on a 4-20% SDS Mini-PROTEAN TGX Precast Gel (BioRAD) and wet-blotting on a polyvinylidene difluoride membrane (GE Healthcare). The membrane was blocked for 2 h at room temperature with 5% milk in PBS containing 0.05% Tween 20 (PBST). Overnight staining with Lin28B rabbit primary antibody (Cell Signaling) was performed at 4 °C at a dilution ratio of 1:3000 in PBST. After washing, the membrane was incubated in peroxidase-labelled goat anti-rabbit secondary antibody (KPL) in a 1:10'000 dilution in PBST for 90 min at RT. Chemiluminescence was induced via ECL prime western blotting detection (Amersham Biosciences) according to the manufacturer's protocol and visualized using a ChemiDoc device (BioRAD). The membrane was stripped for 15 min with stripping buffer (Thermo Fisher), followed by washing, blocking and overnight incubation with GAPDH antibody (mouse monoclonal antibody, OriGene) in a 1:10'000 dilution in PBST

at 4°C. Then the membrane was washed and incubated with a 1:10'000 dilution of peroxidase-labelled goat anti-mouse secondary antibody (KPL) in PBST for 1 h at room temperature. Visualization as described above. Protein bands were quantified by densitometry using the analysis software ImageJ.

7.2.3 SYBR Green RT-qPCR

Lipofectamine 2000-transfection of siRNAs was performed as described for western blot experiments. Total RNA was extracted using TRIzol (Invitrogen) according to the manufacturer's protocol. RNA concentrations were measured on a NanoDrop 2000 spectrophotometer. For mRNA analysis, 1 µg of total RNA was reverse transcribed using the TaqMan microRNA reverse transcription kit (Applied Biosystems) according to the manufacturer's protocol. Final concentrations in the RT reaction mix were: 1x RT buffer, 4 mM dNTP mix, 12.5 µM random hexamer primers (Microsynth), 12.5 µM oligo(dT)₁₅ primers (Promega), 2.5u multiscribe reverse transcriptase and 2u RNase inhibitor (RNasin, Promega). RT was performed on a thermocycler C1000 or S1000 (BioRad) according to the following program: 25°C, 10 min; 37°C, 120 min; 85°C, 5min.

SYBR Green qPCR was performed on a LightCycler 480 instrument (Roche) using KAPA SYBR FAST for Roche LightCycler 480 (KK4610, Sigma-Aldrich). PCR primers were designed using the Universal ProbeLibrary System Assay Design (Roche) and were ordered from Microsynth (Balgach, Switzerland). Cycling conditions were 95°C, 10 min and 40 cycles of 95°C, 15 s; 60°C, 1 min. Each reaction was carried out in three technical replicates. Cp values were extracted with the LightCycler software V1.5 (Roche). The sequences of qPCR primers are given in table 6.6. Mock treatment was Lipofectamine 2000 alone.

Table 7. 6. Primers used for SYBR Green RT-qPCR

Gene symbol, transcript ID	Primer orientation	Sequence (5'-3')
Lin28B NM_001004317.4	Forward Reverse	GAAAAGAAAACCAAAGGGAGATAGA GAGGTAGACTACATTCCTTAGCATGA
GAPDH NM_002046.7	Forward Reverse	AGCCACATCGCTCAGACAC GCCCAATACGACCAAATCC
ACTB NM_001101.5	Forward Reverse	CCAACCGCGAGAAGATGA CCAGAGGCGTACAGGGATAG

7.2.4 TaqMan RT-qPCR

TaqMan RT-qPCR was performed using commercially available TaqMan assay kits. Stem-loop primer, TaqMan probe and qPCR primers were designed by Thermo Fisher. Two TaqMan sets were evaluated. TaqMan set 1: CT9HHW6; TaqMan set 2: CS9KC6U.

Step 1, reverse transcription. Reverse transcription was either performed using the TaqMan microRNA Reverse Transcription kit (4366597, Applied Biosystems) including the use of multiscribe reverse transcriptase or the SuperScript III assay kit (Thermo Fisher) including the use of SuperScript III reverse transcriptase. RT program for multiscribe reverse transcriptase was: 16°C, 30 min; 42°C, 30 min; 85°C, 5 min. RT program for Superscript III reverse transcriptase was: 55°C, 30min, 70°C, 15min. Total RNA concentration was adjusted to 100 ng/ μ l. For the generation of calibration curves, PS siLin28B was either analyzed in H₂O or spiked into mouse liver lysate (provided by Dr. Paulina Cwiek). RT mix was first prepared without siLin28B and kept at 4°C on a thermocycler (Bio Rad). In order to separate siRNA strands prior to RT, siRNA standards were heated to 95°C for 5 min on an adjacent thermocycler and then quickly transferred to the previously prepared RT-mix as described by [208]. The mastermix for reverse transcription is given in table 6.7.

Table 7. 7. Mastermix for reverse transcription for TaqMan RT-qPCR

Component	Volume per reaction (μ l)
100mM dNTPs	0.0825
Reverse transcriptase	0.55
10X RT buffer	0.825
Rnase inhibitor	0.1045
RNAse free H ₂ O	2.288
RT primer	1.5

5 μ l RT-mastermix were pipetted into PCR stripes on a thermocycler and 2.5 μ l of denatured siRNA standards were added.

Step 2, TaqMan qPCR. TaqMan qPCR was performed using the GoTaq probe qPCR assay kit (Promega) according to the manufacturer's protocol. The mastermix for TaqMan qPCR is given in table 6.8.

Table 7. 8. Mastermix for TaqMan qPCR

Component	Volume per reaction (µl)
TaqMan assay (primer + probe)	0.48
2x GoTaq probe master mix	4.8
RNase free H ₂ O	3.68

24.6 µl qPCR master mix was mixed with 1.76 µl RT product in PCR stripes. Samples were then distributed on a 384-well hard-shell PCR plate (8 µl/ well) and the plate was sealed. TaqMan qPCR was performed on a LightCycler 480 instrument (Roche) using the following program: Activation: 10 min, 95°C, followed by 45 cycles: 10 s, 95°C; 30 s, 60°C; 1 s, 72°C.

7.2.5 Chemical ligation-qPCR

For the generation of calibration curves, siRNA standards were prepared at concentrations of 500 nM, 100 nM, 10 nM, 1 nM, 500 pM, 100 pM, 1 pM and 100 fM and 0 fM (NTC). For qPCR quantification, the FastStart Taq DNA polymerase assay kit (Roche, including 10x PCR buffer) was used.

Step 1, chemical ligation. A CL mastermix was prepared on ice containing the components given in table 6.9.

Table 7. 9. Mastermix for chemical ligation

Component	Volume per reaction (µl)
Mouse liver total RNA (100 ng/ µl)	5.0
10x PCR buffer (20 mM Mg ²⁺)	1
Poly A (1 µg/ µl)	1
10 µM PS ligator	0.3
10 µM BPS ligator	0.3
RNase-free H ₂ O	0.4

8 µl Cl mastermix were added to a PCR tube and kept at room temperature on a thermocycler (BioRad). On an adjacent thermocycler, siRNA standards were denatured at 95°C for 5 min

and 2 μ l standard were quickly transferred to each CL master mix. Chemical ligation was performed at 33°C for 1 h.

Step 2, qPCR. qPCR quantification was prepared in technical triplicates. A qPCR master mix containing the components listed in table 6.10 was prepared on ice.

Table 7. 10. Mastermix for qPCR after CL

Component	Volume per reaction (μ l)
H ₂ O, nanopure	5.85
dNTPs, 100mM	0.15
10x PCR buffer (20 mM Mg ²⁺)	1
10 μ M Fwd primer	0.3
10 μ M Rev primer	0.3
10 μ M BHQ anti primer	0.3
Hot Start Taq Polymerase (5 U/ μ l)	0.1

A sub-mastermix for technical triplicates was prepared in a 96 well plate by addition of 26.4 μ l qPCR master mix and 6.6 μ l CL-mix (10% overage). Plate was sealed and centrifuged for 15 s at 1000 rpm. Samples were then distributed on a 384-well hard-shell PCR plate (8 μ l/ well) and the plate was sealed. qPCR was performed on a LightCycler 480 instrument (Roche) using the following program: Activation: 10 min, 95°C, followed by 50 cycles: 3 s, 95°C; 30 s, 48°C; 10 s, 72°C.

7.2.6 Northern blot

Step 1, T4-PNK radiolabeling of RNA probes. Each RNA probe was radioactively labeled (15 μ Ci) using T4-polynucleotide kinase (New England Biolabs) and [γ -³²P] adenosine triphosphate (ATP, 6000 Ci/ mmol, 150 mCi/ ml; Perkin Elmer). 1 μ l of RNA probe (100 nM final) was mixed with RNAsin, RNase-free water, PNK buffer, T4 PNK, and [γ -³²P] ATP (table 6.11) in a dedicated Type C laboratory and incubated at 37°C for 30 min followed by 5 min of heat inactivation at 95°C. Probes were purified using G-25 sephadex spin columns (GE healthcare).

Table 7. 11. Radiolabeling of RNA-probes for northern blots

Reagent	Volume (μ l)
RNase-free H ₂ O	5
1 μ M (cold) RNA	1
10x PNK buffer	1
RNasin	0.5
T4 PNK (10'000U/ml ; M0201S)	1
[γ - ³² P]ATP (6000Ci/mmol, 150mCi/ml)	1.5

Step 2, denaturing polyacrylamide gel electrophoresis (dPAGE). A 12% denaturing polyacrylamide gel was prepared by mixing the reagents listed in table 6.12.

Table 7. 12. Gel composition for 12% dPAGE for northern blots

Reagent	Volume
National diagnostics Urea gel system Concentrate (25%)	24 ml
National diagnostics Urea gel system Diluent	21 ml
National diagnostics Urea gel system Buffer	5 ml
10% ammonium peroxodisulfate (APS)	400 μ l
TEMED	20 μ l

PS siLin28B standards were spiked into mouse liver lysate (provided by Dr. Paulina Cwiek). Total RNA extracted from cyCLIP samples was used as an aqueous solution.

Before loading, gel was prerun at 100 V, 20 mA for 15 min. RNA samples were mixed with 2x formamide loading dye (95% formamide, 0.005% bromphenol blue, 0.05% xylene cyanol FF, 4 mM EDTA) and heated at 95°C for 5 min. After loading, gel was run in 0.5x TBE buffer at 25 mA for 4 h. RNA was transferred on a Biorad Trans-Blot SD semidry blotter to a Hybond-NX membrane (Amersham) at 2.5 mA/ cm² with the voltage limited to 25 V. RNA was crosslinked for 2 h at 60°C using a freshly prepared mix of solution A (12.5 M 1-methylimidazole, pH= 8.) and solution B (0.16 M 1-Ethyl-3-(3-

dimethylaminopropyl)carbodiimid). Membrane was rinsed with 0.5x TBE buffer and stored overnight at 4°C.

Step 3, Prehybridisation. Prehybridisation of the membrane was performed in a dedicated Type C laboratory for 30 min at 40.5°C with in a rotary oven (Thermo Fisher) with the hybridization buffer given in table 6.13.

Table 7. 13. Hybridization buffer for northern blots

Reagent	Volume
20x saline sodium citrate buffer (SSC)	7.5 ml
1M Na ₂ HPO ₄ , pH 7.2	0.6 ml
20% SDS	3 ml
50x Denhardts	0.6 ml
H ₂ O	(18.3 ml ad 30 ml)
Spatula tip of "Roche Nucl. Acid blocking agent"	

20x SSC: 3.0 M NaCl, 0.3 M trisodium citrate, pH= 7.2

50x Denhardts: 1% Ficoll 400, 1% polyvinylpyrrolidone, 1% bovine serum albumin.

After prehybridisation, radioactively labeled probe was added and hybridization performed at 40.5°C overnight. Afterwards, hybridization buffer was discarded and membrane was washed twice with washing buffers 1 (table 6.14) and 2 (table 6.15).

Table 7. 14. Washing buffer 1 for northern blots

Reagent	Volume
5x SSC	125 ml of 20x SSC
1% SDS	25 ml of 20% SDS
H ₂ O	350ml (ad 500 ml)

Table 7. 15. Washing buffer 2 for northern blots

Reagent	Volume
5x SSC	125 ml of 20x SSC
1% SDS	25 ml of 20% SDS
H ₂ O	350ml (ad 500 ml)

After washing, the membrane was exposed to a phosphor screen (Thermo Fisher) overnight. Read-out was performed on a Typhoon scanner at a pixel size of 200 microns and membrane was stripped with stripping buffer (table 6.16).

Table 7. 16. Stripping buffer for northern blots

Reagent	Volume
20% SDS	25 ml
H ₂ O	475 ml

7.2.7 Dual-Luciferase reporter assays

Dual-Luciferase assays were performed in 96 well-plates in HeLa and Huh7 cells. 8000 cells/ well were seeded in 80 μ l DMEM supplemented with 10% FBS. SiRNAs were transfected in Opti-MEM (Invitrogen) serum-free medium after 8 h using Lipofectamine 2000 according to the manufacturer's recommendations. Final siRNA concentrations were 20, 5 and 1.25 nM for HeLa and 40, 10 and 2.5 nM for Huh7 cells. Mock-treated samples were treated with Opti-MEM only. The positive control was unmodified siRenilla, negative control was scrambled siRenilla with a single spermine or phenethylamine modification at the 3' end of the AS strand (scr_si-spm and scr_si-phen, respectively). The negative control for miRNA>p Dual-Luciferase assays was a previously described randomized siRNA[580]. 24 h after siRNA transfection, psiCHECK-2 reporter plasmids (Promega) were transfected with jetPEI (Polyplus Transfection) at a final concentration of 40 ng /well according to the manufacturer's recommendations. Each replicate experiment was performed in technical triplicates. Mean +/- SD are given from 3 independent biological replicates for Huh7 and 3-6 replicates for HeLa cells. For reporter assays using siRenilla conjugates, unmodified psi-CHECK-2 plasmids were used. For reporter assays using miRNA>p, plasmids contained the target sites listed in table 6.17.

For gymnosis studies, Huh7 cells were seeded as described above. SiRNAs were added 8 h after seeding without transfection reagent at final concentrations of 1, 0.5, 0.25 and 0 μ M. Prior to transfection of the psiCHECK-2 vector as above, the growth medium was removed and cells were washed 3x with PBS and 90 μ l fresh DMEM (10% FBS) was added.

For polyamine depletion, a final concentration of 100 μ M APCHA and 500 μ M DFMO was added to the medium 6 h and 48 h after seeding of Huh7 cells. Cells were cultured for 6 days after first APCHA/ DFMO treatment before starting the luciferase assay.

Readout was performed 48 h after transfection of the reporter-plasmid using the Dual-Glo Luciferase Assay System (E2980, Promega), according to the manufacturer's instructions. Luminescence was measured on a Mithras LB940 multimode microplate reader (Berthold Technologies). Renilla luminescence was normalized to the firefly signal and to the mean of all mock treatments across the respective plate.

Table 7. 17. Sequences used for reporter plasmid cloning

Reporter plasmids	Sequence (5'-3')
hsa-miR-106a (1x target site, fully complementary)	<i>CCTCCACTTCAGCCAGGACTCGAGGTTAGGGGTATATGATGGGGAGTAGATCTTTCTAGGAGGGAGACACTGGCCCCTCAAATCGTCCAGCGACCTTCCTCATCCACCCCATCTACCTGCACTGTAAGCACTTTTATTAGCAGCGGAACAAGGAGTCAGACATTTTAA</i> <i>GATGGCGGCCGC</i> <i>TGAGTCTTCGGACCTCGC</i>
hsa-miR-34a (3x target sites, fully complementary)	<i>CCTCCACTTCAGCCAGGACTCGAGAGGGTTTGAAATATAGCTGTTCTTTATGCATAAAACACACAACCAGCTAAGACACTGCCAGAGAAAAAATCGTATTGAATGGCCATTTCCCTACTTATAAGATGTCTCAATCTGAATTTGCGGCCGC</i> <i>TGAGTCTTCGGACCTCGC</i>
hsa-let-7g (1x target site, fully complementary)	<i>CCTCCACTTCAGCCAGGACTCGAGTTTTTCATTTTGAAGGGGCCTCACCGAGTGGGGGCATCATCAAAAACCTTTAACTATACAACCTACTACCTCAGGAGTCCCCTCACCTCCTCTAAGGTTGGGCAGGTGACCCTGAAGTGAGCACAGCCTAGGGCTGAGCTGGGGACCTGGTGCGGCCGC</i> <i>TGAGTCTTCGGACCTCGC</i>

Restriction sites are underlined, primer binding sites are indicated as italicized letters.

7.3 *In vitro* experiments

7.3.1 Tritosome stability assays

Tritosome stability assays were performed based on literature protocols[182, 202].

Rat liver tritosomes (R0610.LT, lot 1610405) were purchased from Xenotech LLC (Kansas City, KS, USA). Lot-specific acid phosphatase levels were 2.827 units/ ml and RNase detection was 23.65 fold above minus control (data provided by Xenotech). Tritosome extracts were standardized to 0.5 units/ ml acid phosphatase in 20 mM citrate buffer (pH=5) as previously described[182, 202]. For each time point, 25 μ l tritosome dilution (4.42 μ l undiluted tritosomes + 20.58 μ l citrate buffer) and 6 μ l 60 μ M siRNA (11.6 μ M final) were incubated at 37°C for the given time points. Collected time points were 0, 0.5, 1, 2, 4, 6 and 24 h. For this, 30 μ l aliquots were drawn from a mastermix containing 33.15 μ l undiluted tritosomes, 154.35 μ l 20 mM Na-citrate (pH=5) and 45 μ l 60 μ M siRNA (calculated for 7.5 aliquots). A mock sample was incubated in H₂O for 24 h. Incubation was quenched by adding 30 μ l of the incubation mixture to 66 μ l MasterPure tissue lysis solution (Epicentre, WI, USA) and 4 μ l proteinase K (20 mg/ ml, Roche). Proteinase K digestion was performed at 65°C for 30 min. Afterwards mixtures were stored at -80°C until analysis.

Shortly before the analysis, samples were thawed on ice and proteinase K was denatured at 95°C for 5 min. Afterwards SDS was precipitated by adding 20 μ l 3 M KCl and shaking for 10 min. SDS was pelleted by centrifugation at 4°C, 12xG for 10 min. Supernatant was transferred to a fresh eppendorff tube and centrifuged again. Cleared supernatants were analyzed on a Hitachi VWR LaChrom Elite HPLC fitted with a DNA Pac PA200 (4x250 mm) anion exchange column and a DNA Pac PA200 (4x50 mm) guard column at 30°C (HPLC gradient in table 6.18). Eluent A was a 1:1 mixture (v:v) of buffer A and ACN. Buffer A was an aqueous solution of 1 mM EDTA and 25 mM Tris.HCl (pH = 8.5). Eluent B was a 1:1 mixture (v:v) of buffer B and ACN. Buffer B was an aqueous solution of 1 mM EDTA, 25 mM Tris.HCl and 1.6 M NaClO₄ (pH = 8.5). Eluents were thoroughly degassed prior to use. Storage solution for DNA Pac PA200 was an aqueous solution of 20 mM Tris.HCl and 1.25 M NaCl (pH= 8.0). UV absorbance was monitored at 260 nm using a Hitachi VWR Elite LaChrom L-2420 UV detector.

Table 7. 18. Gradient for anion exchange HPLC analysis

Time (min)	Eluent A (%)	Eluent B (%)	flow rate (ml/ min)
0.0	100	0	1.0
2.0	100	0	1.0
7.0	46	54	1.0
9.0	0	100	1.0
10.0	0	100	1.0
12.0	100	0	1.0
17.0	100	0	1.0

7.3.2 Mouse serum stability assays

Serum stability assays were performed exactly as described for the tritosome assay, except that the tritosome dilution was replaced by a 1:1 mixture (v:v) of mouse serum (S-25 M, Sigma Aldrich) and H₂O.

7.3.3 PNA hybridization assay

PNA hybridization assays were performed based on literature protocols[108-113]. Frozen tissues were pulverized with a mortar and pestle in liquid nitrogen. Pulverized tissues were homogenized in 1 ml MasterPure tissue lysis solution (Epicentre) supplemented with 40 µl Proteinase K (20 mg/ ml, Roche) in a tissue lyser (Qiagen, Germany) using Qiagen stainless steel beads (5 mm) for 6 min with a frequency of 30 Hz. Tissue homogenates were centrifuged at 10xG, 4°C for 5 min and supernatant was transferred to clean Eppendorff tubes. Then, proteinase K digestion was performed at 65°C for 30 min. SDS was precipitated by adding 20 µl 3 M KCl per 100 µl tissue lysate and centrifugation at 14XG for 10 min, followed by another 2 centrifugation steps to clear the lysate. After each centrifugation, the supernatant was transferred to a clean Eppendorff tube. For blood samples, 300 µl blood were mixed with 600 µl lysis buffer. To 100 µl of cleared lysate was added 95 µl hybridization buffer and 5 µl atto425-PNA probe (8 µM in 20% ACN). Hybridization buffer was an aqueous solution of 50 mM Tris (pH= 8.8) containing 10% ACN. PNA probe was hybridized to the PS siLin28B AS strand in 50 µl aliquots on a thermocycler according to the following temperature program: 95°C for 15 min followed by 20°C for 15 min. After hybridization, supernatants were pooled and centrifuged again (10xG, 4°C for 15 min). Cleared supernatants were subjected to anion

exchange HPLC as described for the tritosome stability assay except that fluorescence at 484 nm was monitored on a Hitachi VWR LaChrom Elite L-2485 detector and column temperature was 50°C. Settings of the fluorescence detector were as follows: Excitation at 436 nm; emission monitored at 484 nm; response time= 1.0 s; sampling period= 50 ms; offset= 0 FLU; emission bandwidth= standard; photomultiplier (PMT) voltage: high; baseline: autozero

7.3.4 FBS stability assays

1.5 µl 80 µM siRenilla, si-spm4 or si-spm6 per aliquot (V= 10 µl per aliquot, 12 µM final) were incubated in 10% FBS at 37°C for the indicated time points. 10 µl aliquots were drawn from a master mix containing 6.5 µl FBS (Sigma Aldrich), 48.75 µl RNase-free H₂O and 9.75 µl 80 µM siRNA (calculated for 6.5 aliquots). A mock sample was incubated in H₂O for 24h. Time points were 0, 1, 2, 4, 8 and 24 h.

Incubation was quenched by addition of 10 µl MasterPure tissue lysis solution (Epicentre) and 2 µl Proteinase K (20 mg/ ml, Roche). Proteinase K digestion was performed at 65°C for 30 min. Aliquots were stored at -80°C until analysis.

5 µl of each aliquot were mixed with 2 µl 6X loading dye purple, no SDS (NEB) and 4 µl H₂O. Samples were analyzed on a 4-20% precast native PA gel (Mini-PROTEAN® TGX Stain-Free™ Protein Gel) using 1x TBE buffer at 60 V for 2 h.

7.3.5 Thermal denaturation studies

UV melting was performed on a Cary 300 instrument (Varian, Palo Alto, CA) equipped with a thermocontroller. 3 µM siRNA solutions were annealed in melting buffer (100 mM NaCl, 10 mM phosphate, 0.1 mM Na₂EDTA, pH = 7.0) by heating to 90°C (5°C/ min) followed by cooling to 20°C. Melting curves were obtained through heating to 90°C (0.5°C/ min) and measuring the absorption at 260 nm. T_m +/- SD was calculated from the maxima of the first derivatives of 3 melting curves.

7.3.6 Electrophoretic mobility shift assay

A PAGE migration assay was used to evaluate siRNA binding to human serum albumin. The protocol was based on previous reports by Sarett et al.[581] and Hvam et al.[582].

An albumin stock solution was prepared by dissolving 2.73 mg HSA (A3782, Sigma Aldrich) in 200 µl PBS (200 µM). 1:1 dilutions were prepared with PBS to obtain the following HSA concentrations: 200, 100, 50 and 25 µM. 0.5 µl of 20 µM siRNA stocks was added to 19.5 µl of the respective HSA solution or PBS. Final concentration of RNA was kept constant at 0.5 µM. Samples were incubated at 37°C for 2 h and then mixed with 6x NEB gel loading dye purple, no SDS (B7025S, New England Biolabs). Samples were analyzed on a 4-20% precast

native PA gel (Mini-PROTEAN® TGX Stain-Free™ Protein Gel) using 1x TBE buffer at 60 V for 2 h. 10 µl of sample were loaded per well. RNA was visualized with SYBR Gold Nucleic Acid stain (Invitrogen). HSA was visualized with Bio-Safe Coomassie stain (BioRad).

7.3.7 Fluorescence displacement assay

Fluorescence displacement assays were performed according to Er et al.[583]. Fluorescence displacement was measured separately for HSA binding sites 1 and 2. Dansylamide (DNSA) was used to measure binding to HSA binding site 1 and BD140 for binding site 2. siRNA/ ORN and HSA stock solutions were prepared at a concentration of 100 µM. The assay buffer was 10% DMSO in phosphate buffer (10 mM, pH= 7.2). The fluorescent dye mix contained 30 µM BD140, 100 µM DNSA and 0.1% (v/v) triton 100 in H₂O. Ibuprofen was used as a positive control. Assay mixtures were prepared according to table 6.19.

Table 7. 19. Pipetting scheme for fluorescence displacement assay

Desired siRNA concentration							Component (V, µl)
50 µM	25 µM	12.5 µM	6.25 µM	3.13 µM	1.56 µM	0.78 µM	
5	5	5	5	5	5	5	Buffer
5	5	5	5	5	5	5	HSA
5	5	5	5	5	5	5	Dye mix
10	22.5	28.8	31.9	33.4	34.2	34.6	H ₂ O
25	12.5	6.2	3.1	1.6	0.8	0.4	siRNA stock

Samples (15 µl/ well) were distributed on a 384 well polypropylene plate (CLS 3658, Corning) and incubated for 30 min at room temperature. Measurement was performed on a Tecan SPARK 20M microplate reader (Tecan, Switzerland). Excitation at 365 nm, fluorescence was measured at 480 nm (DNSA) or 585 nm (BD140). Each measurement was performed in technical triplicates.

7.3.8 Ligation assay in HeLa lysate

Step 1, preparation of HeLa lysate. HeLa cells were cultured in 10 cm² dishes (Techno Plastic Products) until 90% confluency was reached. Cells were washed with PBS (Gibco, Life Technologies) and lysed through scraping on ice with 400 µl lysis buffer (30 mM HEPES-KOH, pH 7.4, 5 mM MgCl₂, 100 mM KCl, 1x cOmplete EDTA-free protease inhibitor, 1 mM DTT, 10% glycerol and 0.5% NP-40). Cell extracts were collected in 1.5 ml microcentrifuge tubes and

incubated for 10 min on ice. Samples were vortexed frequently to ensure efficient lysis. Cell extracts were centrifuged at 17,000xG at 4°C for 10 min and the supernatant was snap-frozen in 50 µl aliquots. Aliquots were stored at -80°C.

Step 2, protein quantification and standardization of cell extracts. Cell extracts were standardized to a protein concentration of 2.1 mg/ ml. Protein concentration was measured according to the Bradford assay standard procedure for microtiter plates (sample: dye= 1:20) as described by the manufacturer (protein assay dye reagent concentrate, BioRad). In brief, 10 µl of cleared cell supernatants of BSA protein standards were mixed in a 96 well plate with 200 µl diluted dye reagent (1:5 dilution in H₂O). The plate was shaken for 30 s and incubated at room temperature for 15 min. Absorption was measured at 620 nm for 1 s per well.

Step 3, ³²P radiolabeling. RNAs were labelled as described for northern blots despite radiolabeling of miR-34a-5p>p was performed using T4 PNK 3'-phosphatase minus (10,000 U/ ml, NEB) to avoid removal of the 2', 3' cycP terminus.

Step 4, ligation assay. Radiolabelled miR-34a-5p>p was annealed to different counterstrands by heating in annealing buffer (30 mM HEPES KOH pH 7.4, 4 mM MgCl₂, 200 mM KCl) at 95°C for 2 min and cooled down to room temperature over 3 h. Where indicated, a bridging ORN (complementary to the 3' end of miR-34a-5p and the 5'-end of the counterstrand) was added in 10-fold excess.

Ligation mixtures in HeLa lysate were prepared as indicated in table 6.20.

Table 7. 20. Ligation mix in HeLa lysate

Component	Volume (µl)
40 nM labelled and annealed RNA	2
HeLa extract (protein conc. 2.1 mg/ ml)	4
Buffer LC*	4

*Buffer LC: 250 µM EDTA (pH 8.0), 100 mM KCl, 3 mM MgCl₂, 12.5 mM DTT, 7.5 mM ATP, 0.5 mM GTP, 1 U/ µL RNasin (Promega), 65 % (w/ v) glycerol.

Ligation mixtures were incubated at 30°C for 30 min. Incubation was quenched through addition of 150 µl proteinase K (Roche) solution (tables 6.21 and 6.22) and incubation at 65°C for 15 min. For non-enzymatic ligation reactions, RNAs were incubated in 1x non-enzymatic buffer (40 mM Tris.HCl pH 7.5, 20 mM NaCl, 6 mM MgCl₂ and 2 mM spermidine.HCl) for 90 min at room temperature. After incubation, non-enzymatic ligation mixtures were diluted to 160 µl with RNase-free H₂O. Ligation mixtures were analyzed by 15% dPAGE as described for northern blots.

Table 7. 21. Composition of proteinase K solution

Component	Volume (μ l)
2x proteinase K digestion buffer	850
Proteinase K	170
RNase-free H ₂ O	680

Table 7. 22. Composition of proteinase K digestion buffer

Component	Volume (μ l)
1 M Tris.HCl, pH 7.5	90
5 M NaCl	27
0.5 M EDTA, pH 8.0	22.5
10% SDS	180
RNase-free H ₂ O	580.5

Step 5, gel drying and read-out. Gels were incubated twice in 500 ml urea removal buffer (10% acetic acid, 5% glycerol, 40% ethanol) for 30 min. Cellophane gel drying sheets (LabForce, GDS-005) and Whatman paper were soaked in RNase-free H₂O for 5 min. The following gel stack was prepared: Whatman paper- gel- drying sheet. Gels were dried under vacuum on an UniGelDryer-4050 device (UniEquip) for 120 min at 80°C. Gels were wrapped with cling film and exposed overnight on a phosphor screen (GE Healthcare). Gels were visualized on a Typhoon scanner as described for northern blots.

7.3.9 RtcB ligation assays

RtcB ligation reactions were performed with RtcB ligase (New England Biolabs, M0458S) in RtcB reaction buffer at 37°C for 1 h. Ligation mix contained the components listed in table 6.23.

Table 7. 23. Composition of RtcB ligation mix

Component	Volume (μ l)
10x RtcB reaction buffer	2
1 mM GTP	2
10 mM MnCl ₂	2
15 μ M RtcB RNA ligase	1
RNase free H ₂ O	12
10 μ M RNA	1

Samples were analyzed by 15% dPAGE. Gel was casted using the SequaGel-urea gel system (National Diagnostics) as described in table 6.24.

Table 7. 24. Gel composition for 15% dPAGE analysis of RtcB reactions

Component	Volume
Urea gel concentrate	12 ml
Urea gel buffer	2 ml
Urea gel diluent	6 ml
TEMED	8 μ l
10% APS	160 μ l

7.3.10 2', 3' cycP stability assays

miR-106a-5p>p and WT were annealed to miR-106a-3p WT and incubated in HeLa lysate for the indicated time points according. Time points were 10, 30, 60, 120 and 180 min. Incubation was quenched through addition of 4 μ l proteinase K (Roche) and incubation at 65°C for 15 min. The composition of the assays mix is given in table 6.25. For t= 0 min, HeLa lysate was inactivated through proteinase K digestion prior to addition of RNA. RNA was isolated by phenol-chloroform extraction and RtcB ligation was performed as described in 6.3.9.

Table 7. 25. Composition of 2', 3' cycP stability assays

Component	Volume (μ l)
10 μ M miR-106a duplex	3
RNasin (Promega)	1
HeLa lysate	2.12
RNase-free H ₂ O	13.88

7.3.11 RNase T1 digestions

50% of confluent HEK293T cells in a T150 flask were seeded into 10 cm dishes. After 24 h, cells were washed with 5 ml PBS on ice. Then, PBS was removed and cells were irradiated twice at 254 nm with 100 mJ (Ultraviolet Crossliner, UVP) on ice. Cells were scraped in 0.5 ml cold PBS and were centrifuged at 200xG at 4°C for 5 min. Cells were lysed with 1 ml NP40 lysis buffer for 15 min, followed by centrifugation at 14,000xG at 4°C for 15 min. Lysate was equally distributed into three eppendorff tubes and 10 μ l RNase T1 (Thermo Scientific) solutions of the indicated concentrations were added. Samples were incubated at 37°C for 3 min, followed by 3 min on ice. 30 μ l of each sample were removed and used as "RNase digested only" fractions. Residual samples were digested with proteinase K (Roche).

50 µl Dynabeads Protein G per dish were washed with 3x 1 ml citrate-phosphate buffer. 25 µg anti-Ago2 antibody (clone 11A9) were immobilized on the beads in a total volume of 500 µl citrate-phosphate buffer by gentle rolling at 4°C for 1 h, followed by washing with 3x 1 ml NP40 lysis buffer and blocking with 1 ml NP40 lysis buffer including BSA at 4°C for 30 min. Then, beads were washed with 3x 1 ml NP40 lysis buffer.

RNase T1 digested lysates were incubated with anti-AGO2 antibody coupled Dynabeads at 4°C for 1 h (Ago2-immunopurification, AGO2-IP). Then, beads were incubated with proteinase K at 65°C for 15 min and RNA was isolated by phenol-chloroform extraction. RNase T1 digested samples were analyzed by 15% dPAGE as described for RtcB ligation assays.

7.3.12 cyCLIP

50% of confluent HEK293T cells in a T150 flask were seeded into 15 cm dishes. 4 dishes were used per replicate. 4 h after seeding, cells were transfected with cyCLIP probes using Lipofectamine RNAiMAX as a transfection reagent. Final concentration of cyCLIP probes was 2.5 nM. 40 µg anti-Ago2 antibodies were coupled to 80 µl Dynabead Protein G per 15 cm dish. The coupling procedure and subsequent RNase T1 digestion including Ago2-IP were performed as described in 6.3.11. RNase T1 concentration was 60.8 U/ µl. Then, beads were resuspended in 50 µl DNase solution (Promega) and incubated at 37°C for 10 min. Afterwards, beads were resuspended in 50 µl of the RtcB ligation mix given in table 6.23. RtcB ligation was performed at 37°C for 1 h. Beads were washed and proteinase K digestion (200 µl, 12 U) was performed for 15 min at 65°C. 1.33 µl glycoBlue was added to each tube and RNA was isolated by phenol-chloroform extraction. RNA was precipitated from the aqueous phase through addition of 600 µl ethanol and storage at -20°C overnight. The RNA pellet was washed with 70% ethanol and dissolved in 20 µl RNase-free H₂O.

Prior to library preparation, ribosomal RNA was removed using the Ribo-zero Gold rRNA removal kit (Illumina, San Diego, CA, USA) according to the manufacturer's protocol. Samples were fragmented, dephosphorylated and phosphorylated as described by Imig et al. [539]. The sequencing library was prepared using the CleanTag Small RNA Library Prep kit (TriLink, San Diego, CA, USA) according to the manufacturer's instructions.

7.4 *In vivo* experiments

All procedures involving animals were conducted by Dr. Gianluca Civenni at the IOR in Bellinzona in conformity with the institutional guidelines for animal experimentation and in compliance with national and international policies. Study protocols were approved by the Swiss Veterinary Authority. Athymic nude mice were purchased from Charles River laboratories and maintained under pathogen-free conditions with food and water *ad libitum*.

The general health status of all animals was monitored daily. For the biodistribution study, five nude mice received a single s.c. injection of 50 mg/ kg PS siLin28B in PBS. In the control group, two mice received a single s.c. injection of PBS alone. Mice were sacrificed 4 h after the injection and the following tissues were collected, snap-frozen and shipped (on dry ice) to ETH for analysis: liver, kidney, spleen, lung, heart, skeletal muscle, prostate and blood.

For the tumor xenograft study, each cohort consisted of seven mice. PC3 cells were inoculated with matrigel in the flank of NSG mice. Treatment was started 7 days after injection of the tumor cells. Mice received three s.c. injections per week for two weeks. Treatment groups were: PS siLin28B (50 mg/ kg, in PBS), scrambled PS siLin28B (50 mg/ kg, in PBS) and PO siLin28B (5 mg/ kg, formulated with *in vivo* jetPEI). Mice were sacrificed on the last day of treatment and tumor weight was measured. Tumor volume was measured after each injection.

7.5 Chemistry

7.5.1 Synthesis of *O*⁴-triazolyluridine-2'-*O*-TBDMS CED phosphoramidite

Synthesis of *O*⁴-triazolyluridine-2'-*O*-TBDMS CED phosphoramidite was performed according to Shah et al. [142]. To 1.6 g (20 eq.) of 1, 2, 4-triazole (Acros) in 10 ml ACN was added on ice: 3 ml TEA (Sigma Aldrich) followed by dropwise addition of 215 μ l (2 eq.) phosphorus oxychloride (Acros). Reaction mixture was stirred for 30 min and a solution of 1 g of 5'-DMT-2'-*O*-TBDMS-uridine CED phosphoramidite (Thermo Fisher) in 10 ml anhydrous ACN was slowly added and the mixture was stirred for another 4 h. Reaction was quenched through addition of 30 ml saturated sodium bicarbonate in H₂O. The aqueous layer was extracted with ethylacetate (EtOAc; 3x 20 ml) and the organic phase was washed with saturated sodium bicarbonate and brine and was then dried over anhydrous Na₂SO₄. Reaction was monitored by thin-layer chromatography (TLC; n-hexane: EtOAc, 2:3). Purification via column chromatography with n-hexane/ EtOAc. ¹H NMR (400 MHz, CDCl₃, ppm) δ 9.23 (s, 1H), 9.22 (s, 1H), 8.88 (d, *J* = 7.3 Hz, 1H), 8.84 (d, *J* = 7.3 Hz, 1H), 8.08 (s, 1H), 8.06 (s, 1H), 7.48 (m, 1H), 7.46 (m, 1H), 7.43 (m, 1H), 7.41 (m, 1H), 7.36 (m, 2H), 7.35 (m, 2H), 7.31 (m, 10H), 6.88 – 6.83 (m, 8H), 6.53 (d, *J* = 7.2 Hz, 1H), 6.37 (d, *J* = 7.2 Hz, 1H), 5.87 (d, *J* = 1.2 Hz, 1H), 5.81 (m, 1H), 4.49 – 4.44 (m, 2H), 4.43 – 4.35 (m, 4H), 3.83 – 3.79 (m, 12H), 3.79 – 3.45 (m, 12H), 2.60 – 2.51 (m, 2H), 2.42 (t, *J* = 6.3 Hz, 2H), 1.21 (t, 1H), 1.17 – 1.09 (m, 18H), 0.98 (d, *J* = 6.7 Hz, 6H), 0.93 (d, *J* = 4.4 Hz, 18H), 0.32 (s, 3H), 0.31 (s, 3H), 0.18 (m, 6H). ³¹P NMR (400 MHz, CDCl₃, ppm) δ 151.19, 148.56

7.5.2 Synthesis of N^2, N^3, N^4 -tri(tert-butoxycarbonyl)-spermine azide

N^2, N^3, N^4 -tri(tert-butoxycarbonyl)spermine azide was synthesized according to Yamada et al. [523]. The reaction was performed on ice and under nitrogen in a dedicated toxtlab (HCl D312, approved by "Stab SGU") due to the explosive potential of the azidation reaction. To a suspension of 1.9 g (1.2 eq.) sodium azide in 40 ml dry ACN was added dropwise 4.1 ml (1 eq.) of trifluoromethane sulfonic anhydride. The reaction mixture was stirred for 2 hours in an ice bath and filtered over cotton to remove the precipitate. The precipitate was washed with 15 ml ACN and the filtrate was added dropwise into a solution of 5.0 g spermine, 61 mg (0.01 eq.) $\text{CuSO}_4 \cdot 5 \text{H}_2\text{O}$ and 6.8 ml (2 eq.) TEA in ACN (ice bath). The reaction mixture was warmed to room temperature and stirred overnight. A solution of 26.7 g (5 eq.) di-tert-butyl dicarbonate in 10 mL ACN was added dropwise and stirring continued for 4 hours. Reaction was monitored by TLC (n-hexane: EtOAc 1:2). The reaction was quenched with 15 ml H_2O and the organic phase was collected and evaporated under vacuum. The residual was partitioned between $\text{H}_2\text{O}/\text{EtOAc}$ and the organic phase was dried over anhydrous MgSO_4 , filtered and evaporated. Column chromatography was performed with n-hexane/ EtOAc. ^1H NMR (400 MHz, DMSO-d_6 , ppm) δ 6.73 (s, 1H), 3.12 – 3.06 (m, 8H), 2.88 (q, $J = 6.5$ Hz, 4H), 1.60 – 1.51 (m, 4H), 1.38 – 1.36 (m, 31H). ESI-MS: m/z calc for $\text{C}_{25}\text{H}_{48}\text{N}_6\text{O}_6$ 528.70, found 529.70 $[\text{M}+\text{H}]^+$

7.5.3 Synthesis of spermine azide

Spermine azide (spm- N_3 .3TFA) was synthesized according to Yamada et al. [523]. 960 mg N^2, N^3, N^4 -tri(tert-butoxycarbonyl)spermine azide were dissolved in 40 ml anhydrous methylene chloride (DCM) and 10 ml trifluoroacetic acid (TFA) was added dropwise at 0 °C. The reaction mixture was stirred for 6 h at room temperature and monitored by TLC (petrol ether: EtOAc 7:3). The solvent was evaporated under vacuum and the crude was dissolved in 2 ml MeOH and precipitated with 50 ml diethyl ether. The precipitate was filtered and washed with diethylether. ^1H NMR (400 MHz, D_2O , ppm) δ 3.19 – 3.07 (m, 12H), 2.14 – 2.05 (m, 4H), 1.78 (p, $J = 3.7$ Hz, 4H).

7.5.4 Synthesis of N^1 -trityl spermine

The synthesis protocol was adapted from Krakowiak et al. [522] but the reactant ratio and conditions for column chromatography were changed in order to isolate the monoprotected spermine derivative. 500 mg spermine (2.5 mmole, anhydrous) was dissolved in 25 ml anhydrous DCM. 866 μl TEA (6.25 mmole, 2.5 eq.) were added to the stirring solution. 348 mg tritylchloride (1.25 mmole, 0.5 eq.) were dissolved in 3 ml anhydrous DCM and added dropwise at -50°C over 30 min. The reaction mixture was stirred at -50°C for 3 h and then evaporated under vacuum. Reaction was monitored by TLC (isopropanol: H_2O : 25% aqueous ammonia,

7:2:1). Purification by column chromatography. Column was packed with isopropanol: H₂O: 25% aqueous ammonia (8:1:1) and thereafter washed with two column volumes of the same solvent mixture. Elution with isopropanol: H₂O: 25% aqueous ammonia (8:1:1), then ratio was changed to 7:2:1. Product containing fractions were pooled, evaporated and dissolved in DCM. Residual silica was removed by filtration (P4 frit) and the solvent was removed under reduced pressure. ¹H NMR (400 MHz, CDCl₃, ppm) δ 7.48 – 7.39 (m, 6H), 7.25 (m, 6H), 7.15 (t, J = 7.3 Hz, 3H), 2.94 – 2.57 (m, 10H), 2.16 (m, 2H), 1.74 (m, 4H), 1.64 (m, 4H). ¹³C NMR (101 MHz, CDCl₃, ppm) δ 146.20, 128.71, 127.85, 126.31, 71.00, 49.58, 48.27, 47.61, 42.07, 40.24, 32.09, 30.55, 27.53, 27.39. ESI-MS: m/z calc for C₂₉H₄₀N₄ 444.67, found 445.33 [M+H]⁺

Bibliography

1. Stephenson, M.L. and P.C. Zamecnik, *Inhibition of Rous sarcoma viral RNA translation by a specific oligodeoxyribonucleotide*. Proceedings of the National Academy of Sciences, 1978. **75**(1): p. 285-288.
2. Zamecnik, P.C. and M.L. Stephenson, *Inhibition of Rous sarcoma virus replication and cell transformation by a specific oligodeoxynucleotide*. Proceedings of the National Academy of Sciences, 1978. **75**(1): p. 280-284.
3. Khvorova, A. and J.K. Watts, *The chemical evolution of oligonucleotide therapies of clinical utility*. Nature Biotechnology, 2017. **35**: p. 238.
4. Crooke, S.T., et al., *RNA-targeted therapeutics*. Cell metabolism, 2018. **27**(4): p. 714-739.
5. Vickers, T.A. and S.T. Crooke, *Development of a quantitative BRET affinity assay for nucleic acid-protein interactions*. PLoS One, 2016. **11**(8): p. e0161930.
6. Röthlisberger, P., C. Berk, and J. Hall, *RNA Chemistry for RNA Biology*. CHIMIA International Journal for Chemistry, 2019. **73**(6): p. 368-373.
7. Eckstein, F., *Phosphorothioates, essential components of therapeutic oligonucleotides*. Nucleic acid therapeutics, 2014. **24**(6): p. 374-387.
8. Shen, X. and D.R. Corey, *Chemistry, mechanism and clinical status of antisense oligonucleotides and duplex RNAs*. Nucleic Acids Research, 2017. **46**(4): p. 1584-1600.
9. Jahns, H., et al., *Stereochemical bias introduced during RNA synthesis modulates the activity of phosphorothioate siRNAs*. Nature communications, 2015. **6**: p. 6317.
10. Clercq, E.D., F. Eckstein, and T.C. Merigan, *Interferon Induction Increased through Chemical Modification of a Synthetic Polyribonucleotide*. Science, 1969. **165**(3898): p. 1137-1139.
11. Krieg, A.M. and C.A. Stein, *Phosphorothioate Oligodeoxynucleotides: Antisense or Anti-Protein?* Antisense Research and Development, 1995. **5**(4): p. 241-241.
12. Sewing, S., et al., *Assessing single-stranded oligonucleotide drug-induced effects in vitro reveals key risk factors for thrombocytopenia*. PLOS ONE, 2017. **12**(11): p. e0187574.
13. Rockwell, P., et al., *Cell-surface perturbations of the epidermal growth factor and vascular endothelial growth factor receptors by phosphorothioate oligodeoxynucleotides*. Proceedings of the National Academy of Sciences, 1997. **94**(12): p. 6523-6528.
14. Guvakova, M.A., et al., *Phosphorothioate Oligodeoxynucleotides Bind to Basic Fibroblast Growth Factor, Inhibit Its Binding to Cell Surface Receptors, and Remove It from Low Affinity Binding Sites on Extracellular Matrix*. Journal of Biological Chemistry, 1995. **270**(6): p. 2620-2627.
15. Geary, R.S., et al., *Pharmacokinetics, biodistribution and cell uptake of antisense oligonucleotides*. Advanced drug delivery reviews, 2015. **87**: p. 46-51.
16. Crooke, S.T., et al., *Cellular uptake and trafficking of antisense oligonucleotides*. Nature Biotechnology, 2017. **35**: p. 230.
17. Rosie, Z.Y., et al., *Cross-species pharmacokinetic comparison from mouse to man of a second-generation antisense oligonucleotide, ISIS 301012, targeting human apolipoprotein B-100*. Drug Metabolism and Disposition, 2007. **35**(3): p. 460-468.
18. Geary, R.S., et al., *Pharmacokinetic Properties of 2'-O-(2-Methoxyethyl)-Modified Oligonucleotide Analogs in Rats*. Journal of Pharmacology and Experimental Therapeutics, 2001. **296**(3): p. 890-897.
19. Duell, P.B., et al., *Long-term mipomersen treatment is associated with a reduction in cardiovascular events in patients with familial hypercholesterolemia*. Journal of Clinical Lipidology, 2016. **10**(4): p. 1011-1021.
20. Finkel, R.S., et al., *Nusinersen versus Sham Control in Infantile-Onset Spinal Muscular Atrophy*. New England Journal of Medicine, 2017. **377**(18): p. 1723-1732.
21. Keam, S.J., *Inotersen: First Global Approval*. Drugs, 2018. **78**(13): p. 1371-1376.

22. Furrer, P., et al., *Structural effect of complete [Rp]-phosphorothioate and phosphorodithioate substitutions in the DNA strand of a model antisense inhibitor-target RNA complex*. Journal of Molecular Biology, 1999. **285**(4): p. 1609-1622.
23. Tong, T., et al., *Occurrence, evolution, and functions of DNA phosphorothioate epigenetics in bacteria*. Proceedings of the National Academy of Sciences, 2018. **115**(13): p. E2988-E2996.
24. Eckstein, F., *Nucleoside phosphorothioates*. Annual review of biochemistry, 1985. **54**(1): p. 367-402.
25. Nukaga, Y., et al., *Stereocontrolled Solid-Phase Synthesis of Phosphorothioate Oligoribonucleotides Using 2'-O-(2-Cyanoethoxymethyl)-nucleoside 3'-O-Oxazaphospholidine Monomers*. The Journal of Organic Chemistry, 2012. **77**(18): p. 7913-7922.
26. Oka, N., et al., *Stereocontrolled Synthesis of Oligoribonucleoside Phosphorothioates by an Oxazaphospholidine Approach*. Organic Letters, 2009. **11**(4): p. 967-970.
27. Oka, N., T. Wada, and K. Saigo, *An Oxazaphospholidine Approach for the Stereocontrolled Synthesis of Oligonucleoside Phosphorothioates*. Journal of the American Chemical Society, 2003. **125**(27): p. 8307-8317.
28. Oka, N., et al., *Solid-Phase Synthesis of Stereoregular Oligodeoxyribonucleoside Phosphorothioates Using Bicyclic Oxazaphospholidine Derivatives as Monomer Units*. Journal of the American Chemical Society, 2008. **130**(47): p. 16031-16037.
29. Wan, W.B., et al., *Synthesis, biophysical properties and biological activity of second generation antisense oligonucleotides containing chiral phosphorothioate linkages*. Nucleic Acids Research, 2014. **42**(22): p. 13456-13468.
30. Iwamoto, N., et al., *Control of phosphorothioate stereochemistry substantially increases the efficacy of antisense oligonucleotides*. Nature Biotechnology, 2017. **35**: p. 845.
31. Li, M., et al., *Synthesis and cellular activity of stereochemically-pure 2'-O-(2-methoxyethyl)-phosphorothioate oligonucleotides*. Chemical Communications, 2017. **53**(3): p. 541-544.
32. Knouse, K.W., et al., *Unlocking P(V): Reagents for chiral phosphorothioate synthesis*. Science, 2018. **361**(6408): p. 1234-1238.
33. Stec, W.J. and G. Zon, *Stereochemical studies of the formation of chiral internucleotide linkages by phosphoramidite coupling in the synthesis of oligodeoxyribonucleotides*. Tetrahedron letters, 1984. **25**(46): p. 5279-5282.
34. Wei, X., *Coupling activators for the oligonucleotide synthesis via phosphoramidite approach*. Tetrahedron, 2013. **69**(18): p. 3615-3637.
35. Dahl, B.H., J. Nielsen, and O. Dahl, *Mechanistic studies on the phosphoramidite coupling reaction in oligonucleotide synthesis. I. Evidence for nudeophilic catalysis by tetrazole and rate variations with the phosphorus substituents*. Nucleic acids research, 1987. **15**(4): p. 1729-1743.
36. Seela, F. and U. Kretschmer, *Diastereomerically pure Rp and Sp dinucleoside H-phosphonates: the stereochemical course of their conversion into P-methylphosphonates, phosphorothioates, and [oxygen-18] chiral phosphates*. The Journal of Organic Chemistry, 1991. **56**(12): p. 3861-3869.
37. Mukhlall, J.A. and W.H. Hersh, *Sulfurization of dinucleoside phosphite triesters with chiral disulfides*. Nucleosides, Nucleotides and Nucleic Acids, 2011. **30**(9): p. 706-725.
38. Cruse, W.B.T., et al., *Chiral phosphorothioate analogues of B-DNA: The crystal structure of Rp-d[Gp(S)CpGp(S)CpGp(S)C]*. Journal of Molecular Biology, 1986. **192**(4): p. 891-905.
39. Bachelin, M., et al., *Structure of a stereoregular phosphorothioate DNA/RNA duplex*. Nature Structural Biology, 1998. **5**(4): p. 271-276.
40. Pauling, L., *The Nature of the Chemical Bond*. Vol. 260. 1960: Cornell university press Ithaca, NY.
41. Liang, C. and L.C. Allen, *Sulfur does not form double bonds in phosphorothioate anions*. Journal of the American Chemical Society, 1987. **109**(21): p. 6449-6453.

42. Iyengar, R., F. Eckstein, and P.A. Frey, *Phosphorus-oxygen bond order in adenosine 5'-O-phosphorothioate dianion*. Journal of the American Chemical Society, 1984. **106**(26): p. 8309-8310.
43. Baraniak, J. and P.A. Frey, *Effect of ion pairing on bond order and charge localization in alkyl phosphorothioates*. Journal of the American Chemical Society, 1988. **110**(12): p. 4059-4060.
44. Frey, P.A. and R.D. Sammons, *Bond order and charge localization in nucleoside phosphorothioates*. Science, 1985. **228**(4699): p. 541-545.
45. Brautigam, C.A. and T.A. Steitz, *Structural principles for the inhibition of the 3'-5' exonuclease activity of Escherichia coli DNA polymerase I by phosphorothioates*. Journal of molecular biology, 1998. **277**(2): p. 363-377.
46. Pecoraro, V.L., J.D. Hermes, and W. Cleland, *Stability constants of magnesium and cadmium complexes of adenine nucleotides and thionucleotides and rate constants for formation and dissociation of magnesium-ATP and magnesium-ADP*. Biochemistry, 1984. **23**(22): p. 5262-5271.
47. Matranga, C., et al., *Passenger-Strand Cleavage Facilitates Assembly of siRNA into Ago2-Containing RNAi Enzyme Complexes*. Cell, 2005. **123**(4): p. 607-620.
48. Schwarz, D.S., Y. Tomari, and P.D. Zamore, *The RNA-Induced Silencing Complex Is a Mg²⁺-Dependent Endonuclease*. Current Biology, 2004. **14**(9): p. 787-791.
49. Koziolkiewicz, M., et al., *Stability of Stereoregular Oligo(nucleoside Phosphorothioate)s in Human Plasma: Diastereoselectivity of Plasma 3' - Exonuclease*. Antisense and Nucleic Acid Drug Development, 1997. **7**(1): p. 43-48.
50. Wójcik, M., et al., *Nucleotide pyrophosphatase/phosphodiesterase 1 is responsible for degradation of antisense phosphorothioate oligonucleotides*. Oligonucleotides, 2007. **17**(1): p. 134-145.
51. Patel, P.C., et al., *Duplex End Breathing Determines Serum Stability and Intracellular Potency of siRNA–Au NPs*. Molecular Pharmaceutics, 2011. **8**(4): p. 1285-1291.
52. Watanabe, D.T.A., R.S. Geary, and A.A. Levin, *Plasma Protein Binding of an Antisense Oligonucleotide Targeting Human ICAM-1 (ISIS 2302)*. Oligonucleotides, 2006. **16**(2): p. 169-180.
53. Yu, R.Z., et al., *Cross-Species Pharmacokinetic Comparison from Mouse to Man of a Second-Generation Antisense Oligonucleotide, ISIS 301012, Targeting Human Apolipoprotein B-100*. Drug Metabolism and Disposition, 2007. **35**(3): p. 460-468.
54. Levin, A.A., Z.Y. Rosie, and R.S. Geary, *Basic principles of the pharmacokinetics of antisense oligonucleotide drugs*, in *Antisense drug technology*. 2007, CRC Press. p. 201-234.
55. Nestle, F.O., et al., *Cationic lipid is not required for uptake and selective inhibitory activity of ICAM-1 phosphorothioate antisense oligonucleotides in keratinocytes*. Journal of investigative dermatology, 1994. **103**(4): p. 569-575.
56. Giachetti, C. and D.J. Chin, *Increased Oligonucleotide Permeability in Keratinocytes of Artificial Skin Correlates with Differentiation and Altered Membrane Function*. Journal of Investigative Dermatology, 1996. **107**(2): p. 256-262.
57. Rappaport, J., et al., *Transport of phosphorothioate oligonucleotides in kidney: Implications for molecular therapy*. Kidney International, 1995. **47**(5): p. 1462-1469.
58. Koller, E., et al., *Mechanisms of single-stranded phosphorothioate modified antisense oligonucleotide accumulation in hepatocytes*. Nucleic Acids Research, 2011. **39**(11): p. 4795-4807.
59. Zhao, Q., et al., *Comparison of Cellular Binding and Uptake of Antisense Phosphodiester, Phosphorothioate, and Mixed Phosphorothioate and Methylphosphonate Oligonucleotides*. Antisense Research and Development, 1993. **3**(1): p. 53-66.
60. Alam, M.R., et al., *The biological effect of an antisense oligonucleotide depends on its route of endocytosis and trafficking*. Oligonucleotides, 2010. **20**(2): p. 103-109.

61. Linnane, E., et al., *Differential uptake, kinetics and mechanisms of intracellular trafficking of next-generation antisense oligonucleotides across human cancer cell lines*. *Nucleic Acids Research*, 2019. **47**(9): p. 4375-4392.
62. Bailey, J.K., et al., *Nucleic acid binding proteins affect the subcellular distribution of phosphorothioate antisense oligonucleotides*. *Nucleic Acids Research*, 2017. **45**(18): p. 10649-10671.
63. Liang, X.-H., et al., *Identification and characterization of intracellular proteins that bind oligonucleotides with phosphorothioate linkages*. *Nucleic Acids Research*, 2015. **43**(5): p. 2927-2945.
64. Wang, S., et al., *Intra-endosomal trafficking mediated by lysobisphosphatidic acid contributes to intracellular release of phosphorothioate-modified antisense oligonucleotides*. *Nucleic Acids Research*, 2017. **45**(9): p. 5309-5322.
65. Colton, M., et al., *Receptor-Mediated Uptake of Phosphorothioate Antisense Oligonucleotides in Different Cell Types of the Liver*. *Nucleic Acid Therapeutics*, 2018. **28**(3): p. 119-127.
66. Flierl, U., et al., *Phosphorothioate backbone modifications of nucleotide-based drugs are potent platelet activators*. *Journal of Experimental Medicine*, 2015. **212**(2): p. 129-137.
67. Harborth, J., et al., *Sequence, chemical, and structural variation of small interfering RNAs and short hairpin RNAs and the effect on mammalian gene silencing*. *Antisense and Nucleic Acid Drug Development*, 2003. **13**(2): p. 83-105.
68. Amarzguioui, M., et al., *Tolerance for mutations and chemical modifications in a siRNA*. *Nucleic acids research*, 2003. **31**(2): p. 589-595.
69. Maja, J., et al., *Impact of Oligonucleotide Structure, Chemistry, and Delivery Method on In Vitro Cytotoxicity*. *Nucleic Acid Therapeutics*, 2017. **27**(1): p. 11-22.
70. Migawa, M.T., et al., *Site-specific replacement of phosphorothioate with alkyl phosphonate linkages enhances the therapeutic profile of gapmer ASOs by modulating interactions with cellular proteins*. *Nucleic Acids Research*, 2019. **47**(11): p. 5465-5479.
71. Stein, C.A., et al., *G3139, an Anti-Bcl-2 Antisense Oligomer That Binds Heparin-Binding Growth Factors and Collagen I, Alters In vitro Endothelial Cell Growth and Tubular Morphogenesis*. *Clinical Cancer Research*, 2009. **15**(8): p. 2797-2807.
72. Janas, M.M., et al., *Selection of GalNAc-conjugated siRNAs with limited off-target-driven rat hepatotoxicity*. *Nature Communications*, 2018. **9**(1): p. 723.
73. Crooke, S.T., et al., *Integrated Safety Assessment of 2'-O-Methoxyethyl Chimeric Antisense Oligonucleotides in NonHuman Primates and Healthy Human Volunteers*. *Molecular Therapy*, 2016. **24**(10): p. 1771-1782.
74. Konarska, M.M., *Site-specific derivatization of RNA with photocrosslinkable groups*. *Methods*, 1999. **18**(1): p. 22-28.
75. Burgin, A.B. and N.R. Pace, *Mapping the active site of ribonuclease P RNA using a substrate containing a photoaffinity agent*. *The EMBO Journal*, 1990. **9**(12): p. 4111-4118.
76. Rosenstein, S.P. and M.D. Been, *Hepatitis delta virus ribozymes fold to generate a solvent-inaccessible core with essential nucleotides near the cleavage site phosphate*. *Biochemistry*, 1996. **35**(35): p. 11403-11413.
77. Musier-Forsyth, K. and P. Schimmel, *Acceptor helix interactions in a class II tRNA synthetase: photoaffinity crosslinking of an RNA miniduplex substrate*. *Biochemistry*, 1994. **33**(3): p. 773-779.
78. Gish, G. and F. Eckstein, *DNA and RNA sequence determination based on phosphorothioate chemistry*. *Science*, 1988. **240**(4858): p. 1520-1522.
79. Yang, X., et al., *Gene silencing activity of siRNA molecules containing phosphorodithioate substitutions*. *ACS chemical biology*, 2012. **7**(7): p. 1214-1220.
80. Seeberger, P.H., E. Yau, and M.H. Caruthers, *2'-Deoxynucleoside Dithiophosphates: Synthesis and Biological Studies*. *Journal of the American Chemical Society*, 1995. **117**(5): p. 1472-1478.

81. Wiesler, W.T. and M.H. Caruthers, *Synthesis of Phosphorodithioate DNA via Sulfur-Linked, Base-Labile Protecting Groups*. The Journal of Organic Chemistry, 1996. **61**(13): p. 4272-4281.
82. Flür, S. and R. Micura, *Chemical synthesis of RNA with site-specific methylphosphonate modifications*. Methods, 2016. **107**: p. 79-88.
83. Hall, A.H., et al., *RNA interference using boranophosphate siRNAs: structure–activity relationships*. Nucleic Acids Research, 2004. **32**(20): p. 5991-6000.
84. Sergueev, D.S. and B.R. Shaw, *H-Phosphonate approach for solid-phase synthesis of oligodeoxyribonucleoside boranophosphates and their characterization*. Journal of the American Chemical Society, 1998. **120**(37): p. 9417-9427.
85. Sood, A., B.R. Shaw, and B.F. Spielvogel, *Boron-containing nucleic acids. 2. Synthesis of oligodeoxynucleoside boranophosphates*. Journal of the American Chemical Society, 1990. **112**(24): p. 9000-9001.
86. Meade, B.R., et al., *Efficient delivery of RNAi prodrugs containing reversible charge-neutralizing phosphotriester backbone modifications*. Nature Biotechnology, 2014. **32**(12): p. 1256.
87. Khvorova, A., M.F. Osborn, and M.R. Hassler, *Taking charge of siRNA delivery*. Nature Biotechnology, 2014. **32**: p. 1197.
88. Kolosenko, I., et al., *RNAi prodrugs targeting Plk1 induce specific gene silencing in primary cells from pediatric T-acute lymphoblastic leukemia patients*. Journal of Controlled Release, 2017. **261**: p. 199-206.
89. Egholm, M., et al., *PNA hybridizes to complementary oligonucleotides obeying the Watson–Crick hydrogen-bonding rules*. Nature, 1993. **365**(6446): p. 566.
90. Nielsen, P.E., et al., *Sequence-selective recognition of DNA by strand displacement with a thymine-substituted polyamide*. Science, 1991. **254**(5037): p. 1497-1500.
91. Heasman, J., *Morpholino oligos: making sense of antisense?* Developmental Biology, 2002. **243**(2): p. 209-214.
92. Mendell, J., et al., *Clinical safety of eteplirsen, a phosphorodiamidate morpholino oligomer (PMO), in Duchenne muscular dystrophy (DMD) patients amenable to skipping exon 51 of the DMD gene*. Neuromuscular Disorders, 2016. **26**: p. S153-S154.
93. Charleston, J., et al., *Long-term treatment with eteplirsen promotes exon 51 skipping and novel dystrophin protein production in Duchenne muscular dystrophy patients*. Neuromuscular Disorders, 2016. **26**: p. S153.
94. Mendell, J.R. and E.M. Kaye, *Reply*. Annals of Neurology, 2014. **75**(2): p. 329-329.
95. Mendell, J.R., et al., *Eteplirsen for the treatment of Duchenne muscular dystrophy*. Annals of Neurology, 2013. **74**(5): p. 637-647.
96. Unger, E.F. and R.M. Califf, *Regarding “Eteplirsen for the treatment of Duchenne muscular dystrophy”*. Annals of Neurology, 2017. **81**(1): p. 162-164.
97. Sarepta. *Sarepta Therapeutics Receives Complete Response Letter from the US Food and Drug Administration for Golodirsen New Drug Application*. 2019 [accessed on 27.08.2019]; Available from: <https://investorrelations.sarepta.com/news-releases/news-release-details/sarepta-therapeutics-receives-complete-response-letter-us-food>.
98. Uhlmann, E., et al., *PNA: Synthetic Polyamide Nucleic Acids with Unusual Binding Properties*. Angewandte Chemie International Edition, 1998. **37**(20): p. 2796-2823.
99. Hyrup, B. and P.E. Nielsen, *Peptide Nucleic Acids (PNA): Synthesis, properties and potential applications*. Bioorganic & Medicinal Chemistry, 1996. **4**(1): p. 5-23.
100. Braasch, D.A., C.J. Nulf, and D.R. Corey, *Synthesis and Purification of Peptide Nucleic Acids*. Current Protocols in Nucleic Acid Chemistry, 2002. **9**(1): p. 4.11.1-4.11.18.
101. McMahon, B.M., Dennis; Lipsky, James; Stewart, Jennifer; Fauq, Abdul; Richelson, Elliott, *Pharmacokinetics and Tissue Distribution of a Peptide Nucleic Acid After Intravenous Administration*. Antisense and Nucleic Acid Drug Development, 2002. **12**(2): p. 65-70.

102. Mardirossian, G., et al., *In vivo hybridization of technetium-99m-labeled peptide nucleic acid (PNA)*. The Journal of Nuclear Medicine, 1997. **38**(6): p. 907.
103. Nielsen, P.E. and M. Egholm, *An introduction to peptide nucleic acid*. Curr Issues Mol Biol, 1999. **1**(1-2): p. 89-104.
104. Nielsen, P.E., et al., *Peptide Nucleic Acids (PNAs) Containing Thymine Monomers Derived from Chiral Amino Acids: Hybridization and Solubility Properties of D-Lysine PNA*. Angewandte Chemie International Edition in English, 1996. **35**(17): p. 1939-1942.
105. Albertshofer, K., et al., *Structure– activity relationship study on a simple cationic peptide motif for cellular delivery of antisense peptide nucleic acid*. Journal of medicinal chemistry, 2005. **48**(21): p. 6741-6749.
106. Wancewicz, E.V., et al., *Peptide nucleic acids conjugated to short basic peptides show improved pharmacokinetics and antisense activity in adipose tissue*. Journal of Medicinal Chemistry, 2010. **53**(10): p. 3919-3926.
107. Beletskii, A., et al., *PNA interference mapping demonstrates functional domains in the noncoding RNA Xist*. Proceedings of the National Academy of Sciences, 2001. **98**(16): p. 9215-9220.
108. Tian, Q., et al., *Quantitative determination of a siRNA (AD00370) in rat plasma using peptide nucleic acid probe and HPLC with fluorescence detection*. Bioanalysis, 2017. **9**(11): p. 861-872.
109. Trubetskoy, V.S., et al., *Phosphorylation-specific status of RNAi triggers in pharmacokinetic and biodistribution analyses*. Nucleic Acids Research, 2016. **45**(3): p. 1469-1478.
110. Roehl, I., M. Schuster, and S. Seiffert, *Oligonucleotide detection method*. 2011, US Patent US20110201006A1.
111. Godinho, B.M., et al., *Pharmacokinetic profiling of conjugated therapeutic oligonucleotides: a high-throughput method based upon serial blood microsampling coupled to peptide nucleic acid hybridization assay*. Nucleic Acid Therapeutics, 2017. **27**(6): p. 323-334.
112. Haraszti, R.A., et al., *5'-Vinylphosphonate improves tissue accumulation and efficacy of conjugated siRNAs in vivo*. Nucleic Acids Research, 2017. **45**(13): p. 7581-7592.
113. Nikan, M., et al., *Docosahexaenoic acid conjugation enhances distribution and safety of siRNA upon local administration in mouse brain*. Molecular Therapy-Nucleic Acids, 2016. **5**: p. e344.
114. Menzi, M., H.L. Lightfoot, and J. Hall, *Polyamine–oligonucleotide conjugates: a promising direction for nucleic acid tools and therapeutics*. Future Medicinal Chemistry, 2015. **7**(13): p. 1733-1749.
115. Menzi, M., et al., *Towards improved oligonucleotide therapeutics through faster target binding kinetics*. Chemistry–A European Journal, 2017. **23**(57): p. 14221-14230.
116. Daniher, A.T., et al., *Modulation of RNase H activity by modified DNA probes: Major groove vs minor groove effects*. Bioorganic & Medicinal Chemistry, 1997. **5**(6): p. 1037-1042.
117. Freier, S.M. and K.-H. Altmann, *The ups and downs of nucleic acid duplex stability: structure-stability studies on chemically-modified DNA: RNA duplexes*. Nucleic Acids Research, 1997. **25**(22): p. 4429-4443.
118. Henry, S., et al., *Chemically modified oligonucleotides exhibit decreased immune stimulation in mice*. Journal of Pharmacology and Experimental Therapeutics, 2000. **292**(2): p. 468-479.
119. Breiling, A. and F. Lyko, *Epigenetic regulatory functions of DNA modifications: 5-methylcytosine and beyond*. Epigenetics & chromatin, 2015. **8**(1): p. 24.
120. Jaenisch, R. and A. Bird, *Epigenetic regulation of gene expression: how the genome integrates intrinsic and environmental signals*. Nature Genetics, 2003. **33**(3s): p. 245.
121. Flanagan, W.M., et al., *A cytosine analog that confers enhanced potency to antisense oligonucleotides*. Proceedings of the National Academy of Sciences, 1999. **96**(7): p. 3513-3518.

122. Lin, K.-Y. and M.D. Matteucci, *A cytosine analogue capable of clamp-like binding to a guanine in helical nucleic acids*. Journal of the American Chemical Society, 1998. **120**(33): p. 8531-8532.
123. Sazani, P., A. Astriab-Fischer, and R. Kole, *Effects of base modifications on antisense properties of 2'-O-methoxyethyl and PNA oligonucleotides*. Antisense and Nucleic Acid Drug Development, 2003. **13**(3): p. 119-128.
124. Wilds, C.J., et al., *Structural Basis for Recognition of Guanosine by a Synthetic Tricyclic Cytosine Analogue: Guanidinium G-Clamp*. Helvetica Chimica Acta, 2003. **86**(4): p. 966-978.
125. Holmes, S.C., A.A. Arzumanov, and M.J. Gait, *Steric inhibition of human immunodeficiency virus type-1 Tat-dependent trans-activation in vitro and in cells by oligonucleotides containing 2'-O-methyl G-clamp ribonucleoside analogues*. Nucleic Acids Research, 2003. **31**(11): p. 2759-2768.
126. Magadum, A., K. Kaur, and L. Zangi, *mRNA-Based Protein Replacement Therapy for the Heart*. Molecular Therapy, 2019. **27**(4): p. 785-793.
127. Karikó, K., et al., *Incorporation of Pseudouridine Into mRNA Yields Superior Nonimmunogenic Vector With Increased Translational Capacity and Biological Stability*. Molecular Therapy, 2008. **16**(11): p. 1833-1840.
128. Kormann, M.S.D., et al., *Expression of therapeutic proteins after delivery of chemically modified mRNA in mice*. Nature Biotechnology, 2011. **29**: p. 154.
129. Rajeev, K.G., T.P. Prakash, and M. Manoharan, *2'-Modified-2-thiothymidine oligonucleotides*. Organic Letters, 2003. **5**(17): p. 3005-3008.
130. Jao, C.Y. and A. Salic, *Exploring RNA transcription and turnover in vivo by using click chemistry*. Proceedings of the National Academy of Sciences, 2008. **105**(41): p. 15779-15784.
131. Phelps, K.J., et al., *Click modification of RNA at adenosine: structure and reactivity of 7-ethynyl- and 7-triazolyl-8-aza-7-deazaadenosine in RNA*. ACS Chemical Biology, 2014. **9**(8): p. 1780-1787.
132. Winz, M.-L., et al., *Site-specific terminal and internal labeling of RNA by poly (A) polymerase tailing and copper-catalyzed or copper-free strain-promoted click chemistry*. Nucleic acids research, 2012. **40**(10): p. e78-e78.
133. Holstein, J.M., D. Schulz, and A. Rentmeister, *Bioorthogonal site-specific labeling of the 5'-cap structure in eukaryotic mRNAs*. Chemical Communications, 2014. **50**(34): p. 4478-4481.
134. Matsuda, S., et al., *siRNA Conjugates Carrying Sequentially Assembled Trivalent N-Acetylgalactosamine Linked Through Nucleosides Elicit Robust Gene Silencing In Vivo in Hepatocytes*. ACS Chemical Biology, 2015. **10**(5): p. 1181-1187.
135. Allerson, C.R., S.L. Chen, and G.L. Verdine, *A chemical method for site-specific modification of RNA: the convertible nucleoside approach*. Journal of the American Chemical Society, 1997. **119**(32): p. 7423-7433.
136. Allerson, C.R. and G.L. Verdine, *Synthesis and biochemical evaluation of RNA containing an intrahelical disulfide crosslink*. Chemistry & Biology, 1995. **2**(10): p. 667-675.
137. Ferentz, A.E. and G.L. Verdine, *Disulfide-crosslinked oligonucleotides*. Journal of the American Chemical Society, 1991. **113**(10): p. 4000-4002.
138. Macmillan, A.M. and G.L. Verdine, *Engineering tethered DNA molecules by the convertible nucleoside approach*. Tetrahedron, 1991. **47**(14-15): p. 2603-2616.
139. Noronha, A.M., D.M. Noll, and P.S. Miller, *Syntheses of DNA duplexes containing AC-C interstrand cross-link*. Nucleosides, Nucleotides and Nucleic Acids, 2001. **20**(4-7): p. 1303-1307.
140. Wiesmayr, A., P. Fournier, and A. Jäschke, *An on-bead tailing/ligation approach for sequencing resin-bound RNA libraries*. Nucleic Acids Research, 2012. **40**(9): p. e68-e68.
141. Koch, M., et al., *Critical 23S rRNA interactions for macrolide-dependent ribosome stalling on the ErmCL nascent peptide chain*. Nucleic Acids Research, 2017. **45**(11): p. 6717-6728.

142. Shah, K., H. Wu, and T.M. Rana, *Synthesis of uridine phosphoramidite analogs: reagents for site-specific incorporation of photoreactive sites into RNA sequences*. Bioconjugate Chemistry, 1994. **5**(6): p. 508-512.
143. Weldon, C., et al., *Identification of G-quadruplexes in long functional RNAs using 7-deazaguanine RNA*. Nature Chemical Biology, 2017. **13**(1): p. 18.
144. Lyons, S.M., et al., *Identification of functional tetramolecular RNA G-quadruplexes derived from transfer RNAs*. Nature Communications, 2017. **8**(1): p. 1127.
145. Yang, W., *Nucleases: diversity of structure, function and mechanism*. Quarterly Reviews of Biophysics, 2011. **44**(1): p. 1-93.
146. Breslow, R., D.L. Huang, and E. Anslyn, *On the mechanism of action of ribonucleases: dinucleotide cleavage catalyzed by imidazole and Zn²⁺*. Proceedings of the National Academy of Sciences, 1989. **86**(6): p. 1746-1750.
147. Cummins, L.L., et al., *Characterization of fully 2'-modified oligoribonucleotide hetero- and homoduplex hybridization and nuclease sensitivity*. Nucleic Acids Research, 1995. **23**(11): p. 2019-2024.
148. Tereshko, V., et al., *Correlating Structure and Stability of DNA Duplexes with Incorporated 2'-O-Modified RNA Analogues*. Biochemistry, 1998. **37**(30): p. 10626-10634.
149. Martin, P., *Ein neuer Zugang zu 2'-O-Alkylribonucleosiden und Eigenschaften deren Oligonucleotide*. Helvetica Chimica Acta, 1995. **78**(2): p. 486-504.
150. Plavec, J., C. Thibaudeau, and J. Chattopadhyaya, *How Does the 2'-Hydroxy Group Drive the Pseudorotational Equilibrium in Nucleoside and Nucleotide by the Tuning of the 3'-Gauche Effect?* Journal of the American Chemical Society, 1994. **116**(15): p. 6558-6560.
151. Thibaudeau, C., et al., *How does the electronegativity of the substituent dictate the strength of the gauche effect?* Journal of the American Chemical Society, 1994. **116**(9): p. 4038-4043.
152. Wan, W.B. and P.P. Seth, *The Medicinal Chemistry of Therapeutic Oligonucleotides*. Journal of Medicinal Chemistry, 2016. **59**(21): p. 9645-9667.
153. Egli, M., et al., *Probing the Influence of Stereoelectronic Effects on the Biophysical Properties of Oligonucleotides: Comprehensive Analysis of the RNA Affinity, Nuclease Resistance, and Crystal Structure of Ten 2'-O-Ribonucleic Acid Modifications*. Biochemistry, 2005. **44**(25): p. 9045-9057.
154. Manoharan, M., *2'-Carbohydrate modifications in antisense oligonucleotide therapy: importance of conformation, configuration and conjugation*. Biochimica et Biophysica Acta (BBA) - Gene Structure and Expression, 1999. **1489**(1): p. 117-130.
155. Guschlbauer, W. and K. Jankowski, *Nucleoside conformation is determined by the electronegativity of the sugar substituent*. Nucleic Acids Research, 1980. **8**(6): p. 1421-1433.
156. Wahl, M.C. and M. Sundaralingam, *Crystal structures of A-DNA duplexes*. Biopolymers, 1997. **44**(1): p. 45-63.
157. Schneider, B., S. Neidle, and H.M. Berman, *Conformations of the sugar-phosphate backbone in helical DNA crystal structures*. Biopolymers, 1997. **42**(1): p. 113-124.
158. Jones, S., et al., *Protein-RNA interactions: a structural analysis*. Nucleic Acids Research, 2001. **29**(4): p. 943-954.
159. Fierro-Monti, I. and M.B. Mathews, *Proteins binding to duplexed RNA: one motif, multiple functions*. Trends in Biochemical Sciences, 2000. **25**(5): p. 241-246.
160. Koshkin, A.A., et al., *LNA (Locked Nucleic Acids): Synthesis of the adenine, cytosine, guanine, 5-methylcytosine, thymine and uracil bicyclonucleoside monomers, oligomerisation, and unprecedented nucleic acid recognition*. Tetrahedron, 1998. **54**(14): p. 3607-3630.
161. Singh, S.K., et al., *LNA (locked nucleic acids): synthesis and high-affinity nucleic acid recognition*. Chemical Communications, 1998(4): p. 455-456.
162. Wengel, J., *Synthesis of 3'-C- and 4'-C-branched oligodeoxynucleotides and the development of locked nucleic acid (LNA)*. Accounts of Chemical Research, 1999. **32**(4): p. 301-310.

163. Obika, S., et al., *Stability and structural features of the duplexes containing nucleoside analogues with a fixed N-type conformation, 2'-O, 4'-C-methyleneribonucleosides*. Tetrahedron Letters, 1998. **39**(30): p. 5401-5404.
164. Obika, S., et al., *Synthesis of 2'-O, 4'-C-methyleneuridine and-cytidine. Novel bicyclic nucleosides having a fixed C3,-endo sugar puckering*. Tetrahedron Letters, 1997. **38**(50): p. 8735-8738.
165. Seth, P.P., et al., *Synthesis and Biophysical Evaluation of 2',4'-Constrained 2'O-Methoxyethyl and 2',4'-Constrained 2'O-Ethyl Nucleic Acid Analogues*. The Journal of Organic Chemistry, 2010. **75**(5): p. 1569-1581.
166. Hong, D., et al., *AZD9150, a next-generation antisense oligonucleotide inhibitor of STAT3 with early evidence of clinical activity in lymphoma and lung cancer*. Science Translational Medicine, 2015. **7**(314): p. 314ra185-314ra185.
167. Morita, K., et al., *2'-O, 4'-C-ethylene-bridged nucleic acids (ENA): highly nuclease-resistant and thermodynamically stable oligonucleotides for antisense drug*. Bioorganic & Medicinal Chemistry Letters, 2002. **12**(1): p. 73-76.
168. Morita, K., et al., *Synthesis and properties of 2'-O, 4'-C-ethylene-bridged nucleic acids (ENA) as effective antisense oligonucleotides*. Bioorganic & Medicinal Chemistry, 2003. **11**(10): p. 2211-2226.
169. Morita, K., et al., *Inhibition of VEGF mRNA by 2'-O, 4'-C- Ethylene-Bridgednucleicacids (ENA®) Antisense Oligonucleotides and Their Influence on Off-Target Gene Expressions*. Nucleosides, Nucleotides and Nucleic Acids, 2006. **25**(4-6): p. 503-521.
170. van der Ree, M.H., et al., *Long-term safety and efficacy of microRNA-targeted therapy in chronic hepatitis C patients*. Antiviral research, 2014. **111**: p. 53-59.
171. Janssen, H.L., et al., *Treatment of HCV infection by targeting microRNA*. New England Journal of Medicine, 2013. **368**(18): p. 1685-1694.
172. Bianchini, D., et al., *First-in-human Phase I study of EZN-4176, a locked nucleic acid antisense oligonucleotide to exon 4 of the androgen receptor mRNA in patients with castration-resistant prostate cancer*. British journal of cancer, 2013. **109**(10): p. 2579.
173. Elmén, J., et al., *Locked nucleic acid (LNA) mediated improvements in siRNA stability and functionality*. Nucleic Acids Research, 2005. **33**(1): p. 439-447.
174. Frieden, M., H.F. Hansen, and T. Koch, *Nuclease stability of LNA oligonucleotides and LNA-DNA chimeras*. Nucleosides, Nucleotides and Nucleic Acids, 2003. **22**(5-8): p. 1041-1043.
175. Swayze, E.E., et al., *Antisense oligonucleotides containing locked nucleic acid improve potency but cause significant hepatotoxicity in animals*. Nucleic Acids Research, 2006. **35**(2): p. 687-700.
176. Teplova, M., et al., *Crystal structure and improved antisense properties of 2'-O-(2-methoxyethyl)-RNA*. Nature Structural Biology, 1999. **6**(6): p. 535-539.
177. Inoue, H., et al., *Synthesis and hybridization studies on two complementary nona (2'-O-methyl) ribonucleotides*. Nucleic Acids Research, 1987. **15**(15): p. 6131-6148.
178. Lamond, A.I. and B.S. Sproat, *Antisense oligonucleotides made of 2'-O-alkylRNA: their properties and applications in RNA biochemistry*. FEBS letters, 1993. **325**(1-2): p. 123-127.
179. Lesnik, E.A., et al., *Oligodeoxynucleotides containing 2'-O-modified adenosine: synthesis and effects on stability of DNA: RNA duplexes*. Biochemistry, 1993. **32**(30): p. 7832-7838.
180. Kawasaki, A.M., et al., *Uniformly modified 2'-deoxy-2'-fluoro-phosphorothioate oligonucleotides as nuclease-resistant antisense compounds with high affinity and specificity for RNA targets*. Journal of Medicinal Chemistry, 1993. **36**(7): p. 831-841.
181. Altmann, K.-H., et al., *Second generation of antisense oligonucleotides: from nuclease resistance to biological efficacy in animals*. CHIMIA International Journal for Chemistry, 1996. **50**(4): p. 168-176.
182. Nair, J.K., et al., *Impact of enhanced metabolic stability on pharmacokinetics and pharmacodynamics of GalNAc-siRNA conjugates*. Nucleic Acids Research, 2017. **45**(19): p. 10969-10977.

183. Foster, D.J., et al., *Advanced siRNA designs further improve in vivo performance of GalNAc-siRNA conjugates*. *Molecular Therapy*, 2018. **26**(3): p. 708-717.
184. Manoharan, M., et al., *Unique gene-silencing and structural properties of 2'-fluoro-modified siRNAs*. *Angewandte Chemie International Edition*, 2011. **50**(10): p. 2284-2288.
185. Thompson, J.D., et al., *Toxicological and pharmacokinetic properties of chemically modified siRNAs targeting p53 RNA following intravenous administration*. *Nucleic Acid Therapeutics*, 2012. **22**(4): p. 255-264.
186. Shen, W., et al., *2'-Fluoro-modified phosphorothioate oligonucleotide can cause rapid degradation of P54nrb and PSF*. *Nucleic acids research*, 2015. **43**(9): p. 4569-4578.
187. Shen, W., et al., *Chemical modification of PS-ASO therapeutics reduces cellular protein-binding and improves the therapeutic index*. *Nature Biotechnology*, 2019. **37**(6): p. 640-650.
188. Shen, W., et al., *Acute hepatotoxicity of 2' fluoro-modified 5–10–5 gapmer phosphorothioate oligonucleotides in mice correlates with intracellular protein binding and the loss of DBHS proteins*. *Nucleic Acids Research*, 2018. **46**(5): p. 2204-2217.
189. Glud, S.Z., et al., *Naked siLNA-mediated gene silencing of lung bronchoepithelium EGFP expression after intravenous administration*. *Oligonucleotides*, 2009. **19**(2): p. 163-168.
190. Gao, S., et al., *The Effect of Chemical Modification and Nanoparticle Formulation on Stability and Biodistribution of siRNA in Mice*. *Molecular Therapy*, 2009. **17**(7): p. 1225-1233.
191. Schlegel, M.K., et al., *Chirality dependent potency enhancement and structural impact of glycol nucleic acid modification on siRNA*. *Journal of the American Chemical Society*, 2017. **139**(25): p. 8537-8546.
192. Nykänen, A., B. Haley, and P.D. Zamore, *ATP Requirements and Small Interfering RNA Structure in the RNA Interference Pathway*. *Cell*, 2001. **107**(3): p. 309-321.
193. Ma, J.-B., et al., *Structural basis for 5'-end-specific recognition of guide RNA by the A. fulgidus Piwi protein*. *Nature*, 2005. **434**(7033): p. 666.
194. Martinez, J., et al., *Single-stranded antisense siRNAs guide target RNA cleavage in RNAi*. *Cell*, 2002. **110**(5): p. 563-574.
195. Frank, F., N. Sonenberg, and B. Nagar, *Structural basis for 5'-nucleotide base-specific recognition of guide RNA by human AGO2*. *Nature*, 2010. **465**(7299): p. 818.
196. Weitzer, S. and J. Martinez, *The human RNA kinase hC1p1 is active on 3' transfer RNA exons and short interfering RNAs*. *Nature*, 2007. **447**(7141): p. 222.
197. Kenski, D.M., et al., *In vivo activity and duration of short interfering RNAs containing a synthetic 5'-phosphate*. *Nucleic Acid Therapeutics*, 2012. **22**(2): p. 90-95.
198. Elkayam, E., et al., *siRNA carrying an (E)-vinylphosphonate moiety at the 5' end of the guide strand augments gene silencing by enhanced binding to human Argonaute-2*. *Nucleic Acids Research*, 2016. **45**(6): p. 3528-3536.
199. Prakash, T.P., et al., *Synergistic effect of phosphorothioate, 5'-vinylphosphonate and GalNAc modifications for enhancing activity of synthetic siRNA*. *Bioorganic & Medicinal Chemistry Letters*, 2016. **26**(12): p. 2817-2820.
200. Lima, W.F., et al., *Single-stranded siRNAs activate RNAi in animals*. *Cell*, 2012. **150**(5): p. 883-894.
201. Prakash, T.P., et al., *Identification of metabolically stable 5'-phosphate analogs that support single-stranded siRNA activity*. *Nucleic Acids Research*, 2015. **43**(6): p. 2993-3011.
202. Parmar, R., et al., *5'-(E)-Vinylphosphonate: A Stable Phosphate Mimic Can Improve the RNAi Activity of siRNA–GalNAc Conjugates*. *ChemBioChem*, 2016. **17**(11): p. 985-989.
203. Schirle, N.T., et al., *Structural analysis of human Argonaute-2 bound to a modified siRNA guide*. *Journal of the American Chemical Society*, 2016. **138**(28): p. 8694-8697.
204. Chen, P.Y., et al., *Strand-specific 5'-O-methylation of siRNA duplexes controls guide strand selection and targeting specificity*. *RNA*, 2008. **14**(2): p. 263-274.

205. Pradère, U., F. Halloy, and J. Hall, *Chemical synthesis of long RNAs with terminal 5'-phosphate groups*. *Chemistry—A European Journal*, 2017. **23**(22): p. 5210-5213.
206. Boos, J.A., et al., *Whole-body scanning PCR; a highly sensitive method to study the biodistribution of mRNAs, noncoding RNAs and therapeutic oligonucleotides*. *Nucleic Acids Research*, 2013. **41**(15): p. e145-e145.
207. Brunschweiger, A., et al., *Site-specific conjugation of drug-like fragments to an anti-miR scaffold as a strategy to target miRNAs inside RISC*. *Chemical Communications*, 2016. **52**(1): p. 156-159.
208. Landesman, Y., et al., *In vivo quantification of formulated and chemically modified small interfering RNA by heating-in-Triton quantitative reverse transcription polymerase chain reaction (HIT qRT-PCR)*. *Silence*, 2010. **1**(1): p. 16.
209. Gu, J., et al., *Formation of 2', 3'-Cyclic Phosphates at the 3' End of Human U6 Small Nuclear RNA in Vitro IDENTIFICATION OF 2', 3'-CYCLIC PHOSPHATES AT THE 3' ENDS OF HUMAN SIGNAL RECOGNITION PARTICLE AND MITOCHONDRIAL RNA PROCESSING RNAs*. *Journal of Biological Chemistry*, 1997. **272**(35): p. 21989-21993.
210. Perkins, K.K., H. Furneaux, and J. Hurwitz, *Isolation and characterization of an RNA ligase from HeLa cells*. *Proceedings of the National Academy of Sciences*, 1985. **82**(3): p. 684-688.
211. Filipowicz, W., et al., *RNA 3'-terminal phosphate cyclase activity and RNA ligation in HeLa cell extract*. *Nucleic Acids Research*, 1983. **11**(5): p. 1405-1418.
212. Schwer, B., et al., *Mammalian 2', 3' cyclic nucleotide phosphodiesterase (CNP) can function as a tRNA splicing enzyme in vivo*. *RNA*, 2008. **14**(2): p. 204-210.
213. Popow, J., et al., *HSPC117 is the essential subunit of a human tRNA splicing ligase complex*. *Science*, 2011. **331**(6018): p. 760-764.
214. Niewoehner, O., et al., *Type III CRISPR-Cas systems produce cyclic oligoadenylate second messengers*. *Nature*, 2017. **548**(7669): p. 543.
215. Kazlauskienė, M., et al., *A cyclic oligonucleotide signaling pathway in type III CRISPR-Cas systems*. *Science*, 2017. **357**(6351): p. 605-609.
216. Peach, S.E., K. York, and J.R. Hesselberth, *Global analysis of RNA cleavage by 5'-hydroxyl RNA sequencing*. *Nucleic Acids Research*, 2015. **43**(17): p. e108-e108.
217. Athukoralage, J.S., et al., *A Type III CRISPR Ancillary Ribonuclease Degrades Its Cyclic Oligoadenylate Activator*. *Journal of Molecular Biology*, 2019. **431**(15): p. 2894-2899.
218. Rouillon, C., et al., *Control of cyclic oligoadenylate synthesis in a type III CRISPR system*. *eLife*, 2018. **7**: p. e36734.
219. Laikhter, A., S.C. Srivastava, and N. Srivastava, *Synthesis of 2', 3'—and 3', 5'—cyclic phosphate mono- and oligonucleotides*. 2013, US Patent US8618279B2.
220. van Boom, J.H., J.F. de Rooy, and C.B. Reese, *The synthesis of oligoribonucleotides. Part X. Preparation of 2', 3'-cyclic phosphates of ribonucleosides and diribonucleoside phosphates via phosphotriester intermediates*. *Journal of the Chemical Society, Perkin Transactions 1*, 1973: p. 2513-2517.
221. Hamm, M.L. and J.A. Piccirilli, *Synthesis and Characterization of Oligonucleotides Containing 2'-S, 3'-O-Cyclic Phosphorothiolate Termini*. *The Journal of Organic Chemistry*, 1999. **64**(15): p. 5700-5704.
222. Nair, J.K., et al., *Multivalent N-acetylgalactosamine-conjugated siRNA localizes in hepatocytes and elicits robust RNAi-mediated gene silencing*. *Journal of the American Chemical Society*, 2014. **136**(49): p. 16958-16961.
223. Lee, H., et al., *Molecularly self-assembled nucleic acid nanoparticles for targeted in vivo siRNA delivery*. *Nature Nanotechnology*, 2012. **7**: p. 389.
224. Dohmen, C., et al., *Defined Folate-PEG-siRNA Conjugates for Receptor-specific Gene Silencing*. *Molecular Therapy - Nucleic Acids*, 2012. **1**: p. e7.
225. Kumar, P., et al., *Transvascular delivery of small interfering RNA to the central nervous system*. *Nature*, 2007. **448**(7149): p. 39.

226. Youn, P., Y. Chen, and D.Y. Furgeson, *A myristoylated cell-penetrating peptide bearing a transferrin receptor-targeting sequence for neuro-targeted siRNA delivery*. *Molecular Pharmaceutics*, 2014. **11**(2): p. 486-495.
227. Wolfrum, C., et al., *Mechanisms and optimization of in vivo delivery of lipophilic siRNAs*. *Nature Biotechnology*, 2007. **25**: p. 1149.
228. Soutschek, J., et al., *Therapeutic silencing of an endogenous gene by systemic administration of modified siRNAs*. *Nature*, 2004. **432**(7014): p. 173-178.
229. Turanov, A.A., et al., *RNAi modulation of placental sFLT1 for the treatment of preeclampsia*. *Nature Biotechnology*, 2018. **36**: p. 1164.
230. Juliano, R.L., *The delivery of therapeutic oligonucleotides*. *Nucleic acids research*, 2016. **44**(14): p. 6518-6548.
231. Osborn, M.F. and Khvorova, A., *Improving siRNA Delivery In Vivo Through Lipid Conjugation*. *Nucleic Acid Therapeutics*, 2018. **28**(3): p. 128-136.
232. Prakash, T.P., et al., *Fatty acid conjugation enhances potency of antisense oligonucleotides in muscle*. *Nucleic Acids Research*, 2019. **47**(12): p. 6029-6044.
233. Kole, R. and A.M. Krieg, *Exon skipping therapy for Duchenne muscular dystrophy*. *Advanced Drug Delivery Reviews*, 2015. **87**: p. 104-107.
234. Lim, K.R.Q., R. Maruyama, and T. Yokota, *Eteplirsen in the treatment of Duchenne muscular dystrophy*. *Drug Design, Development and Therapy*, 2017. **11**: p. 533-545.
235. Sazani, P., et al., *Nonclinical pharmacokinetic evaluation of Eteplirsen, SRP-4045, and SRP-4053: Three Phosphorodiamidate morpholino oligomers (PMOs) for the treatment of patients with Duchenne muscular dystrophy (DMD)*. *Neuromuscular Disorders*, 2015. **25**: p. S263.
236. EMA, E.M.A. *EMA/H/C/004355/0000*. 2018 [accessed on 17.08.2019]; Available from: https://www.ema.europa.eu/en/documents/assessment-report/exondys-epar-refusal-public-assessment-report_en.pdf.
237. Lefebvre, S., et al., *Identification and characterization of a spinal muscular atrophy-determining gene*. *Cell*, 1995. **80**(1): p. 155-165.
238. Wu, H., et al., *Determination of the role of the human RNase H1 in the pharmacology of DNA-like antisense drugs*. *Journal of Biological Chemistry*, 2004. **279**(17): p. 17181-17189.
239. Geary, R.S., *Antisense oligonucleotide pharmacokinetics and metabolism*. *Expert Opinion on Drug Metabolism & Toxicology*, 2009. **5**(4): p. 381-391.
240. Raal, F.J., et al., *Mipomersen, an apolipoprotein B synthesis inhibitor, for lowering of LDL cholesterol concentrations in patients with homozygous familial hypercholesterolaemia: a randomised, double-blind, placebo-controlled trial*. *The Lancet*, 2010. **375**(9719): p. 998-1006.
241. Prakash, T.P., et al., *Targeted delivery of antisense oligonucleotides to hepatocytes using triantennary N-acetyl galactosamine improves potency 10-fold in mice*. *Nucleic Acids Research*, 2014. **42**(13): p. 8796-8807.
242. Tanowitz, M., et al., *Asialoglycoprotein receptor 1 mediates productive uptake of N-acetylgalactosamine-conjugated and unconjugated phosphorothioate antisense oligonucleotides into liver hepatocytes*. *Nucleic Acids Research*, 2017. **45**(21): p. 12388-12400.
243. Lee, R.C., R.L. Feinbaum, and V. Ambros, *The C. elegans heterochronic gene lin-4 encodes small RNAs with antisense complementarity to lin-14*. *cell*, 1993. **75**(5): p. 843-854.
244. Wightman, B., I. Ha, and G. Ruvkun, *Posttranscriptional regulation of the heterochronic gene lin-14 by lin-4 mediates temporal pattern formation in C. elegans*. *Cell*, 1993. **75**(5): p. 855-862.
245. Olsen, P.H. and V. Ambros, *The lin-4 regulatory RNA controls developmental timing in Caenorhabditis elegans by blocking LIN-14 protein synthesis after the initiation of translation*. *Developmental Biology*, 1999. **216**(2): p. 671-680.
246. Pasquinelli, A.E., et al., *Conservation of the sequence and temporal expression of let-7 heterochronic regulatory RNA*. *Nature*, 2000. **408**(6808): p. 86.

247. Reinhart, B.J., et al., *The 21-nucleotide let-7 RNA regulates developmental timing in *Caenorhabditis elegans**. *Nature*, 2000. **403**(6772): p. 901.
248. Llave, C., et al., *Endogenous and silencing-associated small RNAs in plants*. *The Plant Cell*, 2002. **14**(7): p. 1605-1619.
249. Reinhart, B.J., et al., *MicroRNAs in plants*. *Genes & Development*, 2002. **16**(13): p. 1616-1626.
250. Mette, M.F., et al., *Short RNAs can identify new candidate transposable element families in *Arabidopsis**. *Plant Physiology*, 2002. **130**(1): p. 6-9.
251. Park, W., et al., *CARPEL FACTORY, a Dicer homolog, and HEN1, a novel protein, act in microRNA metabolism in *Arabidopsis thaliana**. *Current Biology*, 2002. **12**(17): p. 1484-1495.
252. Ha, M. and V.N. Kim, *Regulation of microRNA biogenesis*. *Nature Reviews Molecular Cell Biology*, 2014. **15**: p. 509.
253. Bartel, D.P., *Metazoan MicroRNAs*. *Cell*, 2018. **173**(1): p. 20-51.
254. Lee, Y., et al., *MicroRNA maturation: stepwise processing and subcellular localization*. *The EMBO journal*, 2002. **21**(17): p. 4663-4670.
255. Lee, Y., et al., *MicroRNA genes are transcribed by RNA polymerase II*. *The EMBO journal*, 2004. **23**(20): p. 4051-4060.
256. Cai, X., C.H. Hagedorn, and B.R. Cullen, *Human microRNAs are processed from capped, polyadenylated transcripts that can also function as mRNAs*. *RNA*, 2004. **10**(12): p. 1957-1966.
257. Lee, Y., et al., *The nuclear RNase III Drosha initiates microRNA processing*. *Nature*, 2003. **425**(6956): p. 415.
258. Nguyen, Tuan A., et al., *Functional Anatomy of the Human Microprocessor*. *Cell*, 2015. **161**(6): p. 1374-1387.
259. Lund, E., et al., *Nuclear export of microRNA precursors*. *Science*, 2004. **303**(5654): p. 95-98.
260. Yi, R., et al., *Exportin-5 mediates the nuclear export of pre-microRNAs and short hairpin RNAs*. *Genes & Development*, 2003. **17**(24): p. 3011-3016.
261. Bohnsack, M.T., K. Czaplinski, and D. GÖRLICH, *Exportin 5 is a RanGTP-dependent dsRNA-binding protein that mediates nuclear export of pre-miRNAs*. *RNA*, 2004. **10**(2): p. 185-191.
262. Hutvagner, G., et al., *A cellular function for the RNA-interference enzyme Dicer in the maturation of the let-7 small temporal RNA*. *Science*, 2001. **293**(5531): p. 834-838.
263. Grishok, A., et al., *Genes and mechanisms related to RNA interference regulate expression of the small temporal RNAs that control *C. elegans* developmental timing*. *Cell*, 2001. **106**(1): p. 23-34.
264. Bernstein, E., et al., *Role for a bidentate ribonuclease in the initiation step of RNA interference*. *Nature*, 2001. **409**(6818): p. 363.
265. Zhang, H., et al., *Single processing center models for human Dicer and bacterial RNase III*. *Cell*, 2004. **118**(1): p. 57-68.
266. Chendrimada, T.P., et al., *TRBP recruits the Dicer complex to Ago2 for microRNA processing and gene silencing*. *Nature*, 2005. **436**(7051): p. 740.
267. Haase, A.D., et al., *TRBP, a regulator of cellular PKR and HIV-1 virus expression, interacts with Dicer and functions in RNA silencing*. *EMBO reports*, 2005. **6**(10): p. 961-967.
268. Wilson, Ross C., et al., *Dicer-TRBP Complex Formation Ensures Accurate Mammalian MicroRNA Biogenesis*. *Molecular Cell*, 2015. **57**(3): p. 397-407.
269. Lee, Y., et al., *The role of PACT in the RNA silencing pathway*. *The EMBO journal*, 2006. **25**(3): p. 522-532.
270. Kok, K.H., et al., *Human TRBP and PACT directly interact with each other and associate with dicer to facilitate the production of small interfering RNA*. *Journal of Biological Chemistry*, 2007. **282**(24): p. 17649-17657.
271. Lee, H.Y., et al., *Differential roles of human Dicer-binding proteins TRBP and PACT in small RNA processing*. *Nucleic Acids Research*, 2013. **41**(13): p. 6568-6576.

272. MacRae, I.J., et al., *Structural basis for double-stranded RNA processing by Dicer*. Science, 2006. **311**(5758): p. 195-198.
273. Park, J.-E., et al., *Dicer recognizes the 5' end of RNA for efficient and accurate processing*. Nature, 2011. **475**(7355): p. 201.
274. MacRae, I.J., K. Zhou, and J.A. Doudna, *Structural determinants of RNA recognition and cleavage by Dicer*. Nature Structural & Molecular Biology, 2007. **14**: p. 934.
275. Iwasaki, S., et al., *Hsc70/Hsp90 chaperone machinery mediates ATP-dependent RISC loading of small RNA duplexes*. Molecular cell, 2010. **39**(2): p. 292-299.
276. MacRae, I.J., et al., *In vitro reconstitution of the human RISC-loading complex*. Proceedings of the National Academy of Sciences, 2008. **105**(2): p. 512-517.
277. Wang, H.-W., et al., *Structural insights into RNA processing by the human RISC-loading complex*. Nature Structural & Molecular Biology, 2009. **16**: p. 1148.
278. Hammond, S.M., et al., *Argonaute2, a Link Between Genetic and Biochemical Analyses of RNAi*. Science, 2001. **293**(5532): p. 1146-1150.
279. Kawamata, T., H. Seitz, and Y. Tomari, *Structural determinants of miRNAs for RISC loading and slicer-independent unwinding*. Nature Structural & Molecular Biology, 2009. **16**: p. 953.
280. Kawamata, T. and Y. Tomari, *Making RISC*. Trends in Biochemical Sciences, 2010. **35**(7): p. 368-376.
281. Kwak, P.B. and Y. Tomari, *The N domain of Argonaute drives duplex unwinding during RISC assembly*. Nature Structural & Molecular Biology, 2012. **19**: p. 145.
282. Schwarz, D.S., et al., *Asymmetry in the Assembly of the RNAi Enzyme Complex*. Cell, 2003. **115**(2): p. 199-208.
283. Khvorovova, A., A. Reynolds, and S.D. Jayasena, *Functional siRNAs and miRNAs Exhibit Strand Bias*. Cell, 2003. **115**(2): p. 209-216.
284. Ui-Tei, K., et al., *Guidelines for the selection of highly effective siRNA sequences for mammalian and chick RNA interference*. Nucleic Acids Research, 2004. **32**(3): p. 936-948.
285. Hu, H.Y., et al., *Sequence features associated with microRNA strand selection in humans and flies*. BMC genomics, 2009. **10**(1): p. 413.
286. Martin, E.C., et al., *Preferential star strand biogenesis of pre-miR-24-2 targets PKC-alpha and suppresses cell survival in MCF-7 breast cancer cells*. Molecular Carcinogenesis, 2014. **53**(1): p. 38-48.
287. Kuchenbauer, F., et al., *Comprehensive analysis of mammalian miRNA* species and their role in myeloid cells*. Blood, 2011. **118**(12): p. 3350-3358.
288. Niederer, F., et al., *Down-regulation of microRNA-34a* in rheumatoid arthritis synovial fibroblasts promotes apoptosis resistance*. Arthritis & Rheumatism, 2012. **64**(6): p. 1771-1779.
289. Chang, K.-W., et al., *Passenger strand miRNA miR-31* regulates the phenotypes of oral cancer cells by targeting RhoA*. Oral Oncology, 2013. **49**(1): p. 27-33.
290. Guo, Z., et al., *Genome-wide survey of tissue-specific microRNA and transcription factor regulatory networks in 12 tissues*. Scientific Reports, 2014. **4**: p. 5150-5150.
291. Choudhury, N.R., et al., *Tissue-specific control of brain-enriched miR-7 biogenesis*. Genes & Development, 2013. **27**(1): p. 24-38.
292. Yang, J.-S. and Eric C. Lai, *Alternative miRNA Biogenesis Pathways and the Interpretation of Core miRNA Pathway Mutants*. Molecular Cell, 2011. **43**(6): p. 892-903.
293. Cipolla, G.A., *A non-canonical landscape of the microRNA system*. Frontiers in Genetics, 2014. **5**(337).
294. Guennewig, B., et al., *Synthetic pre-microRNAs reveal dual-strand activity of miR-34a on TNF- α* . RNA, 2014. **20**(1): p. 61-75.
295. Bartel, D.P., *MicroRNAs: Target Recognition and Regulatory Functions*. Cell, 2009. **136**(2): p. 215-233.
296. Sheu-Gruttadauria, J., et al., *Beyond the seed: structural basis for supplementary microRNA targeting by human Argonaute2*. The EMBO Journal, 2019. **38**(13): p. e101153.

297. Lim, L.P., et al., *Vertebrate MicroRNA Genes*. Science, 2003. **299**(5612): p. 1540-1540.
298. Brennecke, J., et al., *Principles of MicroRNA–Target Recognition*. PLOS Biology, 2005. **3**(3): p. e85.
299. Doench, J.G. and P.A. Sharp, *Specificity of microRNA target selection in translational repression*. Genes & Development, 2004. **18**(5): p. 504-511.
300. Grimson, A., et al., *MicroRNA targeting specificity in mammals: determinants beyond seed pairing*. Molecular Cell, 2007. **27**(1): p. 91-105.
301. Wee, L.M., et al., *Argonaute divides its RNA guide into domains with distinct functions and RNA-binding properties*. Cell, 2012. **151**(5): p. 1055-1067.
302. Moore, M.J., et al., *miRNA–target chimeras reveal miRNA 3'-end pairing as a major determinant of Argonaute target specificity*. Nature communications, 2015. **6**: p. 8864.
303. Broughton, J.P., et al., *Pairing beyond the seed supports microRNA targeting specificity*. Molecular Cell, 2016. **64**(2): p. 320-333.
304. Agarwal, V., et al., *Predicting effective microRNA target sites in mammalian mRNAs*. eLife, 2015. **4**: p. e05005.
305. Schirle, N.T., et al., *Water-mediated recognition of t1-adenosine anchors Argonaute2 to microRNA targets*. eLife, 2015. **4**: p. e07646.
306. Schirle, N.T., J. Sheu-Gruttadauria, and I.J. MacRae, *Structural basis for microRNA targeting*. Science, 2014. **346**(6209): p. 608-613.
307. Guo, H., et al., *Mammalian microRNAs predominantly act to decrease target mRNA levels*. Nature, 2010. **466**(7308): p. 835.
308. Gebert, L.F.R. and I.J. MacRae, *Regulation of microRNA function in animals*. Nature Reviews Molecular Cell Biology, 2019. **20**(1): p. 21-37.
309. Treiber, T., N. Treiber, and G. Meister, *Regulation of microRNA biogenesis and its crosstalk with other cellular pathways*. Nature Reviews Molecular Cell Biology, 2019. **20**(1): p. 5-20.
310. Meister, G., et al., *Identification of novel argonaute-associated proteins*. Current Biology, 2005. **15**(23): p. 2149-2155.
311. Liu, J., et al., *A role for the P-body component GW182 in microRNA function*. Nature Cell Biology, 2005. **7**(12): p. 1261.
312. Ding, L., et al., *The developmental timing regulator AIN-1 interacts with miRISCs and may target the argonaute protein ALG-1 to cytoplasmic P bodies in C. elegans*. Molecular Cell, 2005. **19**(4): p. 437-447.
313. Rehwinkel, J., et al., *A crucial role for GW182 and the DCP1: DCP2 decapping complex in miRNA-mediated gene silencing*. RNA, 2005. **11**(11): p. 1640-1647.
314. Jinek, M., et al., *Structural insights into the human GW182-PABC interaction in microRNA-mediated deadenylation*. Nature Structural & Molecular Biology, 2010. **17**(2): p. 238.
315. Braun, Joerg E., et al., *GW182 Proteins Directly Recruit Cytoplasmic Deadenylation Complexes to miRNA Targets*. Molecular Cell, 2011. **44**(1): p. 120-133.
316. Chen, C.-Y.A., et al., *Ago–TNRC6 triggers microRNA-mediated decay by promoting two deadenylation steps*. Nature Structural & Molecular Biology, 2009. **16**(11): p. 1160.
317. Behm-Ansmant, I., et al., *mRNA degradation by miRNAs and GW182 requires both CCR4: NOT deadenylase and DCP1: DCP2 decapping complexes*. Genes & Development, 2006. **20**(14): p. 1885-1898.
318. Chekulaeva, M., et al., *miRNA repression involves GW182-mediated recruitment of CCR4–NOT through conserved W-containing motifs*. Nature Structural & Molecular Biology, 2011. **18**(11): p. 1218.
319. Fabian, M.R., et al., *miRNA-mediated deadenylation is orchestrated by GW182 through two conserved motifs that interact with CCR4–NOT*. Nature Structural & Molecular Biology, 2011. **18**(11): p. 1211.
320. Braun, J.E., et al., *A direct interaction between DCP1 and XRN1 couples mRNA decapping to 5' exonucleolytic degradation*. Nature Structural & Molecular Biology, 2012. **19**: p. 1324.

321. Krol, J., I. Loedige, and W. Filipowicz, *The widespread regulation of microRNA biogenesis, function and decay*. Nature Reviews Genetics, 2010. **11**: p. 597.
322. Wang, Y., *Tailoring CLIP-Based Methods for Exploring the miRNA Targetome*. 2019, ETH Zurich.
323. Friedman, R.C., et al., *Most mammalian mRNAs are conserved targets of microRNAs*. Genome Research, 2009. **19**(1): p. 92-105.
324. Esteller, M., *Non-coding RNAs in human disease*. Nature Reviews Genetics, 2011. **12**: p. 861.
325. Lekka, E. and J. Hall, *Noncoding RNAs in disease*. FEBS Letters, 2018. **592**(17): p. 2884-2900.
326. Lu, J., et al., *MicroRNA expression profiles classify human cancers*. Nature, 2005. **435**(7043): p. 834-838.
327. Ventura, A., et al., *Targeted Deletion Reveals Essential and Overlapping Functions of the miR-17~92 Family of miRNA Clusters*. Cell, 2008. **132**(5): p. 875-886.
328. Misso, G., et al., *Mir-34: A New Weapon Against Cancer?* Molecular Therapy - Nucleic Acids, 2014. **3**: p. e195.
329. Albino, D., et al., *Activation of the Lin28/let-7 Axis by Loss of ESE3/EHF Promotes a Tumorigenic and Stem-like Phenotype in Prostate Cancer*. Cancer Research, 2016. **76**(12): p. 3629-3643.
330. Yu, F., et al., *let-7 Regulates Self Renewal and Tumorigenicity of Breast Cancer Cells*. Cell, 2007. **131**(6): p. 1109-1123.
331. Zhu, H., et al., *The Lin28/let-7 Axis Regulates Glucose Metabolism*. Cell, 2011. **147**(1): p. 81-94.
332. Frost, R.J.A. and E.N. Olson, *Control of glucose homeostasis and insulin sensitivity by the Let-7 family of microRNAs*. Proceedings of the National Academy of Sciences, 2011. **108**(52): p. 21075-21080.
333. Weiler, J., J. Hunziker, and J. Hall, *Anti-miRNA oligonucleotides (AMOs): ammunition to target miRNAs implicated in human disease?* Gene Therapy, 2006. **13**(6): p. 496-502.
334. Krützfeldt, J., et al., *Silencing of microRNAs in vivo with 'antagomirs'*. Nature, 2005. **438**(7068): p. 685-689.
335. Hogan, D.J., et al., *Anti-miRs Competitively Inhibit microRNAs in Argonaute Complexes*. PLOS ONE, 2014. **9**(7): p. e100951.
336. Beg, M.S., et al., *Phase I study of MRX34, a liposomal miR-34a mimic, administered twice weekly in patients with advanced solid tumors*. Investigational New Drugs, 2017. **35**(2): p. 180-188.
337. Hong, D.S., et al., *MRX34, a liposomal miR-34 mimic, in patients with advanced solid tumors: Final dose-escalation results from a first-in-human phase I trial of microRNA therapy*. Journal of Clinical Oncology, 2016. **34**(15_suppl): p. 2508-2508.
338. Huang, Y., *Preclinical and Clinical Advances of GalNAc-Decorated Nucleic Acid Therapeutics*. Molecular Therapy - Nucleic Acids, 2017. **6**: p. 116-132.
339. Elmén, J., et al., *LNA-mediated microRNA silencing in non-human primates*. Nature, 2008. **452**(7189): p. 896.
340. Elmen, J., et al., *Antagonism of microRNA-122 in mice by systemically administered LNA-antimiR leads to up-regulation of a large set of predicted target mRNAs in the liver*. Nucleic Acids Research, 2007. **36**(4): p. 1153-1162.
341. Gebert, L.F.R., et al., *Miravirsen (SPC3649) can inhibit the biogenesis of miR-122*. Nucleic Acids Research, 2013. **42**(1): p. 609-621.
342. van der Ree, M.H., et al., *Safety, tolerability, and antiviral effect of RG-101 in patients with chronic hepatitis C: a phase 1B, double-blind, randomised controlled trial*. The Lancet, 2017. **389**(10070): p. 709-717.
343. Bonneau, E., et al., *How close are miRNAs from clinical practice? A perspective on the diagnostic and therapeutic market*. EJIFCC, 2019. **30**(2): p. 114-127.
344. Obad, S., et al., *Silencing of microRNA families by seed-targeting tiny LNAs*. Nature Genetics, 2011. **43**: p. 371.

345. Fire, A., et al., *Potent and specific genetic interference by double-stranded RNA in *Caenorhabditis elegans**. *Nature*, 1998. **391**(6669): p. 806-811.
346. Elbashir, S.M., et al., *Duplexes of 21-nucleotide RNAs mediate RNA interference in cultured mammalian cells*. *Nature*, 2001. **411**(6836): p. 494.
347. Liu, J., et al., *Argonaute2 is the catalytic engine of mammalian RNAi*. *Science*, 2004. **305**(5689): p. 1437-1441.
348. Elbashir, S.M., et al., *Functional anatomy of siRNAs for mediating efficient RNAi in *Drosophila melanogaster* embryo lysate*. *The EMBO Journal*, 2001. **20**(23): p. 6877-6888.
349. Burchard, J., et al., *MicroRNA-like off-target transcript regulation by siRNAs is species specific*. *RNA*, 2009. **15**(2): p. 308-315.
350. Jackson, A.L., et al., *Widespread siRNA "off-target" transcript silencing mediated by seed region sequence complementarity*. *RNA*, 2006. **12**(7): p. 1179-1187.
351. Setten, R.L., J.J. Rossi, and S.-p. Han, *The current state and future directions of RNAi-based therapeutics*. *Nature Reviews Drug Discovery*, 2019. **18**(6): p. 421-446.
352. Siolas, D., et al., *Synthetic shRNAs as potent RNAi triggers*. *Nature Biotechnology*, 2005. **23**(2): p. 227-231.
353. Menzi, M., et al., *Site-Specific Labeling of MicroRNA Precursors: A Structure–Activity Relationship Study*. *ChemBioChem*, 2016. **17**(21): p. 2012-2017.
354. Marjorie Robbins, A.J., Ellen Ambegia, Catherine Choi, Ed Yaworski, Lorne Palmer, Kevin McClintock, Ian MacLachlan, *Misinterpreting the Therapeutic Effects of Small Interfering RNA Caused by Immune Stimulation*. *Human Gene Therapy*, 2008. **19**(10): p. 991-999.
355. Adams, D., et al., *Patisiran, an RNAi therapeutic, for hereditary transthyretin amyloidosis*. *New England Journal of Medicine*, 2018. **379**(1): p. 11-21.
356. Coelho, T., et al., *Safety and Efficacy of RNAi Therapy for Transthyretin Amyloidosis*. *New England Journal of Medicine*, 2013. **369**(9): p. 819-829.
357. Suhr, O.B., et al., *Efficacy and safety of patisiran for familial amyloidotic polyneuropathy: a phase II multi-dose study*. *Orphanet Journal of Rare Diseases*, 2015. **10**(1): p. 109.
358. Jackson, A.L., et al., *Position-specific chemical modification of siRNAs reduces "off-target" transcript silencing*. *RNA*, 2006. **12**(7): p. 1197-1205.
359. Kumar, P., et al., *5'-Morpholino modification of the sense strand of an siRNA makes it a more effective passenger*. *Chemical Communications*, 2019. **55**(35): p. 5139-5142.
360. Judge, A.D., et al., *Sequence-dependent stimulation of the mammalian innate immune response by synthetic siRNA*. *Nature Biotechnology*, 2005. **23**(4): p. 457-462.
361. Marques, J.T. and B.R.G. Williams, *Activation of the mammalian immune system by siRNAs*. *Nature Biotechnology*, 2005. **23**(11): p. 1399-1405.
362. Alexopoulou, L., et al., *Recognition of double-stranded RNA and activation of NF- κ B by Toll-like receptor 3*. *Nature*, 2001. **413**(6857): p. 732-738.
363. Reynolds, A., et al., *Induction of the interferon response by siRNA is cell type- and duplex length-dependent*. *RNA*, 2006. **12**(6): p. 988-993.
364. Hornung, V., et al., *Sequence-specific potent induction of IFN- α by short interfering RNA in plasmacytoid dendritic cells through TLR7*. *Nature Medicine*, 2005. **11**(3): p. 263-270.
365. Judge, A.D., et al., *Design of noninflammatory synthetic siRNA mediating potent gene silencing in vivo*. *Molecular Therapy*, 2006. **13**(3): p. 494-505.
366. Robbins, M., et al., *2'-O-methyl-modified RNAs Act as TLR7 Antagonists*. *Molecular Therapy*, 2007. **15**(9): p. 1663-1669.
367. Koller, E., et al., *Competition for RISC binding predicts in vitro potency of siRNA*. *Nucleic Acids Research*, 2006. **34**(16): p. 4467-4476.
368. Liang, X.-h., C.E. Hart, and S.T. Crooke, *Transfection of siRNAs can alter miRNA levels and trigger non-specific protein degradation in mammalian cells*. *Biochimica et Biophysica Acta (BBA)-Gene Regulatory Mechanisms*, 2013. **1829**(5): p. 455-468.

369. Grimm, D., et al., *Fatality in mice due to oversaturation of cellular microRNA/short hairpin RNA pathways*. *Nature*, 2006. **441**(7092): p. 537-541.
370. Janas, M.M., et al., *Safety evaluation of 2'-deoxy-2'-fluoro nucleotides in GalNAc-siRNA conjugates*. *Nucleic Acids Research*, 2019. **47**(7): p. 3306-3320.
371. Taubel, J.Z., et al., *Phase 1 Study of ALN-TTRsc02, a Subcutaneously Administered Investigational RNAi Therapeutic for the Treatment of Transthyretin-Mediated Amyloidosis*, [accessed on 17.08.2019]; Available from: https://www.alnylam.com/wp-content/uploads/2018/03/10.-TTR-SCO2_FINAL.pdf
372. Garber, K., *Alnylam terminates revusiran program, stock plunges*. *Nature Biotechnology*, 2016. **34**: p. 1213.
373. Prakash, T.P., et al., *Positional Effect of Chemical Modifications on Short Interference RNA Activity in Mammalian Cells*. *Journal of Medicinal Chemistry*, 2005. **48**(13): p. 4247-4253.
374. Zlatev, I., et al., *Reversal of siRNA-mediated gene silencing in vivo*. *Nature Biotechnology*, 2018. **36**: p. 509.
375. Johannes, L. and M. Lucchino, *Current challenges in delivery and cytosolic translocation of therapeutic RNAs*. *Nucleic Acid Therapeutics*, 2018. **28**(3): p. 178-193.
376. Shukla, R.S., B. Qin, and K. Cheng, *Peptides Used in the Delivery of Small Noncoding RNA*. *Molecular Pharmaceutics*, 2014. **11**(10): p. 3395-3408.
377. McNamara, J.O., et al., *Cell type-specific delivery of siRNAs with aptamer-siRNA chimeras*. *Nature Biotechnology*, 2006. **24**(8): p. 1005-1015.
378. Steirer, L.M., et al., *The asialoglycoprotein receptor regulates levels of plasma glycoproteins terminating with sialic acid alpha2,6-galactose*. *The Journal of Biological Chemistry*, 2009. **284**(6): p. 3777-3783.
379. Willoughby, J.L.S., et al., *Evaluation of GalNAc-siRNA Conjugate Activity in Pre-clinical Animal Models with Reduced Asialoglycoprotein Receptor Expression*. *Molecular therapy: The Journal of the American Society of Gene Therapy*, 2018. **26**(1): p. 105-114.
380. Bon, C., et al., *Capacity limits of asialoglycoprotein receptor-mediated liver targeting*. *mAbs*, 2017. **9**(8): p. 1360-1369.
381. Fernández, M., F. Javaid, and V. Chudasama, *Advances in targeting the folate receptor in the treatment/imaging of cancers*. *Chemical Science*, 2018. **9**(4): p. 790-810.
382. Demirjian, S., et al., *Safety and Tolerability Study of an Intravenously Administered Small Interfering Ribonucleic Acid (siRNA) Post On-Pump Cardiothoracic Surgery in Patients at Risk of Acute Kidney Injury*. *Kidney International Reports*, 2017. **2**(5): p. 836-843.
383. Barrangou, R., et al., *CRISPR Provides Acquired Resistance Against Viruses in Prokaryotes*. *Science*, 2007. **315**(5819): p. 1709-1712.
384. Brouns, S.J.J., et al., *Small CRISPR RNAs Guide Antiviral Defense in Prokaryotes*. *Science*, 2008. **321**(5891): p. 960-964.
385. Marraffini, L.A. and E.J. Sontheimer, *CRISPR Interference Limits Horizontal Gene Transfer in Staphylococci by Targeting DNA*. *Science*, 2008. **322**(5909): p. 1843-1845.
386. Koonin, E.V., K.S. Makarova, and F. Zhang, *Diversity, classification and evolution of CRISPR-Cas systems*. *Current Opinion in Microbiology*, 2017. **37**: p. 67-78.
387. Knott, G.J. and J.A. Doudna, *CRISPR-Cas guides the future of genetic engineering*. *Science*, 2018. **361**(6405): p. 866-869.
388. Jinek, M., et al., *A Programmable Dual-RNA-Guided DNA Endonuclease in Adaptive Bacterial Immunity*. *Science*, 2012. **337**(6096): p. 816-821.
389. Urnov, F.D., et al., *Genome editing with engineered zinc finger nucleases*. *Nature Reviews Genetics*, 2010. **11**: p. 636.
390. Carroll, D., *Genome Engineering with Targetable Nucleases*. *Annual Review of Biochemistry*, 2014. **83**(1): p. 409-439.

391. Urnov, F.D., *Genome Editing B.C. (Before CRISPR): Lasting Lessons from the “Old Testament”*. The CRISPR Journal, 2018. **1**(1): p. 34-46.
392. Pannunzio, N.R., G. Watanabe, and M.R. Lieber, *Nonhomologous DNA end-joining for repair of DNA double-strand breaks*. Journal of Biological Chemistry, 2018. **293**(27): p. 10512-10523.
393. Pawelczak, K.S., et al., *Modulating DNA Repair Pathways to Improve Precision Genome Engineering*. ACS Chemical Biology, 2018. **13**(2): p. 389-396.
394. Savic, N., et al., *Covalent linkage of the DNA repair template to the CRISPR-Cas9 nuclease enhances homology-directed repair*. eLife, 2018. **7**: p. e33761.
395. Mojica, F.J.M., et al., *Short motif sequences determine the targets of the prokaryotic CRISPR defence system*. Microbiology, 2009. **155**(3): p. 733-740.
396. Marraffini, L.A. and E.J. Sontheimer, *Self versus non-self discrimination during CRISPR RNA-directed immunity*. Nature, 2010. **463**: p. 568.
397. Sternberg, S.H., et al., *DNA interrogation by the CRISPR RNA-guided endonuclease Cas9*. Nature, 2014. **507**: p. 62.
398. Zetsche, B., et al., *Cpf1 Is a Single RNA-Guided Endonuclease of a Class 2 CRISPR-Cas System*. Cell, 2015. **163**(3): p. 759-771.
399. East-Seletsky, A., et al., *Two distinct RNase activities of CRISPR-C2c2 enable guide-RNA processing and RNA detection*. Nature, 2016. **538**: p. 270.
400. Abudayyeh, O.O., et al., *C2c2 is a single-component programmable RNA-guided RNA-targeting CRISPR effector*. Science, 2016. **353**(6299): p. aaf5573.
401. Konermann, S., et al., *Transcriptome Engineering with RNA-Targeting Type VI-D CRISPR Effectors*. Cell, 2018. **173**(3): p. 665-676.e14.
402. Tamulaitis, G., Č. Venclovas, and V. Siksnys, *Type III CRISPR-Cas Immunity: Major Differences Brushed Aside*. Trends in Microbiology, 2017. **25**(1): p. 49-61.
403. Kampmann, M., *CRISPRi and CRISPRa Screens in Mammalian Cells for Precision Biology and Medicine*. ACS Chemical Biology, 2018. **13**(2): p. 406-416.
404. Zheng, Y., et al., *CRISPR interference-based specific and efficient gene inactivation in the brain*. Nature Neuroscience, 2018. **21**(3): p. 447-454.
405. Chavez, A., et al., *Highly efficient Cas9-mediated transcriptional programming*. Nature Methods, 2015. **12**: p. 326.
406. Komor, A.C., et al., *Programmable editing of a target base in genomic DNA without double-stranded DNA cleavage*. Nature, 2016. **533**: p. 420.
407. Villiger, L., et al., *Treatment of a metabolic liver disease by in vivo genome base editing in adult mice*. Nature Medicine, 2018. **24**(10): p. 1519-1525.
408. Gaudelli, N.M., et al., *Programmable base editing of A•T to G•C in genomic DNA without DNA cleavage*. Nature, 2017. **551**: p. 464.
409. Grünewald, J., et al., *Transcriptome-wide off-target RNA editing induced by CRISPR-guided DNA base editors*. Nature, 2019. **569**(7756): p. 433-437.
410. Wrighton, K.H., *Cytosine base editors go off-target*. Nature Reviews Genetics, 2019. **20**(5): p. 254-255.
411. Kim, D., et al., *Genome-wide target specificity of CRISPR RNA-guided adenine base editors*. Nature Biotechnology, 2019. **37**(4): p. 430-435.
412. Pickar-Oliver, A. and C.A. Gersbach, *The next generation of CRISPR–Cas technologies and applications*. Nature Reviews Molecular Cell Biology, 2019. **20**(8): p. 490-507.
413. Kaczmarek, J.C., P.S. Kowalski, and D.G. Anderson, *Advances in the delivery of RNA therapeutics: from concept to clinical reality*. Genome Medicine, 2017. **9**(1): p. 60.
414. Kim, S., et al., *Highly efficient RNA-guided genome editing in human cells via delivery of purified Cas9 ribonucleoproteins*. Genome Research, 2014. **24**(6): p. 1012-1019.
415. Rouet, R., et al., *Receptor-Mediated Delivery of CRISPR-Cas9 Endonuclease for Cell-Type-Specific Gene Editing*. Journal of the American Chemical Society, 2018. **140**(21): p. 6596-6603.
416. Sahin, U., K. Karikó, and Ö. Türeci, *mRNA-based therapeutics — developing a new class of drugs*. Nature Reviews Drug Discovery, 2014. **13**: p. 759.

417. Pardi, N., et al., *mRNA vaccines — a new era in vaccinology*. Nature Reviews Drug Discovery, 2018. **17**: p. 261.
418. Trepotec, Z., et al., *Delivery of mRNA Therapeutics for the Treatment of Hepatic Diseases*. Molecular Therapy, 2019. **27**(4): p. 794-802.
419. Dunn, M.R., R.M. Jimenez, and J.C. Chaput, *Analysis of aptamer discovery and technology*. Nature Reviews Chemistry, 2017. **1**: p. 0076.
420. Neff, C.P., et al., *An aptamer-siRNA chimera suppresses HIV-1 viral loads and protects from helper CD4+ T cell decline in humanized mice*. Science Translational Medicine, 2011. **3**(66): p. 66ra6-66ra6.
421. Esposito, C.L., et al., *STAT3 Gene Silencing by Aptamer-siRNA Chimera as Selective Therapeutic for Glioblastoma*. Molecular Therapy - Nucleic Acids, 2018. **10**: p. 398-411.
422. Mehlhorn, A., P. Rahimi, and Y. Joseph, *Aptamer-based biosensors for antibiotic detection: a review*. Biosensors, 2018. **8**(2): p. 54.
423. Ng, E.W.M., et al., *Pegaptanib, a targeted anti-VEGF aptamer for ocular vascular disease*. Nature Reviews Drug Discovery, 2006. **5**(2): p. 123-132.
424. Shirota, H., D. Tross, and D.M. Klinman, *CpG Oligonucleotides as Cancer Vaccine Adjuvants*. Vaccines, 2015. **3**(2): p. 390-407.
425. Reeman, S., et al., *Protection of Mice from Lethal Vaccinia Virus Infection by Vaccinia Virus Protein Subunits with a CpG Adjuvant*. Viruses, 2017. **9**(12): p. 378.
426. Ludwig, A., et al., *Ribozyme Cleavage of Telomerase mRNA Sensitizes Breast Epithelial Cells to Inhibitors of Topoisomerase*. Cancer Research, 2001. **61**(7): p. 3053-3061.
427. Behlke, M.A., *Chemical Modification of siRNAs for In Vivo Use*. Oligonucleotides, 2008. **18**(4): p. 305-320.
428. Robbins, M.A., et al., *Stable expression of shRNAs in human CD34+ progenitor cells can avoid induction of interferon responses to siRNAs in vitro*. Nature Biotechnology, 2006. **24**(5): p. 566.
429. Heidel, J.D., et al., *Lack of interferon response in animals to naked siRNAs*. Nature biotechnology, 2004. **22**(12): p. 1579.
430. Alterman, J.F., et al., *Hydrophobically Modified siRNAs Silence Huntingtin mRNA in Primary Neurons and Mouse Brain*. Molecular Therapy - Nucleic Acids, 2015. **4**: p. e266.
431. Braasch, D.A., et al., *RNA Interference in Mammalian Cells by Chemically-Modified RNA*. Biochemistry, 2003. **42**(26): p. 7967-7975.
432. Braasch, D.A., et al., *Biodistribution of phosphodiester and phosphorothioate siRNA*. Bioorganic & Medicinal Chemistry Letters, 2004. **14**(5): p. 1139-1143.
433. Chiu, Y.-L. and T.M. Rana, *siRNA function in RNAi: A chemical modification analysis*. RNA, 2003. **9**(9): p. 1034-1048.
434. Winkler, J., et al., *Off-target effects related to the phosphorothioate modification of nucleic acids*. ChemMedChem, 2010. **5**(8): p. 1344-1352.
435. Kraynack, B.A. and B.F. Baker, *Small interfering RNAs containing full 2'-O-methylribonucleotide-modified sense strands display Argonaute2/eIF2C2-dependent activity*. RNA, 2006. **12**(1): p. 163-176.
436. Moss, E.G., R.C. Lee, and V. Ambros, *The cold shock domain protein LIN-28 controls developmental timing in C. elegans and is regulated by the lin-4 RNA*. Cell, 1997. **88**(5): p. 637-646.
437. Moss, E.G. and L. Tang, *Conservation of the heterochronic regulator Lin-28, its developmental expression and microRNA complementary sites*. Developmental Biology, 2003. **258**(2): p. 432-442.
438. Yang, D.-H. and E.G. Moss, *Temporally regulated expression of Lin-28 in diverse tissues of the developing mouse*. Gene Expression Patterns, 2003. **3**(6): p. 719-726.
439. Richards, M., et al., *The Transcriptome Profile of Human Embryonic Stem Cells as Defined by SAGE*. STEM CELLS, 2004. **22**(1): p. 51-64.
440. Nam, Y., et al., *Molecular basis for interaction of let-7 microRNAs with Lin28*. Cell, 2011. **147**(5): p. 1080-1091.

441. Guo, Y., et al., *Identification and characterization of lin-28 homolog B (LIN28B) in human hepatocellular carcinoma*. *Gene*, 2006. **384**: p. 51-61.
442. Loughlin, F.E., et al., *Structural basis of pre-let-7 miRNA recognition by the zinc knuckles of pluripotency factor Lin28*. *Nature Structural & Molecular Biology*, 2012. **19**(1): p. 84.
443. Piskounova, E., et al., *Lin28A and Lin28B Inhibit let-7 MicroRNA Biogenesis by Distinct Mechanisms*. *Cell*, 2011. **147**(5): p. 1066-1079.
444. Balzer, E. and E.G. Moss, *Localization of the Developmental Timing Regulator Lin28 to mRNP Complexes, P-bodies and Stress Granules*. *RNA Biology*, 2007. **4**(1): p. 16-25.
445. Balzeau, J., et al., *The LIN28/let-7 Pathway in Cancer*. *Frontiers in Genetics*, 2017. **8**(31).
446. Hagan, J.P., E. Piskounova, and R.I. Gregory, *Lin28 recruits the TUTase Zcchc11 to inhibit let-7 maturation in mouse embryonic stem cells*. *Nature Structural & Molecular Biology*, 2009. **16**: p. 1021.
447. Heo, I., et al., *TUT4 in Concert with Lin28 Suppresses MicroRNA Biogenesis through Pre-MicroRNA Uridylation*. *Cell*, 2009. **138**(4): p. 696-708.
448. Nguyen, L.H., et al., *Lin28b is sufficient to drive liver cancer and necessary for its maintenance in murine models*. *Cancer Cell*, 2014. **26**(2): p. 248-261.
449. Roos, M., et al., *A Small-Molecule Inhibitor of Lin28*. *ACS Chemical Biology*, 2016. **11**(10): p. 2773-2781.
450. Roos, M., et al., *Short loop-targeting oligoribonucleotides antagonize Lin28 and enable pre-let-7 processing and suppression of cell growth in let-7-deficient cancer cells*. *Nucleic Acids Research*, 2014. **43**(2): p. e9-e9.
451. GlenResearch Report 18.13. [accessed on 10.09.2019]; Available from: <https://www.glenresearch.com/reports/gr18-13>.
452. Ravikumar, V.T., et al., *Development of siRNA for therapeutics: efficient synthesis of phosphorothioate RNA utilizing phenylacetyl disulfide (PADS)*. *Bioorganic & Medicinal Chemistry Letters*, 2006. **16**(9): p. 2513-2517.
453. Scotson, J.L., et al., *Phosphorothioate anti-sense oligonucleotides: the kinetics and mechanism of the generation of the sulfurising agent from phenylacetyl disulfide (PADS)*. *Organic & Biomolecular Chemistry*, 2016. **14**(35): p. 8301-8308.
454. Krotz, A.H., et al., *Phosphorothioate oligonucleotides with low phosphate diester content: greater than 99.9% sulfurization efficiency with "aged" solutions of phenylacetyl disulfide (PADS)*. *Organic Process Research & Development*, 2004. **8**(6): p. 852-858.
455. Reddy, M.P., N.B. Hanna, and F. Farooqui, *Fast cleavage and deprotection of oligonucleotides*. *Tetrahedron Letters*, 1994. **35**(25): p. 4311-4314.
456. IDT. [accessed on 10.09.2019]; Available from: <https://eu.idtdna.com/pages/support/faqs/how-does-the-efficiency-of-rna-synthesis-compare-with-dna->.
457. Devor, E.J. and M.A. Behlke, *Oligonucleotide yield, resuspension, and storage*. *Integrated DNA Technologies*, 2005: p. 1-11.
458. Leighton, F., et al., *The large-scale separation of peroxisomes, mitochondria, and lysosomes from the livers of rats injected with Triton WR-1339: improved isolation procedures, automated analysis, biochemical and morphological properties of fractions*. *The Journal of Cell Biology*, 1968. **37**(2): p. 482-513.
459. Lübke, T., P. Lobel, and D.E. Sleaf, *Proteomics of the lysosome*. *Biochimica et Biophysica Acta (BBA) - Molecular Cell Research*, 2009. **1793**(4): p. 625-635.
460. Bettencourt, B., *Methods of Treating Transthyretin (TTR) Mediated Amyloidosis*. 2017, US Patent US10060921B2.
461. Akinc, A., et al., *Methods and compositions for treating a serpincl1-associated disorder*. 2017, US Patent US20170159053A1.
462. Geary, R.S., et al., *Pharmacokinetics and Metabolism in Mice of a Phosphorothioate Oligonucleotide Antisense Inhibitor of C-raf-1 Kinase Expression*. *Drug Metabolism and Disposition*, 1997. **25**(11): p. 1272-1281.

463. Garin, D., et al., *In vivo siRNA distribution and pharmacokinetics assessed by nuclear imaging are modulated according to radiolabelling site*. Nuclear Medicine and Biology, 2015. **42**(12): p. 958-966.
464. Hsieh, J.-C., S. Zinnen, and P. Modrich, *Kinetic mechanism of the DNA-dependent DNA polymerase activity of human immunodeficiency virus reverse transcriptase*. Journal of Biological Chemistry, 1993. **268**(33): p. 24607-24613.
465. Van Nostrand, E.L., et al., *Variation in single-nucleotide sensitivity of eCLIP derived from reverse transcription conditions*. Methods, 2017. **126**: p. 29-37.
466. Van de Water, F.M., et al., *Intravenously administered short interfering RNA accumulates in the kidney and selectively suppresses gene function in renal proximal tubules*. Drug Metabolism and Disposition, 2006. **34**(8): p. 1393-1397.
467. Merkel, O.M., et al., *In Vivo SPECT and Real-Time Gamma Camera Imaging of Biodistribution and Pharmacokinetics of siRNA Delivery Using an Optimized Radiolabeling and Purification Procedure*. Bioconjugate Chemistry, 2009. **20**(1): p. 174-182.
468. Endoh, T. and T. Ohtsuki, *Cellular siRNA delivery using cell-penetrating peptides modified for endosomal escape*. Advanced Drug Delivery Reviews, 2009. **61**(9): p. 704-709.
469. Veldhoen, S., et al., *Cellular delivery of small interfering RNA by a non-covalently attached cell-penetrating peptide: quantitative analysis of uptake and biological effect*. Nucleic Acids Research, 2006. **34**(22): p. 6561-6573.
470. Hirsch, M. and M. Helm, *Live cell imaging of duplex siRNA intracellular trafficking*. Nucleic Acids Research, 2015. **43**(9): p. 4650-4660.
471. Igarashi, K. and K. Kashiwagi, *Modulation of cellular function by polyamines*. The International Journal of Biochemistry & Cell Biology, 2010. **42**(1): p. 39-51.
472. Lightfoot, H.L. and J. Hall, *Endogenous polyamine function—the RNA perspective*. Nucleic Acids Research, 2014. **42**(18): p. 11275-11290.
473. Antony, T., et al., *Selectivity of Polyamines on the Stability of RNA–DNA Hybrids Containing Phosphodiester and Phosphorothioate Oligodeoxyribonucleotides*. Biochemistry, 1999. **38**(33): p. 10775-10784.
474. Jovine, L., S. Djordjevic, and D. Rhodes, *The crystal structure of yeast phenylalanine tRNA at 2.0 Å resolution: cleavage by Mg²⁺ in 15-year old crystals*. Journal of Molecular Biology, 2000. **301**(2): p. 401-414.
475. Bolton, P.H. and D.R. Kearns, *Hydrogen bonding interactions of polyamines with the 2' OH of RNA*. Nucleic Acids Research, 1978. **5**(4): p. 1315-1324.
476. Quigley, G.J., M.M. Teeter, and A. Rich, *Structural analysis of spermine and magnesium ion binding to yeast phenylalanine transfer RNA*. Proceedings of the National Academy of Sciences, 1978. **75**(1): p. 64-68.
477. Holbrook, S.R., et al., *Crystal structure of yeast phenylalanine transfer RNA: II. Structural features and functional implications*. Journal of Molecular Biology, 1978. **123**(4): p. 631-660.
478. Ouameur, A.A., P. Bourassa, and H.-A. Tajmir-Riahi, *Probing tRNA interaction with biogenic polyamines*. RNA, 2010. **16**(10): p. 1968-1979.
479. Ikemura, T., *The relation between the strong binding of spermine to polynucleotides and the conformation of polynucleotides*. Biochimica et Biophysica Acta (BBA)-Nucleic Acids and Protein Synthesis, 1969. **195**(2): p. 389-395.
480. Stevens, L. and G. Pascoe, *The location of spermine in bacterial ribosomes as indicated by 1, 5-difluoro-2, 4-dinitrobenzene and by ethidium bromide*. Biochemical Journal, 1972. **128**(2): p. 279-289.
481. Kolhatkar, V., et al., *Star-Shaped Tetraspermine Enhances Cellular Uptake and Cytotoxicity of T-Oligo in Prostate Cancer Cells*. Pharmaceutical Research, 2015. **32**(1): p. 196-210.
482. Meng, T., et al., *A spermine conjugated stearic acid-g-chitosan oligosaccharide polymer with different types of amino groups for efficient p53 gene therapy*. Colloids and Surfaces B: Biointerfaces, 2016. **145**: p. 695-705.

483. Moreau, V., et al., *Zip Nucleic Acids: new high affinity oligonucleotides as potent primers for PCR and reverse transcription*. *Nucleic Acids Research*, 2009. **37**(19): p. e130-e130.
484. Noir, R., et al., *Oligonucleotide– Oligospermine Conjugates (Zip Nucleic Acids): A Convenient Means of Finely Tuning Hybridization Temperatures*. *Journal of the American Chemical Society*, 2008. **130**(40): p. 13500-13505.
485. Paris, C.m., et al., *Conjugating phosphospermines to siRNAs for improved stability in serum, intracellular delivery and RNAi-Mediated gene silencing*. *Molecular Pharmaceutics*, 2012. **9**(12): p. 3464-3475.
486. Nothisen, M., et al., *Cationic siRNAs provide carrier-free gene silencing in animal cells*. *Journal of the American Chemical Society*, 2009. **131**(49): p. 17730-17731.
487. Prakash, T., et al., *Synthesis of site-specific oligonucleotide-polyamine conjugates*. *Bioorganic & Medicinal Chemistry Letters*, 1994. **4**(14): p. 1733-1738.
488. Brzezinska, J., et al., *Polyaminooligonucleotide: NMR structure of duplex DNA containing a nucleoside with spermine residue, N-[4, 9, 13-triazatridecan-1-yl]-2'-deoxycytidine*. *Biochimica et Biophysica Acta (BBA)-General Subjects*, 2014. **1840**(3): p. 1163-1170.
489. Domingo, O., et al., *Intermolecular 'cross-torque': the N4-cytosine propargyl residue is rotated to the 'CH'-edge as a result of Watson–Crick interaction*. *Nucleic Acids Research*, 2015. **43**(11): p. 5275-5283.
490. Lou, C., et al., *Oligonucleotides Containing Aminated 2'-Amino-LNA Nucleotides: Synthesis and Strong Binding to Complementary DNA and RNA*. *Bioconjugate Chemistry*, 2017. **28**(4): p. 1214-1220.
491. Godzina, P., K. Adrych-Rozek, and W.T. Markiewicz, *Synthetic oligonucleotide combinatorial libraries. 3. Synthesis of polyamevonucleosides*. *Nucleosides and Nucleotides*, 1999. **18**(11-12): p. 2397-2414.
492. Markiewicz, W.T., P. Godzina, and M. Markiewicz, *Synthesis of polyaminooligonucleotides and their combinatorial libraries*. *Nucleosides & Nucleotides*, 1999. **18**(6-7): p. 1449-1454.
493. Potier, P., A. Abdennaji, and J.P. Behr, *Synthesis and Hybridization Properties of Oligonucleotides Containing Polyamines at the C-2 Position of Purines: A Pre-synthetic Approach for the Incorporation of Spermine into Oligodeoxynucleotides Containing 2-(4, 9, 13-Triazatridecyl)-2'-deoxyguanosine*. *Chemistry—A European Journal*, 2000. **6**(22): p. 4188-4194.
494. Potier, P., et al., *Synthesis of oligonucleotides bearing polyamine groups for recognition of DNA sequences*. *Nucleosides & Nucleotides*, 1999. **18**(6-7): p. 1467-1468.
495. Schmid, N. and J.-P. Behr, *Recognition of DNA sequences by strand replacement with polyamino-oligonucleotides*. *Tetrahedron Letters*, 1995. **36**(9): p. 1447-1450.
496. Daigle, N.D., et al., *Molecular characterization of a human cation-Cl⁻ cotransporter (SLC12A8A, CCC9A) that promotes polyamine and amino acid transport*. *Journal of Cellular Physiology*, 2009. **220**(3): p. 680-689.
497. Pegg, A.E., *Polyamine metabolism and its importance in neoplastic growth and as a target for chemotherapy*. *Cancer Research*, 1988. **48**(4): p. 759-774.
498. Casero Jr, R.A. and L.J. Marton, *Targeting polyamine metabolism and function in cancer and other hyperproliferative diseases*. *Nature Reviews Drug Discovery*, 2007. **6**(5): p. 373.
499. Damiani, E. and H.M. Wallace, *Polyamines and Cancer. Polyamines: Methods and Protocols*, 2018. p. 469-488.
500. Phanstiel, O.t., N. Kaur, and J.-G. Delcros, *Structure-activity investigations of polyamine-anthracene conjugates and their uptake via the polyamine transporter*. *Amino Acids*, 2007. **33**(2): p. 305-313.
501. Li, M., et al., *Antitumor effects and preliminary systemic toxicity of ANISpm in vivo and in vitro*. *Anti-cancer Drugs*, 2013. **24**(1): p. 32-42.

502. Tomasi, S., et al., *Targeting the polyamine transport system with benzazepine-and azepine-polyamine conjugates*. Journal of Medicinal Chemistry, 2010. **53**(21): p. 7647-7663.
503. Vida, N., et al., *Polyamine conjugates of stigmasterol*. Steroids, 2012. **77**(12): p. 1212-1218.
504. Bailly, C., *Cell-targeted cytotoxics: a new generation of cytotoxic agents for cancer treatment*. Phytochemistry Reviews, 2014. **13**(1): p. 171-181.
505. Guminski, Y., et al., *Synthesis of conjugated spermine derivatives with 7-nitrobenzoxadiazole (NBD), rhodamine and bodipy as new fluorescent probes for the polyamine transport system*. Bioorganic & Medicinal Chemistry Letters, 2009. **19**(9): p. 2474-2477.
506. Kruczynski, A., et al., *Preclinical activity of F14512, designed to target tumors expressing an active polyamine transport system*. Investigational New Drugs, 2011. **29**(1): p. 9-21.
507. Annereau, J.-P., et al., *A fluorescent biomarker of the polyamine transport system to select patients with AML for F14512 treatment*. Leukemia Research, 2010. **34**(10): p. 1383-1389.
508. Kruczynski, A., et al., *F14512, a polyamine-vectorized anti-cancer drug, currently in clinical trials exhibits a marked preclinical anti-leukemic activity*. Leukemia, 2013. **27**: p. 2139.
509. Thibault, B., et al., *F14512, a polyamine-vectorized inhibitor of topoisomerase II, exhibits a marked anti-tumor activity in ovarian cancer*. Cancer Letters, 2016. **370**(1): p. 10-18.
510. Leary, A., et al., *Phase I dose-escalation study of F14512, a polyamine-vectorized topoisomerase II inhibitor, in patients with platinum-refractory or resistant ovarian cancer*. Investigational New Drugs, 2019. **37**(4): p. 693-701.
511. Aouida, M., R. Poulin, and D. Ramotar, *The human carnitine transporter SLC22A16 mediates high affinity uptake of the anticancer polyamine analogue bleomycin-A5*. Journal of Biological Chemistry, 2010. **285**(9): p. 6275-6284.
512. Enomoto, A., et al., *Molecular Identification of a Novel Carnitine Transporter Specific to Human Testis: INSIGHTS INTO THE MECHANISM OF CARNITINE RECOGNITION*. Journal of Biological Chemistry, 2002. **277**(39): p. 36262-36271.
513. Okabe, M., et al., *Characterization of the organic cation transporter SLC22A16: A doxorubicin importer*. Biochemical and Biophysical Research Communications, 2005. **333**(3): p. 754-762.
514. Macmillan, A.M. and G.L. Verdine, *Engineering tethered DNA molecules by the convertible nucleoside approach*. Tetrahedron, 1991. **47**(14): p. 2603-2616.
515. MacMillan, A.M. and G.L. Verdine, *Synthesis of functionally tethered oligodeoxynucleotides by the convertible nucleoside approach*. The Journal of Organic Chemistry, 1990. **55**(24): p. 5931-5933.
516. Allerson, C.R., S.L. Chen, and G.L. Verdine, *A Chemical Method for Site-Specific Modification of RNA: The Convertible Nucleoside Approach*. Journal of the American Chemical Society, 1997. **119**(32): p. 7423-7433.
517. Diaz, A.R., R. Eritja, and R.G. Garcia, *Synthesis of Oligodeoxynucleotides Containing 2-Substituted Guanine Derivatives Using 2-Fluoro-2'-Deoxyinosine as Common Nucleoside Precursor*. Nucleosides and Nucleotides, 1997. **16**(10-11): p. 2035-2051.
518. Guennewig, B.S., Moritz; Menzi, Mirjam; Dogar, Afzal M; Hall, Jonathan, *Properties of N4-Methylated Cytidines in miRNA Mimics*. Nucleic Acid Therapeutics, 2012. **22**(2): p. 109-116.
519. Petri, S., et al., *Increased siRNA duplex stability correlates with reduced off-target and elevated on-target effects*. RNA, 2011. **17**(4): p. 737-749.
520. Kanavarioti, A., E.E. Baird, and P.J. Smith, *Use of phosphoimidazolide-activated guanosine to investigate the nucleophilicity of spermine and spermidine*. The Journal of Organic Chemistry, 1995. **60**(15): p. 4873-4883.

521. Kanavarioti, A., et al., *Large steric effect in the substitution reaction of amines with phosphoimidazolid-activated nucleosides*. The Journal of Organic Chemistry, 1995. **60**(3): p. 632-637.
522. Krakowiak, K.E. and J. Bradshaw, *Selective protection of the primary amine functions of linear tetraamines using the trityl group*. Synthetic Communications, 1998. **28**(18): p. 3451-3459.
523. Yamada, T., et al., *Versatile site-specific conjugation of small molecules to siRNA using click chemistry*. The Journal of organic chemistry, 2011. **76**(5): p. 1198-1211.
524. Andrews, P.W., *Human teratocarcinomas*. Biochimica et Biophysica Acta (BBA) - Reviews on Cancer, 1988. **948**(1): p. 17-36.
525. Ferrari, A., et al., *Immature human NT2 cells grafted into mouse brain differentiate into neuronal and glial cell types*. FEBS Letters, 2000. **486**(2): p. 121-125.
526. proteinatlas. [accessed on 23.09.2019]; Available from: <https://www.proteinatlas.org/ENSG00000187772-LIN28B/cell#rna>.
527. Lightfoot, H.L., et al., *Control of the polyamine biosynthesis pathway by G2-quadruplexes*. eLife, 2018. **7**: p. e36362.
528. Behr, J.-P., *Synthetic Gene Transfer Vectors II: Back to the Future*. Accounts of Chemical Research, 2012. **45**(7): p. 980-984.
529. Broughton, J.P. and A.E. Pasquinelli, *A tale of two sequences: microRNA-target chimeric reads*. Genetics Selection Evolution, 2016. **48**(1): p. 31.
530. Lewis, B.P., C.B. Burge, and D.P. Bartel, *Conserved seed pairing, often flanked by adenosines, indicates that thousands of human genes are microRNA targets*. Cell, 2005. **120**(1): p. 15-20.
531. Lewis, B.P., et al., *Prediction of mammalian microRNA targets*. Cell, 2003. **115**(7): p. 787-798.
532. Steinkraus, B.R., M. Toegel, and T.A. Fulga, *Tiny giants of gene regulation: experimental strategies for microRNA functional studies*. Wiley Interdisciplinary Reviews: Developmental Biology, 2016. **5**(3): p. 311-362.
533. Lee, F.C.Y. and J. Ule, *Advances in CLIP Technologies for Studies of Protein-RNA Interactions*. Molecular Cell, 2018. **69**(3): p. 354-369.
534. Chi, S.W., et al., *Argonaute HITS-CLIP decodes microRNA-mRNA interaction maps*. Nature, 2009. **460**: p. 479.
535. Ascano, M., et al., *Identification of RNA-protein interaction networks using PAR-CLIP*. Wiley Interdisciplinary Reviews: RNA, 2012. **3**(2): p. 159-177.
536. Hafner, M., et al., *Transcriptome-wide identification of RNA-binding protein and microRNA target sites by PAR-CLIP*. Cell, 2010. **141**(1): p. 129-141.
537. Hafner, M., et al., *PAR-CLIP-a method to identify transcriptome-wide the binding sites of RNA binding proteins*. JoVE (Journal of Visualized Experiments), 2010(41): p. e2034.
538. Hafner, M., et al., *Genome-wide identification of miRNA targets by PAR-CLIP*. Methods, 2012. **58**(2): p. 94-105.
539. Imig, J., et al., *miR-CLIP capture of a miRNA targetome uncovers a lincRNA H19-miR-106a interaction*. Nature Chemical Biology, 2015. **11**(2): p. 107.
540. Kudla, G., et al., *Cross-linking, ligation, and sequencing of hybrids reveals RNA-RNA interactions in yeast*. Proceedings of the National Academy of Sciences, 2011. **108**(24): p. 10010-10015.
541. Grosswendt, S., et al., *Unambiguous identification of miRNA: target site interactions by different types of ligation reactions*. Molecular cell, 2014. **54**(6): p. 1042-1054.
542. Filipowicz, W. and A.J. Shatkin, *Origin of splice junction phosphate in tRNAs processed by HeLa cell extract*. Cell, 1983. **32**(2): p. 547-557.
543. Moore, M.J., et al., *miRNA-target chimeras reveal miRNA 3'-end pairing as a major determinant of Argonaute target specificity*. Nature Communications, 2015. **6**: p. 8864.
544. Popow, J., et al., *HSPC117 Is the Essential Subunit of a Human tRNA Splicing Ligase Complex*. Science, 2011. **331**(6018): p. 760-764.

545. Popow, J., A. Schleiffer, and J. Martinez, *Diversity and roles of (t)RNA ligases*. Cellular and Molecular Life Sciences, 2012. **69**(16): p. 2657-2670.
546. Desai, K.K., et al., *Structures of the noncanonical RNA ligase RtcB reveal the mechanism of histidine guanylylation*. Biochemistry, 2013. **52**(15): p. 2518-2525.
547. Chakravarty, A.K. and S. Shuman, *The sequential 2', 3'-cyclic phosphodiesterase and 3'-phosphate/5'-OH ligation steps of the RtcB RNA splicing pathway are GTP-dependent*. Nucleic Acids Research, 2012. **40**(17): p. 8558-8567.
548. Chakravarty, A.K., et al., *RNA ligase RtcB splices 3'-phosphate and 5'-OH ends via covalent RtcB-(histidinyl)-GMP and polynucleotide-(3') pp (5') G intermediates*. Proceedings of the National Academy of Sciences, 2012. **109**(16): p. 6072-6077.
549. Maughan, W.P. and S. Shuman, *Distinct contributions of enzymic functional groups to the 2', 3'-cyclic phosphodiesterase, 3'-phosphate guanylylation, and 3'-ppG/5'-OH ligation steps of the Escherichia coli RtcB nucleic acid splicing pathway*. Journal of Bacteriology, 2016. **198**(8): p. 1294-1304.
550. Tanaka, N., et al., *Novel mechanism of RNA repair by RtcB via sequential 2', 3'-cyclic phosphodiesterase and 3'-Phosphate/5'-hydroxyl ligation reactions*. Journal of Biological Chemistry, 2011. **286**(50): p. 43134-43143.
551. Tanaka, N., B. Meineke, and S. Shuman, *RtcB, a novel RNA ligase, can catalyze tRNA splicing and HAC1 mRNA splicing in vivo*. Journal of Biological Chemistry, 2011. **286**(35): p. 30253-30257.
552. Tanaka, N. and S. Shuman, *RtcB is the RNA ligase component of an Escherichia coli RNA repair operon*. Journal of Biological Chemistry, 2011. **286**(10): p. 7727-7731.
553. Englert, M., et al., *Structural and mechanistic insights into guanylylation of RNA-splicing ligase RtcB joining RNA between 3'-terminal phosphate and 5'-OH*. Proceedings of the National Academy of Sciences, 2012. **109**(38): p. 15235-15240.
554. Nandakumar, J., et al., *RNA Repair: An Antidote to Cytotoxic Eukaryal RNA Damage*. Molecular Cell, 2008. **31**(2): p. 278-286.
555. Nandakumar, J., S. Shuman, and C.D. Lima, *RNA Ligase Structures Reveal the Basis for RNA Specificity and Conformational Changes that Drive Ligation Forward*. Cell, 2006. **127**(1): p. 71-84.
556. Schwer, B., et al., *Portability and fidelity of RNA-repair systems*. Proceedings of the National Academy of Sciences of the United States of America, 2004. **101**(9): p. 2788-2793.
557. Winter, J. and S. Diederichs, *Argonaute proteins regulate microRNA stability: Increased microRNA abundance by Argonaute proteins is due to microRNA stabilization*. RNA Biology, 2011. **8**(6): p. 1149-1157.
558. Usher, D. and A. McHale, *Nonenzymic joining of oligoadenylates on a polyuridylic acid template*. Science, 1976. **192**(4234): p. 53-54.
559. Buzayan, J.M., A. Hampel, and G. Bruening, *Nucleotide sequence and newly formed phosphodiester bond of spontaneously ligated satellite tobacco ringspot virus RNA*. Nucleic Acids Research, 1986. **14**(24): p. 9729-9743.
560. Sharmeen, L., M. Kuo, and J. Taylor, *Self-ligating RNA sequences on the antigenome of human hepatitis delta virus*. Journal of virology, 1989. **63**(3): p. 1428-1430.
561. Lutay, A., et al. *Nonenzymatic template-dependent ligation of 2', 3'-cyclic phosphate-containing oligonucleotides catalyzed by metal ions*. in *Doklady Biochemistry and Biophysics*. 2005.
562. Verlander, M., R. Lohrmann, and L. Orgel, *Catalysts for the self-polymerization of adenosine cyclic 2', 3'-phosphate*. Journal of Molecular Evolution, 1973. **2**(4): p. 303-316.
563. Uesugi, S. and M. Ikehara, *Polynucleotides. 41. Synthesis and template-directed polymerization of adenylyl (3'-5') adenosine cyclic 2', 3'-phosphate*. Biochemistry, 1977. **16**(3): p. 493-498.
564. Zhao, G., et al., *MicroRNA-34a suppresses cell proliferation by targeting LMTK3 in human breast cancer mcf-7 cell line*. DNA and cell biology, 2013. **32**(12): p. 699-707.
565. Jacob, J., et al., *LMTK3 escapes tumour suppressor miRNAs via sequestration of DDX5*. Cancer letters, 2016. **372**(1): p. 137-146.

566. Honda, S., K. Morichika, and Y. Kirino, *Selective amplification and sequencing of cyclic phosphate-containing RNAs by the cP-RNA-seq method*. Nature Protocols, 2016. **11**: p. 476.
567. Zhu, D., et al., *MicroRNA-17/20a/106a modulate macrophage inflammatory responses through targeting signal-regulatory protein α* . Journal of Allergy and Clinical Immunology, 2013. **132**(2): p. 426-436. e8.
568. Das, U. and S. Shuman, *Mechanism of RNA 2',3'-cyclic phosphate end healing by T4 polynucleotide kinase-phosphatase*. Nucleic Acids Research, 2012. **41**(1): p. 355-365.
569. Abe, N., H. Abe, and Y. Ito, *Dumbbell-Shaped Nanocircular RNAs for RNA Interference*. Journal of the American Chemical Society, 2007. **129**(49): p. 15108-15109.
570. Abe, N., H. Abe, and Y. Ito, *Synthesis of Dumbbell-Shaped Cyclic RNAs for RNA Interference*. Current Protocols in Nucleic Acid Chemistry, 2012. **48**(1): p. 16.4.1-16.4.11.
571. Abe, N., et al., *Synthesis, Structure, and Biological Activity of Dumbbell-Shaped Nanocircular RNAs for RNA Interference*. Bioconjugate Chemistry, 2011. **22**(10): p. 2082-2092.
572. Jiang, W., P. Samai, and L.A. Marraffini, *Degradation of phage transcripts by CRISPR-associated RNases enables type III CRISPR-Cas immunity*. Cell, 2016. **164**(4): p. 710-721.
573. Ceccaldi, R., B. Rondinelli, and A.D. D'Andrea, *Repair pathway choices and consequences at the double-strand break*. Trends in Cell Biology, 2016. **26**(1): p. 52-64.
574. Savić, N., et al., *In vitro Generation of CRISPR-Cas9 Complexes with Covalently Bound Repair Templates for Genome Editing in Mammalian Cells*. Bio-protocol, 2019. **9**(1): p. e3136.
575. Liu, T., et al., *Cycling Li-O₂ batteries via LiOH formation and decomposition*. Science, 2015. **350**(6260): p. 530-533.
576. Walder, B.J., et al., *One- and Two-Dimensional High-Resolution NMR from Flat Surfaces*. ACS Central Science, 2019. **5**(3): p. 515-523.
577. Kong, X., et al., *Mapping of Functional Groups in Metal-Organic Frameworks*. Science, 2013. **341**(6148): p. 882-885.
578. Pradère, U. and J. Hall, *Site-specific difunctionalization of structured RNAs yields probes for microRNA maturation*. Bioconjugate Chemistry, 2016. **27**(3): p. 681-687.
579. Pradère, U., et al., *Chemical Synthesis of Mono- and Bis-Labeled Pre-MicroRNAs*. Angewandte Chemie International Edition, 2013. **52**(46): p. 12028-12032.
580. Zagalak, J.A., et al., *Properties of short double-stranded RNAs carrying randomized base pairs: toward better controls for RNAi experiments*. RNA, 2015. **21**(12): p. 2132-2142.
581. Sarett, S.M., et al., *Lipophilic siRNA targets albumin in situ and promotes bioavailability, tumor penetration, and carrier-free gene silencing*. Proceedings of the National Academy of Sciences, 2017. **114**(32): p. E6490-E6497.
582. Hvam, M.L., et al., *Fatty Acid-Modified Gapmer Antisense Oligonucleotide and Serum Albumin Constructs for Pharmacokinetic Modulation*. Molecular Therapy, 2017. **25**(7): p. 1710-1717.
583. Er, J.C., et al., *Fluorescent Dye Cocktail for Multiplex Drug-Site Mapping on Human Serum Albumin*. ACS Combinatorial Science, 2013. **15**(9): p. 452-457.

Appendix

Appendix – Project 1

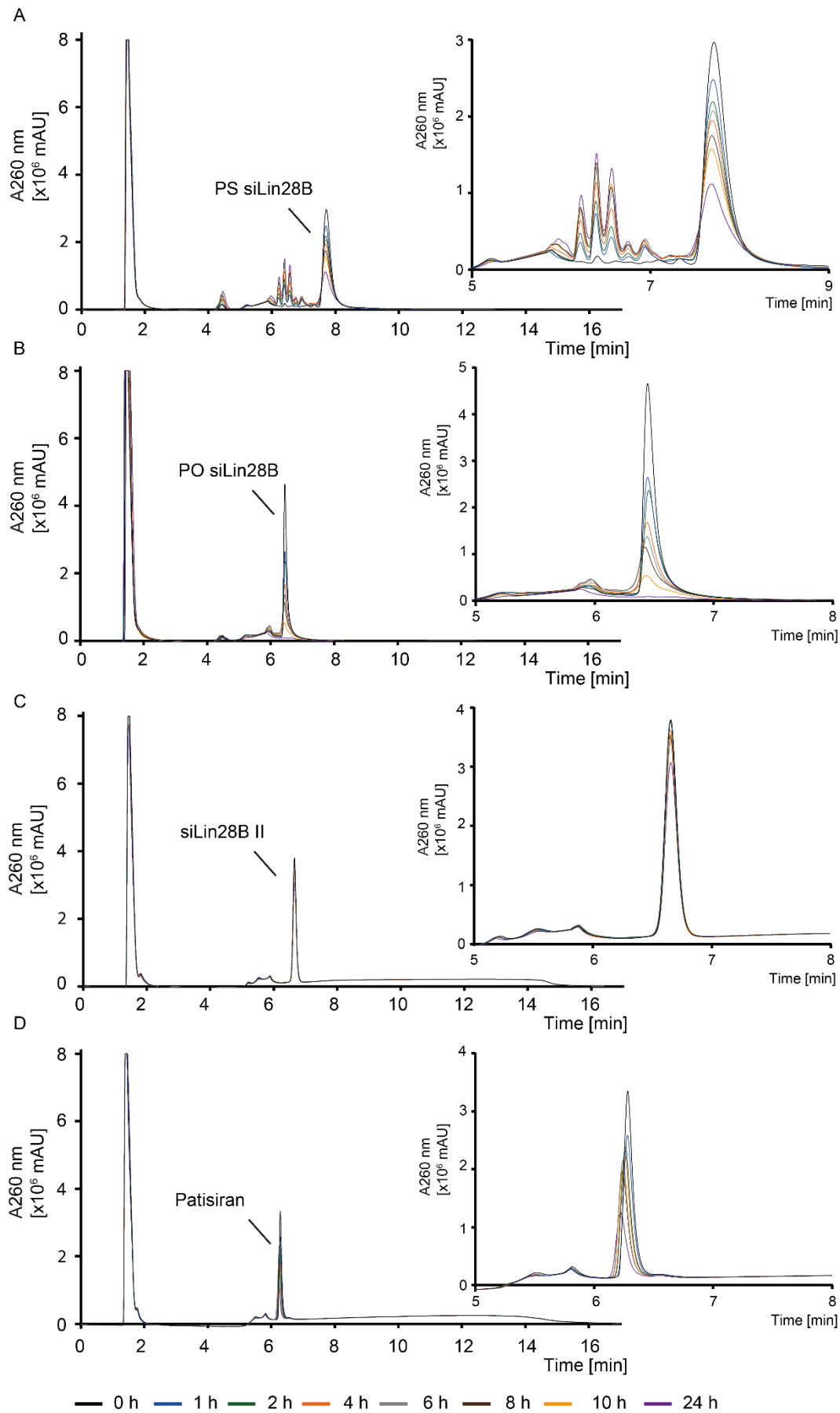
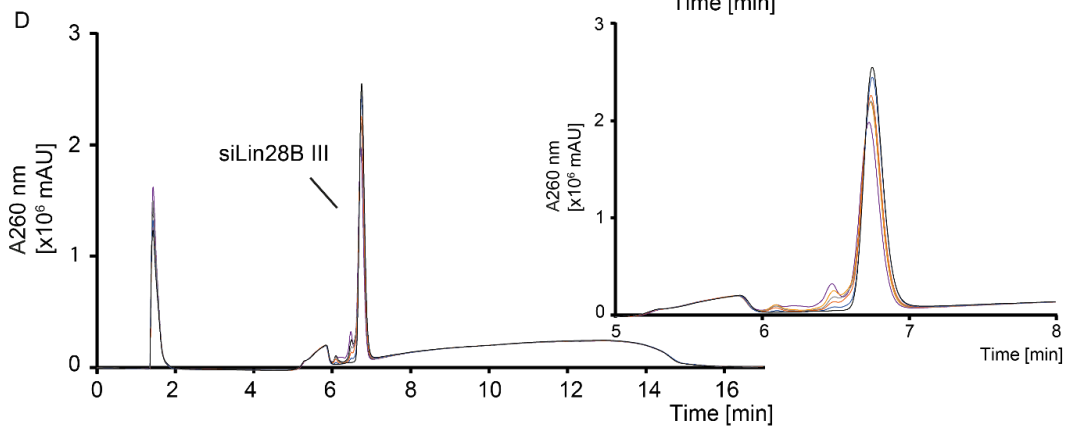
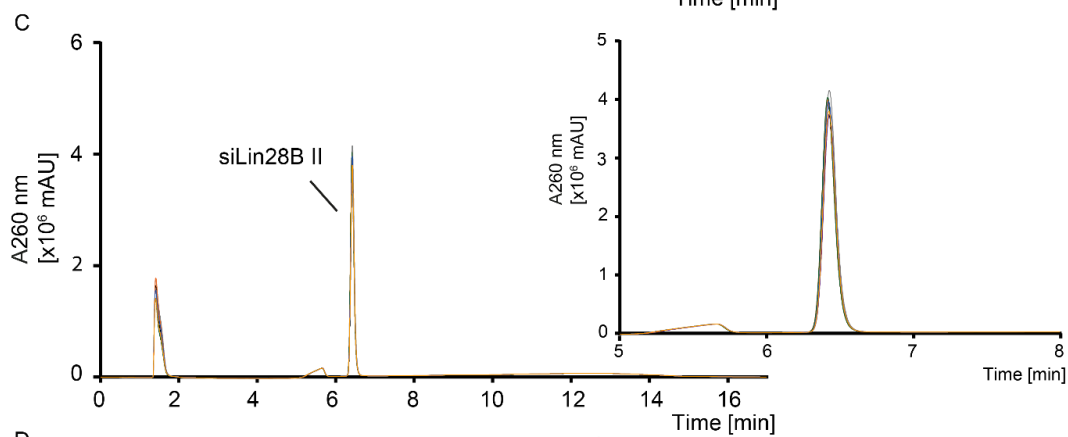
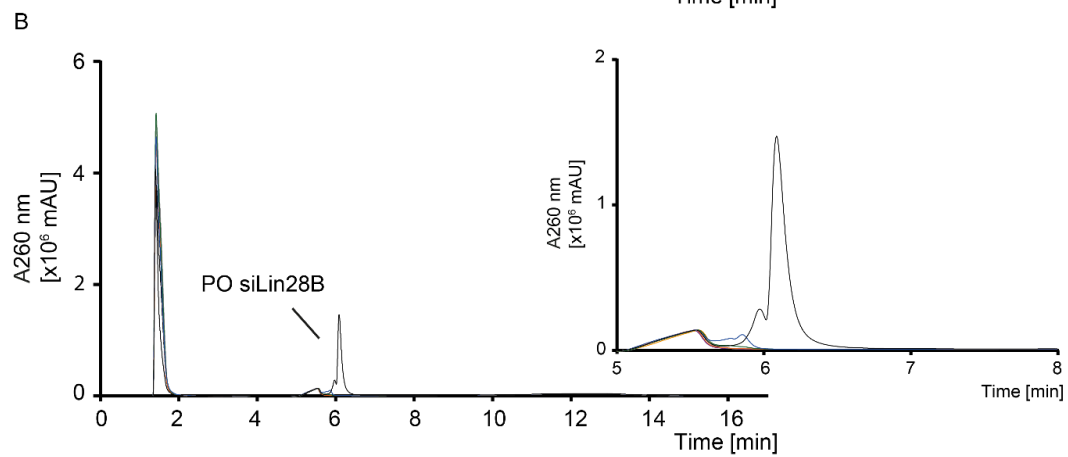
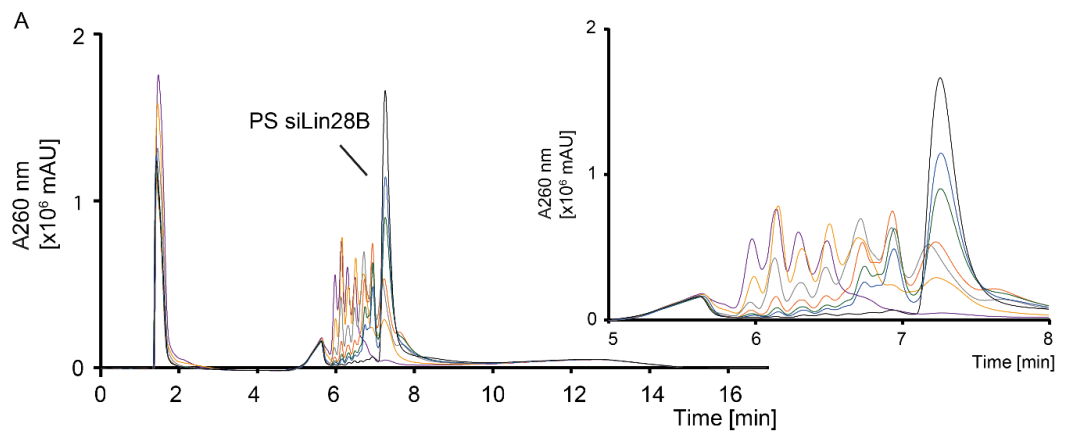


Figure 8. 1. Anion-exchange HPLC chromatograms from serum stability assays. A) PS siLin28B. B) PO siLin28B. C) siLin28B II. D) Patisiran



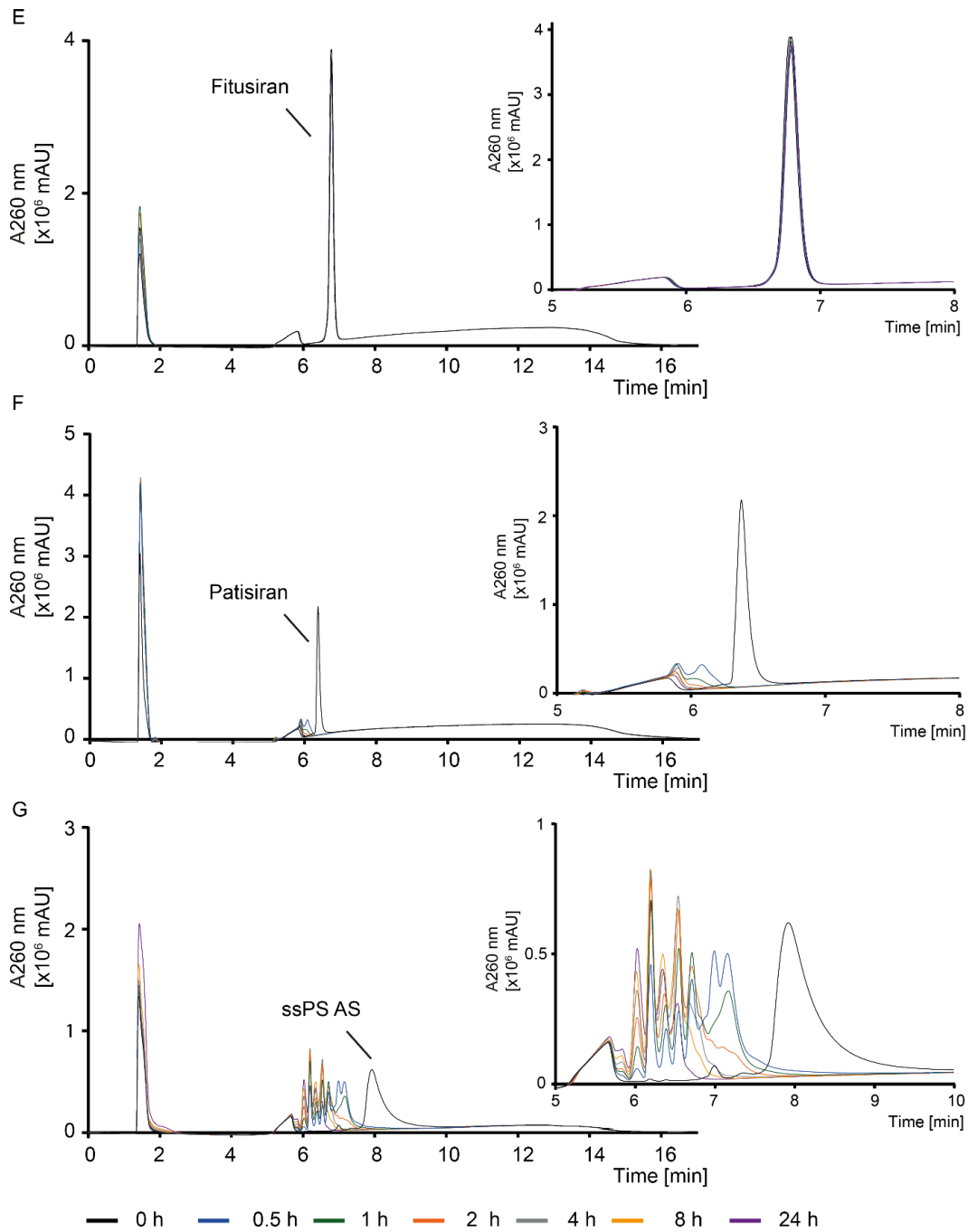
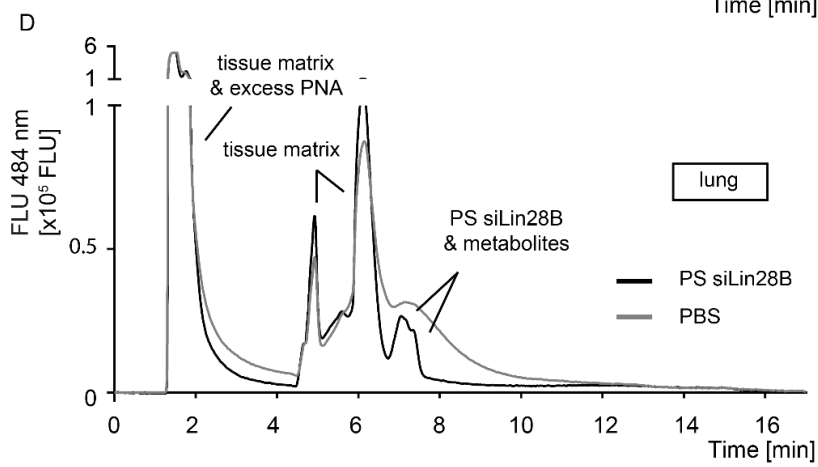
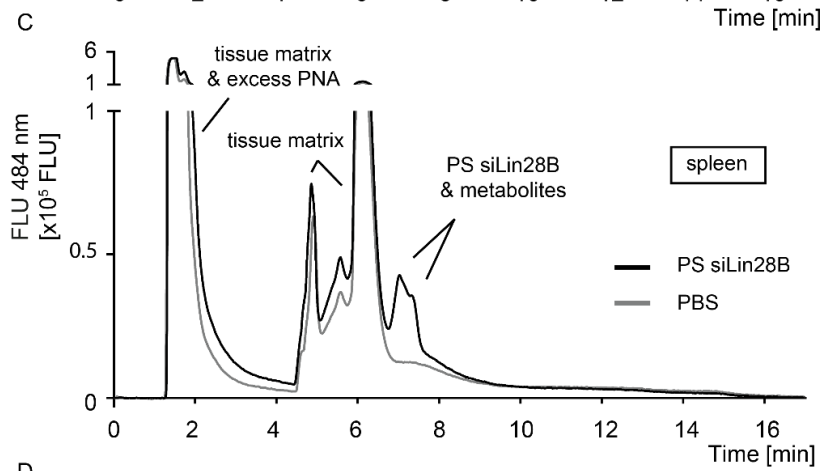
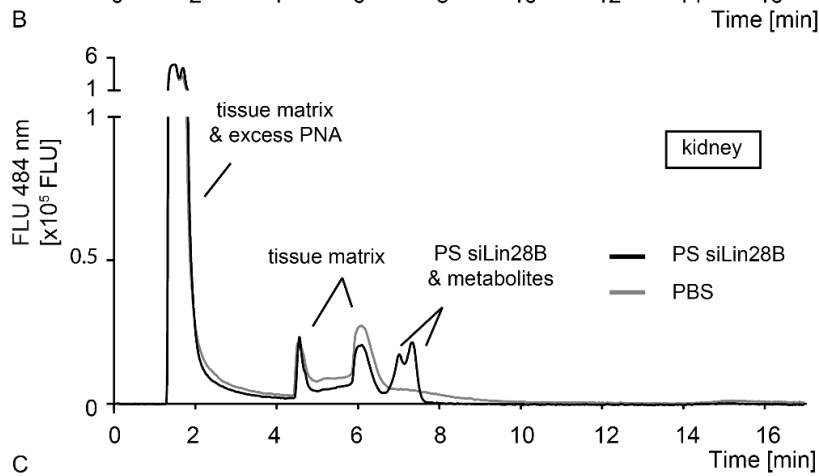
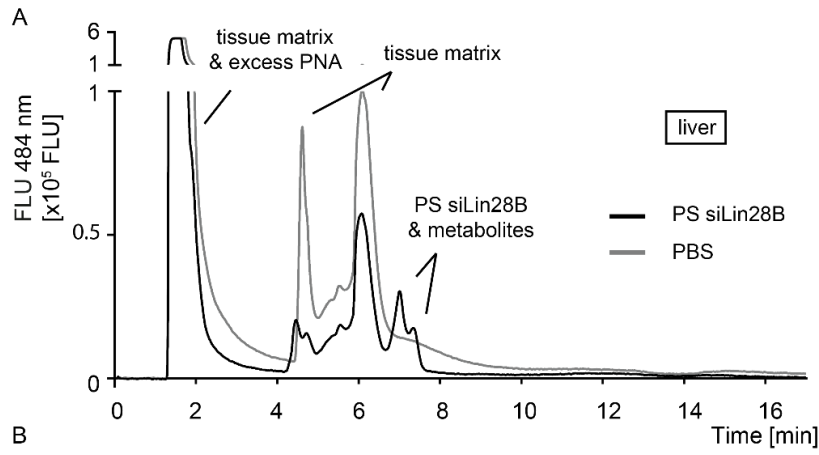


Figure 8. 2. Anion-exchange HPLC chromatograms from tritosome stability assays. A) PS siLin28B. B) PO siLin28B. C) siLin28B II. D) siLin28B III. E) Fitusiran. F) Patisiran. G) ssPS AS



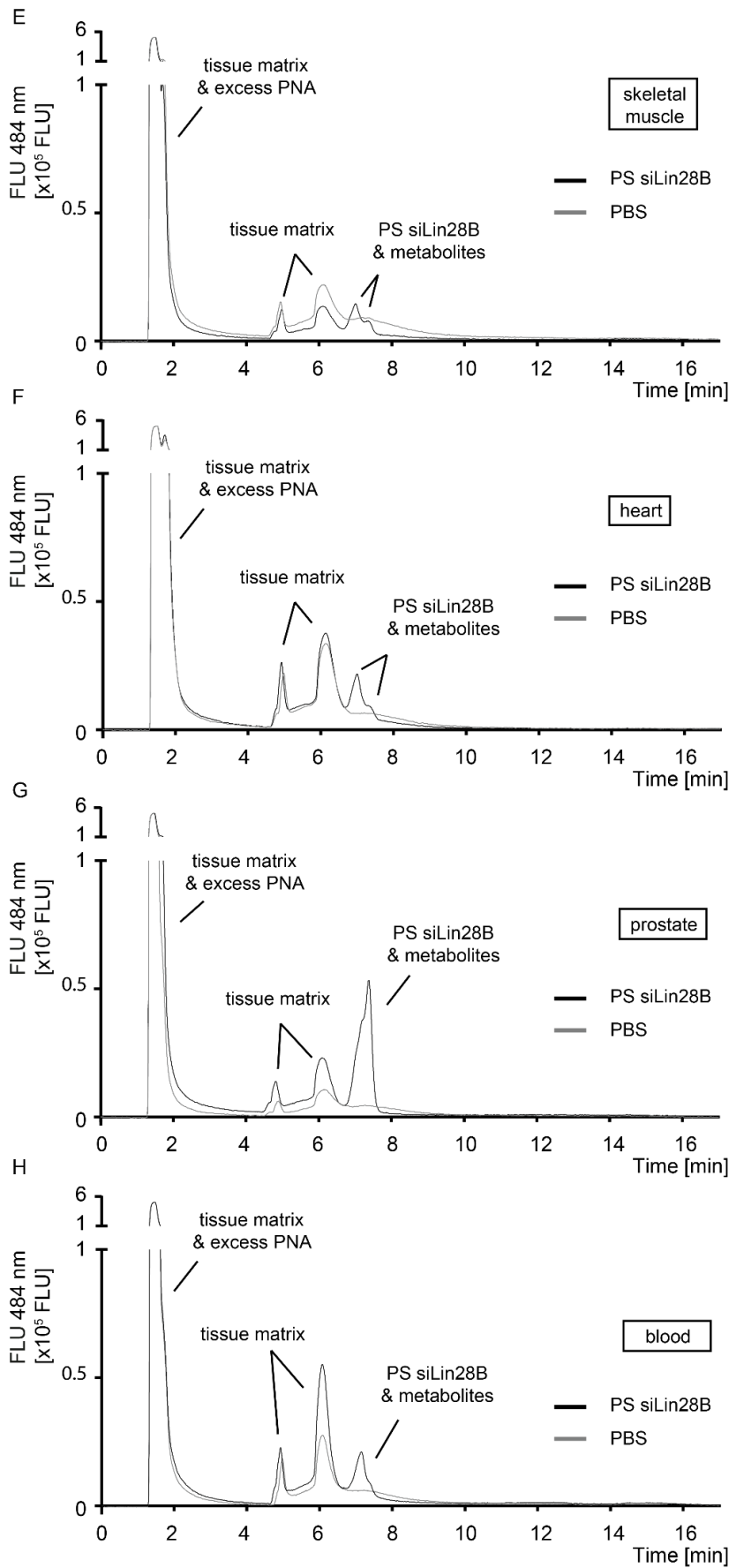


Figure 8. 3. Anion-exchange HPLC analysis (fluorescence trace) from biodistribution study. Overlays of tissues from a mouse that was injected with 50 mg/ kg PS siLin28B and a mouse that received PBS treatment. A) Liver. B) Kidney. C) Spleen. D) Lung. E) Skeletal muscle. F) Heart. G) Prostate. H) Blood

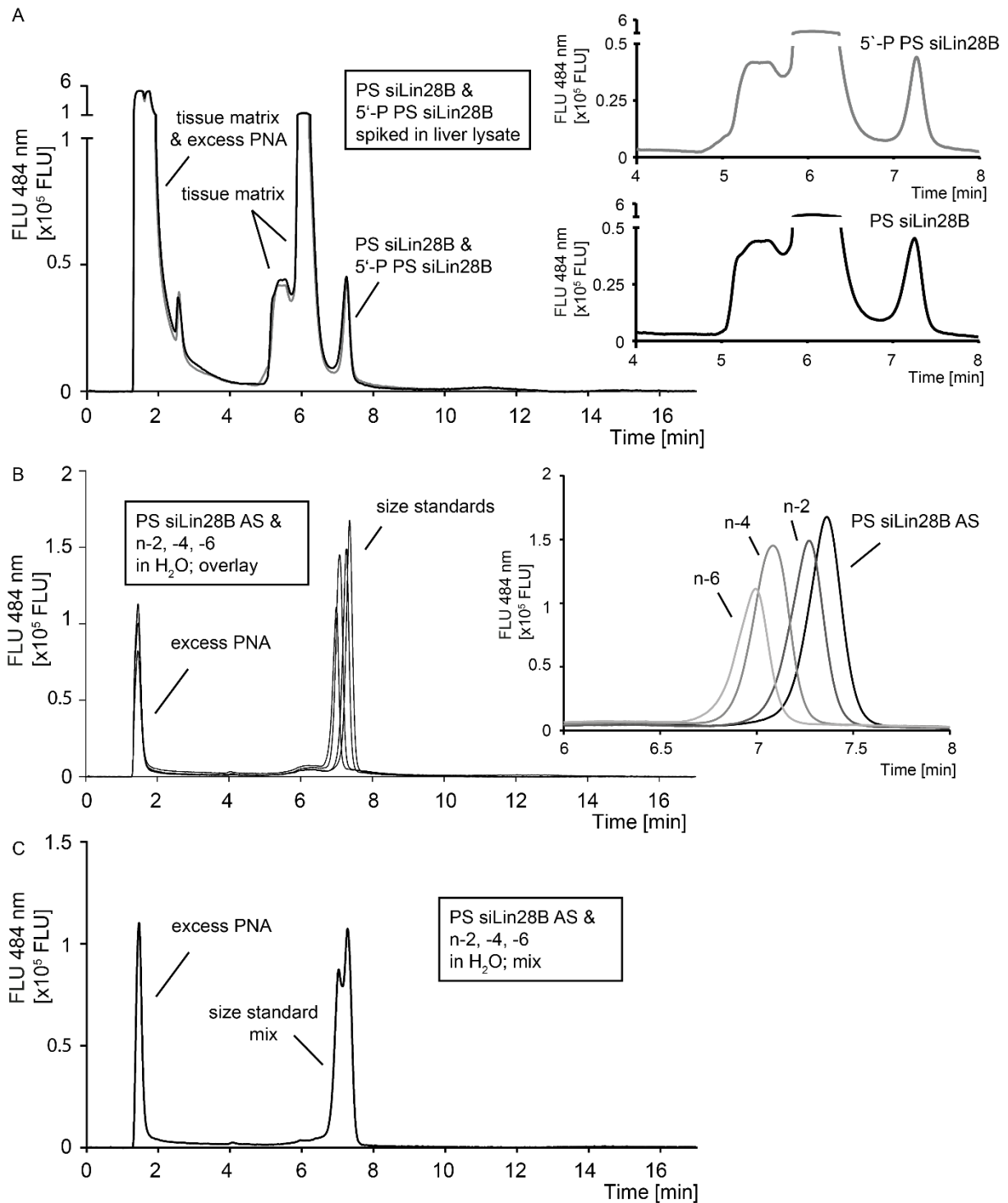


Figure 8. 4. Anion exchange HPLC (fluorescence trace) of PS siLin28B standards. A) Overlay of mouse liver lysate spiked with PS siLin28B or 5'-phosphorylated (AS-strand) PS siLin28B. B) Overlay of potential PS siLin28B AS metabolites in H₂O. PS siLin28B AS strands were truncated from the 3'-end. C) Mixture of truncated AS strands from B in H₂O.

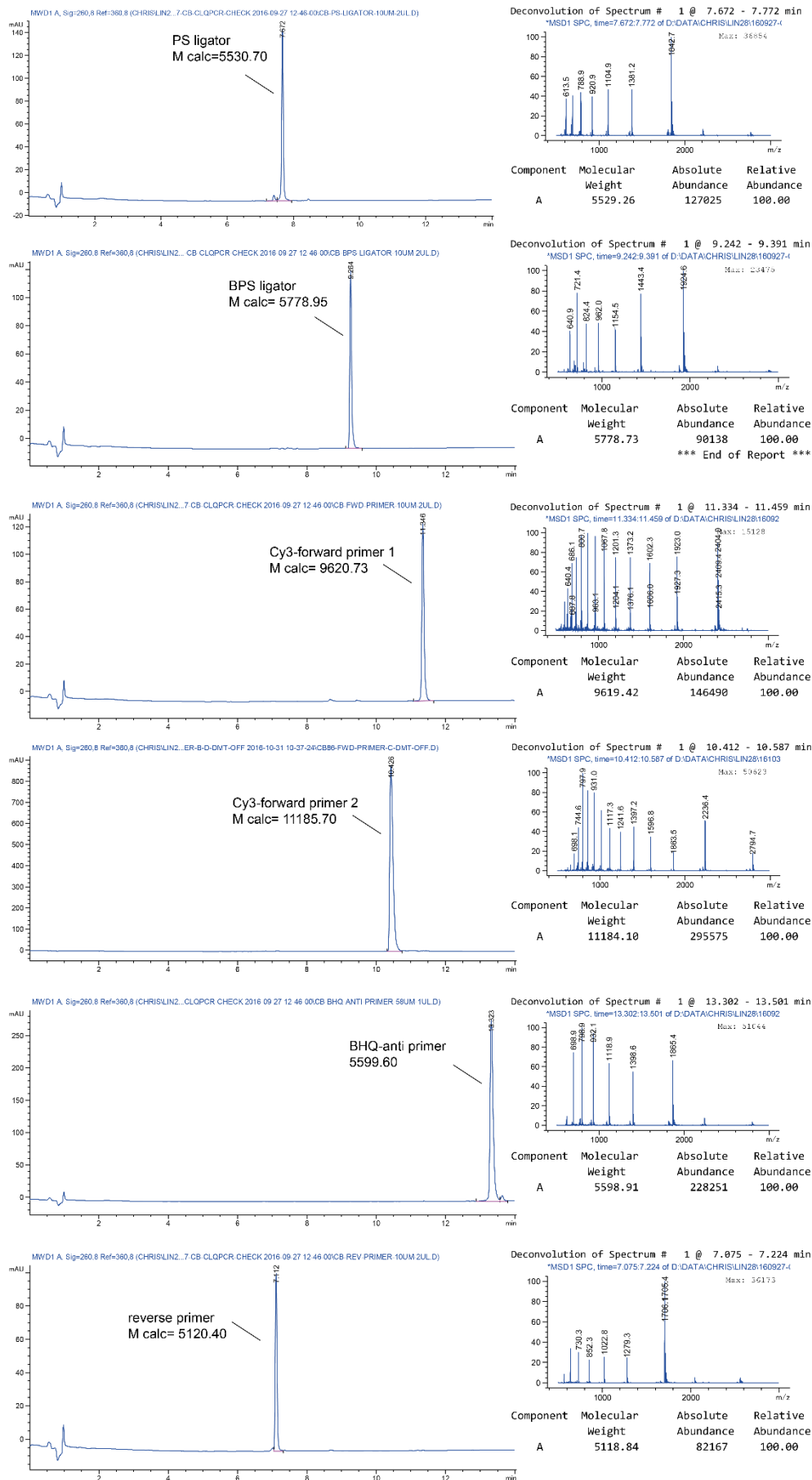


Figure 8. 5. LC-MS analysis of ligators and primers for CL-qPCR

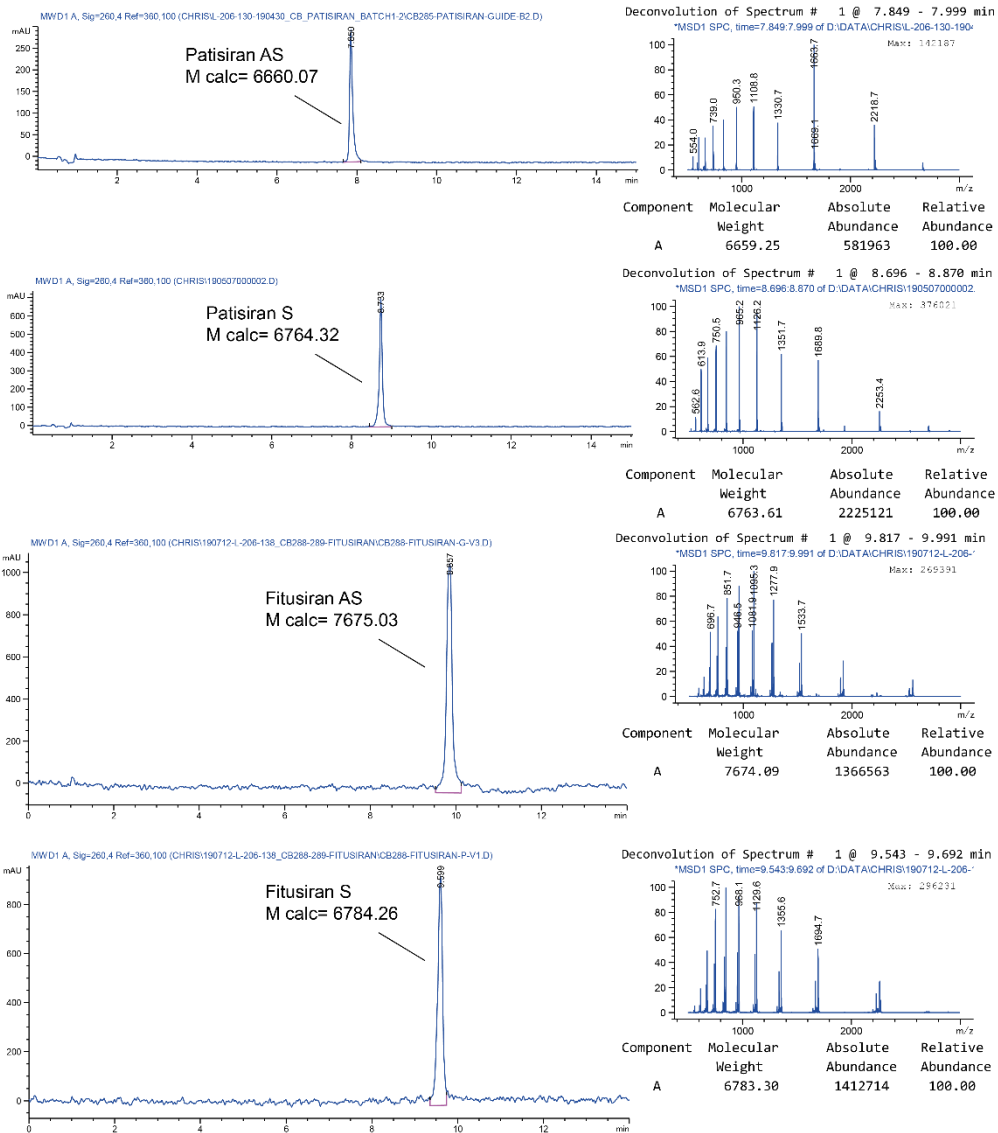


Figure 8. 6. LC-MS analysis of modified siRNAs for nuclease stability assays

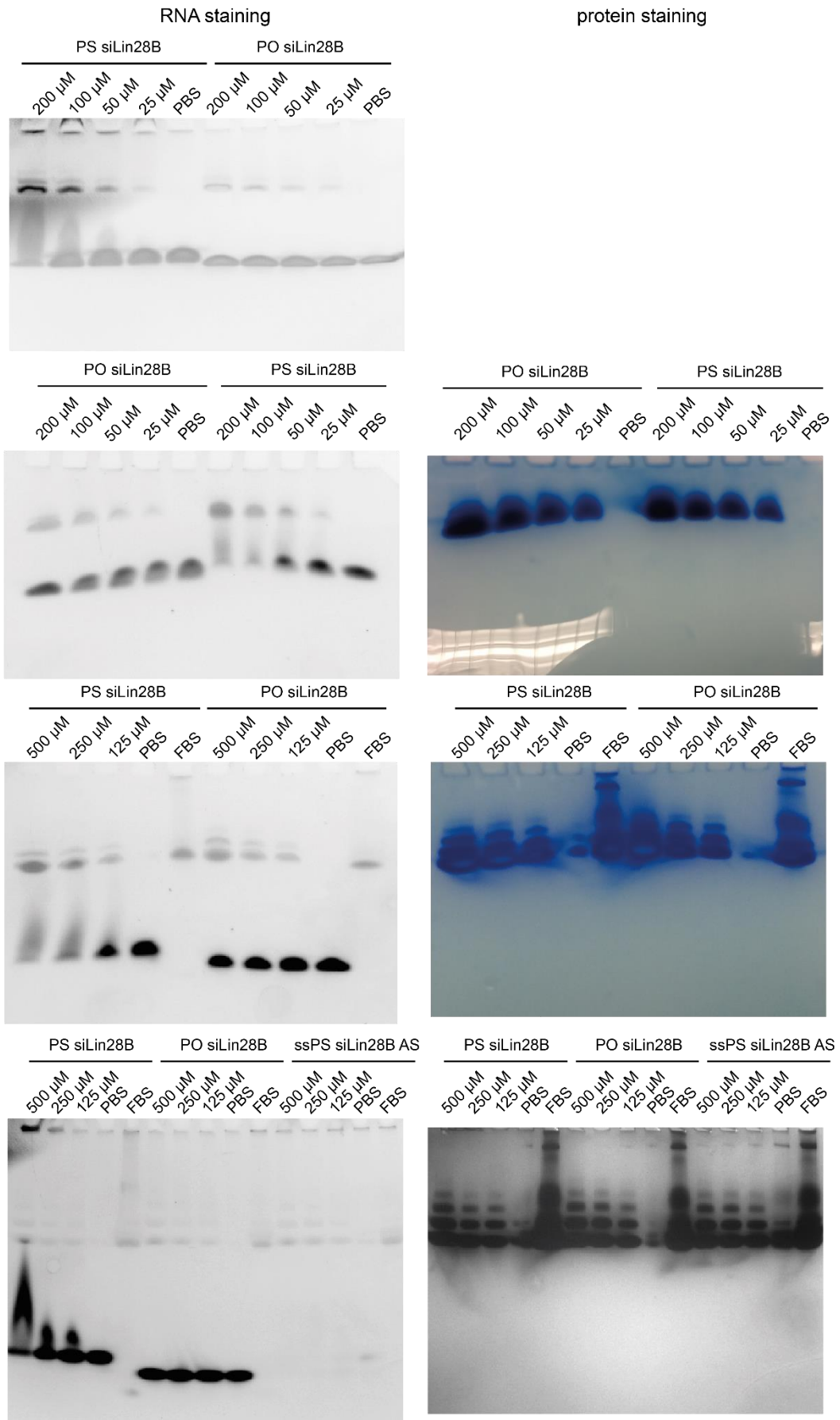
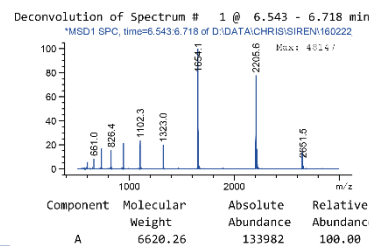
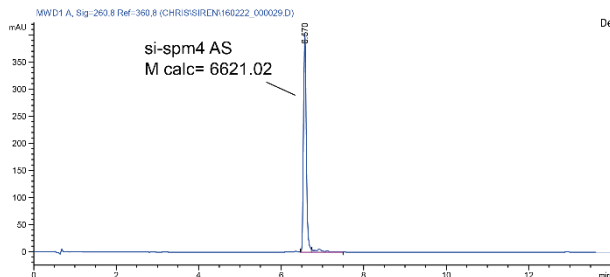
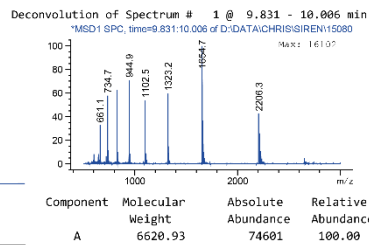
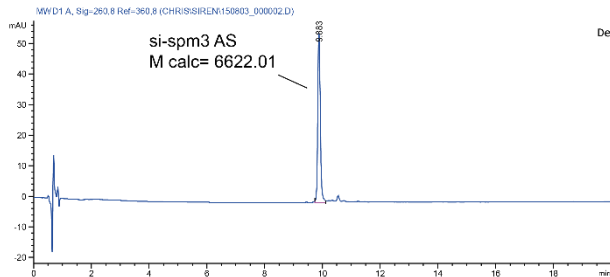
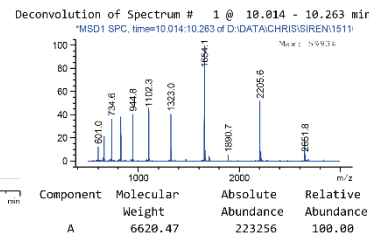
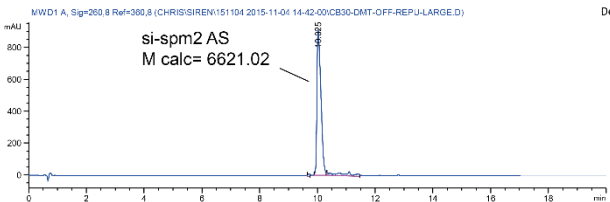
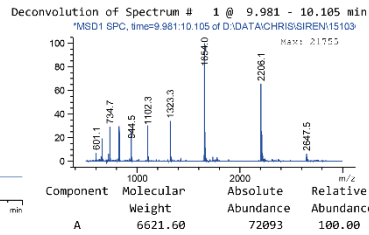
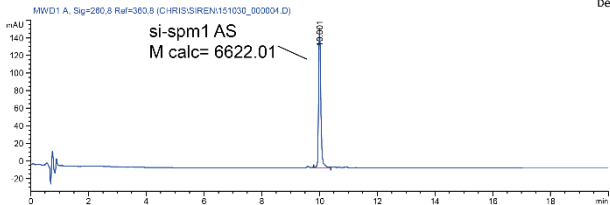
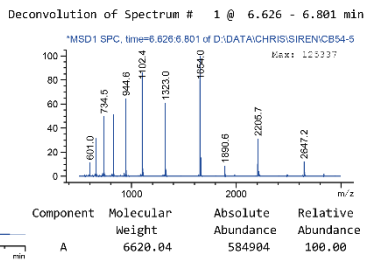
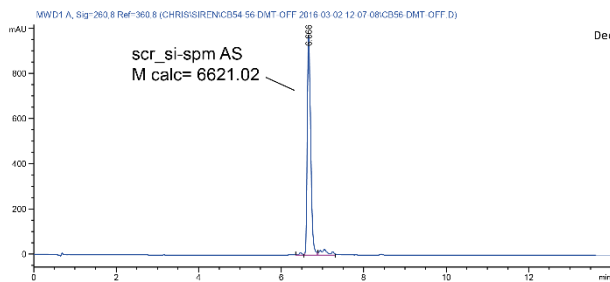
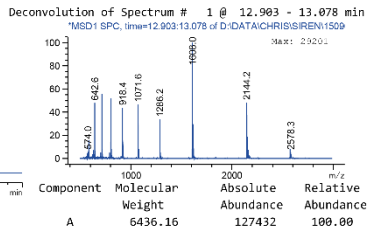
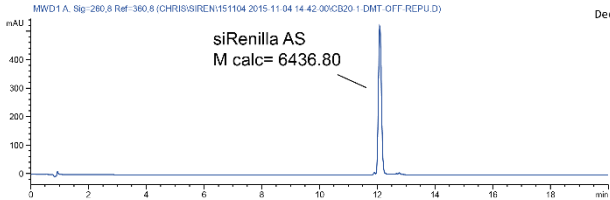
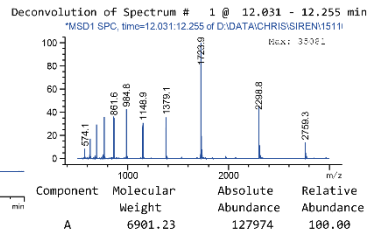
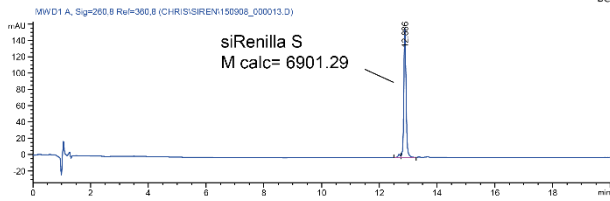


Figure 8. 7. Electrophoretic mobility shift assays to evaluate albumin binding of PS and PO siLin28B

Appendix – Project 2



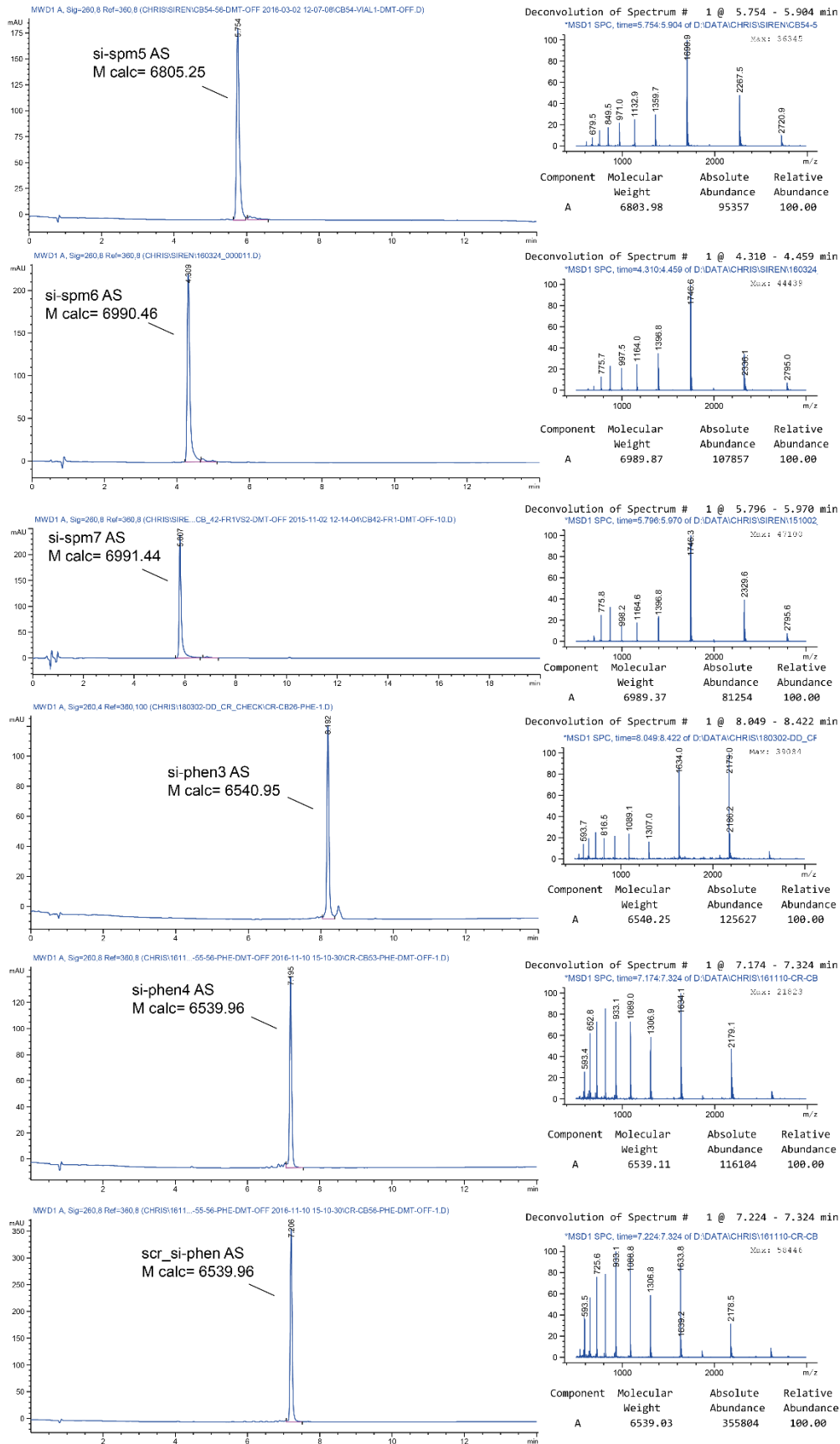


Figure 8. 8. LC-MS analysis of siRenilla-spermine and -phenethylamine conjugates

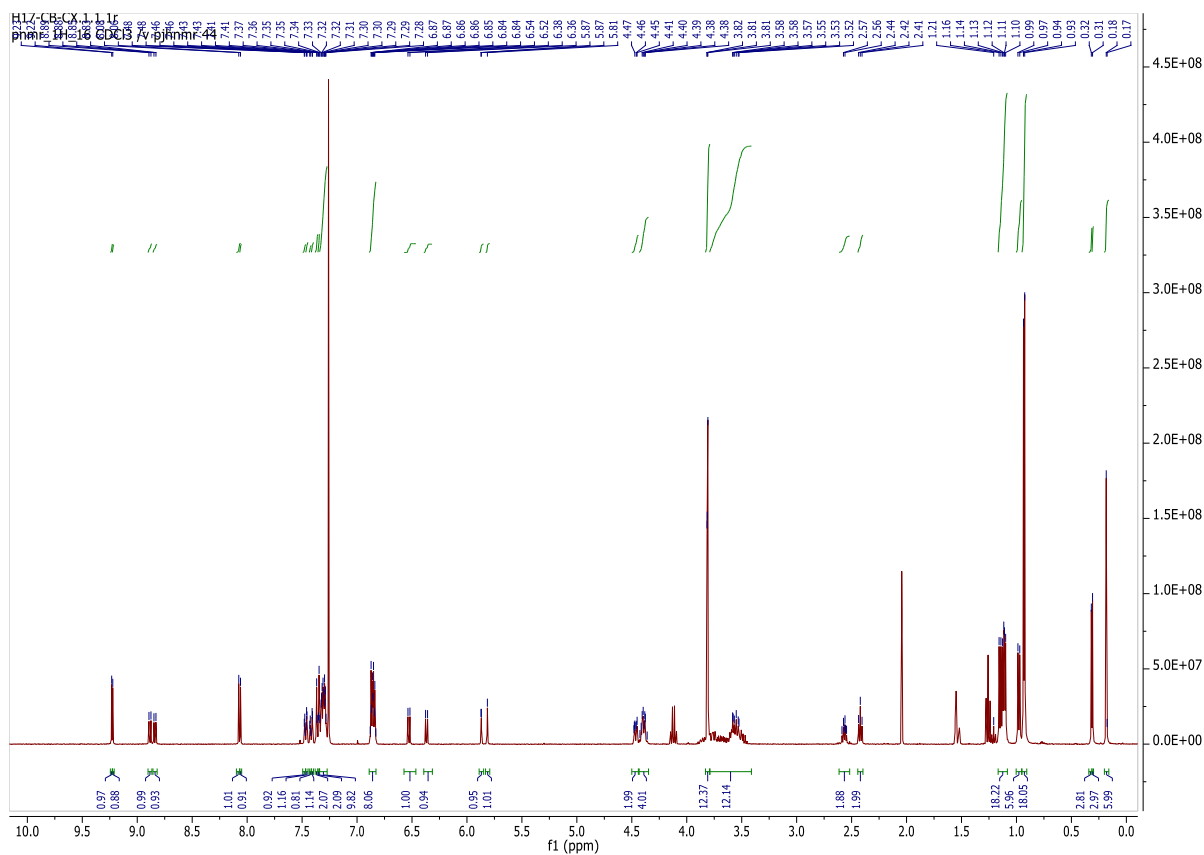


Figure 8. 9. ^1H NMR of O^4 -triazolyluridine-2'-O-TBDMS CED phosphoramidite

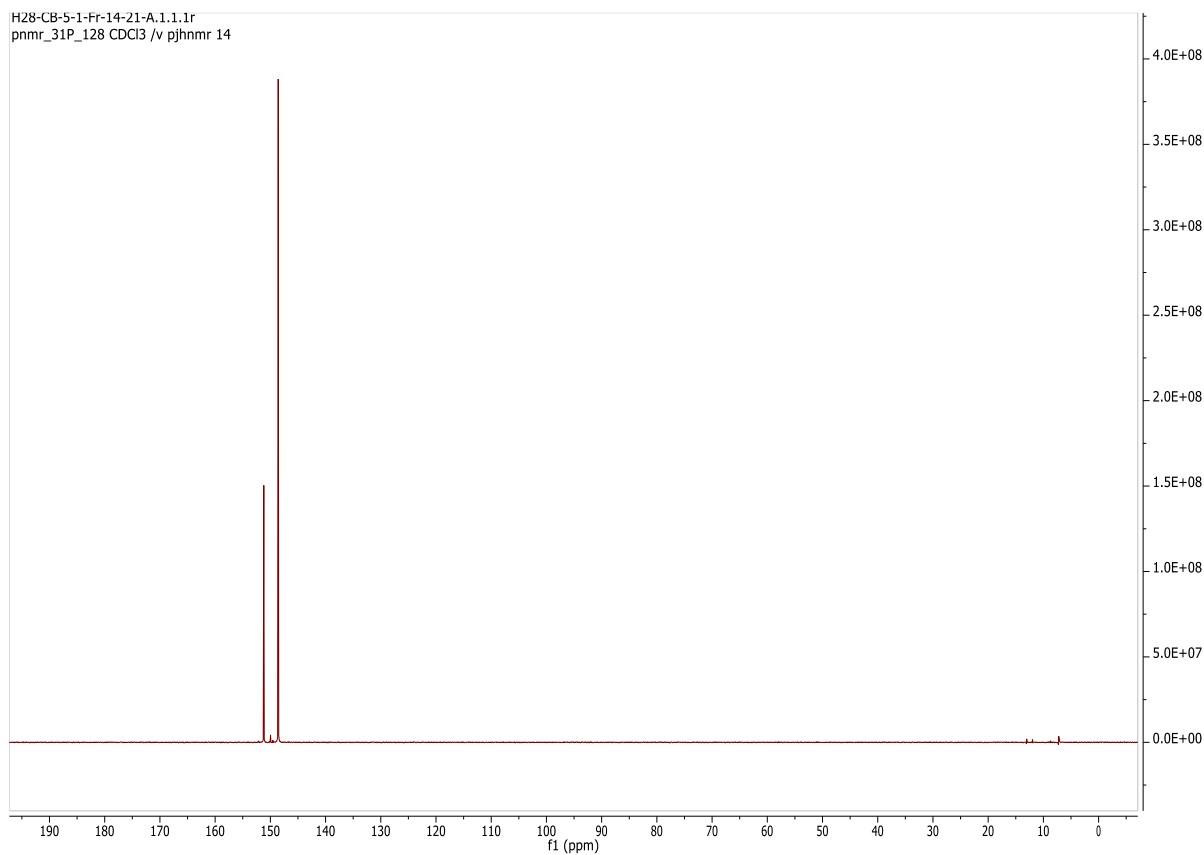


Figure 8. 10. ^{31}P NMR of O^4 -triazolyluridine-2'-O-TBDMS CED phosphoramidite

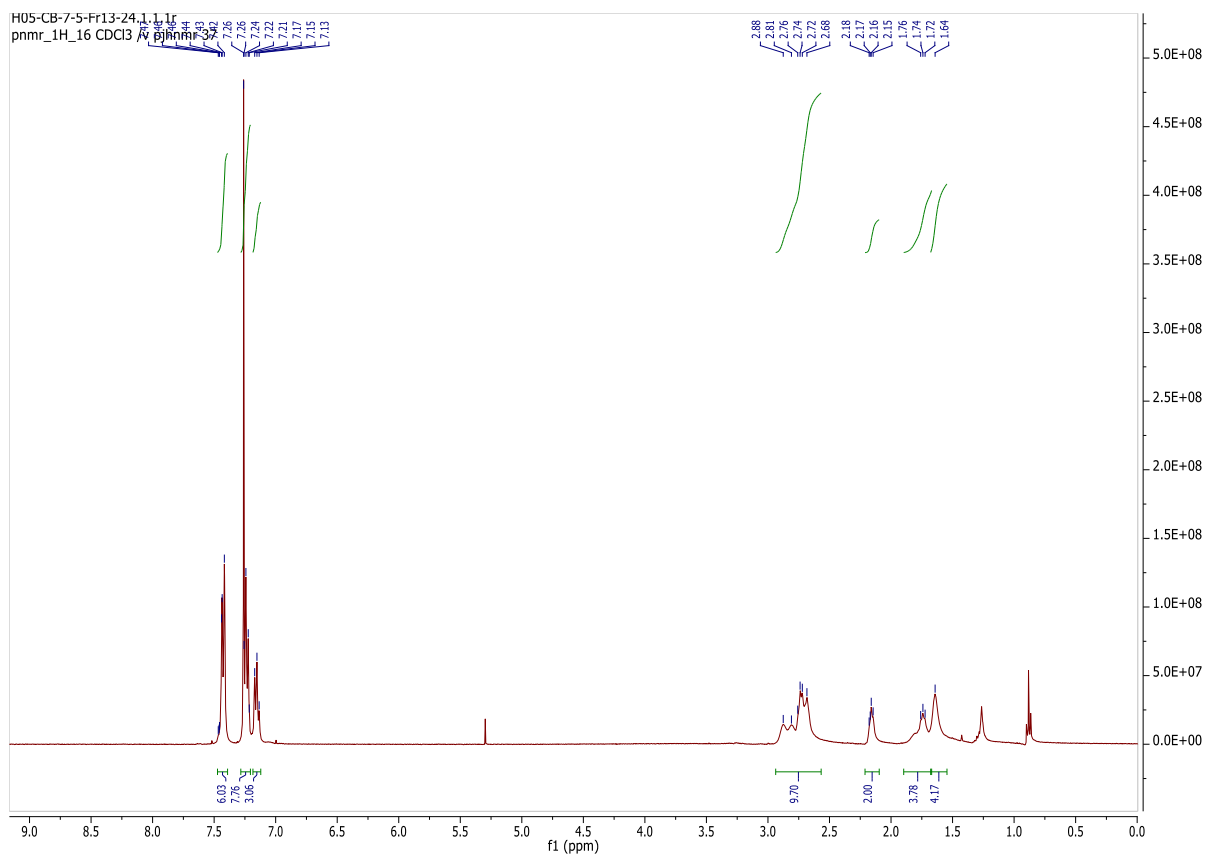


Figure 8. 11. ^1H NMR of N^1 -trityl spermine

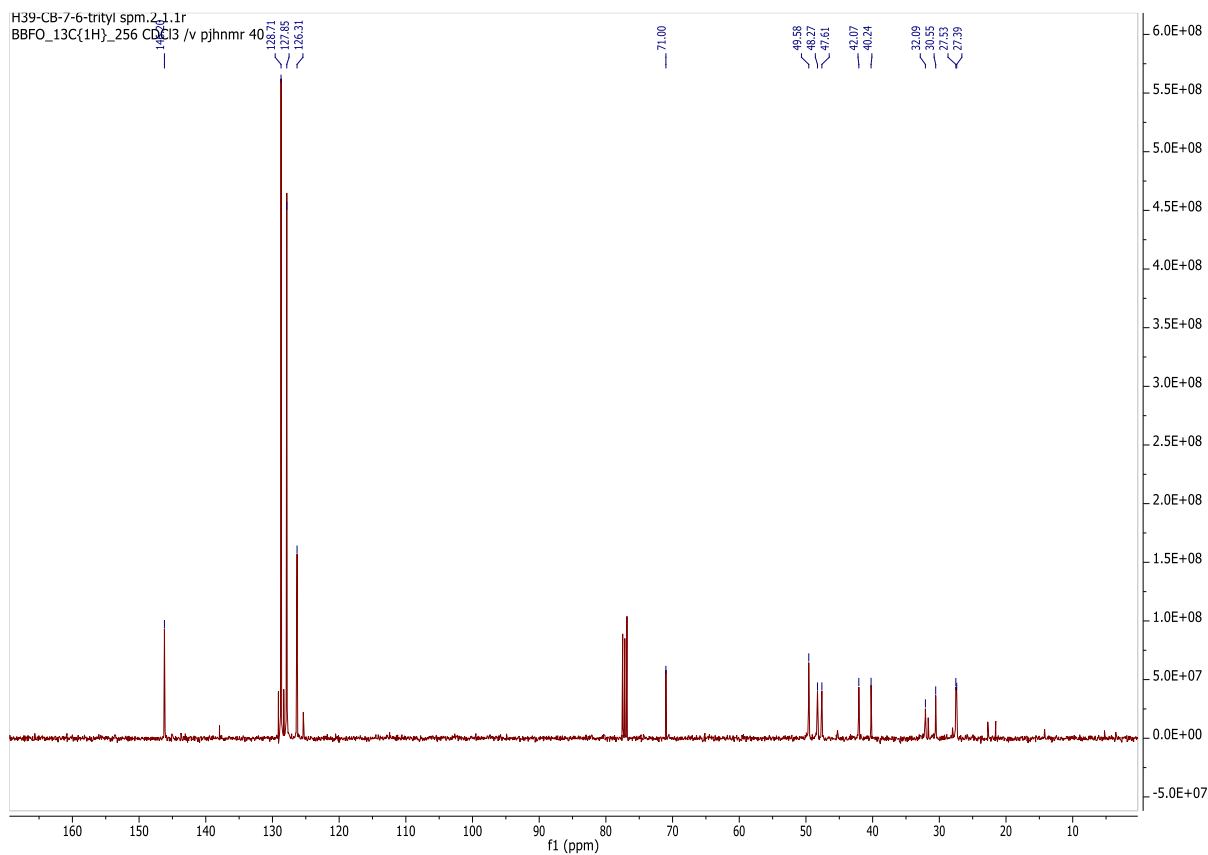


Figure 8. 12. ^{13}C NMR of N^1 -trityl spermine

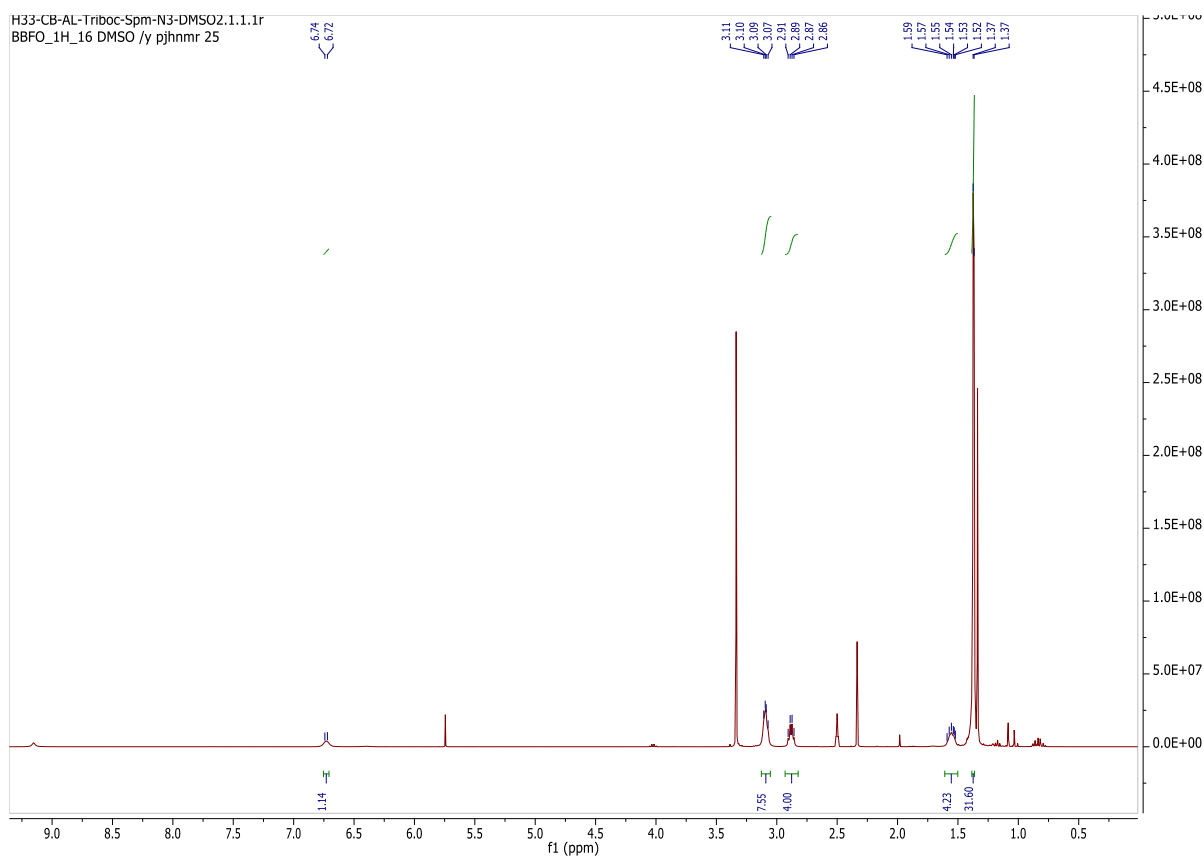


Figure 8. 13. ^1H NMR of N^2,N^β,N^4 -tri(tert-butoxycarbonyl)spermine azide

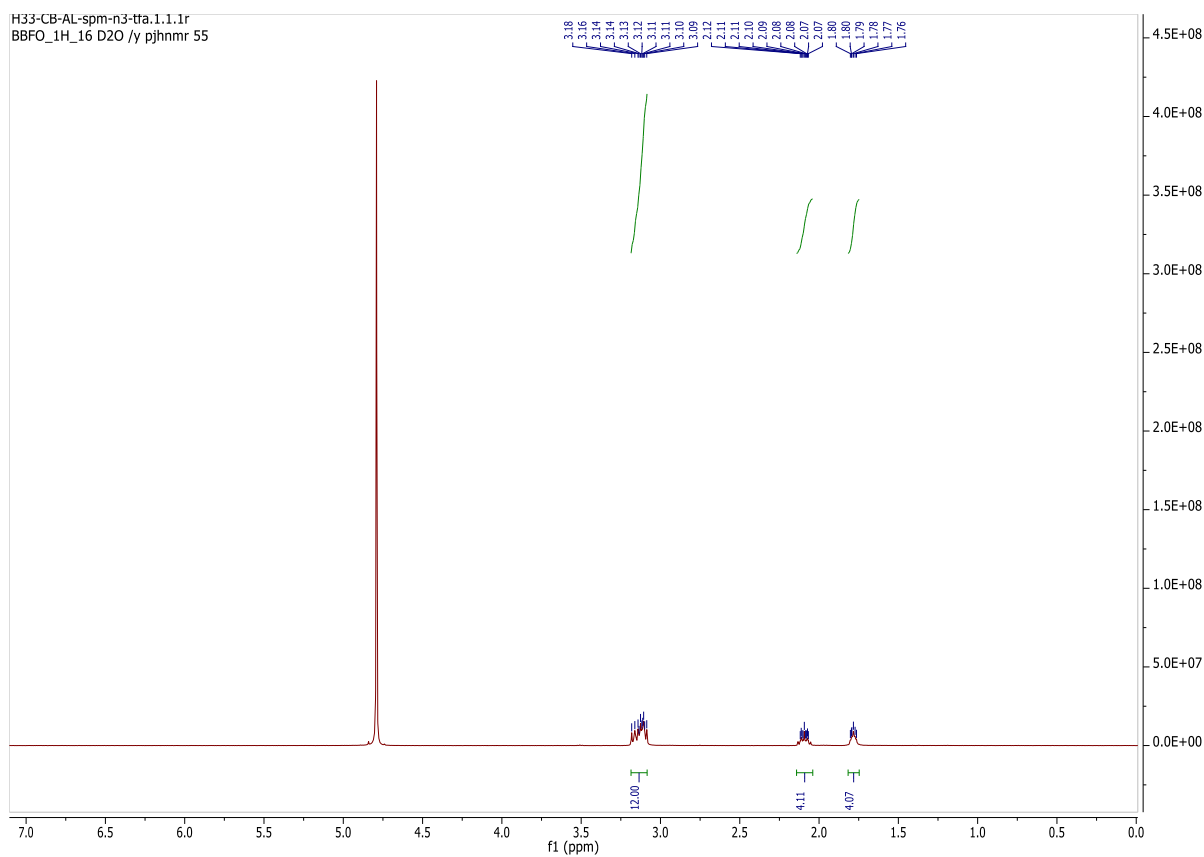


Figure 8. 14. ^1H NMR of spermine azide.3TFA

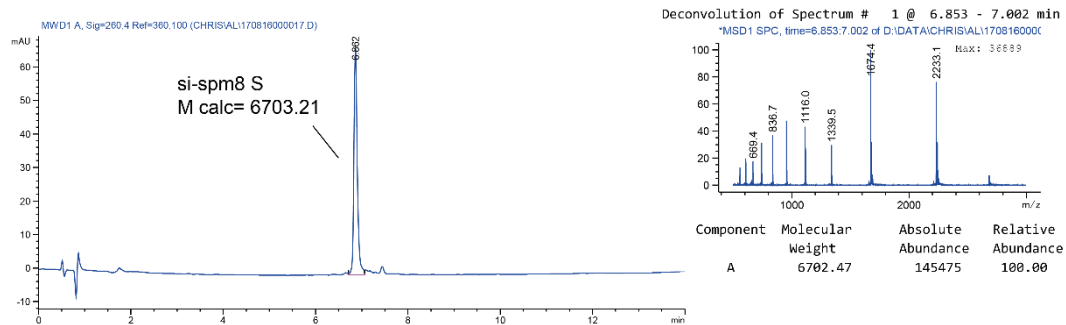


Figure 8. 15. LC-MS analysis of si-spm8 sense strand after click reaction with spermine-N₃. Sequence of si-spm8 S (5'-3'): GAGCGAAGAGGGCGAGAAUY. Y indicates 2'-O-propargyl cytosine.

Appendix – Project 3

Table 8. 1. Sequences of ORNs used for project 3

Compound	Sequence (5'-3')
hsa-miR-34a-5p	UGGCAGUGUCUUAGCUGGUUGU (>p)
hsa-miR-34a-3p	CAAUCAGCAAGUAUACUGCCCU
hsa-miR-106a-5p	AAAAGUGCUUACAGUGCAGGUAG (>p)
hsa-miR-106a-3p	CUGCAAUGUAAGCACUUCUUAC
hsa-let-7g-5p	UGAGGUAGUAGUUUGUACAGUU (>p)
hsa-let-7g-3p	CUGUACAGGCCACUGCCUUGC
siLin28B- dumbbell>P	AGUACCAAAGUGCUCAUAGUGCAGGUAGUUUUGGCAUGACUCU ACUGUAGUAUGGGCACUUCAGUACU>p
truncated pre- miR-20b>p	UGCAGGUAGUUUUGGCAUGACUCUACUGUA>p
8CS(0)	GUGGAUGACGGCGCCACUGCCACCACCGCAGACGCCGCCUCU
8CS(+2)	CUGUGGAUGACGGCGCCACUGCCACCACCGCAGACGCCGCCU CU
8CS(+8)	AAUCCUCUGUGGAUGACGGCGCCACUGCCACCACCGCAGACGC CGCCUCU
LigProd8CS(0)	UGGCAGUGUCUUAGCUGGUUGUGUGGAUGACGGCGCCACUGC CACCACCGCAGACGCCGCCUCU
LigProd8CS(+2)	UGGCAGUGUCUUAGCUGGUUGUCUGUGGAUGACGGCGCCACU GCCACCACCGCAGACGCCGCCUCU
LigProd8CS(+8)	UGGCAGUGUCUUAGCUGGUUGUAAUCCUCUGUGGAUGACGGC GCCACUGCCACCACCGCAGACGCCGCCUCU
14CS(0)	GUGGAUGACUAAGACACUGCCACCACCGCAGACGCCGCCUCU
14CS(+2)	CUGUGGAUGACUAAGACACUGCCACCACCGCAGACGCCGCCUC U
14CS(+8)	AAUCCUCUGUGGAUGACUAAGACACUGCCACCACCGCAGACGC CGCCUCU
LigProd14CS(0)	UGGCAGUGUCUUAGCUGGUUGUGUGGAUGACUAAGACACUGC CACCACCGCAGACGCCGCCUCU
LigProd14CS(+8)	UGGCAGUGUCUUAGCUGGUUGUAAUCCUCUGUGGAUGACUAA GACACUGCCACCACCGCAGACGCCGCCUCU
Bridging ORN	CCACAGAGGAUUACAACCAGCUAA

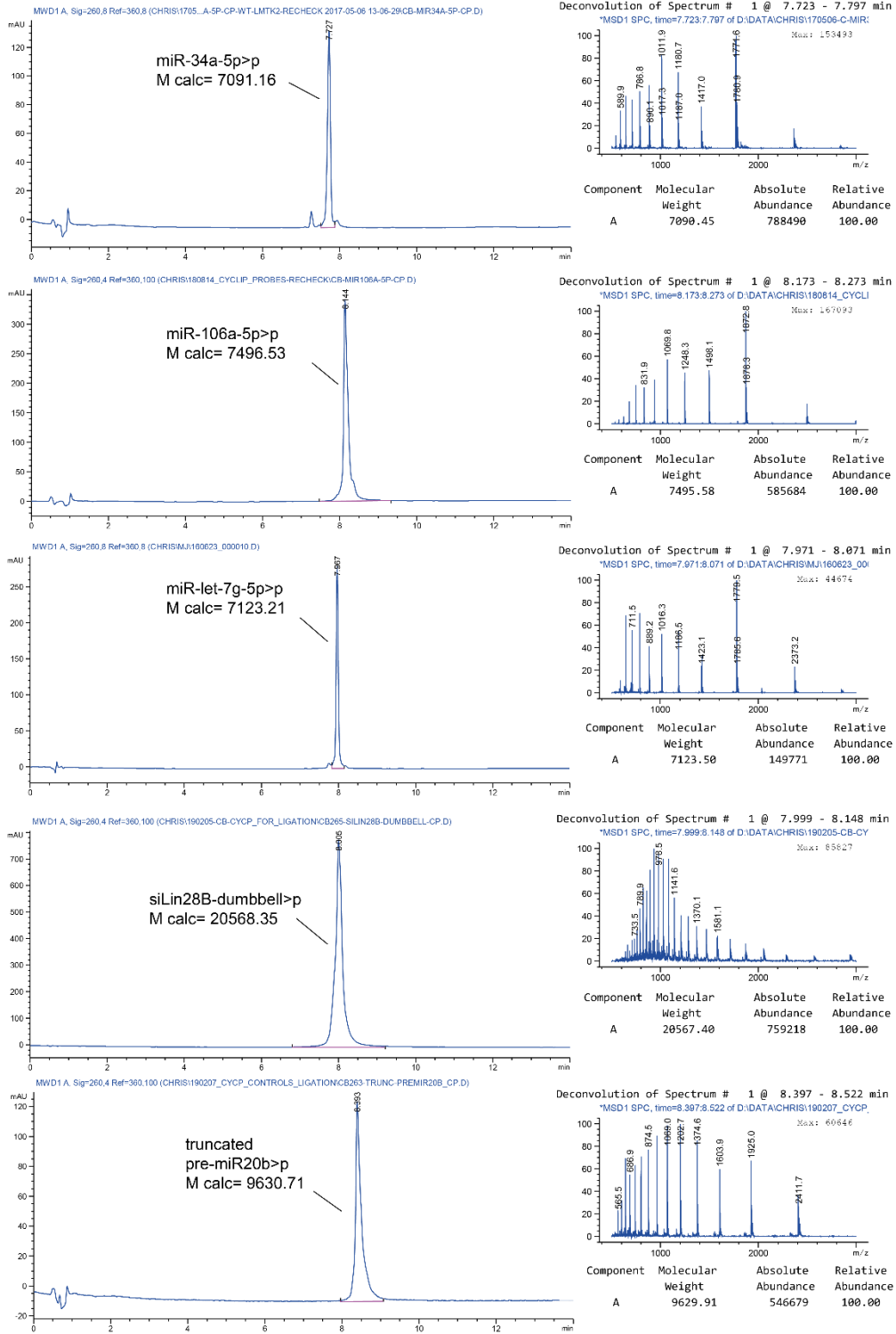


Figure 8. 16. LC-MS analysis of RNA>p

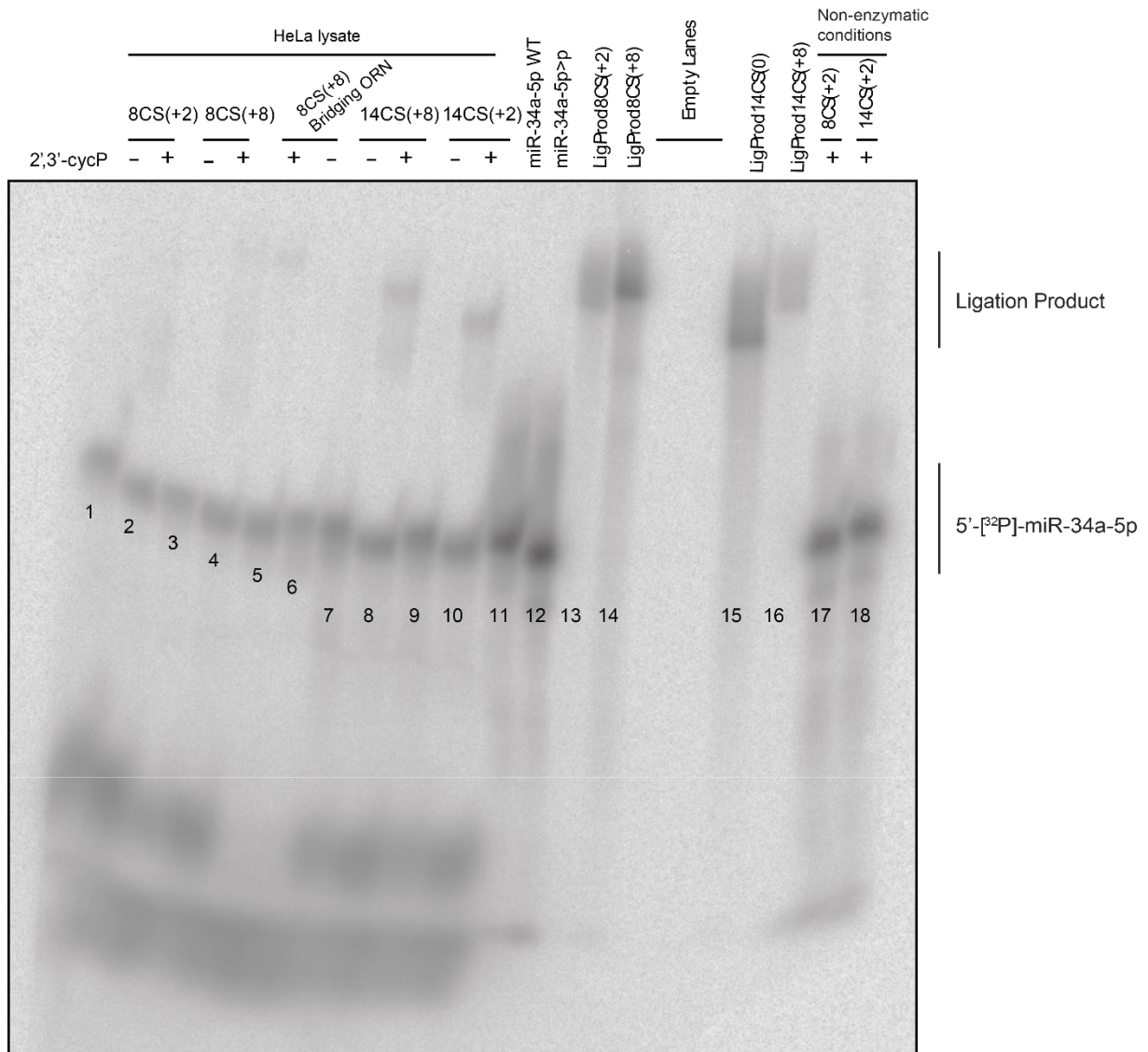


Figure 8. 17. Ligation of 5'-³²P-labelled miR-34a-5p>p to different counterstrands in HeLa lysate. 15% dPAGE, replicate 1 for figure 4.4 C.

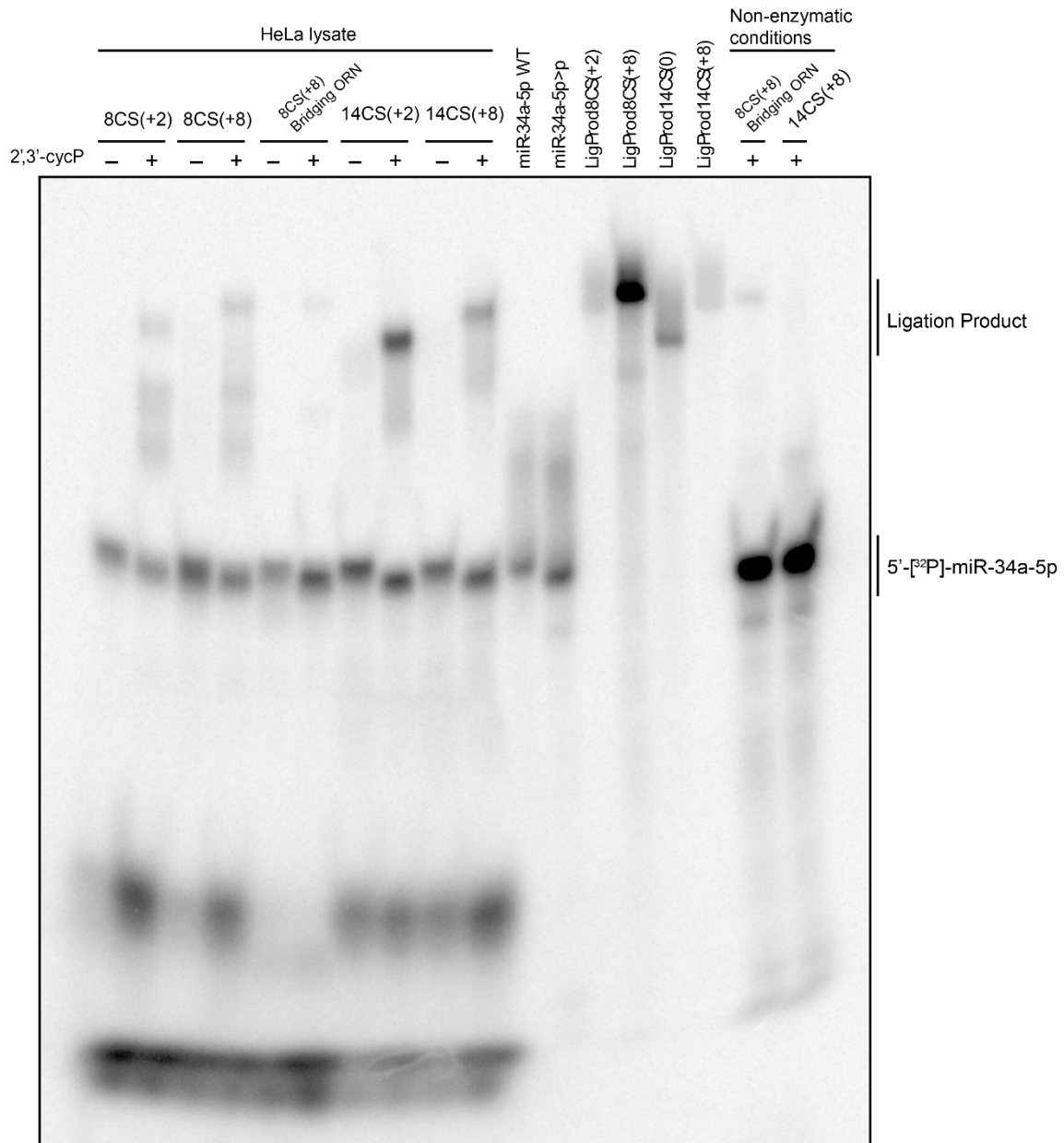


Figure 8. 18. Ligation of 5'-³²P-labelled miR-34a-5p>p to different counterstrands in HeLa lysate. 15% dPAGE, uncropped gel (replicate 2) of figure 4.4 C.

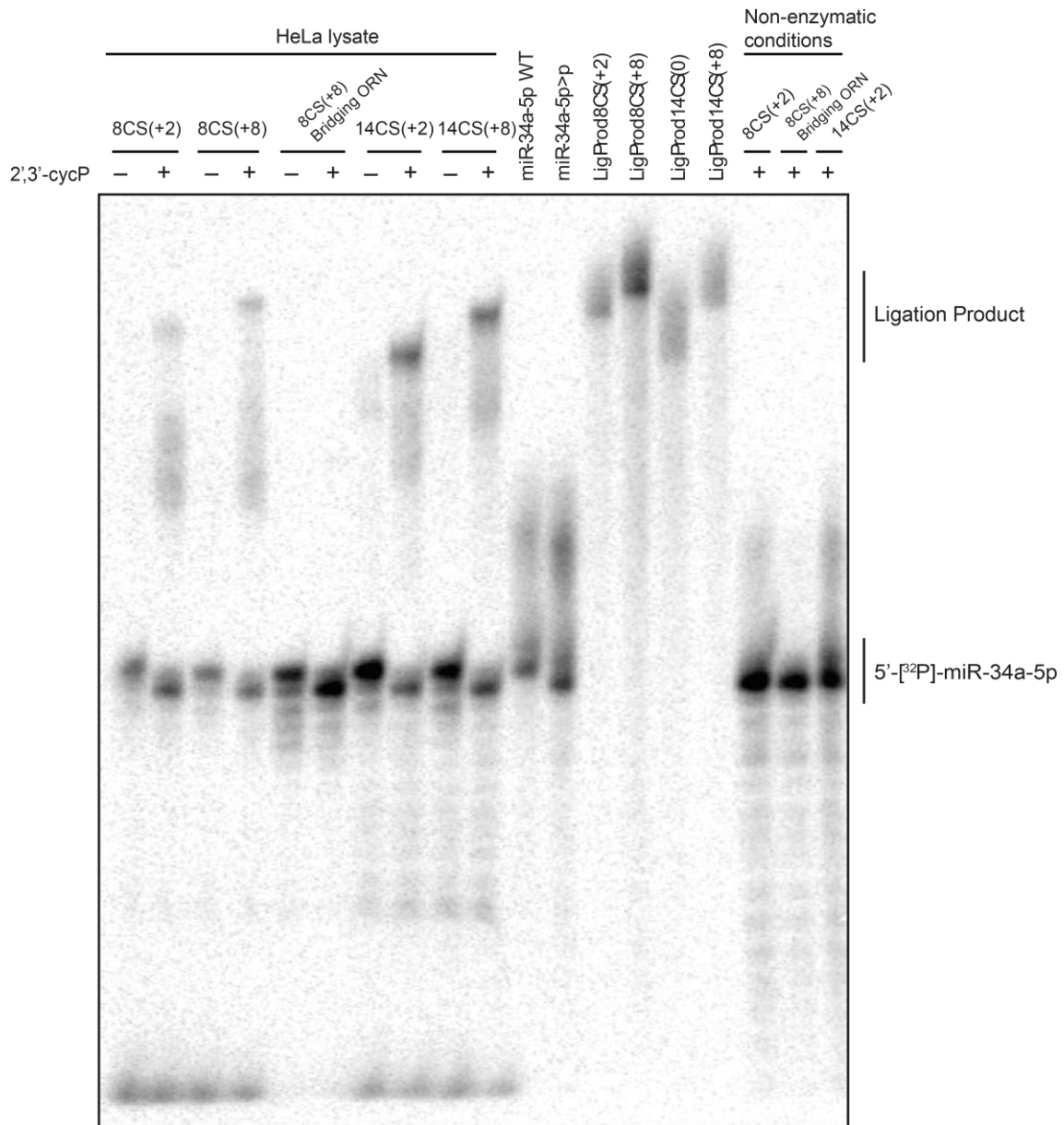


Figure 8. 19. Ligation of 5'-³²P-labelled miR-34a-5p>p to different counterstrands in HeLa lysate. 15% dPAGE, replicate 3 for figure 4.4 C.

Curriculum vitae

Personal data

Name	Christian Berk
Date of birth	02.08.1989
Place of birth	Andernach, Germany
Citizenship	Germany

Education

Since	ETH Zurich
03/ 2015	Department of Chemistry and Applied Biosciences Prof. Dr. Jonathan Hall PhD candidate
12/ 2014	Approbation German license to practice as a pharmacist
05/ 2014 – 10/ 2014	Kaiser Apotheke, Berlin, Germany Practical training for pharmacists
11/ 2013 – 04/ 2014	University of Cambridge, United Kingdom Department of Biochemistry Prof. Dr. Peter F. Leadlay Visiting student (diploma thesis)
10/ 2009 – 10/ 2013	University of Freiburg Pharmacy (state exam)
08/ 2000 – 03/ 2009	Kurfürst-Salentin Gymnasium Andernach, Germany